Konformationsanalyse von Naturstoffen und ihren Derivaten anhand von NMR-Parametern und computerchemischen Rechnungen

von

Dr. Uwe Michael Reinscheid

aus Meschede

Schriftliche Habilitationsleistung am Fachbereich Pharmazie der Universität Marburg gemäß §6 (2) der Habilitationsordnung

November 2006

Vorwort

Die vorliegende Habilitation wurde im Zeitraum 2004-2006 am Max-Planck-Institut für biophysikalische Chemie, Abteilung NMR II, angefertigt.

Für die großzügige Unterstützung von Prof. Griesinger (Max-Planck-Institut Göttingen) und Prof. Keusgen (Pharmazie, Universität Marburg) möchte ich mich herzlich bedanken.
Ich freue mich, dass so viele Kollegen und Mitarbeiter mir fachlich und persönlich geholfen haben.

Danksagung

Ohne die Hilfe und den liebevollen Rückhalt meiner Mutter, meines Bruders Dieter, meiner Frau Frauke und meiner Schwiegereltern Ursula und Wolfgang gäbe es diese Arbeit nicht.

Ich hoffe, das Geben und Nehmen aller Beteiligten hielt sich einigermaßen in der Waage.

Ich danke dem Herrn, dass er mir Zuversicht, Glauben und Hoffnung schenkte, als ich davon nicht genug hatte.

Für den stärksten und tapfersten Papa der Welt.

"Wenn die Maus satt ist, ist das Mehl bitter."

(Karl-Heinz Reinscheid)

Inhaltsverzeichnis

Inhaltsverzeichnis

1. Überblick

Das übergeordnete Ziel dieser Arbeit ist eine genaue Konformationsanalyse komplexer Naturstoffe durch eine neue Kombination aus experimentellen und mittels DFT(Dichtefunktionaltheorie) berechneten NMR-Parametern. Ausgehend vom klassischen MD(Moleküldynamik)/NMR-Ansatz werden Konformationen durch einen MD/NMR/DFT-Ansatz bestimmt. Auf diese Weise ist erstmals eine geometrische, quantenmechanische und energetische Beschreibung von komplexen Naturstoffen möglich, als Ausgangspunkt für ihre Evaluierung als Wirkstoffe. Die Leistungsfähigkeit der Ansätze wird an einer Serie von Naturstoffen großer Diversität nachgewiesen.
Im Einzelnen werden u. a. folgende Fragestellungen bearbeitet:

1. Welche Konformation nimmt das zyklische Depsipeptid Hormaomycin in Lösung an ?
2. Wie flexibel ist Hormaomycin in Lösung ?
3. Besitzt der Zuckersubstituent des immunogenen MUC1-abgeleiteten Glykopeptids eine strukturierende Wirkung ?
4. Welche Konformation besitzt ein lineares, trimeres Cyclopropan in Lösung ?
5. Sind zyklische Cyclopropane durch Elektronendelokalisation stabilisiert und aromatisch ?
6. Welcher Zusammenhang besteht zwischen der $^{3}J_{C6H1'}$ Kopplung und dem glykosidischen Diederwinkel in Cytidin ?
7. Lässt sich die Konformation von Menthol in Lösung anhand der ^{13}C Verschiebungen bestimmen ?

Im Folgenden wird der Aufbau der Arbeit kurz vorgestellt.
Im einleitenden Teil wird zunächst die Bedeutung der Konformation chemischer Verbindungen dargelegt. Es wird mit Literaturbeispielen belegt, dass eine quantenmechanische Beschreibung für das Verständnis einer ermittelten Konformation notwendig ist. Anschließend werden Naturstoffe als "privilegierte" Strukturen in der Wirkstoffsuche vorgestellt. Als eine universelle Methode zur Konformationsanalyse behandeln die folgenden zwei Kapitel die NMR-Spektroskopie, die hierfür traditionell die

Lage (chemische Verschiebung) und Form (J-Kopplung) der NMR-Signale, sowie die Messung von Relaxationseffekten (NOE/ROE) und in jüngster Zeit von dipolaren Restkopplungen im orientierenden Medium nutzt. Als weitere neue Parameter stehen quantenmechanisch berechnete chemische Verschiebungen und J-Kopplungen der Konformationsanalyse zur Verfügung, wofür einige Literaturbeispiele für Rechnungen auf dem DFT Niveau genannt werden. Die letzten beiden Kapitel der Einleitung behandeln die verwendeten Werkzeuge zur Modellierung der Verbindungen: Moleküldynamik, DFT Rechnungen und Natural-Bond-Orbital(NBO)-Analyse. Im Hauptteil "Ergebnisse und Diskussion" werden die Veröffentlichungen vorgestellt. Den Abschluß bilden die Zusammenfassung, die Listen der zitierten Literatur und eigener Veröffentlichungen, sowie der Lebenslauf.

Einleitung

2.1 Konformationsanalyse und Naturstoffe als privilegierte Strukturen

Die Eignung einer Verbindung für eine molekulare Funktion hängt von ihrer Konstitution, Konfiguration und ihrer Konformation ab. Umgekehrt gilt, dass eine Änderung der letztgenannten drei chemischen Charakteristika, zu einer "Fehl"funktion führen kann.
Insbesondere Konformationsänderungen biologischer Verbindungen wurden in den letzten Jahren zu einem wichtigen medizinischen Forschungsgebiet, da sie in einem ursächlichen Zusammenhang mit schwerwiegenden Krankheiten stehen. So sind unlösliche β-Faltblattstrukturen vormals löslicher Proteine das charakteristische Kennzeichen degenerativer Erkrankungen wie Morbus Alzheimer [Sommer, 2002; Hammerström, 2003]. Auch die physiologische PrP^{c}-Form des Prionenproteins wandelt sich durch einen Übergang von einer α-Helix zu einem β-Faltblatt in die pathologische PrP^{sc}-Form um [Taylor, 2002; Soto, 2003].

Ein weiteres Beispiel für die Bedeutung der Konformation von Verbindungen findet sich im Bereich der antibiotischen Naturstoffe, wo Vancomycin ein "letztes Mittel" aufgrund fortschreitender Resistenzbildung gegenüber Standard-Antibiotika wie Penicilline und Makrolide darstellt [Williams, 1999]. Seine Wirksamkeit nimmt mit dem Grad seiner Dimerisierung zu. In einer NMR-Studie wurde gezeigt, dass der Disaccharid-Substituent die Konformation des zyklischen Peptids beeinflusst [Grdadolnik, 1998]. Ein weiterer Zuckersubstituent verstärkte die Dimerisierung und steigerte damit die Aktivität [Mackay, 1994].

Wie subtil elektronische Einflüsse auf die Konformation sein können, zeigt das Beispiel des Guanosin-3´,5´-bisphosphats als Modellverbindung für Oligonukleotide [Acharya, 1999]. Der Ladungszustand des Aglykons moduliert über anomere Effekte die Vorzugskonformation des Zucker-Phosphat Rückgrats am 3´-Ende. Erst eine detaillierte Analyse der bindenden und antibindenden Orbitale erlaubte eine prädiktive Beschreibung der Modellverbindung. Weitere Beispiele für den Einfluss eines Substituenten auf die Konformation sind die diagnostisch interessanten, modifizierten Amino-Oligonucleoside. Die Stickstoffsubstitution verändert den γ-Diederwinkel am 5´-Ende und schwächt damit die Hybridisierung mit dem komplementären Strang [Obika, 2005].

Anhand von DFT Rechnungen können NMR-Parameter durch stereoelektronische Effekte interpretiert werden. So wurde mit Hilfe einer NBO-Analyse an *cis*-1,3-disubstituieren Cyclohexanen gezeigt, dass der γ-Effekt einer OH- bzw. OCH_3-Gruppe auf die Protonverschiebung durch Hyperkonjugation erklärt werden kann [de Oliveira, 2006]. Eine ebensolche ist verantwortlich für die experimentell gefundenen, kleineren $^1J_{CH}$ Kopplungen für axiale Positionen in anomeren Systemen im Gegensatz zu solchen für äquatoriale Positionen. Die resultierende Verstärkung bzw. Verkürzung der äquatorialen CH-Bindung [Eliel, 1995] wurde in einer Reihe von anomeren Systemen berechnet [Martínez-Mayorga, 2004].

Derartige Zusammenhänge sind aufgrund quantenmechanischer Rechnungen an konformativ interessanten Verbindungen durch DFT-Methoden möglich geworden und können Ausgangspunkt für ein Konformationsdesign sein, wie die Erzeugung "flexibler Moleküle mit definierter Gestalt" [Hoffmann, 1998; Hoffmann, 2000] durch Methylierungen von Polyketiden gezeigt hat. Obwohl Naturstoffe wie Bleomycin A_2 auf diese Weise präorganisierte Konformationen einnehmen [Kato, 1988; Owa, 1992; Boger, 1998; Boger, 1999], war ein synthetischer Nachbau lange Zeit nicht möglich [Hoffmann, 1992]. Seit Mitte der 90er Jahre gelingt die Umsetzung dieses Konzeptes [Stahl, 1996; Böhm, 1996; Stahl, 1997], auch im Bereich der Wirkstoffforschung in Gestalt der Optimierung einer Ligand-Protein Bindung. Weil der Gibbs-Energieunterschied zwischen einem "mittelmäßigen" und einem "guten" Liganden in der Größenordnung von 4 kcal/mol liegt, reagieren Affinitäten sehr empfindlich auf eine veränderte Dynamik des Liganden und des Proteins. Eine Prä-Organisation des Liganden in seiner "Aktivkonformation" erscheint daher ein lohnender Versuch zu sein, um seine Affinität zu steigern. Wie das bereits erwähnte Bleomycin A2 zeigt, sind besonders im Bereich der Naturstoffe interessante Beispiele für ein solches "natürliches" Konformationsdesign vorhanden. Ein synthetisches Derivat mit erhöhter Population der Aktivkonformation der *L*-Threonin Einheit zeigte eine gesteigerte Wirksamkeit [Boger, 1998; Boger, 1999].

Diesen pharmazeutisch relevanten Fall von molekularer Erkennung versuchen Docking und Scoring Programme zu simulieren [Stahl, 2002; Gohlke, 2000; 2002]. Als Grundlage diente die Schlussfolgerung aus der Analyse der Kristallstruktur von Benzol-Einschlussverbindungen, dass die molekulare Selbsterkennung in der Festphase als Anleitung für das Ligand-Design dienen kann [Klebe, 1993]. Diese Hypothese konnte bereits erfolgreich genutzt werden [Gurrath, 1998; Vedani, 1995], gestützt durch die hohe Qualität der Programme bei der Beschreibung von Amino- und Nukleinsäuren. Die ungemein große

chemische Diversität niedermolekularer Verbindungen verhindert eine ebensolche für die Charakterisierung der Liganden/Wirkstoffe im Komplex.

Ein wichtiger Schritt auf diesem Weg ist die computerchemische Untersuchung der isolierten Liganden. Hieraus können zum einen Schlüsse gezogen werden, inwieweit der kraftfeldbasierte Ansatz beim Docking verlässlich die Chemie der Verbindung beschreibt. Zum anderen können experimentelle Daten wie chemische Verschiebungen und J-Kopplungen evaluiert und gedeutet werden im Hinblick auf die jeweilige Konformation des Liganden.

Der Wert einer computerchemischen Analyse bereits bei der Strukturaufklärung belegte eine retrospektive Literaturrecherche [Nicolaou, 2005]. Es wurden mehr als 300 sogenannte "revidierte Strukturen" von Naturstoffen aus dem Zeitraum 1990 bis 2004 gefunden. Als ein Beispiel seien die zwei Vorschläge für ein zyklisches Heptapeptid, Axinastatin 1 oder Malaysiatin, genannt. Ausgang war vermutlich die Fehlinterpretation eines Massenspektrums Durch Synthese und NMR-Analyse konnte dem Naturstoff der Strukturvorschlag des Axinastatin 1 zugeordnet werden [Konat, 1995]. Die ^{13}C- Verschiebungen der beiden Vorschläge differierten teilweise um mehr als 5 ppm, so dass eine Berechnung auch zum Ziel hätte führen können.

Eine neuer Aspekt auf dem Gebiet der molekularen Erkennung ist die differenzielle Bindung [Lavigne, 2001]. Im Gegensatz zur spezifisch oder selektiven Bindung werden Rezeptoren hergestellt, die verschiedene Bindungseigenschaften aufweisen. Für diesen Zweck können auch dynamische Bibliotheken verwendet werden. Die Einführung eines Gastmoleküls verschiebt das dynamische Gleichgewicht einer Monomeren Mischung in Richtung eines Komplexes, der einen zum Gastmolekül komplementären Rezeptor darstellt [Cardullo, 2000].

Als ein Beispiel aus dem Bereich der Naturstoffe seien hier Nukleotide genannt, da sie sowohl an Nukleotid-triphosphat Hydrolasen als auch an Proteinkinasen binden [Denessiouk, 2000]. Die Suche nach Leitstrukturen unter den allseits bekannten Naturstoffen in der oben gemachten Definition, ist daher ein bisher vernachlässigtes, aber lohnendes Gebiet.

Entsprechend wurden in den letzten Jahren neben Diversitäts-orientierten Bibliotheken auch Naturstoff-basierte Sammlungen potentieller Wirkstoffe aufgebaut [Koehn, 2005; Davis, 1999; Wess, 2001] und Naturstoffe erleben eine Renaissance als Wirkstoffkandidaten [Paterson, 2005; Butler, 2005]; eine paradoxe Entwicklung, da seit Beginn der Arzneimitteltherapie und auch in der modernen Wirkstoffsuche, Naturstoffe eine große Rolle spielen, wie eine Übersicht der neu eingeführten Wirkstoffe des Zeitraums 1981-2002 mit

einem Naturstoffanteil von ca. 30 % belegt [Newman, 2003]. Aus diesem reichhaltigen Fundus schöpfend, versucht eine neue Strategie, Naturstoffe synthetisch miteinander zu einem Hybrid zu kombinieren [Tietze, 2003; Mehta, 2002]. Der Naturstoff Vitamin E dokumentiert mit seiner Phytylkette, verantwortlich für die Membran Wechselwirkung, und der Phenol Teilstruktur, wirksam als Radikalfänger, die Effektivität dieses Ansatzes.

Als Ursache für ihren Erfolg als Wirkstoffe nimmt man an, dass Naturstoffe biologisch validierte Startpunkte im Screening nach Leitstrukturen darstellen [Breinbauer, 2002]. Eng verknüpft damit ist der Begriff der "privilegierten Struktur". Der Begriff wurde für die Gruppe der Benzodiazepine eingeführt, als festgestellt wurde, dass sie sowohl an den Benzodiazepin-Rezeptor als auch an Cholecystokinin-Rezeptoren binden [Evans, 1988]. Ein Ligand ist somit privilegiert, falls er an verschiedene Faltungstypen binden kann. Der Faltungstyp spielt eine wichtige Rolle in der Leitstruktursuche, weil ähnliche Faltungstypen, mit gewissen Ausnahmen, ähnliche Liganden binden. Bei einer Zahl der menschlichen Proteine von mehr als 100 000 werden nur bis zu 8000 verschiedene Faltungstypen angenommen und somit die Leitstruktursuche vereinfacht.
Naturstoffe weisen privilegierte Strukturen aus mehreren Gründen auf. Zum einen wurden sie von verschiedenen Proteinen synthetisiert und teilweise transportiert. Daher müssen sie ausgewogene Bindungseigenschaften aufweisen. Zum anderen dienen sie vermutlich immer einem biologischen Zweck, der in der Regel durch Bindung an eine Zielstruktur erreicht wird. Entscheidend ist nun, dass diese beiden Eigenschaften in der Entwicklungsgeschichte des jeweiligen Produzenten und seiner jeweiligen Umgebung optimiert wurden. Ergebnis dieser Optimierung ist oft eine Kombination aus Flexibilität und Starrheit, die die sogenannte "Enthalpie-Entropie-Kompensation" widerspiegelt: je stärker die Wechselwirkungen, desto stärker wird die Beweglichkeit von Ligand und Protein eingeschränkt [Liu, 2001; Williams, 2004]. Diese Kombination aus Flexibilität und Starrheit findet sich nicht nur auf Substanzebene, sondern auch in der Biogenese und damit auf Organismusebene. Als prägnantes Beispiel möge hier die Resistenzentwicklung bei Mikroorganismen dienen [Bode, 2005].

Der oben genannten "Privilegierung" der Naturstoffe durch die Evolution steht das menschliche Bewerten potentieller Leitstrukturen gegenüber. In zwei Studien wurde belegt, wie schwierig diese Evaluierung ist [Martin, 2002; Lajiness, 2004]. So wurden bei einer zweiten Durchsicht 50 % der vorher abgelehnten Verbindungen nunmehr akzeptiert. Eine Ursache hierfür ist ihre unzureichende Charakterisierung.

In dieser Hinsicht ermöglicht die geometrische, quantenmechanische und energetische Beschreibung von Verbindungen in der vorliegenden Arbeit nicht nur die Weiterentwicklung von Naturstoffen zu Wirkstoffen, sondern auch die Evaluierung potentieller Leitstrukturen.

2.2 NMR-Parameter in der Konformationsanalyse

Chemische Verschiebungen

Obwohl chemische Verschiebungen Informationen über die Konformation enthalten, war es in der Vergangenheit schwierig, quantitative Zusammenhänge vorherzusagen. Frühe Berechnungen lieferten demnach nur grobe Werte [Ando, 1983]. Durch die Fortschritte in den letzten 10 Jahren ermöglicht, wurden durch den MD/NMR/DFT-Ansatz chemische Verschiebungen berechnet, die in der vorliegenden Arbeit zur Konformationsanalyse von Tercyclopropandimethanol (Kapitel 3.4), Cytidin (Kapitel 3.6) und Menthol-Diastereomeren (Kapitel 3.7) eingesetzt wurden. Im Bereich der Strukturevaluierung von Naturstoffen haben mehrere Gruppen einen MD/NMR/DFT-Ansatz erfolgreich angewandt [Torres-Valencia, 2004; Barone, 2002a].

Speziell für Peptide und Proteine wird die temperaturabhängige chemische Verschiebung der Amidprotonen als Strukturinformation verwendet. Änderungen kleiner als 3 ppb/K deuten auf eine Abschirmung vom Lösungsmittel hin und können daher eine Wasserstoffbrücke anzeigen [Kessler, 1982]. Diese Information wurde als Hinweis auf strukturierte Bereiche in der Konformationsanalyse von Hormaomycin (Kapitel 3.2) und von MUC1-abgeleiteten Glykopeptiden (Kapitel 3.3) eingesetzt.

Für die von MUC1-abgeleiteten Glykopeptide wurde die Sekundärstruktur durch Vergleich der chemischen Verschiebungen von Hα, Cα und CO mit bekannten Werten aus Helix- bzw. Faltblattstrukturen bestätigt (Kapitel 3.3). Grundlage hierfür sind gegenläufige Tendenzen in den beiden Strukturen im Vergleich mit Werten aus unstrukturierten Bereichen [Wishart, 1994; Wishart, 2001].

NOE/ROE-Daten

Abstände zwischen Protonen können aufgrund der Dipol-Dipol-Relaxation abgeschätzt werden [Neuhaus, 2000]. Der zugrunde liegende Effekt (Nuclear Overhauser Effect, NOE,

bzw. das Analogon im rotierenden System, ROE) skaliert mit r^{-6} bezüglich des Abstandes zwischen den Protonen und ist somit nur auf atomar kurzen Distanzen messbar. Die Intensitäten in Form des integrierten Signals können semiquantitativ oder nach Kalibrierung mit einem bekannten, fixierten Abstand (z. B. ein Methylen-Protonenpaar) in Moleküldynamik-Rechnungen verwendet werden [Gronenborn, 1985]. Wird ein Abstandsfehler von 5 % akzeptiert, so resultiert daraus bereits eine Toleranz in der NOE-Intensitätsmessung von 35 %. Daher wurde der semiquantitative Ansatz mit einer Klassifizierung in drei oder vier Abstandsbeschränkungen und einer möglichst großen Zahl an NOE/ROE pro Struktureinheit für die Konformationsanalyse von Hormaomycin (Kapitel 3.2) und den MUC1-abgeleiteten Glykopeptiden (Kapitel 3.3) angewandt.

J-Kopplungen

Traditionell am wichtigsten ist die ^{3}J-Kopplung, welche vom Diederwinkel abhängt [Haasnoot, 1980]. Die sogenannte Karplus-Gleichung vom Typ (1) [Karplus, 1959] wurde im Rahmen der Valence-Bond(VB) Theorie abgeleitet und mit empirischen Daten korreliert:

$$^3J = A\cos^2(\Phi + \omega) + B\cos(\Phi + \omega) + C \qquad (1)$$

A, B, C sind Parameter für eine Serie verwandter Substanzen, Φ ist der Diederwinkel und ω beschreibt die Phasenverschiebung.
Es existiert eine große Zahl an Parametrisierungen, die in der Regel empirisch ermittelt wurden so z. B. für die ^{3}J-Kopplung zwischen den Amidprotonen und den α-Protonen in Peptiden und Proteinen [Pardi, 1984]. Aufgrund des trigonometrischen Zusammenhanges existieren jedoch bis zu vier verschiedene Diederwinkel je gemessener Kopplungskonstante. Zudem wird bei Änderungen des Diederwinkels, die schnell auf der NMR-Zeitskala sind, nur die gemittelte Kopplungskonstante gemessen. In der Moleküldynamik-Rechnung wird dieses teilweise berücksichtigt, indem ein entsprechend großer Konformationsraum erlaubt bleibt. Eine konformationelle Heterogenität als Ursache für die Inkompatibilität der NMR-Parameter wurde von Kessler et al. bereits 1988 beschrieben [Kessler, 1988].
In neuerer Zeit werden auch ^{1}J und ^{2}J, sowie weitreichende Kopplungen (^{n}J mit n > 3) für Strukturuntersuchungen verwendet. Dabei werden oft keine einfachen, quantitativen Zusammenhänge empirisch gefunden. Die quantenmechanische Berechnung dieser J-

Kopplungen hat daher einen besonders großen Wert für die Konformationsanalyse und auch die elektronische Charakterisierung einer Substanz.

Aus E.COSY Spektren [Griesinger, 1985; Müller, 1987] können homonukleare ^{3}J-Kopplungen (Hormaomycin in Kapitel 3.2 und MUC1-abgeleitete Glykopeptide in Kapitel 3.3), aus heteronuklearen HSQC Spektren ^{1}J-Kopplungen (Cytidin in Kapitel 3.6) und aus HMBC/HSQC Spektren [Verdier, 2003] heteronukleare ^{3}J-Kopplungen (Tercyclopropandimethanol in Kapitel 3.4) erhalten werden.

Von der Arbeitsgruppe Murata wurde eine Methode zur Bestimmung der relativen Konfiguration anhand von $^{2}J_{CH}$, $^{3}J_{CH}$ und $^{3}J_{HH}$ Kopplungen entwickelt [Matsumori, 1999]. Auf diese Weise konnte u.a. die alizyklische Seitenkette von Maiotoxin [Matsumori, 1999], ein neues Isomer von Latrunculin B [Hoye, 2002] und das cytotoxische Apratoxin A [Luesch, 2001] stereochemisch charakterisiert werden. Somit besteht die experimentelle Basis für die Kombination aus berechneten und experimentellen J-Kopplungen in der stereochemischen Analyse (siehe Kapitel 2.3).

Dipolare Restkopplungen (RDCs)

Durch den Raum wechselwirken zwei NMR-aktive Kerne aufgrund ihrer Dipoleigenschaften. Die Stärke dieser Wechselwirkung hängt vom Abstand der Kerne und der Orientierung des internuklearen Vektors bezüglich des statischen Magnetfeldes ab. In isotroper Lösung mittelt sich der Effekt aufgrund der schnellen, ungerichteten Reorientierung des Moleküls aus. In partiell anisotropen Medien wird diese Reorientierung teilweise behindert und die ansonsten starke Wechselwirkung (im kHz Bereich) wird auf Frequenzen im Bereich 0-20 Hz skaliert. Somit wird einerseits die schmale Linienbreite, andererseits die Strukturinformation aufgrund der dipolaren Kopplung erhalten, die man nun als dipolare Restkopplungen (residual dipolar coupling, RDC) bezeichnet.

Die Strukturbestimmung von Proteinen konnte für zwei günstige Fälle allein aufgrund von RDC Daten erzielt werden [Hus, 2001; Blackledge, 2005]. RDC Daten niedermolekularer Substanzen werden erst seit einigen Jahren erhalten, da neue Orientierungsmedien für organische Lösungsmittel entwickelt werden mussten. Nun steht eine Reihe von skalierbaren Medien zur Verfügung (z. B. gestreckte, gestauchte Polymergele [Luy, 2004; Freudenberger, 2004; Freudenberger, 2005; Haberz, 2005]) und die Anwendung auf stereochemische und dynamische Fragestellungen nimmt eine rasche Entwicklung [Geschwind, 2005]. Die

Berechnungen starten mit dem Orientierungstensor anhand eines Strukturmodells. Hiervon ausgehend werden theoretische RDCs berechnet und mit den experimentellen Daten verglichen [Zweckstetter, 2000]. Als eine weitere Möglichkeit wurden sie in der Konformationsanalyse von Hormaomycin in DMSO als Randbedingungen in Molekulardynamik-Rechnungen verwendet (Kapitel 3.2). In diesem Fall werden sie wie Abstands- und Winkelinformationen aus NOE/ROE-Messungen und J-Kopplungskonstanten eingesetzt [Hus, 2000]. Da eine Mindestzahl von 5 unabhängigen RDCs pro starrer Einheit notwendig sind, wurden bisher oft Moleküle mit starren Einheiten untersucht: Zucker [Yan, 2003, Freedberg, 2002], Polycyclen [Luy, 2004; Freudenberger, 2004; Freudenberger, 2005; Thiele, 2003; Thiele, 2004; Yan, 2004] und konformativ stabile Ringe [Verdier, 2003; Haberz, 2005]. In jüngster Zeit wird versucht, auch flexiblere Moleküle anhand von RDC Daten und computerchemischen Berechnungen stereochemisch zu analysieren [Thiele, 2006].

2.3 Berechnung von NMR-Parametern und deren Anwendung

Die direkte Wechselwirkung der magnetischen Momente $\hat{m}_K$ des Atomkerns K mit einem äußeren Magnetfeld $\hat{B}$ führt durch die Aufspaltung der Energieniveaus zu folgendem Korrekturterm der Energie:

$$\Delta E = -\hat{m}_K \hat{B} \tag{2}$$

In einem Molekül induziert das Magnetfeld einen Strom und dieser nach dem Biot-Savartschen Gesetz wiederum ein magnetisches Feld, welches das angelegte Feld überlagert. Am Ort des Kerns wirkt also in Gegenwart der Elektronen ein effektives Feld $\hat{B}_{eff}$:

$$\Delta E = -\hat{m}_K \hat{B}_{eff} = -\hat{m}_K \left(\tilde{1} - \tilde{\sigma}_K\right)\hat{B} \tag{3}$$

Zusätzlich zur direkten Wechselwirkung (2) ergibt sich ein durch die Elektronen induzierter Anteil, der mittels des chemischen Verschiebungstensors $\tilde{\sigma}_K$ charakterisiert wird. Außer der chemischen Verschiebung treten im Molekül Kopplungen der Kernspins untereinander auf, die zur weiteren Aufspaltung der Signale führen. Die direkte Kopplung der magnetischen

Momente der Atomkerne K und L ($\tilde{D}_{KL}$) ist eine anisotrope Größe, die sich in der Gasphase und in Lösung herausmittelt. Die indirekte Kopplung $\tilde{J}_{KL}$ wird über Spin- und Bahndrehimpuls der Elektronen vermittelt und ist damit, wie die chemische Verschiebung, ein elektronischer Effekt [Atkins, 1994].
Die Interpretation der NMR-Spektren geschieht phänomenologisch mittels eines effektiven Hamiltonoperators $\hat{H}_{NMR}$ [Helgaker, 1999]:

$$\hat{H}_{NMR} = -\sum_K \gamma_K \hbar \hat{B}\left(\tilde{1} - \tilde{\sigma}_K\right)\hat{I}_K + \sum_{K>L} h\hat{I}_K \tilde{J}_{KL} \hat{I}_L \tag{4}$$

Der erste Term beschreibt die chemische Verschiebung mittels des Verschiebungstensors $\tilde{\sigma}_K$, wobei das kernmagnetische Moment über das gyromagnetische Verhältnis γ_K mit dem Kernspin $\hat{I}_K$ verknüpft ist ($\hat{m}_K = \gamma_K \hat{I}_K$). Die indirekte J-Kopplung wird durch den zweiten Term beschrieben, der den Spin-Spin-Kopplungstensor $\tilde{J}_{KL}$ enthält. In Lösung und Gasphase sind aufgrund der statistischen Ausrichtung nur die isotropen NMR-Parameter messbar, die sich aus der Spur der Tensoren ergeben:

$$\sigma_K^{isotrop} = \frac{1}{3} Tr\left(\tilde{\sigma}_K\right) \tag{5}$$

$$J_{KL}^{isotrop} = \frac{1}{3} Tr\left(\tilde{J}_{KL}\right) \tag{6}$$

Im Experiment bezieht man die chemische Verschiebung auf eine Referenzsubstanz (für ^{1}H und ^{13}C Tetramethylsilan [Friebolin, 1999]) und gibt die relative chemische Verschiebung an:

$$\delta = \sigma_{ref} - \sigma_K \tag{7}$$

Aus Gleichung (3) lassen sich NMR-Parameter durch eine Taylor-Entwicklung der elektronischen Energie nach $\hat{B}$ und $\hat{m}_K$ berechnen:

$$
\begin{aligned}
&E\left(\hat{B},\hat{m}_K\right) = E(0) \\
&+\left(\frac{dE}{d\hat{B}}\right)_{\hat{B}=0}\hat{B} \\
&+\sum_K\left(\frac{dE}{d\hat{m}_K}\right)_{\hat{m}_K=0}\hat{m}_K \\
&+\frac{1}{2}\hat{B}^T\left(\frac{d^2E}{d\hat{B}^2}\right)_{\hat{B}=0}\hat{B} \\
&+\frac{1}{2}\sum_{KL}\hat{m}_K^T\left(\frac{d^2E}{d\hat{m}_K\cdot d\hat{m}_L}\right)_{\hat{m}_{K,L=0}}\hat{m}_L \\
&+\sum_K\hat{B}^T\left(\frac{d^2E}{d\hat{B}\cdot d\hat{m}_K}\right)_{\hat{B},\hat{m}_K=0}\hat{m}_K+\ldots
\end{aligned}
\tag{8}
$$

Ausdrücke für $\tilde{\sigma}_K$ und $\tilde{J}_{KL}$ erhält man durch Vergleich mit den Energiebeiträgen, die sich aus dem NMR-Hamiltonoperator (4) ergeben:

$$\tilde{\sigma}^K = \left.\frac{d^2E}{d\hat{B}\cdot d\hat{m}_K}\right|_{\hat{B},\hat{m}_K=0} \tag{9}$$

$$\tilde{J}_{KL} = \left.\frac{d^2E}{d\hat{m}_K\cdot d\hat{m}_L}\right|_{\hat{m}_{K,L=0}} \tag{10}$$

In Anwesenheit eines homogenen, externen magnetischen Feldes wird der Hamilton-Operator der Gleichung (4) abhängig von einem Vektorpotential $\hat{A}(r)$. Das Vektorpotential $\hat{A}(r)$ ist zu einem gegebenen magnetischen Feld $\hat{B}$ jedoch nicht eindeutig festgelegt. Für ein statisches, homogenes Magnetfeld in der Coulomb-Eichung

$$\nabla\cdot\hat{A}(\vec{r}) = 0 \tag{11}$$

nimmt es die folgende Form an:

$$\hat{A}(r) = \frac{1}{2}\left(\hat{B}\times\left(\vec{r}-\vec{R}_0\right)\right) \tag{12}$$

mit $\vec{R}_0$ als einem beliebigen Parameter, dem sogenannten Eichursprung.

Diese Ursprungsabhängigkeit (gauge dependence) oder auch Eichvarianz muss für die Berechnung chemischer Verschiebungen aufgehoben werden [Helgaker, 1999]. Ein erfolgreicher Ansatz diese Abhängigkeit zu verringern, verwendet sogenannte "gauge including atomic orbitals" (GIAO) Θ_μ [Ditchfield, 1972]:

$$\Theta_\mu\left(\hat{B}\right) = \chi_\mu \exp\left[-\frac{ie}{\hbar}\hat{A}_\mu \cdot \vec{r}\right] \tag{13}$$

mit $\hat{A}_\mu$ als Vektorpotential aus Gleichung (12).

Die Atomorbitale χ_μ werden mit einem Phasenfaktor versehen, der vom Eichursprung des Vektors abhängt. Im Rechenzyklus wird dieser Phasenfaktor optimiert, so dass die erste Ableitung nach $\hat{B}$ gegen null geht.

Die Implementierung der GIAO Methode in das DFT Schema kombinierte Qualität mit Geschwindigkeit [Wolinski, 1990; Cheeseman, 1996]. Somit wurden Verbindungen mit einer Molekülmasse größer 100 Da einer Rechnung zugänglich. Die weiterhin notwendige Abwägung zwischen Qualität und Geschwindigkeit zeigten Berechnungen von ^{13}C Verschiebungen auf rechenintensivem MP2 Niveau, die größere Übereinstimmung mit experimentellen Werten als DFT Rechnungen aufwiesen (Cheeseman, 1996).

In einer Reihe von Studien wurde der Einfluß der verschiedenen Funktionale und Basissätze in DFT Rechnungen untersucht. Für die Kombination aus dem B3LYP Funktional und dem 6-311++G(2d,2p) Basissatz wurde eine gute Übereinstimmung zwischen berechneten und experimentellen chemischen Verschiebungen und J-Kopplungen gefunden (Bagno, 2001; 2003). Für Geometrieoptimierungen reichte ein 6-31G(d,p) Basissatz, analog einer Untersuchung von Cheeseman et al. (1996), die eine Geometrieooptimierung auf B3LYP/6-31G(d) Niveau für ausreichend fanden. ^{13}C Verschiebungen berechnet auf B3LYP/6-311+G(2d,p) Niveau wiesen einen um den Faktor 3 kleineren Fehler auf als Hartree-Fock Rechnungen. Besonders für Verbindungen mit einer delokalisierten Elektronenverteilung, verhindert die fehlende Elektronenkorrelation in Hartree-Fock Rechnungen eine adäquate Vorhersage der chemischen Verschiebungen (Cheeseman, 1996).

Als ein typisches Beispiel mögen die Ergebnisse der Gruppe Bagno (2001; 2003) dienen. Die berechneten ^{13}C Verschiebungen für eine heterogene Reihe von aliphatischen und

aromatischen Verbindungen zeigten für Kohlenstoff Atome ohne Halogensubstituent eine durchschnittliche, absolute Abweichung von 6,0 ppm gegenüber den experimentellen Werten. Diese erhöhte sich auf 16,4 ppm für Kohlenstoff Atome mit Chlorsubstituent. $^{1}J_{CH}$ Kopplungen wurden unterschätzt mit einer durchschnittlichen, absoluten Abweichung von 7,6 Hz. Für $^{1}J_{CH}$, $^{3}J_{CH}$ und J_{HH} Kopplungen dominierte der FC-Term; entweder weil die DSO und PSO Terme klein waren oder sich gegenseitig auslöschten. Die empirische Karplus-Beziehung für $^{3}J_{HH}$ in Ethan wurde vom FC-Term dominiert [Helgaker, 2000].

Relativistische Effekte wurden für Halogenverbindungen beobachtet und können für C,H,O,N-Verbindungen vernachlässigt werden [Bagno 2001; 2003]. Entsprechend wurde in einer Studie gezeigt, dass Protonverschiebungen von zwei Chlorpyrimidinen nur unter Einbeziehung von Korrelations- und Lösungsmitteleffekten, sowie großer Basissätze in guter Übereinstimmung mit experimentellen Werten berechnet werden konnten [Perez, 2006].

Im Folgenden werden Anwendungen vornehmlich der chemischen Verschiebung in der Konformationsanalyse organischer Verbindungen genannt.

Im Bereich der Vorhersage von Spektren bzw. der Strukturvalidierung wurden in den letzten Jahren große Fortschritte erzielt. So wurden mit DFT-Methoden die Proton- und Kohlenstoffspektren von Naphtalin-Derivaten [Bagno, 2001; 2003], einem Norbornanderivat [Bassarello, 2003], komplexer Naturstoffe wie Strychnin [Bagno, 2006], sowie die ^{13}C-Verschiebungen einer Reihe von Alkaloiden, Terpenen [Barone, 2002a] und Zuckern [Taubert, 2005] berechnet. Im letztgenannten Beispiel wurden systematisch erhöhte ^{13}C Verschiebungen erhalten, die oft bei DFT Rechnungen auftreten. Für C1 der α-D-Lxyofuranose wurde mit 8,5 ppm die größte Abweichung zum experimentellen Wert festgestellt [Taubert, 2005]. Interessanterweise brachte die Modellierung von Lösungsmitteleffekten keine Verbesserung. Jedoch wurde durch die Wahl von Methanol anstelle von TMS (Tetramethylsilan) als Referenzverbindung die größte Abweichung zum experimentellen Wert auf 4 ppm gesenkt. Im Gegensatz zum obigen Fall verbesserte die Verwendung eines Kontinuummodells (PCM: polarizable continuum model) zur Modellierung der Lösungsmitteleffekte die Übereinstimmung zwischen berechneten und gemessenen Daten, wenn in polaren Lösungsmitteln gemessene NMR-Werte genutzt wurden (Bagno, 2006). Für unpolare Lösungsmittel ist der Fehler einer Rechnung in vacuo jedoch meist in der Größenordnung anderer verwendeter Näherungen: Vernachlässigung von Rotations- und Schwingungseffekten, konformative Beweglichkeit und unvollständiger Basissatz. Darüberhinaus sind die Funktionale und die Lösungsmittel Modellierung schwer

abzuschätzende Fehlerquellen. Umso wichtiger ist die Korrelation mit experimentellen Daten anhand einer Reihe von Verbindungen bzw. innerhalb einer Verbindungsklasse.

In flexiblen Verbindungen kann durch berechnete NMR-Parameter die relative Stereochemie bestimmt werden. Anhand von experimentellen und berechneten J-Kopplungen wurde die relative Konfiguration des marinen Makrolids Reidispongiolid A bestimmt [Bifulco, 2004]. Durch experimentelle J-Kopplungen und chemische Verschiebungen kombiniert mit DFT-Rechnungen der NMR-Parameter wurde die relative Konfiguration von neuen Steroidglykosiden erhalten [Plaza, 2004]. Experimentelle ^{13}C-Verschiebungen der Propionat-Einheiten in Naturstoffen ermöglichten eine stereochemische Vorhersage, wie am Beispiel der Makrolid-Gruppe der Desertomycine gezeigt wurde [Kobayashi, 1999; Lee, 1999; Tan, 2000; Kobayashi, 2000; Kobayashi, 2001a,b]. Die Fragmente des verwandten Oasomycin konnten stereochemisch auf Grundlage der Berechnung von ^{13}C Verschiebungen auf Hartree-Fock Niveau differenziert werden [Barone, 2002b]. Wegen ihrer Flexibilität mussten entsprechend der Boltzmann Verteilung gewichtete chemische Verschiebungen eingesetzt werden. Auch für 1,3-Dimethyl-Fragmente wurde die relative Konfiguration anhand berechneter ^{13}C Verschiebungen bestimmt [Stahl, 1996; 1997].

In der Konformationsanalyse von Benzoxazinen wurden mit Hilfe von berechneten Protonen Verschiebungen und J-Kopplungen das Konformeren-Verhältnis bestimmt und damit Schwierigkeiten von NMR Messungen bei verschiedenen Temperaturen wie Löslichkeit und Linienverbreiterung umgangen [Tähtinen, 2003]. Die Kombination aus DFT-Rechnungen und NMR-Daten wurde für die Konformationsanalyse von Carvedilol, einem nicht-selektiven β-Blocker und Inhibitor der β-Amyloidbildung, durchgeführt [Almeida, 2004]. Hierfür wurde die Verbindung in drei Fragmente zerlegt und diese getrennt berechnet, um den Rechenaufwand zu verringern. Die gute Übereinstimmung von experimentellen zu berechneten Werten rechtfertigte diesen Ansatz. Eine weitere Verbesserung der Berechnung von ^{13}C-Verschiebungen wurde durch die Einbeziehung empirischer Korrekturfaktoren erreicht, die zuvor an einem Satz von 37 kleinen organischen Verbindungen ermittelt wurden [Giesen, 2002].

Dagegen wurde ein relativ geringer Regressionskoeffizient von 0,94 und eine hohe Standardabweichung von 2,8 ppm zwischen experimentellen und berechneten ^{13}C Verschiebungen für eine Serie der umweltrelevanten PCBs (polychlorierte Biphenyle) erhalten [Kolehmainen, 2006]. Jedoch wurde in diesem Fall für die Berechnung der chemischen Verschiebung ein 3-21G(d) Basissatz gewählt, der sicher für die große Ungenauigkeit der berechneten Werte verantwortlich ist.

Im Gegensatz zu den chemischen Verschiebungen sind die Spin-Spin-Kopplungskonstanten feldunabhängige Parameter, welche als Größen zweiter Ordnung in den Kernmomenten im NMR-Hamiltonoperator auftreten (Gleichung (8)). Die magnetischen Momente der Atomkerne treten sowohl über den Bahndrehimpuls als auch den Spin der Elektronen in Wechselwirkung. Zur Beschreibung von $\widetilde{J}_{KL}$ wird der Hamiltonoperator erweitert. Es resultieren vier Terme:

DSO (diamagnetischer Spin-Orbit)-,
PSO (paramagnetischer Spin-Orbit)-,
SD (Spin-Dipol)- und
FC (Fermi-Kontakt)-Term.

Der letzte Term (FC) ist meist dominant und beschreibt die nicht-klassische Wechselwirkung zwischen Kern- und Elektronenspin, wenn sich Elektron und Kern am selben Ort befinden. Es resultiert eine langsame Basissatzkonvergenz und die Notwendigkeit großer Basissätze für ausreichend präzise Ergebnisse.
Während Hartree-Fock Rechnungen Proton Verschiebungen gut reproduzieren, werden Kopplungskonstanten stark überschätzt [Bagno, 2001]. Die Einbeziehung von Korrelationseffekten durch die Verwendung des Hybrid-Funktionals B3LYP in DFT Rechnungen führte zu hoher Genauigkeit der berechneten Kopplungskonstanten und begründete die große Verbreitung dieses Funktionals [Sychrovský, 2000; Helgaker, 2000].

In einer systematischen Studie wurde die Basissatzabhängigkeit für die Berechnung von J-Kopplungen mit dem Hybridfunktional B3LYP untersucht [Peralta, 2003]. Für Elemente der ersten beiden Perioden wurde mit einem erweiterten Basissatz von Dunning [Dunning, 1989] der FC-Term gut repräsentiert, so dass die größte Abweichung nur 1,4 % für $^{1}J_{OH}$ betrug. In der Simulation von Protonenspektren einer Reihe von organischen Verbindungen zeigte der relativ kleine 6-31G(d,p) Basissatz bereits gute Übereinstimmung mit den experimentellen Kopplungskonstanten [Bagno, 2001].

In einer systematischen Studie reproduzierte das B3LYP Funktional $^{1}J_{CH}$ Kopplungen einer heterogenen Gruppe von 72 Testverbindungen mit einer Standardabweichung von 6,7 Hz und einer durchschnittlich absoluten Abweichung von 15,89 Hz. Hierfür wurde ein erweiterter Dunning Basissatz verwendet [Maximoff, 2005].
Auf dem DFT-Niveau wurden bisher homo- und heteronukleare ^{3}J Kopplungen unterschätzt gegenüber den experimentellen Werten [Bouř, 1999]. Die homonuklearen $^{3}J_{HH}$ Kopplungen

von 48 substituierten Ethanen wurden mit dem B3LYP Funktional berechnet [Díez, 2005]. Mit einem Skalierungsfaktor von 0,904 ergab sich eine Standardabweichung von 0,1 Hz bezüglich der experimentellen Werte.

Neue Entwicklungen erlauben die Berechnung der chemischen Verschiebung und J-Kopplungen großer Systeme (1000 Atome) [Watson, 2004; Ochsenfeld, 2004]. Durch Korrelationen mit experimentellen Werten muss die Genauigkeit dieser Methoden evaluiert werden.

2.4 Simulationen mit Kraftfeldmethoden und Moleküldynamik

Kraftfeldmethoden gehören zu den ältesten Simulationskonzepten der theoretischen Chemie [Jensen, 1999]. Sie gehen von Atomen als Massepunkte aus, sowie von mehr oder weniger deformierten Bindungslängen, Bindungswinkeln und Diederwinkeln. Es wird angenommen, dass die tatsächliche Geometrie eine möglichst geringe Abweichung von Standardwerten aufweist. Darüberhinaus werden valenzunabhängige Wechselwirkungen (z. B. elektrostatische und van der Waals) berücksichtigt.

Im Unterschied zu den quantenmechanischen Methoden untersuchen Kraftfeldmethoden lediglich die Bewegungen der Kerne und vernachlässigen die Elektronen. Die Energie eines Punktes der Energiehyperfläche ist damit nicht der Eigenwert einer Zustandsfunktion, sondern die Summe aus verschiedenen Potentialen, die allein von den Kernpositionen und der Parametrisierung abhängt. Eine einfache Superposition der einzelnen Kräfte, abgeleitet aus den Energien, ist möglich, da sie stark voneinander entkoppelt sind. Zur Festlegung der Thermodynamik wird meist das NVT Ensemble gewählt, bei dem die Teilchenzahl N, das Volumen V und die Temperatur T des Systems konstant gehalten werden.

Je nach Substanzklasse und Zielstellung wurde eine Vielzahl von Kraftfeldern entwickelt ("Consistent Valence Force Field", CVFF [Leach, 1996, Dauber-Osguthorpe, 1988; Lifson, 1979], AMBER [Weiner, 1984], CHARMM [Brooks, 1983]. Das CVFF wurde für eine große Zahl von Verbindungen getestet (Kohlenwasserstoffe, Peptide, Nucleinsäure, Zucker etc.) und enthält anharmonische Terme und Kreuzterme, um die Wechselwirkung zwischen zwei Parametern zu simulieren. Seine Eignung für die Simulation von Zuckerderivaten wurde

durch eine Korrelation zwischen kristallographischen und simulierten geometrischen Werten gezeigt [Martín-Pastor, 1997].

Optimierung der Molekülgeometrie bedeutet, lokale und globale Energieminima (stabilste Konformation) auf der Energiehyperfläche zu suchen. Während man ein lokales Minimum durch Algorithmen gezielt suchen kann (einfaches [Wiberg, 1965] und konjugiertes Gradientenverfahren [Fletcher, 1964]), ist das Auffinden des globalen Minimums nur annähernd durch Abtasten des Konformationsraumes möglich. Neben stochastischen Methoden (Monte Carlo) ist hier vor allem die Molekulardynamik (MD) [Alder, 1957] zu nennen. MD-Simulationen basieren auf der analytischen Ableitung von Kraftvektoren, wobei die Geschwindigkeiten der Atome mit einer Modelltemperatur des Systems verbunden sind. Durch Steuerung dieser Temperatur können lokale Energiebarrieren und Sattelpunkte überwunden werden, so dass das globale Minimum erreicht werden kann. Dabei wird das Molekül im thermischen Gleichgewicht seinen Gleichgewichtszustand als Folge reversibler Geometrieänderungen einnehmen. Ein Protokoll aus definierten Temperaturschritten wird auch als simuliertes Tempern (Simulated Annealing, SA) bezeichnet [Brünger, 1993; Kirkpatrick, 1983].

Der Zustand eines Systems wird im Allgemeinen durch ein Boltzmann-Ensemble von Konformationen bestimmt (im makromolekularen Bereich oft Strukturen genannt). Im Allgemeinen weisen fast alle experimentellen Daten drei Charakteristika auf, die mehr oder weniger die Aussagekraft abgeleiteter, simulierter Strukturen schwächen [van Gunsteren, 2006]. Zum einen sind experimentelle Daten über Zeit und Raum gemittelt. Daher werden Mittelwerte über den zugänglichen Konformationsraum während eines experimentell festgelegten Zeitraums erhalten. Zum zweiten ist die Zahl der gemessenen, unabhängigen Werte oft klein gegenüber einer oft großen Zahl an Freiheitsgraden. Die Folge ist eine Unterbestimmung des Systems. So wurden für ein Heptapeptid durch Simulation vier Konformationsfamilien identifiziert, die alle mit den 21 gemessenenen ^{3}J-Kopplungskonstanten in Übereinstimmung waren [Bellanda, 2001; Bavoso 1988]. Die Simulation eines 20mer β-Peptids erbrachte unterschiedliche Konformationen, die alle mit den verfügbaren NMR-Daten in Übereinstimmung waren [Glättli, 2004]. Eine Moleküldynamik-Simulation zeigte, dass einige der untersuchten β-Schleifenmimetika eine konformative Heterogenität aufwiesen, die ihre Funktion als "Mimetikum" in Frage stellte [Müller, 2000]. Ein drittes Charakteristikum ist, dass die Genauigkeit der experimentellen Daten teilweise zu gering für die Kalibrierung und Validierung einer Simulation ist.

In der vorliegenden Arbeit erlaubte erst die Einbeziehung von RDC-Daten den Ausschluß einer Konformation von Hormaomycin in DMSO, als Zeichen für eine Unterbestimmung allein aufgrund von ^{3}J-Kopplungskonstaten und NOE-Daten (Kapitel 3.2).

2.5 Quantenmechanische DFT Rechnungen und Natural-Bond-Orbital(NBO)-Analyse

Die Eigenzustände $\Psi(\vec{r}_1,\ldots,\vec{r}_N)$ für ein System aus N Elektronen können durch die Lösung der Schrödingergleichung erhalten werden:

$$\hat{H}\Psi(\vec{r}_1,\ldots,\vec{r}_N) = E\Psi(\vec{r}_1,\ldots,\vec{r}_N) \tag{14}$$

Die Grundidee der Dichtefunktionaltheorie ist, die komplizierte N-Elektronen-Wellenfunktion $\Psi(\vec{r}_1,\ldots,\vec{r}_N)$ und die dazugehörige Schrödingergleichung durch die viel einfachere Elektronendichte ρ und ein entsprechendes Schema ihrer Berechnung zu ersetzen.

Hohenberg und Kohn zeigten bereits 1964, dass die Grundzustandselektronendichte ρ_0 eindeutig den zugehörigen Hamiltonoperator und damit das externe Potential v_{ext}, (z. B. das Coulomb Potential der Atomkerne in der Born-Oppenheimer Näherung, [Born, 1927]) sowie alle weiteren physikalischen Eigenschaften eines elektronischen Systems bestimmt [Hohenberg, 1964].

Mit der Definition eines Funktionals (die Funktion einer Funktion, Schreibweise mit [] Klammern) wird somit die Grundzustandsenergie E_0 ein Funktional der Elektronendichte ρ_0, was die Bezeichnung Dichtefunktionaltheorie erklärt.

Die elektronische Grundzustandsenergie E_0 lässt sich durch folgenden Ansatz bestimmen:

$$E_0 = \underbrace{\min}_{\rho}\left(\int dr\rho v_{ext}(\vec{r}) + F[\rho]\right) \tag{15}$$

$F[\rho]$ ist ein universelles, vom externen Potential unabhängiges Funktional. Einsetzen der Grundzustandselektronendichte ρ_0 minimiert den Ansatz und liefert damit die Grundzustandsenergie E_0. Jedoch ist die genaue Form des Funktionals $F[\rho]$ nicht bekannt. Für Approximationen an das exakte Funktional $F[\rho]$ gilt nicht mehr das Variationsprinzip. Eine mittels DFT berechnete Grundzustandsenergie ist daher nicht notwendigerweise eine obere Schranke für E_0. Der "sichere Weg zu guten Rechenergebnissen" ist somit nur für die *ab-initio* Methoden bekannt und führt über größere Basissätze zum Verfahren der vollständigen Konfigurationswechselwirkung (full configuration interaction, FCI) [Pople, 1999].

Trotz dieses methodischen Nachteils gegenüber *ab-initio* Methoden legte eine Veröffentlichung von Kohn und Sham 1965 den Grundstein für die weitere sehr erfolgreiche Entwickung der DFT Methoden [Kohn, 1965]. Es wurde vorgeschlagen, das Funktional $F[\rho]$ in mehrere Anteile aufzuspalten:

$$F[\rho] = T_s[\rho] + J[\rho] + E_{xc}[\rho] \tag{16}$$

mit

$T_s[\rho]$: kinetische Energie des nicht-wechselwirkenden Referenzsystems mit derselben Grundzustandsdichte wie das betrachtete, wechselwirkende

$J[\rho]$: klassische Coulomb-Wechselwirkung der Ladungsdichte mit sich selbst

$E_{xc}[\rho]$: Austauschkorrelationsfunktional, welches die Unterschiede zwischen der tatsächlichen kinetischen Energie und T_s sowie der vollen Elektron-Elektron Wechselwirkung J beschreibt

Das nicht-wechselwirkende System lässt sich als Slater-Determinante schreiben. So ergeben sich für die entsprechenden Spin-Orbitale $\varphi_i(x)$ (hier: Kohn-Sham-Orbitale) die folgenden Einteilchen-Gleichungen:

$$\left(-\frac{1}{2}\nabla^2 + v_{eff}\right)\varphi_i(x) = \varepsilon_i \varphi_i(x) \tag{17}$$

Der Laplace-Operator ist definiert durch: $\nabla^2 = \left(\frac{\partial^2}{\partial x^2} + \frac{\partial^2}{\partial y^2} + \frac{\partial^2}{\partial z^2}\right)$

Das effektive Potential v_{eff} wird durch die Bedingung festgelegt, dass das nicht-wechselwirkende System dieselbe Grundzustandselektronendichte haben soll wie das betrachtete, wechselwirkende:

$$v_{eff} = v_{ext} + v_j + v_{xc} \tag{18}$$

mit v_j als Elektron-Elektron Coulomb-Potential.

Das Austauschkorrelationspotential v_{xc} wird durch Ableitung von $E_{xc}[\rho]$ nach der Elektronendichte ρ erhalten:

$$v_{xc} = \frac{dE_{xc}[\rho]}{d\rho} \tag{19}$$

Die Gleichungen (17)-(19) werden als Kohn-Sham-Gleichungen bezeichnet und müssen selbstkonsistent gelöst werden. In Analogie zu HF-Methoden werden auch die Kohn-Sham-Orbitalfunktionen in den Gleichungen (17)-(19) durch Linearkombination geeigneter Basisfunktionen (LCAO-Ansatz) dargestellt. Es resultiert ein Säkulargleichungssystem, dessen Lösung unter anderem vom Austauschkorrelationspotential v_{xc} abhängt.

Unterschiedliche DFT-Methoden differieren in der Form des Austausch-korrelationsfunktionals $E_{xc}[\rho]$ (19).

In der vorliegenden Arbeit wurde das Hybrid-Funktional B3LYP verwendet [Koch, 2001]. Der Erfolg der Hybrid-Methoden resultiert aus der Kompensation der Über- und Unterbewertungen bestimmter Energieanteile durch empirische Koeffizienten. Da keine allgemeine Form des Austauschkorrelationspotentials bekannt ist, kann über die Qualität der derzeit angewandten DFT Methoden keine allgemeingültige Aussage getroffen werden.

Untersuchungen von stereoelektronischen Effekten in Alkan Isomeren sowie von intramolekularen van der Waals Wechselwirkungen bei der Photodimerisierung von

Anthracen zeigten Schwächen einer DFT Rechnung [Grimme, 2006a; 2006b]. Im ersten Fall wurden Energiedifferenzen nicht einmal qualitativ richtig bezüglich experimenteller Daten erhalten. Ursache scheint zu sein, dass derzeitige Hybridfunktionale relevante Effekte der Elektronenkorrelation bei mittleren Elektron-Elektron Abständen vernachlässigen. Im zweiten Fall entsprach zwar der berechnete Wert dem experimentellen. Da aber intermolekulare und intramolekulare van der Waals Effekte betragsmäßig zufällig gleich waren und beide unberücksichtig blieben, wurde das korrekte Ergebnis erhalten.

Aufgrund dieser Einschränkungen sollte vornehmlich eine Serie von Verbindungen bzw. eine Reihe von Eigenschaften untersucht werden. Weitere Rechnungen werden zeigen, wie relevant die oben genannten Probleme derzeitiger Hybridfunktionale sind. Relativistische Effekte wurden in der vorliegenden Arbeit nicht berücksichtigt, da diese für Elemente der ersten beiden Perioden nur eine geringe Rolle spielen [Kutzelnigg, 2004; Autschbach, 2004].

Natural-Bond-Orbital(NBO)-Analyse

Die von Weinhold entwickelte Methode der Natürlichen Bindungsorbitale (NBO) ist eine etablierte Variante der Populationsanalysen [Reed, 1988]. Ausgehend von quantenmechanischen Molekülberechnungen, werden die Elektronen auf Einzentren-NBOs (einsame Elektronenpaare) und Zweizentren NBOs (Bindungspaare) verteilt. Die Optimierung dieser Verteilung führt zur wichtigsten Lewisstruktur. In dieser konnte die maximale Zahl der Elektronen untergebracht werden. Neben den bindenden werden auch antibindende Orbitale berechnet und die Analyse ihrer Besetzungszahlen erlaubt eine stereoelektronische Interpretation. Ein Anwendungsgebiet besteht in der noch immer kontroversen Ursachenforschung bezüglich der Rotationsbarriere in Ethan [Bickelhaupt, 2003; Weinhold, 2003; Pophristic, 2001; Weinhold, 2001; Goodman, 1999; Mo, 2004]. In der vorliegenden Arbeit wurde eine NBO-Analyse des Cytidins (Kapitel 3.6) und der Rondelane (Kapitel 3.5) durchgeführt, um Zusammenhänge zwischen quantenmechanischer Beschreibung und Konformation bzw. J-Kopplungen herzustellen.

3. Ergebnisse und Diskussion

3.1 Veröffentlichungen

Hormaomycin:

U. M. Reinscheid, B. D. Zlatopolskiy, C. Griesinger, A. Zeeck, A. de Meijere, Chem Eur. J. 2005, 11, 2929
U. M. Reinscheid, J. Farjon, P. Haberz, M. Blackledge, C. Griesinger, ChemBioChem 2006, 7, 287

Glykopeptide:

S. Dziadek, H. Kunz, C. Griesinger, **U. M. Reinscheid**, Chem. Eur. J. 2006, 12, 4981

Oligomere Cyclopropane:

A. G. M. Barrett, R. A. James, G. E. Morton, P. A. Procopiou, C. Boehme, A. de Meijere, C. Griesinger, **U. M. Reinscheid**, J. Org. Chem. 2006, 71, 2756

zyklische Cyclopropane

S. G. Wehner, C. Boehme, **U. M. Reinscheid**, J. Mol. Struct. (THEOCHEM) 2006, eingereicht

Cytidin:

J. T. Fischer, **U. M. Reinscheid**, Eur. J. Org. Chem. 2006, 9, 2074

J. T. Fischer, S. G. Wehner, **U. M. Reinscheid**, J. Mol. Struct. (THEOCHEM) 2006, 767, 81

Menthol-Diastereomere

J. Härtner, **U. M. Reinscheid**, J. Mol. Struct. 2006, eingereicht

3.2 Hormaomycin

Hormaomycin ist ein aus *Streptomyces griseoflavus* W-384 isoliertes Cyclodepsipeptid mit neuartigen Aminosäurederivaten: einem substituierten Prolin (4-Propenyl-prolin) sowie diastereomeren cyclopropyl-substituierten D- und L-(3-(2-Nitrocyclopropyl)alaninen [Reinscheid, 2005; Rössner, 1990]. Die Totalsynthese von Hormaomycin **1** und einigen Derivaten (2a-2c) gelang in den letzten Jahren [Reinscheid, 2005] und bewies das aufgestellte Formelbild (Abb. 1).

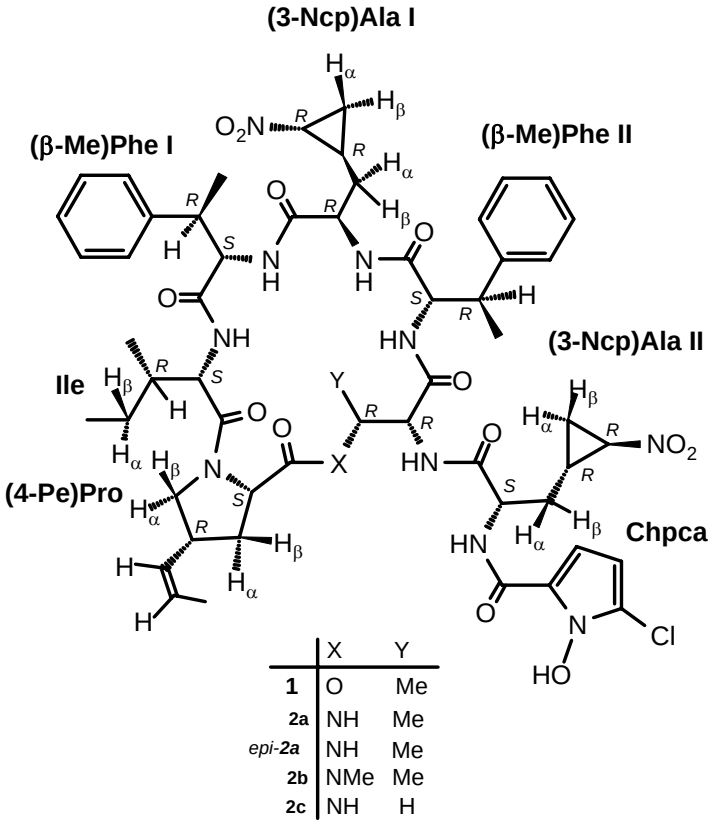

	X	Y
1	O	Me
2a	NH	Me
*epi-**2a***	NH	Me
2b	NMe	Me
2c	NH	H

Abbildung 1: Formelbild von Hormaomycin und seinen Komponenten

Hormaomycin ist spezifisch antibiotisch wirksam gegen *Arthrobacter* Arten und weist eine inhibitorische Aktivität gegen *Plasmodium* Arten auf [Otoguro, 2006]. Als Ausgangspunkt für Struktur-Wirkungsbeziehungen wurden in der vorliegenden Arbeit die Konformationen von Hormaomycin **1** in zwei unterschiedlichen Lösungsmitteln, $CDCl_3$ und DMSO, bestimmt. Die Konformationsanalyse in $CDCl_3$ zeigte, dass beide Verbindungen eine kompakte Struktur

aufweisen, mit einer parallelen Anordnung des Pyrrolidin-Rings der Komponente Chpca mit der Phenyl-Seitenkette von (β-Me)Phe II (Abb. 2). Beide Verbindungen zeigen ein ähnliches antibiotisches Spektrum.

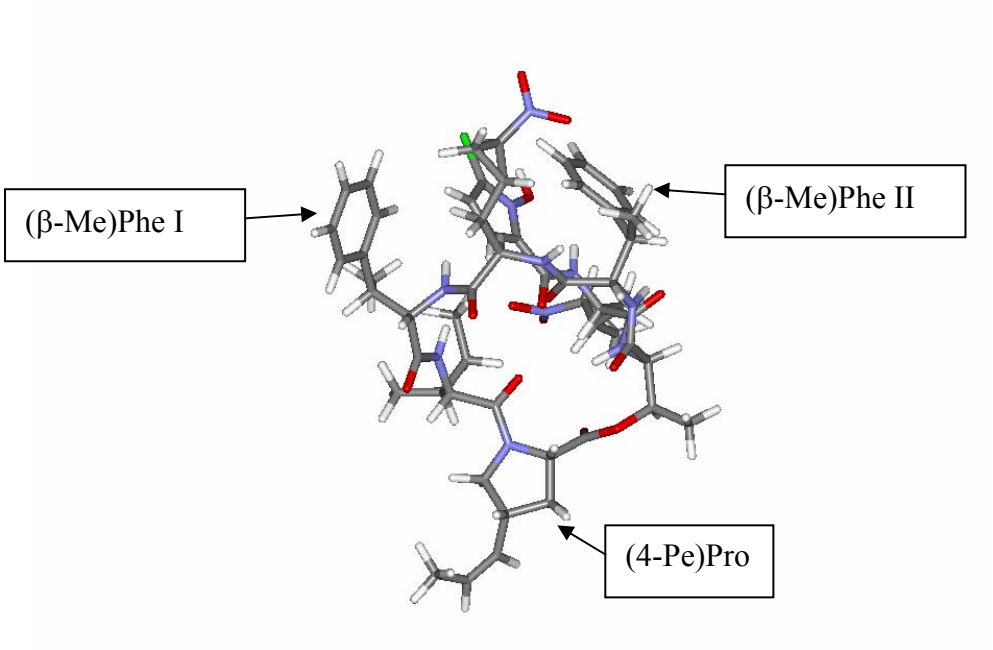

Abbildung 2: Konformation von Hormaomycin in $CDCl_3$ anhand von ^3J und ROE-Daten

Das Epimer von 2a (*epi*-2a, Abb. 1) dagegen besitzt ein verändertes ^1H NMR-Spektrum im Vergleich zu 2a, was auf eine unterschiedliche Konformation hindeutet, in Übereinstimmung mit der Abwesenheit einer antibiotischen Aktivität. Die Konformationsanalyse von Hormaomycin in einem anderen Lösungsmittel (DMSO) zeigte jedoch, dass vermutlich kein einfacher Zusammenhang zwischen ermittelter Konformation und Bioaktivität aufgestellt werden kann, da in diesem Lösungsmittel Hormaomycin allgemein eine größere Flexibilität aufwies und eine andere Konformation als in $CDCl_3$ einnahm [Reinscheid, 2006]. Ein Hinweis auf Flexibilität war die Bestimmung von zwei Konformationsfamilien, deren makrozyklischer Ring in Abb. 3 dargestellt ist, basierend auf NOE-Daten und J-Kopplungen. Unter Verwendung von RDC-Daten, erhalten aus Messungen an einer Polyacrylamid-Probe von Hormaomycin [Haberz, 2005], konnte eine Familie ausgeschlossen werden. Die so ermittelte Konformationsfamilie in DMSO (NJb) (Abb. 3) ähnelt stärker der Konformation in $CDCl_3$ als die ausgeschlossene NJa.

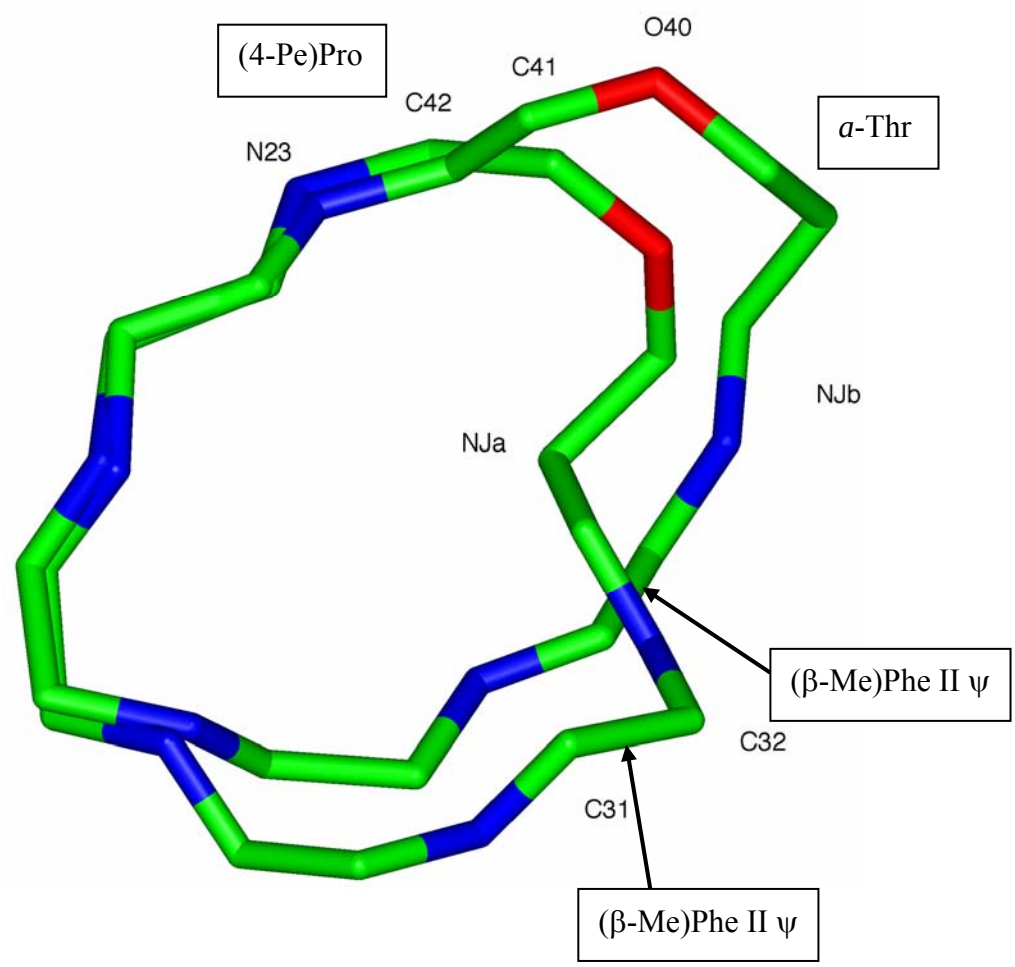

Abbildung 3: Zwei Konformationsfamilien (NJa und NJb) von Hormaomycin in DMSO anhand von ^{3}J und NOE-Daten

Die größten Unterschiede im makrozyklischen Ring zeigen die Diederwinkel des *a*-Threonins zusammen mit der Esterbindung (Tab. 1). In $CDCl_3$ ist der Diederwinkel HNCOCαCβ annähernd antiperiplanar (170°), im Gegensatz zu einer *gauche* Orientierung in DMSO (-57°). Der benachbarte Diederwinkel CαCβOCO ist *gauche* (+) in $CDCl_3$, aber *gauche* (-) in DMSO.

In beiden Lösungsmitteln $CDCl_3$ und DMSO werden *β*-Schleifen aus jeweils den gleichen Komponenten gebildet [Reinscheid, 2005; Reinscheid, 2006]. Die Orientierung der Seitenketten differiert jedoch beträchtlich und weist vermutlich auf eine erhöhte Flexibilität der Seitenkette aus (3-Ncp)Ala II und Chpca in DMSO hin (Abb. 4). Als Indizien hierfür wurden gemittelte J-Kopplungen gemessen, sowie eine verringerte Zahl von NOE-Signalen

Tabelle 1: Diederwinkel des makrozyklischen Rings der Konformation in DMSO, in $CDCl_3$ und aus einer Kristallstruktur. Die Werte in Fettdruck zeigen an, dass eine weitere Konformation mit einer Abweichung von weniger als 20° existiert.

	ϕ			ψ			ω ILE NACH (β-ME)PHE I		
	DMSO	$CDCl_3$	Kristall	DMSO	$CDCl_3$	Kristall	DMSO	$CDCl_3$	Kristall
(β-Me)Phe I	**–83**	**–90**	**–80**	**–7**	–47	**–15**	**180**	**173**	**173**
(3-Ncp)Ala I	**116**	69	**131**	**–133**	**–135**	–163	**178**	**–168**	**–179**
(β-Me)Phe II	**–98**	–67	**–103**	**126**	180	**133**	**170**	**166**	**172**
a-Thr (OCCαCβO)	–80	**43**	**54**				**–173**	**170**	**180**
a-Thr (HNCOCαCβ)				–57	170	–89			
Ester (CaCbOCO)				–68	90	158			
Ester (CβOCOCα)							143	**–173**	**168**
(4-Pe)Pro	**–66**	**–61**	**–58**				**174**	**–176**	**179**
(4-Pe)Pro (OCOCαN)				41	**143**	**152**			
Ile	**–128**	**–93**	**–110**	**160**	**152**	**167**			

langer Reichweite und eine verringerte Differenz der chemischen Verschiebungen ähnlicher Komponenten gefunden.

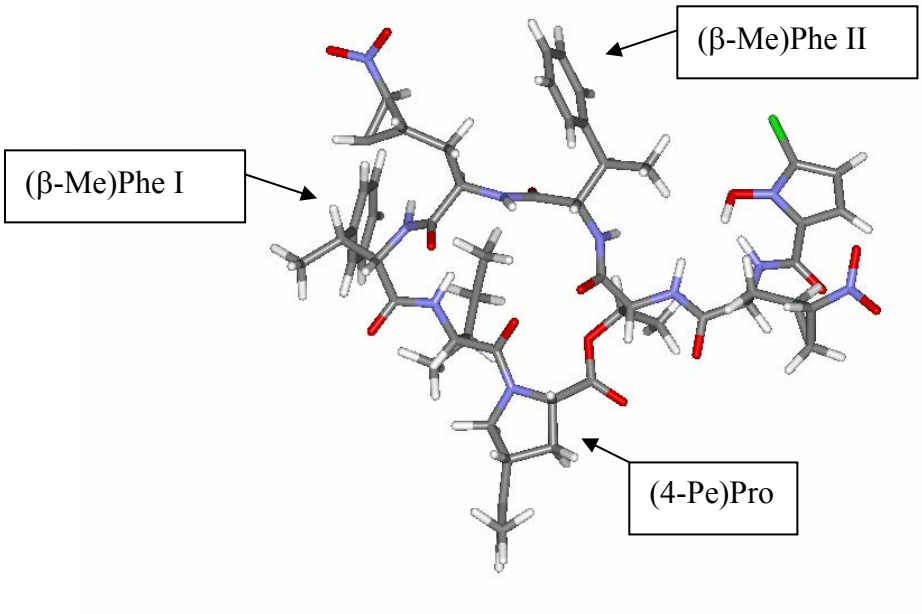

Abbildung 4: Konformation von Hormaomycin in DMSO anhand von ^3J, NOE- und RDC-Daten

D-Aminosäuren finden sich häufig in Schleifenstrukturen, da sich die Rückgrat-Diederwinkel in erlaubten Regionen entsprechend einer Ramachandran-Analyse befinden. Eine systematische Studie der Gruppe von Wishart zeigte an Gramicidin S Derivaten, dass die Heterochiralität des Rückgrats für die Mehrzahl der erzeugten Typ II` β-Schleifen verantwortlich ist [Gibbs, 2002]. Auch in den Hormaomycin Strukturen sind sie an den Positionen i+1 [3-(2-Nitrocyclopropyl)Alanin I] und i+2 [*allo*-Threonin] der beiden *β*-Schleifen zu finden. Die *β*-Schleifen entsprechen nicht genau den Standard-Typen aus Proteinen und Peptiden. Damit übereinstimmend wurden in einer Datenbank-Recherche für *D*-Aminosäuren überwiegend Schleifentypen gefunden, die keinem Standard-Typ zugeordnet werden konnten [Mitchell, 2003].

Der Vergleich zwischen Hormaomycin und dem Aza-analogen hatte bereits gezeigt, dass die Esterbindung nicht die Ursache für die abweichenden Schleifentypen ist, da für beide Verbindungen eine ähnliche makrozyklische Konformation ermittelt wurde. Im Gegensatz zu den Konformationen in Lösung, lag Hormaomycin in einer Kristallstruktur als Dimer mit anderen Komponenten als *β*-Schleifen vor (Abb. 5) [Gruene, 2006]. Die Position des Prolinderivats (4-Pe)Pro erscheint um eine Position im Uhrzeigersinn gedreht beim Übergang von den Lösungskonformationen zu der Konformation im Kristall. Zudem fand sich nur in einer Schleife eine *D*-Aminosäure (*allo*-Threonin). Welchem Lösungsmittel diese Konformation zuzuordnen ist, lässt sich wegen der Unbestimmtheit des Kristallisationsprozesses aus einem Lösungsmittelgemisch nicht sagen. Die Unterschiede zwischen der Kristallstruktur und den NMR-Lösungsstrukturen können daher auf Lösungsmitteleffekten, der Anwesenheit/Abwesenheit von Metallionen aber auch Packungseffekten beruhen.

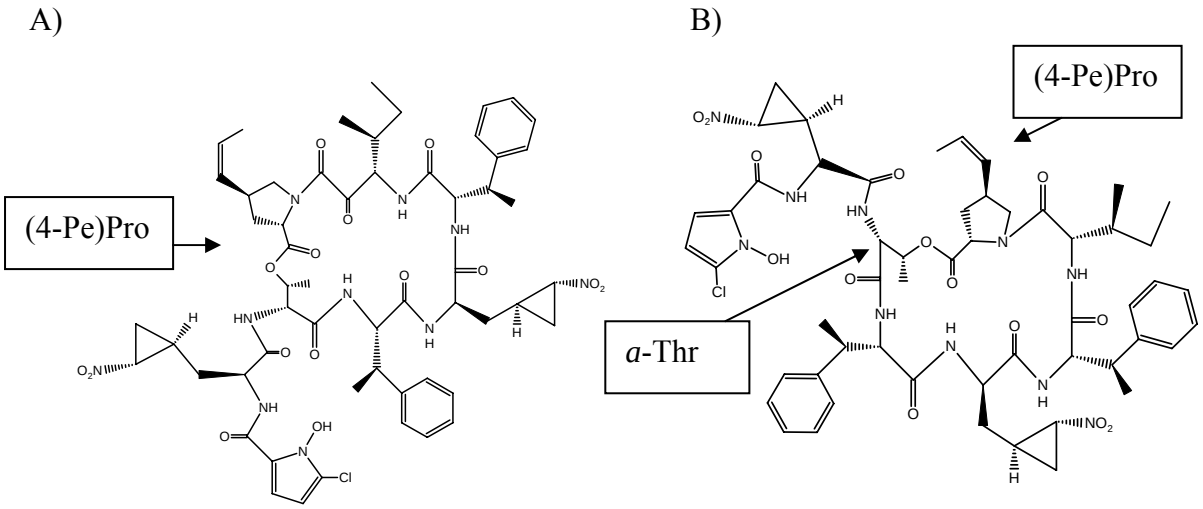

Abbildung 5: Schematischer Aufbau der β-Schleifen von Hormaomycin in $CDCl_3$ und DMSO (A) sowie in der Kristallstruktur (B)

3.2 MUC1-abgeleitetes Glykopeptid

Peptide, die biologische Funktionen von Proteien nachahmen, eignen sich als Leitstrukturen [Reineke, 1998]. So wurde mit der Phagen-Display-Technik [Smith, 1985] ein 20mer Peptid gefunden, welches die Funktion des Proteinhormons Erythropoetin (EPO, 165 Aminosäuren) nachahmt [Wrighton, 1996]. Peptide eignen sich auch als Leitstrukturen in der immunologischen Tumortherapie [Blattman, 2004]. Für eine immunologische Behandlung sollten Unterschiede zwischen den Zelloberflächen gesunder und entarteter Zellen bestehen. Für das epitheliale Mucin MUC1 konnte eine solche Tumorassoziation nachgewiesen werden [Hanisch, 2000]. Die antigene Struktur des Mucins besteht aus der extrazellulären Domäne, die aus Sequenzwiederholungen eines komplex-O-glykosylierten 20mer Peptids aufgebaut ist [Swallow, 1987]. Tumorassoziiertes MUC1 weist ein verändertes Glykosylierungmuster auf. Mit diesen Informationen war es möglich, einen synthetischen Impfstoff herzustellen, der eine spezifische, humorale Immunantwort in der Maus auslöste [Dziadek, 2005a; Dziadek, 2005b].

Eine ähnliche Strategie der Gruppe von Boons zur Synthese von immunaktiven Glykopeptiden basiert auf einer Aminosäuresequenz aus *Neisseria meningitides* [Buskas, 2005].

Im Rahmen der vorliegenden Arbeit wurde eine Konformationsanalyse eines 20mer Peptids, O-substituiert mit (2,6)-sialyl T an Threonin 11 (Abb. 6) anhand von ROE Intensitäten, ^{3}J-

Kopplungskonstanten und Temperaturabhängigkeiten der NH-Protonen durchgeführt, um einen Zusammenhang zwischen Konformation und antigener Wirkung herstellen zu können [Dziadek, 2006] (Abb. 7).

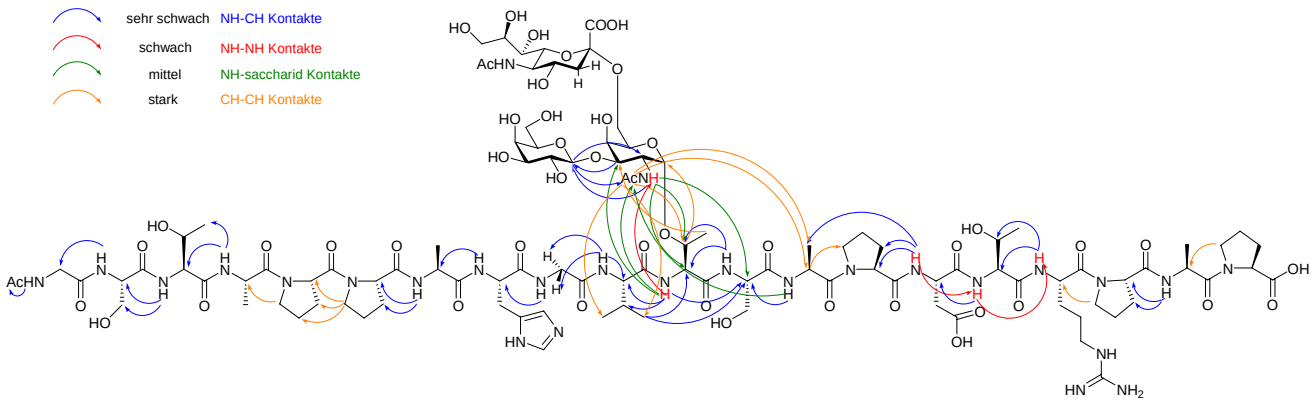

Abbildung 6: Glykopeptid abgeleitet aus MUC1 mit ROE-Kontakten

	G9	V10	T11	S12	A13	P14	D15	T16	R17	
(i, i+1)										
dNN							▬	▬		
dαN	▬	▬	▬	▬	▬	▬		▬	▬	
dβN			▬			—		▬		
(i, i+2)										
dβN					—	—				
$^3J_{N\alpha}$ (Hz)		**4.5/6.5**	**8.7**	**10.0**	**8.6**	**7.5**	**--**	**8.1**	**8.7**	**7.7**
Δδ/ΔT (ppb/K)	**5.3**	**3.5**	**-2.8**	**3.2**	**3.5**	**--**	**3.5**	**4.8**	**5.2**	

Abbildung 7: ROE Kontakte, $^3J_{N\alpha}$ und Temperaturkoeffizienten der NH-Protonen von MUC-1 abgeleitetem Glykopeptid. Die Liniendicke zeigt die ROE Intensität an. Für Prolin wird statt NH das δ Proton genommen.

Anhand der ermittelten Konformationsfamilie der 20mer Wiederholungseinheit von MUC1, substituiert mit tumor-assoziierten komplexen Zuckern, konnte der strukturierende Einfluß der Zucker auf das Peptidrückgrat nachgewiesen werden [Dziadek, 2006]. Sekundärstrukturen

wurden in Substratregionen für GalNAc Transferasen (GVTSAP) (Abb. 8) als auch in immundominanten Regionen (PDTRP) (Abb. 9) induziert. Dies korrelierte mit den *in-vivo* Ergebnissen, in denen die Anwesenheit, die Art und die Position des Zucker-Substituenten die immunologische Wirkung eines Glykopeptids veränderten [Dziadek, 2005a; Dziadek, 2005b]. Als ein zusätzlicher Hinweis auf die Bedeutung der komplexen Zuckersubstituenten kann eine Phase I Studie mit einem rein peptidischen Impfstoff aus 5 Wiederholungseinheiten gewertet werden. In dieser Studie an 16 Personen wurden nur geringe immunologische Effekte nachgewiesen [Ramanathan, 2005].

Welche Rolle die Zuckersubstituenten bei der Bindung spielen, wurde an einer Reihe von 22 monoklonalen Antikörpern von der Gruppe Karsten untersucht [Karsten, 2004]. Hierunter fanden sich 11 monoklonale Antikörper, die an nicht-glykosylierte Peptide über das Motif DTR binden. Da die Bindung in gleichem Ausmaße zunahm, wenn das Peptid mit GalNAcα1 oder Galβ1-3GalNAcα1 substituiert wurde, und in einem ELISA keine Bindung an die Glykane allein beobachtet wurde, scheinen in diesem Fall die Zucker nicht direkt an der Bindung beteiligt zu sein. Dies unterstützt die Annahme, dass für das MUC1-abgeleitete Glykopeptid der Zuckersubstituent nicht allein das Bindungsepitop darstellt, sondern die Bindung zumindest zum Teil auf den strukturierenden Effekt auf das Peptidrückgrat zurückzuführen ist.

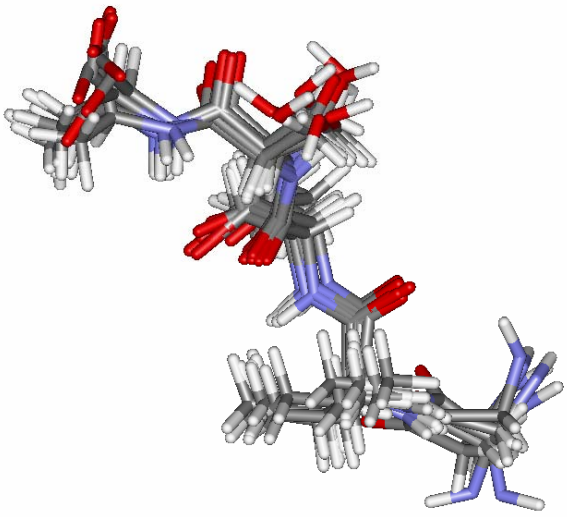

Abbildung 8: Gestreckte Konformation der GVTSA Sequenz des MUC1-abgeleiteten Glykopeptids

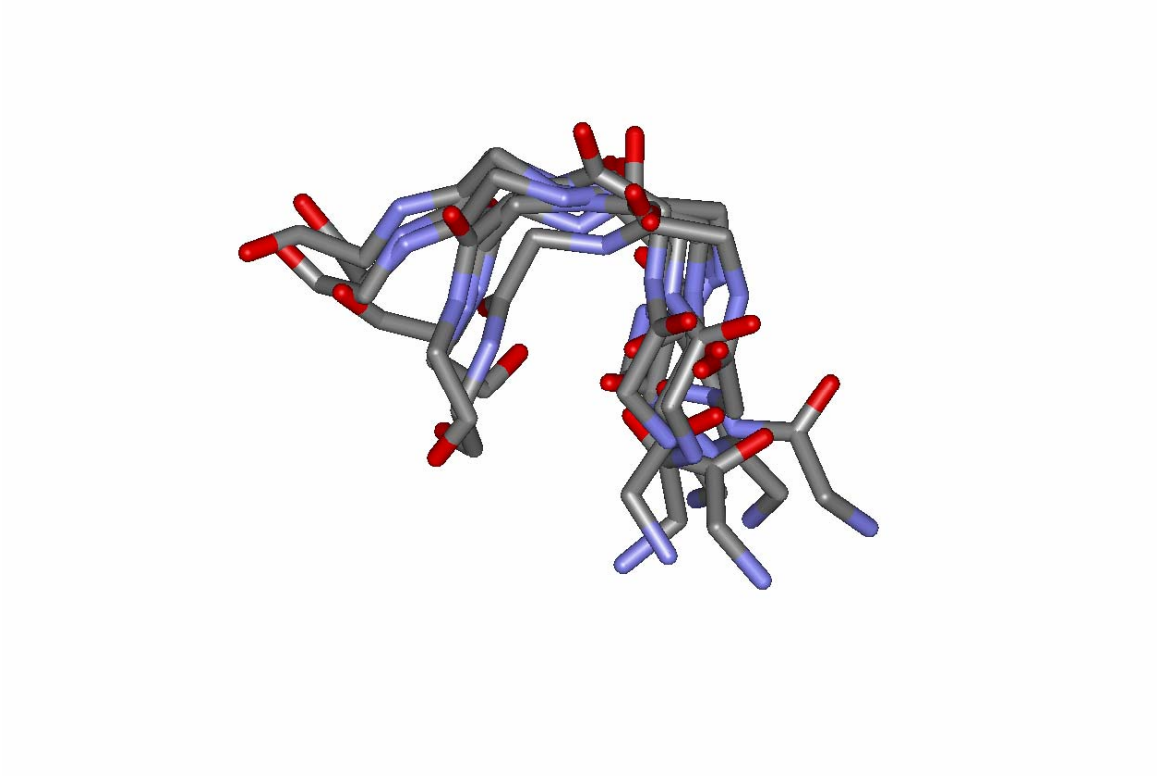

Abbildung 9: Schleifenartige Konformation der APDTR Sequenz des MUC1-abgeleiteten Glykopeptids

Trotz des geringen und lokalen Einflusses des Zuckersubstituenten auf das Peptidrückgrat, können kleine Energieänderungen kinetisch und thermodynamisch bedeutsam sein. So unterdrückte die O-Glykosylierung durch α-GalNAc an Ser-135 eines Prion-Peptids die Bildung unlöslicher Fibrillen, wogegen O-Glykosylierung an Ser-132 die Bildung verstärkte im Vergleich zum nicht-substituierten Peptid [Chen, 2002]. Die chemischen Verschiebungen der Peptide unterschieden sich nur lokal, in der Region des Substituenten.

Große Bedeutung kommt daher der Wahl der Modellverbindung und der Untersuchungsbedingungen zu. Bisherige Untersuchungen wurden meist mit unphysiologischen Parametern wie Temperaturen von + 4°C, Glykosylierungen mit einem Monosaccharid bzw. mit stark reduzierten Peptiden durchgeführt, so dass die Übertragbarkeit der ermittelten Konformationen auf die in vivo Bedingungen problematisch erscheint [Schuman, 2003; Liu, 2004; Kirnarsky, 2000]. In der vorliegenden Untersuchung dagegen wurden physiologische Bedingungen, ein komplexes Trisaccharid als Substituent und Peptide der maximalen Sequenzwiederholung gewählt, wodurch ein Zusammenhang zwischen lokaler Sekundärstruktur und Wirkung fundierter belegt werden konnte.

Entsprechend der NMR-Analyse des MUC1-Glykopeptids wurde in der Kristallstruktur des Komplexes aus dem FAB-Fragment des Antikörpers SM3, welcher gegen MUC1 gerichtet ist,

und einem 13er-MUC1-Peptid, eine gestreckte Konformation für den Peptid-Liganden gefunden [Dokurno, 1998]. Ohne Zucker-Substituent zeigte das hierbei verwendete Peptid in Lösung keine ausreichend stabile Sekundärstruktur im Gegensatz zu den Glykopeptiden der vorliegenden Arbeit. Eine Übertragbarkeit der Ergebnisse scheint aufgrund der fehlenden Glykosylierung und verringerten Peptidlänge nicht möglich.

3.4 Tercyclopropandimethanol

Theoretisch- und präparativ-arbeitende Chemiker zeigen großes Interesse für die Chemie der Cyclopropan-Verbindungen seit der ersten Synthese im 19. Jahrhundert. In der Folge stellte man das ubiquitäre Vorkommen des Dreirings im Bereich der Naturstoffe fest, mit der 1-Aminocyclopropancarbonsäure als Vorstufe des Pflanzenhormons Ethylen [Yang, 1984].
Auch das zyklische Depsipeptid Hormaomycin enthält ein bisher neuartiges Nitrocylopropyl-substituiertes Alanin [Rössner, 1990]. Ein Novum in der natürlich vorkommenden Cyclopropan-Architektur war die Isolierung von zwei bakteriellen Naturstoffen, die in einer Seitenkette oligomere Cyclopropanringe linear angeordnet enthalten [Yoshida, 1990; Kuo, 1995]. Spiroverknüpfte Cyclopropane, sogenannte [*n*]Triangulane, zeigen eine helikale Anordnung und werden als σ-Analoga der aromatischen [*n*]Helicene angesehen [de Meijere, 2004; de Meijere, 1999]. Im Kristall ihrer Dimethanol-Derivate wurden supramolekulare Spiralen beobachtet, die durch Wasserstoffbrücken zwischen den terminalen Hydroxygruppen assoziiert sind. Die Kristallstrukturen der oligomeren Cyclopropane zeigten jedoch unterschiedliche Konformationen mit unterschiedlichen Diederwinkeln zwischen den Cyclopropan-Einheiten [Barrett, 1997; Barrett, 2001; Charette, 1996]. Die Konformationsanalyse aufgrund des MD/NMR/DFT-Ansatzes von Tercyclopropandimethanol (Abb. 10) sollte nun die vorherrschende Konformation in Lösung bestimmen [Barrett, 2006a].

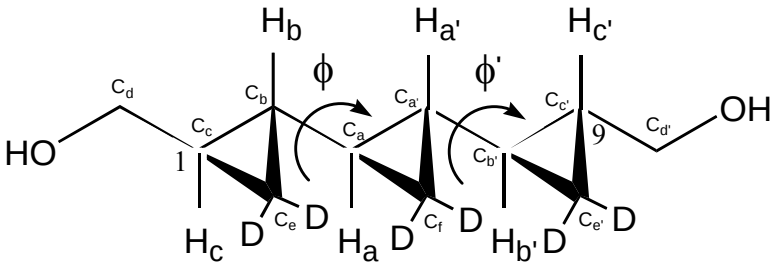

Abbildung 10: Formelbild von Tercyclopropandimethanol

Bisher war bekannt, dass das kleinste oligomere Cyclopropan, Bicyclopropyl, in Lösung vornehmlich als *gauche*-Konformer vorliegt [de Meijere, 1974]. Für die verschiedenen Konformationen durch Variation des Diederwinkels ϕ zwischen den Cyclopropaneinheiten wurden ^{3}J-Kopplungskonstanten (Abb. 11A) und die chemische Verschiebung von C_c durch DFT-Rechnungen ermittelt (Abb. 11B).

A) B)

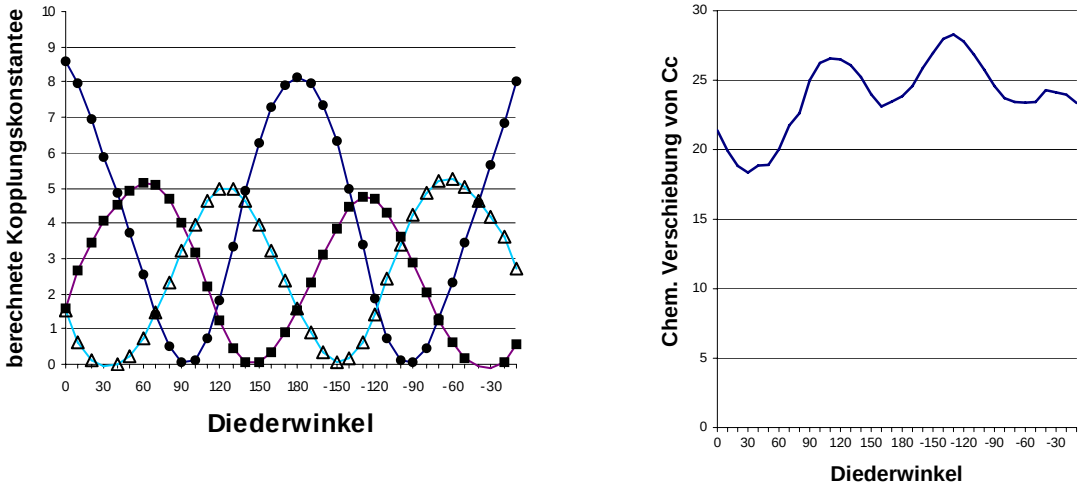

Abbildung 11: Zusammenhang zwischen den Kopplungskonstanten und der chemischen Verschiebung bei verändertem Diederwinkel ϕ zwischen den Cyclopropaneinheiten aufgrund DFT-Rechnungen A) gefüllter Kreis: $^3J_{HaHb}$ Kopplungskonstante; gefülltes Quadrat: $^3J_{HaCc}$ Kopplungskonstante; offenes Dreieck: $^3J_{HaCe}$ Kopplungskonstante. B) Chemische Verschiebung von C_c bei verändertem Diederwinkel ϕ

Die Berechnung der Varianz zwischen den experimentellen und theoretischen Daten für die verschiedenen Konformationen des Tercyclopropandimethanol erlaubte die Bestimmung der vorherrschenden Konformation [Barrett, 2006a]. Diejenige Konformation mit der geringsten Abweichung, ausgedrückt als Varianz, stellt die Lösungskonformation dar (Abb. 12).

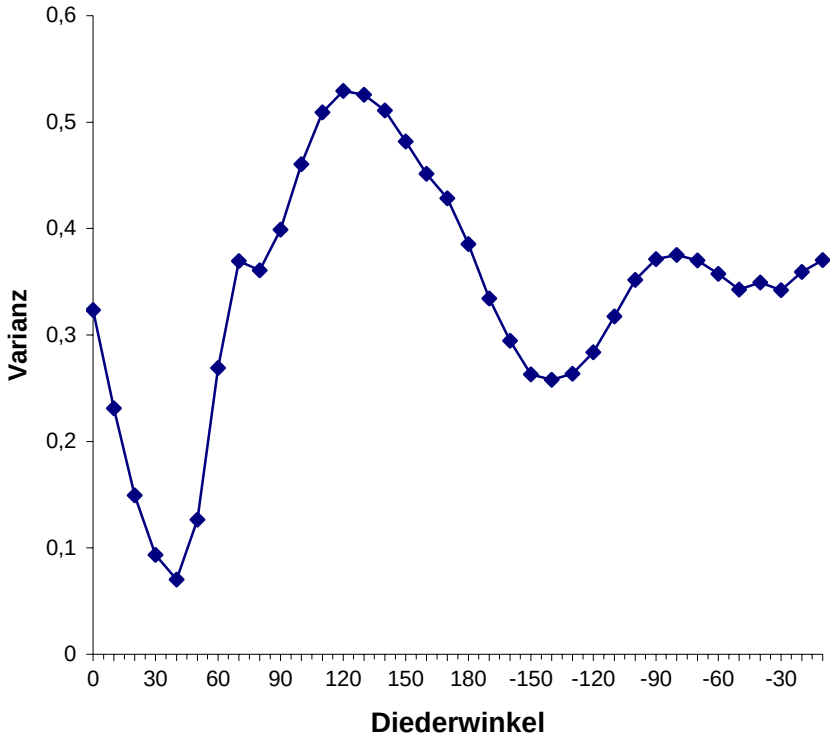

Abbildung 12: Varianz zwischen theoretischen und experimentellen Werten für verschiedene Diederwinkel zwischen zwei Cyclopropan-Einheiten (zwei ^{3}J-Kopplungen, eine ^{13}C-Verschiebung und zwei NOE-Werte).

Für Tercyclopropandimethanol ist dies der Fall bei einem Diederwinkel von + 40°, so dass eine helikale Konformation entsteht (Abb. 13).

Diese *gauche* (+) Konformation stimmt mit der Konformation in der Kristallstruktur von *syn*,*trans*-Quinquecyclopropandimethanol überein, jedoch nicht mit einem anders konfigurierten Derivat [Charette, 1996]. Dies deutet auf eine Konformationskontrolle durch die Konfiguration hin. Die abweichende Kristallstruktur von Tercyclopropandimethanol zeigt, dass z. B. Effekte der Kristallpackung die Bildung der durchgängigen Helix verhindern können und die Energieunterschiede zwischen den Konformationen gering sind.

Im Allgemeinen entstehen helikale Verbindungen durch sterische Spannung rigider Einheiten (Beispiel Helicene), stabilisierende nicht-kovalente, intramolekulare Wechselwirkungen (Beispiel α-Helix in Proteinen), oder durch supramolekulare Wechselwirkungen (Beispiel DNA). Weitere Untersuchungen sind notwendig, um die Stabilisierung der helikalen Struktur der oligomeren Cyclopropane erklären zu können. Denkbar ist die Verstärkung der lokalen *gauche*-Präferenz zwischen zwei Cyclopropan-Ringen mit zunehmender Kettenlänge, aber

auch ein Einfluss der terminalen Hydroxygruppen, wie im obigen Fall der [*n*]Triangulane beobachtet wurde.

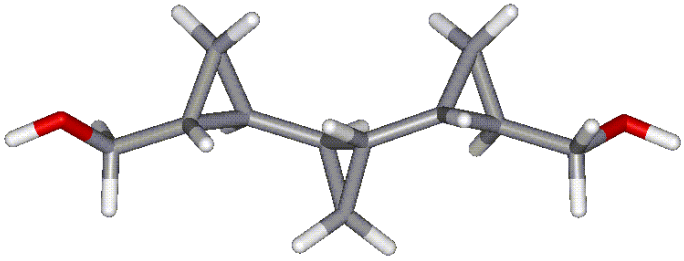

Abbildung 13: Helikale, *gauche* (+) Konformation von Tercyclopropandimethanol in Aceton[D6]

3.5 Zyklische Cyclopropane (Rondelane)

Der Ringschluß eines oligomeren Cyclopropans führt zu einer Reihe von Nano-Ringen, den [N]Rondelanen [Wehner, 2006] (Abb. 14). Aufgrund ihrer potentiell interessanten Eigenschaften als Nanomaterialien, wurden in den letzten Jahren Versuche zu ihrer Herstellung unternommen, die bisher erfolglos blieben [Barrett, 2006b].

Jedoch erlauben quantenmechanische Rechnungen die theoretische Analyse dieser Verbindungen. So wurde aufgrund des MD/NMR/DFT-Ansatzes untersucht, ob eine besonders große Ringspannung die Synthese unmöglich macht und ob die Rondelane einen aromatischen Charakter aufweisen und damit eine Stabilisierung erfahren.

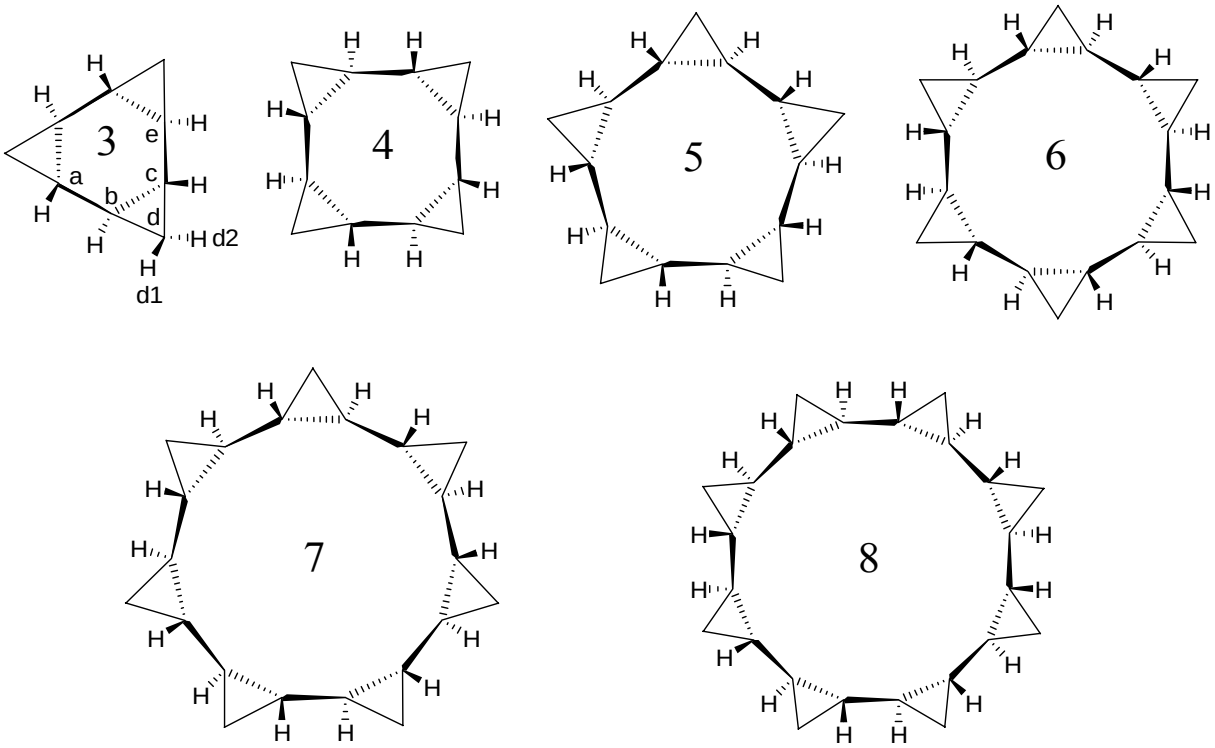

Abbildung 14: Formelbilder der Serie von [3]Rondelan bis [8]Rondelan

Durch eine MD-Rechnung wurden Startstrukturen für eine DFT-Analyse erhalten. Die Geometrie-optimierte Struktur für [3]Rondelan ist in Abb. 15 dargestellt.

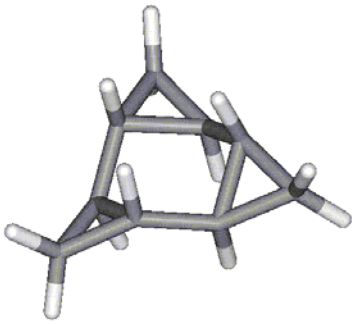

Abbildung 15: Berechnete Konformation von [3]Rondelan

Es wurden thermochemische Reaktionstypen definiert (Schema 1), anhand derer die Spannung für den Ringschluß ausgehend von einem linearen, offenkettigen Oligocyclopropan berechnet wurde (Typ I).

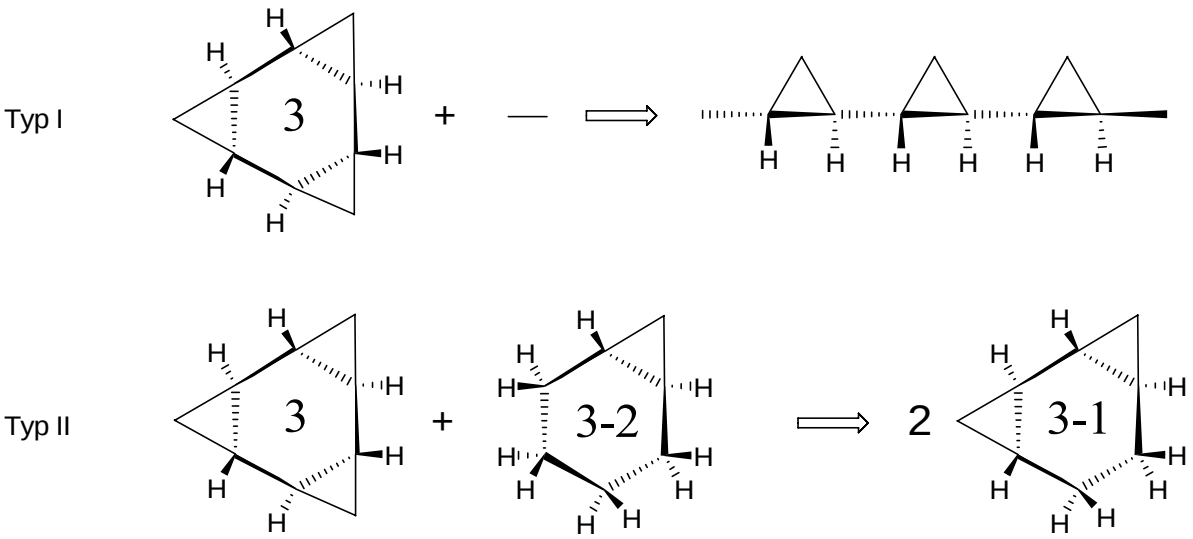

Schema 1: Thermochemische Reaktionstypen am Beispiel von [3]Rondelan

Höhere Homologe wie [8]Rondelan zeigen nur eine geringe Destabilisierung (-6,82 kcal/Mol, im Vergleich Cyclopropan: -26,13 kcal/Mol), so dass eine erfolgreiche Synthese möglich erscheint (Tab. 2).

Tabelle 2: Thermochemische Reaktionen der [N]Rondelane (in kcal/Mol)

	Typ I	Typ II
[3]Rondelan	-106,0	+2,3
[4]Rondelan	-59,2	-15,1
[5]Rondelan	-33,0	-15,3
[6]Rondelan	-18,8	-3,7
[7]Rondelan	-11,1	+2,2
[8]Rondelan	-6,8	+1,0

Für [3]Rondelan ist die destabilisierende Energie so groß (Typ I: -106,0 kcal/Mol), dass diese Verbindung vermutlich unter Laborbedingungen nicht stabil ist.
Die positiven Energiewerte des Reaktionstyps II korrespondieren mit einer Stabilisierung aufgrund einer Elektronendelokalisation. Diese ist nur für [3]Rondelan (+2,3 kcal/Mol), [7]Rondelan (+2,2 kcal/Mol) und [8]Rondelan (+1,0 kcal/Mol) vorhanden. Neben diesem energetischen Aromatizitätskriterium wurden auch die geometrischen (Bindungslängen, auch im Rahmen einer NBO-Analyse) und magnetischen Eigenschaften [Chen, 2005; Schleyer, 1996] (kernunabhängige chemische Verschiebung, "Nucleus Independent Chemical Shift", NICS) untersucht. Als aromatisch werden im klassischen Sinne planare, zyklische Elektronensysteme mit [4n+2] π-Elektronen bezeichnet, als antiaromatisch mit [4n] π-Elektronen. Cyclopropan wird durch σ-Aromatizität stabilisiert [Cremer, 1986]. Hinweise hierfür sind die hochfeld-verschobenen ^{1}H Verschiebungen und die negativen NICS-Werte oberhalb des Rings [Moran, 2003; Exner, 2001]. Nur für [3]Rondelan wurden NICS-Werte und Bindungslängen berechnet, die auf einen schwach aromatischen Charakter hinweisen. Für die höheren Homologen wurden keine geometrischen und magnetischen Eigenschaften gefunden, die auf Aromatizität hinweisen. Für den kleinsten Vertreter der Rondelane ist trotz geringer Stabilisierung durch Elektronendelokalisation, die Destabilisierung durch Spannung vermutlich zu groß für eine Herstellung dieser Verbindung.

3.6 Cytidin

Am Beispiel des Nukleosids Cytidin wurde der Zusammenhang zwischen Konformation, stereoelektronischen Effekten, sowie chemischen Verschiebungen und J-Kopplungen analysiert [Fischer, 2006a; Fischer, 2006b]. Korrelationen können zur Parametrisierung von Karplus-Beziehungen genutzt werden und die Strukturaufklärung von Oligonukleotiden verbessern. Eine Herausforderung ist hierbei die inhärente Flexibilität der Ribose, des glykosidischen Diederwinkels und der Base. Im Allgemeinen werden in Nukleinsäuren *anti* (240° bzw. -120°) und *syn* (60°) Konformationen für den glykosidischen Diederwinkel χ gefunden [Wijmenga, 1998] (Abb. 16).
Bisherige computerchemische Untersuchungen wurden vielfach an verkleinerten Modellverbindungen durchgeführt, so dass Zusammenhänge für die natürlich vorkommenden Nukleoside nur abgeleitet werden konnten [Ghose, 1994; Dejaegere, 1998]. In der

vorliegenden Arbeit wurde das vollständige Modell von Cytidin in zwei Schritten untersucht: zunächst wurden durch Moleküldynamik Rechnungen stabile Konformere ermittelt, die dann als Startpunkte für Berechnungen der Geometrie und von NMR-Parametern auf DFT-Niveau dienten.

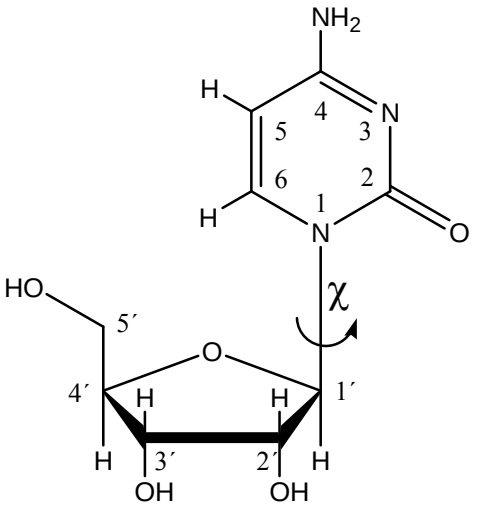

Abbildung 16: Formelbild von Cytidin mit dem glykosidischen Diederwinkel χ

Die Ribose nimmt in den Pyrimidinbasen vornehmlich eine Nord-Konformation (N für Nord: C3′ ausserhalb der Ringebene; S für Süd: C2′ ausserhalb der Ringebene) [Altona, 1973]. Der MD/NMR/DFT-Ansatz lieferte für Cytidin die stabile Konformation in Abb. 17 mit der Nord-Konformation der Ribose und einer *anti*-Orientierung der Base. Im Rahmen einer Strukturevaluierung korrelierten die berechneten ^{13}C-Verschiebungen für diese Konformation mit experimentellen Daten [Fischer, 2006a; Ebrahimi, 2001].

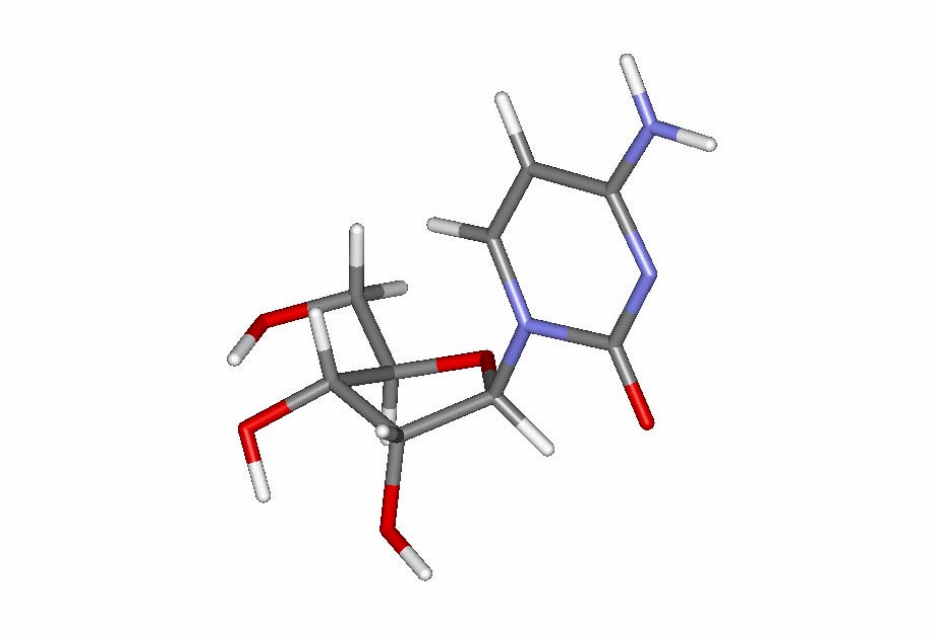

Abbildung 17: Berechnete Konformation von Cytidin mit der Nord-Konformation der Ribose und einer *anti*-Orientierung der Base

Für Modellverbindungen wurde bereits ein Zusammenhang zwischen der Ribofuranose-Konformation und der Substitution an C1 nachgewiesen [Cloran, 2000]. Cytidin zeigte im Rahmen des MD/NMR/DFT-Ansatzes darüber hinaus einen Zusammenhang zwischen dem glykosidischen Diederwinkel und den ^{13}C chemischen Verschiebungen sowie den $^{1}J_{C1'H1'}$, $^{1}J_{C2'H2'}$, $^{1}J_{C3'H3'}$, und $^{1}J_{C4'H4'}$ Kopplungskonstanten (Tab. 3) [Fischer, 2006a; Fischer, 2006b], der in früheren Untersuchungen nicht beobachtet wurde [Ebrahimi, 2001; Bandyopadhyay, 1997]. Die Abweichungen zwischen berechneten und experimentellen Werten sind geringer für $^{1}J_{CH}$ Kopplungen der Ribose im Vergleich zur Base (Tab. 3). Die $^{1}J_{C3'H3'}$ Kopplung reagiert am empfindlichsten auf eine Rotation der Base, so dass eine Differenz von ca. 15 Hz zwischen der *anti* und *syn* Konformation besteht, die für die Analyse von Spektren von Oligonukleotiden genutzt werden kann. Nimmt man die fast gleichen experimentellen $^{1}J_{C2'H2'}$ und $^{1}J_{C3'H3'}$ Kopplungen für Cytidin, korreliert dieses Paar am besten mit den berechneten Werten für die *anti* Konformation.

Tabelle 3: Berechnete Ribose $^{1}J_{CH}$ Kopplungskonstanten von Cytidin in der Nord-(N) bzw. Süd(S)-Konformation mit festgelegtem glykosidischen Diederwinkel χ (experimentelle Werte in DMSO als Lösungsmittel)

ϕ/ Atompaar	N60°	N110°	N180°	N–145°	N–120°	N–60°	S–120°	experimentell
C5-H5	143,3	143,4	143,4	143,4	143,2	143,5	146,5	172,4
C6-H6	150,0	153,3	155,3	153,4	150,2	146,7	153,9	180,1
C1´-H1´	164,2	170,3	178,3	175,1	169,5	175,7	169,2	169,0
C2´-H2´	157,3	170,1	159,2	155,2	152,1	154,8	158,1	147,5
C3´-H3´	167,1	163,6	155,5	154,4	152,3	154,3	162,8	146,5
C4´-H4´	150,5	151,7	159,8	159,7	159,1	153,6	155,3	142,4

Eine NBO-Analyse von Cytidin lieferte die Wechselwirkungsenergien aufgrund der Elektronendelokalisation von besetzten in unbesetzte Anti-Bindungen. Danach wurden die Energien für alle an der Kopplung zwischen C6 und H1´ beteiligten Bindungsorbitale für den Elektronentransfer $\sigma_{\text{(Bindungspfad der Kopplung)}} \rightarrow \sigma^*$ (B in Abb. 18) und für den Elektronentransfer $\sigma \rightarrow \sigma^*_{\text{(Bindungspfad der Kopplung)}}$ summiert. Die Differenz dieser Summen (B-A) zeigt für einen posititven Wert eine verstärkte Delokalisierung der beteiligten Bindungselektronen in Antibindungen an. Es wurde eine Korrelation zwischen der Differenz (B-A) und der entsprechenden ^{3}J-Kopplung zwischen C6 und H1´ (und damit auch dem glykosidischen Diederwinkel) nachgewiesen (Abb. 18). Dabei ergab sich, dass mit zunehmend positiver Differenz der Wechselwirkungsenergien, die $^{3}J_{C6H1´}$ Kopplungskonstante zunimmt und somit hyperkonjugative Effekte die Kopplung vornehmlich bestimmen. Bei einem glykosidischen Diederwinkel von -120° tritt die größte Elektronendelokalisation entlang des Bindungspfades von C6 nach H1´auf.

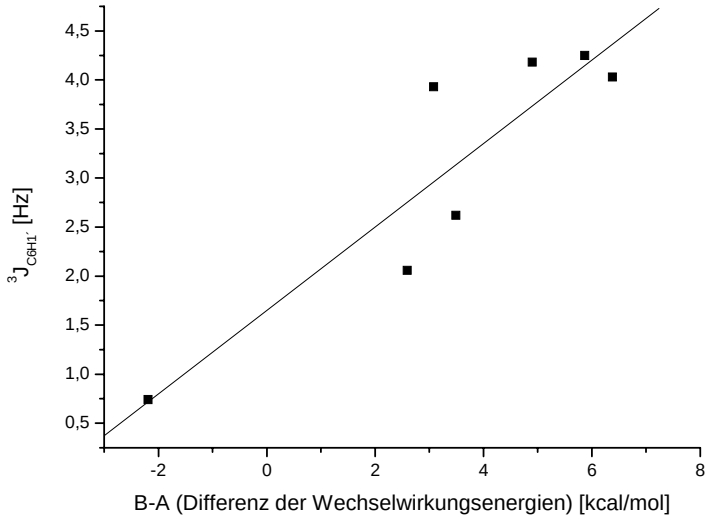

Abbildung 18: Korrelation zwischen $^3J_{C6H1'}$ und der Differenz der Wechselwirkungsenergien

Ein weiteres Ergebnis der computerchemischen Analyse betrifft die Flexibilität der Nukleinsäuren, die für die Verringerung von H-H Abstoßungen der Basenpaare wichtig ist. Sie beruht u.a. auf der Pyramidalisierung des Basen-Stickstoffs und ist schwierig zu messen, da die Energiedifferenzen nur sehr gering sind. Berechnungen zeigten eine pyramidale Geometrie abhängig vom glykosidischen Diederwinkel und einer Abweichung von ca. 8° von der Planarität für die *anti*-Konformation der Base (Tab. 4 und Abb. 19) [Fischer, 2006a]. Somit erleichtert die Pyramidalisierung des Basen-Stickstoffs Basenpaarungen durch eine erhöhte Flexibilität der Base.

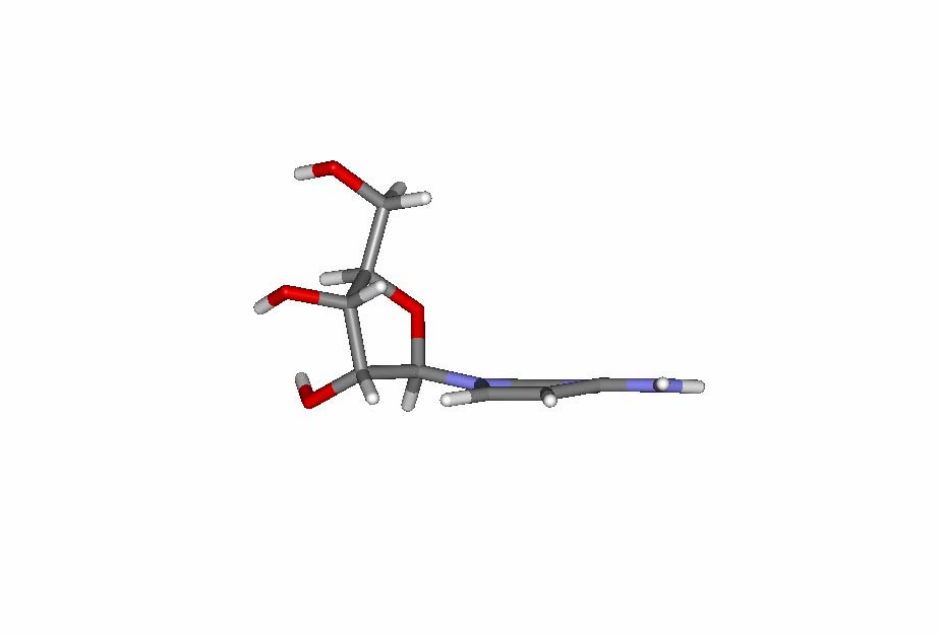

Abbildung 19: Pyramidalisierung des Basen-Stickstoffs in Cytidin mit der Ribose in der Nord-Konformation

Tabelle 4: Berechnete Diederwinkel von Cytidin in der Nord-(N) bzw. Süd(S)-Konformation in Bezug zur Basenplanarität bei festgelegtem glykosidischen Diederwinkel χ

ϕ/ Diederwinkel	N60°	N110°	N180°	N–145°	N–120°	N–60°	S–120°
C6-N1-C2-N3	1,3°	-6,9°	1,4°	5,9°	8,8°	1,8°	6,5°
C2-N1-C6-C5	1,3°	4,5°	-1,0°	-6,7°	-8,7°	-3,5°	-5,8°
N1-C2-N3-C4	-2,5°	4,8°	-0,9°	-1,7°	-3,7°	0,2°	-3,0°
C2-N3-C4-C5	1,1°	-0,3°	0,1°	-1,8°	-1,5°	-0,5°	-1,1°
N3-C4-C5-C6	1,6°	-2,4°	0,3°	1,2°	1,9°	-1,1°	2,1°
C4-C5-C6-N1	-2,7°	0,1°	0,2°	3,0°	3,3°	3,1°	1,5°
Summe der positiven Diederwinkel	5,3°	9,4°	2,0°	10,1°	14,0°	5,1°	10,1°
C1´-N1-C6-C5	172,6°	-179,6°	-179,1°	-174,0°	-171,8°	-166,9°	-177,6°
C1´-N1-C2-N3	-169,8°	177,6°	179,6°	174,1°	172,7°	166,8°	178,6°

Als letzter Punkt soll die experimentell schwierige Konformationsanalyse der OH-Gruppen der Ribose erwähnt werden. Bisher wurde angenommen, dass in RNA die 2`-OH-Gruppe in die Richtung des Rückgrats orientiert ist [Acharya, 2002]. Jedoch zeigten MD-Simulationen und NMR-Messungen, dass auch eine Ausrichtung des Protons zur Base vorliegen kann [Hennig, 2005; Auffinger, 1997]. Die hierfür wichtige Kalibrierung einer Karplus-Beziehung wurde quantenmechanisch durchgeführt [Fohrer, 2006].

3.7 Menthol und seine Diastereomere

Die Korrektur von Literaturdaten als Teil einer Strukturevaluierung ist mit einem MD/NMR/DFT-Ansatz möglich. Bei der Fermentation des Pilzes *Phomopsis amygdali* wurde (+)-Menthol als Metabolit identifiziert [Sassa, 2003] (Abb. 20A).

In der vorliegenden Arbeit ergab der Vergleich mit Literaturdaten [Senda, 1975] und die quantenmechanische Rechnung, dass die veröffentlichten ^{13}C Werte weder Menthol noch einem der Diastereomere zugeordnet werden konnten [Härtner, 2006] und somit ein Fehler vorliegen muss.

A

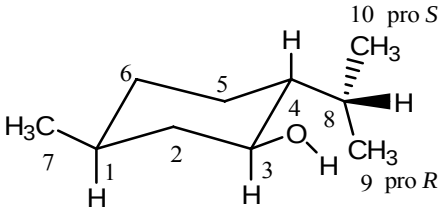

B

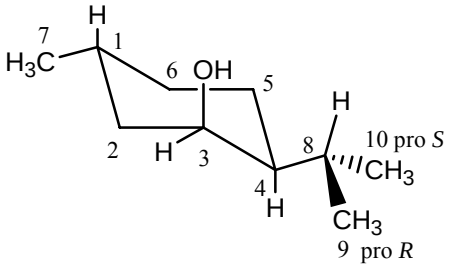

C

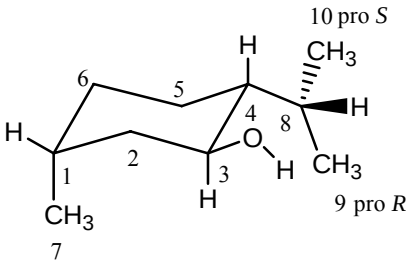

D

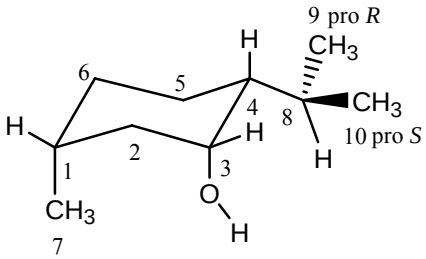

E

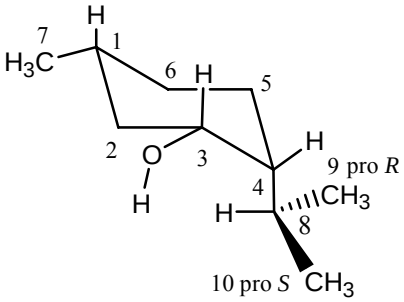

Abbildung 20 A-E: Formelbilder der vorherrschenden Konformere von A: (+) Menthol ($1_{eq}3_{eq}4_{eq}$) und den zugehörigen Diastereomeren B: Neomenthol ($1_{eq}3_{ax}4_{eq}$), C: Isomenthol ($1_{ax}3_{eq}4_{eq}$), D: Neoisomenthol ($1_{ax}3_{ax}4_{eq}$) und Neoisomenthol ($1_{eq}3_{eq}4_{ax}$)

Weiterhin ergab im Falle des Menthols ein Diederwinkel des Isopropyl-Substituenten von 60° die beste Übereinstimmung zwischen experimentellen (NMR-Messung in Lösung) und theoretischen ^{13}C-Verschiebungen (Abb. 20A und Abb. 21A-C, Tab. 5). Das Vertauschen der beiden prochiralen Methylgruppen des Isopropyl-Substituenten erlaubte zudem die Bestimmung der Prochiralität. Das Ergebnis für Menthol stimmte mit einer Kristallstrukturanalyse überein, die wegen einer schnellen Sublimation und entsprechender Schwierigkeit, geeignete Kristalle zu erhalten, erst 1999 gelang. [Bombicz, 1999]. Die Kristallstruktur zeigte alle Substituenten in äquatorialen Positionen eines Cyclohexan Sessels.

A) Diederwinkel = 60°

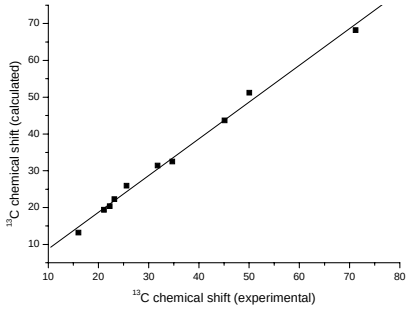

B) Diederwinkel = 180°

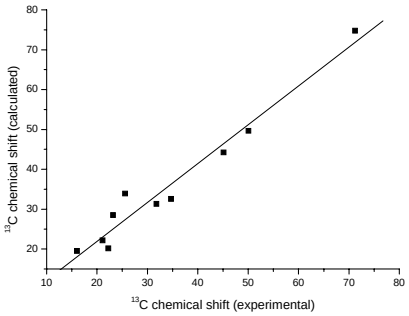

C) Diederwinkel = 300°

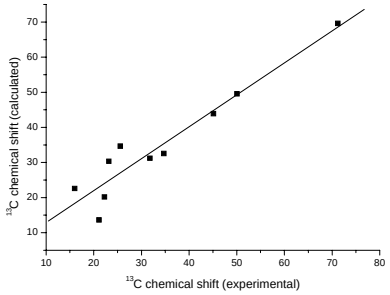

Abbildung 21 A-C: Korrelation zwischen experimentellen und theoretischen ^{13}C-Verschiebungen für Menthol-Konformere mit unterschiedlichem Diederwinkel der Isopropyl-Gruppe (H8-C8-C4-H4)

Entsprechend wurde für das Menthol-Diastereomer Neomenthol die Konformation der Isopropyl-Gruppe auf Grundlage des höchsten Korrelationskoeffizienten bestimmt (Tab. 5), in Übereinstimmung mit $^{3}J_{H4H8}$ Kopplungskonstanten. Im Fall von Isomenthol wurden nur schwache Korrelationen zwischen berechneten und experimentellen ^{13}C Verschiebungen gefunden (Tab. 5). Eine Berechnung der Energiedifferenzen favorisierte das 60° Rotamer der

Abbildung 20C. Darüberhinaus wurde in MD-Simulationen zusätzlich ein Sessel mit einer axialen Isopropyl-Gruppe gefunden. Energieberechnungen wiesen auf die Dominanz des 60° Rotamers mit einer äquatorialen Isopropyl-Gruppe hin ($1_{ax}3_{eq}4_{eq}$: 60°/180°/300°: 0 / +1,78 / +0,67 kcal/Mol; $1_{eq}3_{ax}4_{ax}$: 180°: +1,47 kcal/Mol). Auch mit einer Gewichtung der beiden hauptsächlich populierten Konformere, ergab die Korrelation zwischen den berechneten und experimentellen ^{13}C Verschiebungen nur einen geringen Korrelationskoeffizient von 0,9786. Der einfache Ansatz, basierend allein auf der Verwendung von ^{13}C Verschiebungen, ist daher nicht in der Lage, das Isopropyl Rotamer in Isomenthol zu bestimmen. Entsprechend zeigte der Messwert der $^3J_{H4H8}$ Kopplung von 5,5 Hz eine Mittelung an, die in den Rechnungen nicht ausreichend abgebildet wurde.

Tabelle 5: Korrelationskoeffizienten und Standardabweichung (in Klammern) der Korrelationen zwischen experimentellen und theoretischen ^{13}C-Verschiebungen von Menthol und seinen Diastereomeren in Abhängigkeit vom Diederwinkel der Isopropyl-Gruppe (H8-C8C4-H4) (das vorherrschende Konformer ist in Fettdruck)

Isomer/Diederwinkel	60°	180°	300°
Menthol (Abb. 20A)	**0,9969 (1,42)**	0,9788 (3,67)	0,9524 (5,24)
Neomenthol (Abb. 20B)	0,9817 (3,33)	**0,9943 (1,85)**	0,9814 (3,81)
Isomenthol (Abb. 20C)	0,9752 (4,32)	0,9824 (3,68)	0,9777 (3,66)
Neoisomenthol (Abb. 20D)	0,9825 (3,47)	0,9935 (1,86)	0,9833 (3,01)

Bisherige NMR-Analysen ergaben für Neoisomenthol eine Dominanz der Sessel Konformation mit einer axialen Isopropyl-Gruppe von 91% [Senda, 1975]. Hiervon abweichend wurde eine höhere Energie des axialen (Abb. 20E) gegenüber dem äquatorialen Konformer (Abb. 20D) und eine schlechtere Korrelation zwischen berechneten und experimentellen ^{13}C Verschiebungen für das axiale Konformer (Korrelationskoeffizient 0,9811 und Standardabweichung 3,17) berechnet. Die berechnete ^3J Kopplung für das axiale Konformer betrug 10,1 Hz ($^3J_{H2axH3ax}$), sowie für das äquatoriale Konformer 2,7 Hz ($^3J_{H2axH3eq}$). Die Messung einer gemittelten ^3J Kopplungskonstanten zwischen H3 und H2 von 6,3 Hz zeigte, dass eine ausgeglichene Mischung der beiden Sessel in Lösung vorliegt. Diese Diskrepanz zu den obigen Korrelationen liegt an der unzureichenden Modellierung der experimentellen Bedingungen (Rechnungen in vacuo), wie die Temperaturabhängigkeit der chemischen Verschiebungen bzw. Konformationen aufgrund einer Wasserstoffbrückenbindung für 3-substituierte Cyclohexanole zeigt [de Oliveira, 2006].

4. Zusammenfassung

Die Konformationsanalysen des komplexen Naturstoffs Hormaomycin und eines von MUC1-abgeleiteten Glykopeptids wurden entsprechend dem MD/NMR-Ansatz durchgeführt.

Hormaomycin zeigte in verschiedenen Lösungsmitteln eine veränderte Konformation. Somit konnte von einer Lösungskonformation nicht direkt auf die bioaktive Konformation geschlossen werden. Hormaomycin lag im Lösungsmittel $CDCl_3$ in einer kompakten Konformation vor, wogegen in DMSO die Seitenketten eine größere Flexibilität aufwiesen. Der makrozyklische Ring war in beiden Lösungsmitteln mit β-Schleifen aus den gleichen Komponenten aufgebaut. Nur der Einsatz von RDC-Daten ermöglichte eine Konformationsanalyse in DMSO.

Für das MUC1-abgeleitete **Glykopeptid** konnte ein für die Wirkung relevanter strukturierender Einfluss des Zuckersubstituenten nachgewiesen werden. So wurde eine gestreckte Konformation für die Erkennungsregion von Transferasen und eine schleifenartige Konformation für die immundominante Peptidregion ermittelt.

Weitere Verbindungen wurden mittels des MD/NMR/DFT-Ansatzes untersucht.
Tercyclopropandimethanol zeigte eine helikale Lösungskonformation in Aceton. Die alleinige Verwendung der experimentellen ^{3}J-Kopplungen und NOE-Daten erlaubte keine eindeutige Bestimmung der Konformation. Erst die quantenmechanische Berechnung der ^{3}J-Kopplungen und ^{13}C-Verschiebungen führte zum Nachweis einer helikalen Konformation.
Nur die kleinen, zyklischen Cyclopropane (**Rondelane**) werden durch hohe Ringspannungen destabilisiert, so dass eine Synthese der höheren Homologen gelingen könnte. Der kleinste Vertreter dieser Serie von bisher nicht synthetisierten Verbindungen wies schwach aromatische Eigenschaften auf.
Für **Cytidin** korrelierten berechnete ^{13}C Verschiebungen mit einer Nord-Konformation der Ribose. Durch eine NBO-Analyse wurde ein Zusammenhang zwischen der $^3J_{C6H1'}$ Kopplung und hyperkonjugativen Effekten ermittelt. DFT Rechnungen zeigten die Pyramidalisierung des Basenstickstoffs und wiesen damit auf eine weitere Flexibilität der Nukleoside hin.
Die Berechnung der ^{13}C-Verschiebungen von **Menthol** erlaubte eine schnelle und effektive Konformationsanalyse und Strukturevaluierung. Das vorherrschende Menthol Konformer in Lösung ist ein Sessel mit der Isopropylgruppe in äquatorialer Position und einem 60° Rotamer

dieses Substituenten. Anhand von Korrelationen konnte für Neomenthol das dominierende 180° Rotamer bestimmt werden.

Die Kombination aus experimentellen NMR-Parametern und theoretischen Daten aufgrund computerchemischer Methoden konnte somit erfolgreich in der Strukturevaluierung einer Reihe von komplexen Naturstoffen unterschiedlicher chemischer Natur eingesetzt werden. In der Konformationsanalyse wurde ein Zusammenhang zwischen quantenmechanischer Beschreibung und geometrischer Struktur hergestellt. Auf diese Weise wurde die Grundlage zur Vorhersage experimenteller Parameter gelegt und dieses prädiktive Potential für bisher nicht-existente Verbindungen wie die Rondelane genutzt.

5. Zitierte Literatur

P. Acharya, A. Trifonova, C. Thibaudeau, A. Földesi. J. Chattopadhyaya, Angew. Chem. 1999, 111, 3861; Angew. Chem. Int. Ed. 1999, 38, 3645

P. Acharya, J. Chattopadhyaya, J. Org. Chem. 2002, 67, 1852

B. J. Alder, T. Wainwright, J. Chem. Phys. 1957, 27, 1208

D. R. P. Almeida, D. M. Gasparro, T. A. Martinek, F. Fülöp, Im G. Csizmadia, J. Phys. Chem. A 2004, 108, 7719

C. Altona, M. Sundaralingam, J. Am. Chem. Soc. 1973, 95, 2333

I. Ando, G. A. Webb, Theory of NMR Parameters, Academic Press, London, 1983

P. W. Atkins, Physical Chemistry, Oxford University Press, 1994

P. Auffinger, E. Westhof, J. Mol. Biol. 1997, 274, 54

J. Autschbach, in: Calculation of NMR and EPR parameters (Eds. M Kaupp, M. Bühl, V. G. Malkin), Wiley-VCH, 2004

R. F. Bader, Atoms in Molecules. A Quantum Theory, Oxford Press, 1990

A. Bagno, Chem. Eur. J. 2001, 7, 1652

A. Bagno, F. Rastrelli, G. Saielli, J. Phys. Chem. A 2003, 107, 9964

A. Bagno, F. Rastrelli, G. Saielli, Chem. Eur. J. 2006, 12, 5514

T. Bandyopadhyay, J. Wu, W. A. Stripe, I. Carmichael, A. S. Serianni, J. Am. Chem. Soc. 1997, 119, 1737

G. Barone, L. Gomez-Paloma, D. Duca, A. Silvestri, R. Riccio, G. Bifulco, Chem. Eur. J. 2002a, 8, 3233

G. Barone, D. Duca, A. Silvestri, L. Gomez-Paloma, R. Riccio, G. Bifulco, Chem. Eur. J. 2002b, 8, 3240

C. Bassarello, P. Cimino, L. Gomez-Paloma, R. Riccio, G. Bifulco, Tetrahedron 2003, 59, 9555

A. G. M. Barrett, D. Hamprecht, A. J. P. White, D. J. Williams, J. Am. Chem. Soc. 1997, 119, 8608

A. G. M. Barrett, D. Hamprecht, R. A. James, M. Ohkubo, P. A. Procopiou, M. A. Toledo, A., A. J. P. White, D. J. Williams, J. Org. Chem. 2001, 66, 2187

A. G. M. Barrett, R. A. James, G. E. Morton, P. A. Procopiou, C. Boehme, A. de Meijere, C. Griesinger, U. M. Reinscheid, J. Org. Chem. 2006a, 71, 2756

A. G. M. Barrett, pers. Mitteilung, Imperial College, London, 2006b

A. Bavoso, E. Benedetti, B. DiBlasio, V. Pavone, C. Pedone, C. Toniolo, G. M. Bonora, F. Formaggio, M. Crisma, J. Biomol. Struct. Dyn. 1988, 6, 803

M. Bellanda, E. Peggion, R. Bürgi, W. F. van Gunsteren, S. Mammi, J. Pept. Res. 2001, 57, 97

F. M. Bickelhaupt, E. J. Baerends, Angew. Chem. 2003, 115, 4315; Angew. Chem. Int. Ed. 2003, 42, 4183

G. Bifulco, C. Bassarello, R. Riccio, L. Gomez-Paloma, Org. Lett. 2004, 6, 1025

M. Blackledge, Prog. NMR Spectrosc. 2005, 46, 23

J. N. Blattman, P. D. Greenberg, Science 2004, 305, 200

H. B. Bode, R. Müller, Angew. Chem. 2005, 117, 6988; Angew. Chem. Int. Ed. 2005, 44, 6828

H.-J. Böhm, G. Klebe, Angew. Chem. 1996, 108, 2750; Angew. Chem. Int. Ed. 1996, 35, 2589

D. L. Boger, T. M. Ramsey, H. Cai, S. T. Hoehn, J. Stubbe, J. Am. Chem. Soc. 1998, 120, 9149

D. L. Boger, H. Cai, Angew. Chem. 1999, 111, 470; Angew. Chem. Int. Ed. 1999, 38, 448

P. Bombicz, J. Buschmann, P. Luger, N. X. Dung, C. B. Nam, Z. Kristallogr. 1999, 214, 420

M. Born, R. J. Oppenheimer, Ann. Physik 1927, 84, 458

P. Bouř, M. Buděšínský, J. Chem. Phys. 1999, 110, 2836

R. Breinbauer, I. R. Vetter, H. Waldmann, Angew. Chem. 2002, 114, 3002; Angew. Chem. Int. Ed. 2002, 41, 2878

B. R. Brooks, R. E. Bruccoleri, B. C. Olafson, D. J. States, S. Swaminathan, M. Karplus, J. Comp. Chem. 1983, 4, 187

A. T. Brünger, M. Nilges, Q. Rev. Biophys. 1993, 26, 49

T. Buskas, S. Ingale, G.-J. Boons, Angew. Chem. 2005, 117, 6139; Angew. Chem. Int. Ed. 2005, 44, 5985

M. S. Butler, Nat. Prod. Rep. 2005, 22, 162

F. Cardullo, M. C. Calama, B. H. M. Snellink-Ruel, J. L. Weidmann, A. Bielejewska, Chem. Commun. 2000, 367

A. B. Charette, H. Lebel, J. Am. Chem. Soc. 1996, 118, 10327

J. R. Cheeseman, G. W. Trucks, T. A. Keith, M. J. Frisch, J. Chem. Phys. 1996, 104, 5497

P.-Y. Chen, C.-C. Lin, Y.-T. Chang, S.-C. Lin, S. I. Chan, Proc. Natl. Acad. Sci. USA 2002, 99, 12633

Z. Chen, C. S. Wannere, C. Corminboeuf, R. Puchta, P. v. R. Schleyer, Chem. Rev. 2005, 105, 3842

F. Cloran, Y. Zhu, J. Osborn, I. Carmichael, A. S. Serianni, J. Am. Chem. Soc. 2000, 122, 6435

D. Cremer, J. Gauss, J. Am. Chem. Soc. 1986, 108, 7467

P. Dauber-Osguthorpe, V. A. Roberts, D. J. Osguthorpe, J. Wolff, M. Genest, A. T. Hagler, Prot. Struct. Funct. Genet. 1988, 4, 31

A. M. Davis, T. I. Oprea, S. J. Teague, P. D. Leeson, Angew. Chem. 1999, 111, 3962; Angew. Chem. Int. Ed. 1999, 38, 3743

A. P. Dejaegere, D. A. Case, J. Phys. Chem. A 1998, 102, 5280

A. de Meijere, W. Lüttke, F. Heinrich, Liebigs Ann. Chem. 1974, 306

A. de Meijere, A. F. Khlebnikov, R. R. Kostikov, S. I. Kozhushkov, P. R. Schreiner, A. Wittkopp, D. S. Yufit, Angew. Chem. 1999, 111, 3682; Angew. Chem. Int. Ed. 1999, 38, 3474

A. de Meijere, A. F. Khlebnikov, S. I. Kozhushkov, K. Miyazawa, D. Frank, P. R. Schreiner, B. C. Rinderspacher, D. S. Yufit, J. A. K. Howard, Angew. Chem. 2004, 116, 6715; Angew. Chem. Int. Ed. 2004, 43, 6553

K. A. Denessiouk, M. S. Johnson, Proteins 2000, 38, 310

P. R. de Oliveira, L. Tasic, S. A. Rocco, R. Rittner, Magn. Reson. Chem. 2006, 44, 790

E. Díez, J. Casanueva, J. S. Fabián, A. L. Esteban, M. P. Galache, V. Barone, J. E. Peralta, R. H. Contreras, Mol. Phys. 2005, 103, 1307

R. Ditchfield, J. Chem. Phys. 1972, 56, 5688

P. Dokurno, P. A. Bates, H. A. Band, L. M. D. Stewart, J. M. Lally, J. M. Burchell, J. Taylor-Papadimitriou, D. Snary, M. J. E. Sternberg, P. S. Freemont, J. Mol. Biol. 1998, 284, 713

T. H. Dunning Jr., J. Chem. Phys. 1989, 90, 1007

S. Dziadek, D. Kowalczyk, H. Kunz, Angew. Chem. 2005a, 117, 7798; Angew. Chem. Int. Ed. 2005a, 44, 7624

S. Dziadek, A. Hobel, E. Schmitt, H. Kunz, Angew. Chem. 2005b, 117, 7803; Angew. Chem. Int. Ed. 2005b, 44, 7630

S. Dziadek, H. Kunz, C. Griesinger, U. M. Reinscheid, Chem. Eur. J. 2006, 12, 4981

M. Ebrahimi, P. Rossi, C. Rogers, G. S. Harbison, J. Magn. Reson. 2001, 150, 1

E. L. Eliel, 100+ Years of Conformational Analysis. In: Conformational Behaviour, and Six-Membered Rings: Analysis, Dynamics, and Stereoelectronic Effects; Ed. E. Juaristi, VCH New York, 1995

B. Evans, K. E. Rittle, M. G. Bock, R. M. DiPrado, R. M. Freidinger, W. L. Whitter, G. F. Lundell, D. F. Veber, P. S. Anderson, R. S. L. Chang, V. J. Lotti, D. J. Cerino, T. B. Chen, P. J. Kling, K. A. Kunkel, J. P. Springer, J. Hirshfield, J. Med. Chem. 1988, 31, 2235

K. Exner, P. v. R. Schleyer, J. Phys. Chem. A 2001, 105, 3407

J. T. Fischer, U. M. Reinscheid, Eur. J. Org. Chem. 2006a, 9, 2074

J. T. Fischer, S. G. Wehner, U. M. Reinscheid, J. Mol. Struct. (THEOCHEM) 2006b, 767, 81

R. Fletcher, C. M. Reeves, J. Comp. 1964, 7, 149

J. Fohrer, U. Reinscheid, M. Hennig, T. Carlomagno, Angew. Chem. Int. Ed. 2006, im Druck

D. I. Freedberg, J. Am. Chem. Soc. 2002, 124, 2358

J. C. Freudenberger, P. Spiteller, R. Bauer, H. Kessler, B. Luy, J. Am. Chem. Soc. 2004, 126, 14690

J. C. Freudenberger, S. Knör, K. Kobzar, D. Heckmann, T. Paululat, H. Kessler, B. Luy, Angew. Chem. 2005, 117, 427; Angew. Chem. Int. Ed. 2005, 44, 433

H. Friebolin, Ein- und zweidimensionale NMR-Spektroskopie, Wiley-VCH, Weinheim, 1999

R. Geschwind, Angew. Chem. 2005, 117, 4744; Angew. Chem. Int. Ed. 2005, 44, 4666

R. Ghose, J. P. Marino, K. B. Wiberg, J. H. Prestegaard, J. Am. Chem. Soc. 1994, 116, 8827

D. J. Giesen, N. Zumbulyadis, Phys. Chem. Chem. Phys. 2002, 4, 5498

A. C. Gibbs, T. C. Bjorndahl, R. S. Hodges, D. S. Wishart, J. Am. Chem. Soc. 2002, 127, 1203

A. Glättli, W. F. van Gunsteren, Angew. Chem. 2004, 116, 6472; Angew. Chem. Int. Ed. 2004, 43, 6312

H. Gohlke, M. Hendlich, G. Klebe, J. Mol. Biol. 2000, 295, 337

H. Gohlke, G. Klebe, Angew. Chem. 2002, 114, 2764; Angew. Chem. Int. Ed. 2002, 41, 2645

L. Goodman, H. Gu, V. Pophristic, J. Chem. Phys. 1999, 110, 4268

S. G. Grdadolnik, P. Pristovsek, D. F. Mierke, J. Med. Chem. 1998, 41, 2090

S. Grimme, Angew. Chem. 2006a, 118, 4571; Angew. Chem. Int. Ed. 2006a, 45, 4460

S. Grimme, C. Diedrich, M. Korth, Angew. Chem. 2006b, 118, 641; Angew. Chem. Int. Ed. 2006b, 45, 625

C. Griesinger, O. W. Soerensen, R. R. Ernst, J. Am. Chem. Soc. 1985, 107, 6394

A. M. Gronenborn, G. M. Clore, Prog. NMR Spectrosc. 1985, 17, 1

T. Gruene, C. Sheldrick, pers. Mitteilung

M. Gurrath, G. Müller, H.-D. Höltje, Perspect. Drug Discovery Des. 1998, 12, 135

C. A. G. Haasnoot, F. A. A. M. de Leeuw, C. Altona, Tetrahedron 1980, 36, 2783

P. Haberz, J. Farjon, C. Griesinger, Angew. Chem. 2005, 117, 431; Angew. Chem. Int. Ed. 2005, 44, 427

J. Härtner, U. M. Reinscheid, J. Mol. Struct. 2006, eingereicht

P. Hammerström, R. L. Wiseman, E. T. Powers, J. W. Kelly, Science 2003, 299, 713

F.-G. Hanisch, S. Müller, Glycobiology 2000, 10, 439

T. Helgaker, M. Jaszúnski, K. Ruud, Chem. Rev. 1999, 99, 293

T. Helgaker, M. Watson, N. C. Handy, J. Chem. Phys. 2000, 113, 9402

M. Hennig, J. Fohrer, T. Carlomagno, J. Am. Chem. Soc. 2005, 127, 2028

R. W. Hoffmann, Angew. Chem. 1992, 104, 1147; Angew. Chem. Int. Ed. 1992, 31, 1124

R. W. Hoffmann, M. Stahl, U. Schopfer, G. Frenking, Chem. Eur. J. 1998, 4, 559

R. W. Hoffmann, Angew. Chem. 2000, 112, 2134; Angew. Chem. Int. Ed. 2000, 39, 2054

P. Hohenberg, W. Kohn, Phys. Rev. 1964, 136, 864

T. R. Hoye, S.-E. N. Ayyad, B. M. Eklov, N. E. Hashish, W. T. Shier, K. A. El Sayed, M. T. Hamann, J. Am. Chem. Soc. 2002, 124, 7405

J.-C. Hus, D. Marion, M. Blackledge, J. Mol. Biol. 2000, 298, 927

J.-C. Hus, D. Marion, M. Blackledge, J. Am. Chem. Soc. 2001, 123, 1541

F. Jensen, Introduction to Computational Chemistry, John Wiley & Sons, Chichester, 1999

M. Karplus, J. Chem. Phys. 1959, 30, 11

U. Karsten, N. Serttas, H. Paulsen, A. Danielczyk, S. Goletz, Glycobiology 2004, 14, 681

Y. Kato, N. Fusetani, S. Matsunaga, K. Hashimoto, K. Koseki, J. Org. Chem. 1988, 53, 3930

H. Kessler, Angew. Chem. 1982, 94, 509; Angew. Chem. Int. Ed. 1982, 21, 512

H. Kessler, C. Griesinger, J. Lautz, A. Muller, W. F. van Gunsteren, H. J. C. Berendsen, J. Am. Chem. Soc. 1988, 110, 3393

S. Kirkpatrick, C. D. Gelatt Jr., M. P. Vecchi, Science 1983, 220, 671

L. Kirnarsky, O. Prakash, S. M. Vogen, M. Nomoto, M. A. Hollingsworth, S. Sherman, Biochemistry 2000, 39, 12076

G. Klebe, F. Diederich, Philos. Trans. R. Soc. London Ser. A 1993, 345, 37

Y. Kobayashi, J. Lee, K. Tezuka, Y. Kishi, Org. Lett. 1999, 1, 2177

Y. Kobayashi, C.-H. Tan, Y. Kishi, Angew. Chem. 2000, 112, 4449; Angew. Chem. Int. Ed. 2000, 39, 4279

Y. Kobayashi, C.-H. Tan, Y. Kishi, J. Am. Chem. Soc. 2001a, 123, 2076

Y. Kobayashi, N. Hayashi, C.-H. Tan, Y. Kishi, Org. Lett. 2001b, 3, 2245

W. Koch, M. C. Holthausen, A Chemist`s Guide to Density Functional Theory, Wiley, New York, 2001

F. E. Koehn, G. T. Carter, Nat. Rev. Drug Discov. 2005, 4, 206

E. Kolehmainen, K. Tuppurainen, S. A. Lanina, E. Sievänen, K. Laihia, V. P. Boyarskiy, V. A. Nikiforov, T. E. Zhesko, Chemosphere 2006, 62, 368

W. Kohn, L. J. Sham, Phys. Rev. A 1965, 140, 1133

R. K. Konat, B. Mathä, J. Winkler, H. Kessler, Liebigs Ann. 1995, 765

M. S. Kuo, R. J. Zielinski, J. I. Cialdella, C. K. Marschke, M. J. Dupuis, G. P. Li, D. A. Kloosterman, C. H. Spilman, V. P. Marshall, J. Am. Chem. Soc. 1995, 117, 10629

W. Kutzelnigg, in: Calculation of NMR and EPR parameters (Eds. M Kaupp, M. Bühl, V. G. Malkin), Wiley-VCH, 2004

M. S. Lajiness, G. M. Maggiora, V. Shanmugasundaram, J. Med. Chem. 2004, 47, 4891

J. F. Lavigne, E. V. Anslyn, Angew. Chem. 2001, 113, 3212; Angew. Chem. Int. Ed. 2001, 40, 3118

A. R. Leach, Molecular Modelling - Principles and Application, Addison Wesley Longman, England, 1996

J. Lee, Y. Kobayashi, K. Tezuka, Y. Kishi, Org. Lett. 1999, 1, 2181

S. Lifson, A. T. Hagler, J. Am. Chem. Soc. 1979, 101, 5111

L. Liu, Q.-X. Guo, Chem. Rev. 2001, 101, 673

M. Liu, B. Acres, J.-M. Balloul, N. Bizouarne, S. Paul, P. Slos, P. Squiban, Proc. Natl. Acad. Sci. USA 2004, 101, 14567

H. Luesch, W. Y. Yoshida, R. E. Moore, V. J. Paul, T. H. Corbett, J. Am. Chem. Soc. 2001, 123, 5418

B. Luy, K. Kobzar, H. Kessler, Angew. Chem. 2004, 116, 1112; Angew. Chem. Int. Ed. 2004, 43, 1092

J. P. Mackay, U. Gerhard, D. A. Beauregard, R. A. Maplestone, D. H. Williams, J. Am. Chem. Soc. 1994, 116, 4573

Y. C. Martin, J. L. Kofron, L. M. Traphagen, J. Med. Chem. 2002, 45, 4350

K. Martínez-Mayorga, E. Juaristi, G. Cuevas, J. Org. Chem. 2004, 69, 7266

M. Martín-Pastor, J. F. Espinosa, J. L. Asensio, J. Jiménez-Barbero, Carbohydr. Res. 1997, 298, 15

N. Matsumori, D. Kaneno, M. Murata, H. Nakamura, K. Tachibana, J. Org. Chem. 1999, 64, 866

S. N. Maximoff, J. E. Peralta, V. Barone, G. E. Scuseria, J. Chem. Theory Comput. 2005, 1, 541

G. Mehta, V. Singh, Chem. Soc. Rev. 2002, 31, 324

J. B. O. Mitchell, J. Smith, Proteins 2003, 50, 563

Y. Mo, W. Wu, L. Song, M. Lin, Q. Zhang, J. Gao, Angew. Chem. 2004, 116, 2020; Angew. Chem. Int. Ed. 2004, 43, 1986

D. Moran, M. Manoharan, T. Heine, P. v. R. Schleyer, Org. Lett. 2003, 5, 23

L. Müller, J. Magn. Reson. 1987, 72, 191

G. Müller, G. Hessler, H. Y. Decornez, Angew. Chem. 2000, 112, 926; Angew. Chem. Int. Ed. 2000, 39, 894

D. Neuhaus, M. P. Williamson, The Nuclear Overhauser Effect in Structural and Conformational Analysis, Wiley-VCH, 2000

D. J. Newman, G. M. Cragg, K. M. Snader, J. Nat. Prod. 2003, 66, 1022

K. C. Nicolaou, S. A. Snyder, Angew. Chem. 2005, 117, 1036; Angew. Chem. Int. Ed. 2005, 44, 1012

S. Obika, M. Sekiguchi, R. Somjing, T. Imanishi, Angew. Chem. 2005, 117, 1980; Angew. Chem. Int. Ed. 2005, 44, 1944

C. Ochsenfeld, J. Kussmann, F. Koziol, Angew. Chem. Int. Ed. 2004, 43, 4485

K. Otoguro, H. Ui, A. Ishiyama, N. Arai, M. Kobayashi, Y. Takahashi, R. Masuma, K. Shiomi, H. Yamada, S. Omura, J. Antibiot. 2006, 56, 322

T. Owa, A. Haupt, M. Otsuka, S. Kobayashi, N. Tomioka, A. Itai, M. Ohno, T. Shiraki, M. Uesugi, Y. Sugiura, K. Maeda, Tetrahedron 1992, 48, 1193

A. Pardi, M. Billeter, K. Wüthrich, J. Mol. Biol. 1984, 180, 741

M. Pérez, T. T. Peakman, A. Alex, P. D. Higginson, J. C. Mitchell, M. J. Snowden, I. Morao, J. Org. Chem. 2006, 71, 3103

I. Paterson, E. A. Anderson, Science 2005, 310, 451

J. E. Peralta, G. E. Scuseria, J. R. Cheeseman, M. J. Frisch, Chem. Phys. Lett. 2003, 375, 452

A. Plaza, S. Piacente, A. Perrone, A. Hamed, C. Pizza, G. Bifulco, Tetrahedron 2004, 60, 12201

J. A. Pople, Angew. Chem. 1999, 111, 2014; Angew. Chem. Int. Ed. 1999, 38, 1894

V. Pophristic, L. Goodman, Nature 2001, 411, 565

R. K. Ramanathan, K. M. Lee, J. McKolanis, E. Hitbold, W. Schraut, A. J. Moser, E. Warnick, T. Whiteside, J. Osborne, H. Kim, R. Day, M. Troetschel, O. J. Finn, Cancer Immunol. Immunother. 2005, 54, 254

A. E. Reed, L. A. Curtiss, F. Weinhold, Chem. Rev. 1988, 88, 899

U. Reineke, J. Schneider-Mergener, Angew. Chem. 1998, 110, 801; Angew. Chem. Int. Ed. 1998, 37, 769

U. M. Reinscheid, B. D. Zlatopolskiy, C. Griesinger, A. Zeeck, A. de Meijere, Chem Eur. J. 2005, 11, 2929

U. M. Reinscheid, J. Farjon, P. Haberz, M. Blackledge, C. Griesinger, ChemBioChem 2006, 7, 287

E. Rössner, A. Zeeck, W. A. König, Angew. Chem. 1990, 102, 84; Angew. Chem. Int. Ed. 1990, 29, 64

T. Sassa, H. Kenmoku, M. Sato, T. Murayama, N. Kato, Biosci. Biotechnol. Biochem. 2003, 67, 475

P. v. R. Schleyer, C. Maerker, A. Dransfeld, H. Jiao, N. J. R. van Eikema Hommes, J. Am. Chem. Soc. 1996, 118, 6317

J. Schuman, A. P. Campbell, R. R. Koganty, B. M. Longenecker, J. Pept. Res. 2003, 61, 91

Y. Senda, S. Imaizumi, Tetrahedron 1975, 31, 2905

G. P. Smith, Science 1985, 228, 1315

B. Sommer, Curr. Opin. Pharmacol. 2002, 2, 87

C. Soto, Nat. Rev. Neurosci. 2003, 4, 49

M. Stahl, U. Schopfer, G. Frenking, R. W. Hoffmann, J. Org. Chem. 1996, 61, 8083

M. Stahl, U. Schopfer, G. Frenking, R. W. Hoffmann, Mol. Phys. 1997, 92, 569

M. Stahl, M. Rarey, G. Klebe, in: Bioinformatics-From Genomes to Drugs, Methods and Principles in Medicinal Chemistry, Vol. 14, 137, Wiley-VCH, 2002

D. M. Swallow, S. J. Gendler, B. Griffith, G. Corney, J. Taylor-Papadimitriou, Nature 1987, 328, 82

V. Sychrosvský, J. Gräfenstein, D. Cremer, J. Chem. Phys. 2000, 113, 3530

P. Tähtinen, A. Bagno, K. D. Klika, K. Pihlaja, J. Am. Chem. Soc. 2003, 105, 4609

C.-H. Tan, Y. Kobayashi, Y. Kishi, Angew. Chem. 2000, 112, 4452; Angew. Chem. Int. Ed. 2000, 39, 4282

S. Taubert, H. Konschin, D. Sundholm, Phys. Chem. Chem. Phys. 2005, 7, 2561

J. P. Taylor, J. Hardy, K. H. Fischbeck, Science 2002, 296, 1991

C. M. Thiele, S. Berger, Org. Lett. 2003, 5. 705

C. M. Thiele, J. Org. Chem. 2004, 69, 7403

C. M. Thiele, A. Marx, R. Berger, J. Fischer, M. Biel, A. Giannis, Angew. Chem. 2006, 118, 4566; Angew. Chem. Int. Ed. 2006, 45, 4455

L. F. Tietze, H. P. Bell, S. Chandrasekhar, Angew. Chem. 2003, 115, 4128; Angew. Chem. Int. Ed. 2003, 42, 3996

J. M. Torres-Valencia, M. Meléndez-Rodríguez, R. Àlvarez-García, C. M. Cerda-García-Rojas, P. Joseph-Nathan, Magn. Reson. Chem. 2004, 42, 898

W. F. van Gunsteren, D. Bakowies, R. Baron, I. Chandrasekhar, M. Christen, X. Daura, P. Gee, D. P. Geerke, A. Glättli, P. H. Hünenberger, M. A. Kastenholz, C. Oostenbrink, M. Schenk, D. Trzesniak, N. F. A. van der Vegt, H. B. Yu, Angew. Chem. 2006, 118, 4168; Angew. Chem. Int. Ed. 2006, 45, 4064

A. Vedani, P. Zbinden, J. P. Snyder, P. A. Greenidge, J. Am. Chem. Soc. 1995, 117, 4987

L. Verdier, P. Sakhaii, M. Zweckstetter, C. Griesinger, J. Magn. Reson. 2003, 163, 353

M. A. Watson, P. Salek, P. Macak, M. Jaszuński, T. Helgaker, Chem. Eur. J. 2004, 10, 4627

S. G. Wehner, C. Boehme, U. M. Reinscheid, J. Mol. Struct. 2006 (THEOCHEM), eingereicht

S. J. Weiner, P. A. Kollmann, D. A. Case, U. C. Singh, C. Chio, G. Alagona, S. Profeda, P. Weiner, J. Am. Chem. Soc. 1984, 106, 765

F. Weinhold, Nature 2001, 411, 539

F. Weinhold, Angew. Chem. 2003, 115, 4320; Angew. Chem. Int. Ed. 2003, 42, 4188

G. Wess, M. Urmann, B. Sickenberger, Angew. Chem. 2001, 113, 3443; Angew. Chem. Int. Ed. 2001, 40, 3341

K. Wiberg, J. Am. Chem. Soc. 1965, 87, 1070

S. S. Wijmenga, B. N. M. van Buuren, Prog. NMR Spectrosc. 1998, 32, 287

D. H. Williams, B. Bardsley, Angew. Chem. 1999, 111, 1264; Angew. Chem. Int. Ed. 1999, 38, 1173

D. H. Williams, E. Stephens, D. P. O`Brien, M. Zhou, Angew. Chem. 2004, 116, 6760; Angew. Chem. Int. Ed. 2004, 43, 6596

D. S. Wishart, B. D. Sykes, Meth. Enzymol. 1994, 239, 363

D. S. Wishart, D. A. Case, Meth. Enzymol. 2001, 338, 3

K. Wolinski, J. F. Hinton, P. Pulay, J. Am. Chem. Soc. 1990, 112, 8251

N. C. Wrighton, F. X. Farrell, R. Chang, A. K. Kashyap, F. P. Barbone, L. S. Mulcahy, D. L. Johnson, R. W. Barrett, L. K. Jolliffe, W. J. Dower, Science 1996, 273, 458

J. L. Yan, A. D. Kline, H. P. Mo, M. J. Shapiro, E. R. Zartler, J. Org. Chem. 2003, 68, 1768

J. L. Yan, F. Delaglio, A. Kaerner, A. D. Kline, H. P. Mo, M. J. Shapiro, T. A. Smitka, G. A. Stephenson, E. R. Zartler, J. Am. Chem. Soc. 2004, 126, 5008

S. F. Yang, N. E. Hoffmann, Annu. Rev. Plant Physiol. 1984, 35, 155

M. Yoshida, M. Ezaki, M. Hashimoto, M. Yamashita, N. Shigematsu, M. Okuhara, M. Kohsaka, K. Horikoshi, J. Antibiot. 1990, 18, 748

M. Zweckstetter, A. Bax, J. Am. Chem. Soc. 2000, 122, 3791

6. Publikationsliste

Mutzel A, Reinscheid UM, Antranikian G, Müller R* (1996) Isolation and characterization of a thermophilic *Bacillus* strain, which degrades phenol and cresols as sole carbon source at 70°C, Appl. Microbiol. Biotechnol., 46: 593

Reinscheid UM, Bauer MP, Müller R* (1997) Biotransformation of halophenols by a thermophilic *Bacillus* sp., Biodegradation, 7: 455

Duffner FM, Reinscheid UM, Bauer MP, Mutzel A, Müller R* (1997) Strain differentiation and taxonomic characterisation of a thermophilic group of phenol-degrading Bacilli, System. Appl. Microbiol., 20: 602

Reinscheid UM, Zuilhof H, Müller R, Vervoort J* (1998) Biological, thermal and photochemical transformation of 2-trifluoromethylphenol, Biodegradation, 9: 487

Liu WZ, Reinscheid UM* (2004) Camptothecin-resistant fungal endophytes of *Camptotheca acuminata*, Mycol. Prog., 3: 189

Reinscheid UM, Zlatopolskiy BD, Griesinger C*, Zeeck A, de Meijere A* (2005) The structure of hormaomycin and one of its all-peptide aza-analogues in solution: Syntheses and biological activities of new hormaomycin analogues, Chem. Eur. J., 11: 2929

Reinscheid UM* (2006) Direct determination of ciprofloxacin in admixtures with metronidazol and ampicillin by NMR, J. Pharm. Biom. Anal., 40: 447

Reinscheid UM, Farjon J, Haberz P, Blackledge M, Griesinger C* (2006) Effect of the solvent on the conformation of a depsipeptide: NMR derived solution structure of hormaomycin in DMSO by using residual dipolar couplings in a novel DMSO compatible alignment medium, ChemBioChem, 7: 287

Barrett AGM, James RA, Morton GE, Procopiou PA, Boehme C, de Meijere A, Griesinger C, Reinscheid UM* (2006) Helical structure of tercyclopropanedimethanol in solution, J. Org. Chem., 71: 2756

Fischer JT, Reinscheid UM* (2006) ^{13}C chemical shifts and $^{1}J_{CH}$ coupling constants of cytidine at different χ dihedrals based on DFT calculations, Eur. J. Org. Chem., 9: 2074

Dziadek S, Kunz H*, Griesinger C*, Reinscheid UM (2006) Structural implication of complex carbohydrates attached to MUC1 derived peptides, Chem. Eur. J., 12: 4981

Fick AC, Reinscheid UM* (2006) Characterization of the binding epitope of ciprofloxacin bound to human serum albumin, J. Pharm. Biom. Anal., 41: 1025

Reinscheid UM*, Zuilhof H, Vervoort J (2006) Mild hydrolysis of 2-trifluoromethylphenol: kinetics, mechanism and environmental relevance, Chemosphere, 65: 318

Fischer JT, Wehner SG, Reinscheid UM* (2006) Interpretation of cytidine proton chemical shifts and J coupling constants calculated by DFT, J. Mol. Structure (THEOCHEM), 767, 81

Härtner J, Reinscheid UM* (2006) Conformational analysis of menthol diastereomers by NMR and DFT computation, J. Mol. Struct., eingereicht

Fohrer J, Reinscheid UM, Hennig M, Carlomagno T* (2006) Determination of 2′-hydroxyl group conformation in RNA: Dependence of homo- and heteronuclear ^{3}J and ^{2}J scalar couplings on the H2′-C2′-O2′-OH dihedral angle, Angew. Chem. Int. Ed., im Druck

Wehner SG, Boehme C, Reinscheid UM* (2006), J. Mol. Struct. (THEOCHEM), eingereicht

* : corresponding author

Vorträge und Poster-Präsentationen

Reinscheid UM, Müller R (1995). Untersuchungen zum mikrobiellen Abbau von Chlorphenolen bzw. Phenol unter thermophilen Bedingungen. Doktorandentagung der DPhG, Banz

Reinscheid UM, Müller R (1995) Screening for thermophilic microorganisms with the ability to degrade chlorophenols. Frühjahrstagung der VAAM, Stuttgart

Reinscheid UM, Müller R (1996) Co-metabolische Transformation von Halophenolen unter thermophilen Bedingungen. Doktorandentagung der DPhG, Salzau

Reinscheid UM, Bauer MP, Müller R (1996) Biotransformation of halophenols by a thermophilic Bacillus species. Biodegradation of Organic Pollutants, UIB-GBF-CSIC-TUB Symposium, Mallorca, Spain

Reinscheid UM (1998) Biological and non-biological transformation of 2-trifluoromethylphenol under thermophilic conditions. Mini Symposium: NMR in Environmental Sciences, Ede, The Netherlands

Haberz P, Farjon J, Reinscheid UM, Junker J, Zweckstetter M, Bermel W, Griesinger C (2006) Dipolar couplings for structure elucidation of small molecules. 47th Experimental Nuclear Magnetic Resonance Conference, Pacific Grove, California, USA

7. Lebenslauf

Persönliche Daten

Name	Dr. Uwe Michael Reinscheid
Geburtsdatum	24.2.1967
Geburtsort	Meschede, Nordrhein-Westfalen
Familienstand	ledig

Ausbildung und Berufstätigkeit

1974-1978	Marien-Grundschule, Meschede
1978-1987	Gymnasium der Benediktiner, Abtei Meschede
1987	Abitur
1988-1992	Pharmaziestudium in Münster
1992	2. Staatsexamen
1992-1993	praktisches Jahr in Kiel (Sophienhof-Apotheke) und an der Université Paris-Sud (Prof. Combet-Farnoux)
1993	3. Staatsexamen, Approbation als Apotheker
1994-1997	Promotion an der Technischen Universität Hamburg-Harburg, Bereich Technische Biochemie (Prof. Müller)
1997	Post-Doc an der Landwirtschaftlichen Universität Wageningen (Holland), Institut für Biochemie, Prof. Vervoort
1998	wissenschaftlicher Mitarbeiter am Bundesinstitut für Arzneimittel und Medizinprodukte, Berlin
1998-2000	Laborleiter Mikrobiologie und Sonderanalytik bei KVP (Bayer AG), Kiel
2000-2001	GMP-Seminarleiter für Pharma Training Service (PTS), Arnsberg
2001	wissenschaftlicher Mitarbeiter am Institut für Pharmazeutische Biologie der Universität Bonn (Prof. Leistner)
2002	wissenschaftlicher Mitarbeiter in der Organischen Chemie der Universität Frankfurt (Prof. Schwalbe)
2003-	wissenschaftlicher Mitarbeiter der Abteilung NMR II am Max-Planck-Institut für biophysikalische Chemie in Göttingen (Prof. Griesinger)

Auszeichnungen

1987	Abitur-Jahrgangsbester mit der Note 1,1
1988-1993	Stipendiat der Studienstiftung des deutschen Volkes

Lehrtätigkeit

SS und WS 2000	Seminar und Praktikum "Cytologie und Histologie des Menschen", und "Pflanzenmorphologie", Universität Bonn
seit SS 2004	Vorlesung "Instrumentelle Analytik für Pharmazeuten", Universität Marburg
	Praktikum im Rahmen des Wahlpflichtfaches für Pharmazeuten, Universität Marburg

The Structure of Hormaomycin and One of Its All-Peptide Aza-Analogues in Solution: Syntheses and Biological Activities of New Hormaomycin Analogues

Uwe M. Reinscheid,[a] Boris D. Zlatopolskiy,[b] Christian Griesinger,*[a] Axel Zeeck,*[b] and Armin de Meijere*[b]

Abstract: Four new aza-analogues of hormaomycin **1**, a secondary metabolite with interesting biological activities produced by *Streptomyces griseoflavus*, were synthesized and subjected to preliminary tests of their antibiotic activity to provide new insights into the structure–activity relationship studies of this class of compounds. The solution structures of hormaomycin **1** and its aza-analogue **2a** were determined by NMR spectroscopy. The data exhibited a reasonably rigid conformation for both molecules, stabilized by stacking interactions between the aromatic moieties attached to the ring and the side chain. According to NMR-spectral data the aza-analogue *epi*-**2a** has a rather different conformation and indeed shows no antibacterial activity whatsoever.

Keywords: amino acids · NMR spectroscopy · peptides · structure elucidation · synthetic methods

Introduction

Hormaomycin **1** is a secondary metabolite produced by *Streptomyces griseoflavus* (strain W-384).[1,2] This peptide lactone contains (*S*)-isoleucine [(*S*)-Ile] as the only proteinogenic amino acid along with two units of (2*S*,3*R*)-3-methylphenylalanine [(βMe)Phe], one of (*R*)-*allo*-threonine [*a*-Thr] as well as two moieties of (1′*R*,2′*R*)-3-(2′-nitrocyclopropyl)alanine [(3-Ncp)Ala; the (2*S*)-diastereomer in the side chain and the (2*R*)-diastereomer in the ring part of the molecule] as well as one residue of (2*S*,4*R*)-4-(*Z*)-propenylproline [(4-Pe)Pro] (Figure 1). The side chain of **1** is terminated by an amide-bound 5-chloro-1-hydroxypyrrole-2-carboxylic acid [Chpca]. The latter three constituents have never been found in any natural product before. Besides challenging structural features, hormaomycin **1** possesses quite an interesting spectrum of biological activities, including a marked influence on the secondary metabolite production of other streptomycetes, an exceptionally selective antibiotic activity against coryneform bacteria,[1] and also an antimalaria activity.[3]

The unique biological properties of **1** prompted feeding experiments with amino acids, which possibly could replace (3-Ncp)Ala. This approach yielded several new analogues of hormaomycin,[4] however, the precursor-directed biosynthesis is apparently limited to such modifications of the building blocks, which are tolerated by the hormaomycin synthetase. Thus, it was for example impossible to isolate analogues of hormaomycin with a substituted or modified *allo*-threonine (*a*-Thr) moiety.[5] On the other hand, it appeared to be interesting to study the biological and, in this context, the conformational properties of hormaomycin and especially its cyclopeptide analogue **2a** with (2*R*,3*R*)-diaminobutyric acid instead of (*R*)-*allo*-threonine in the macrocycle. The more rigid additional amide bond might have a significant influence on the intramolecular hydrogen bonds and thereby on the global structure in solution as compared to that of the peptide lactone. This comparison might provide insights into the structural requirements for biological activities of hormaomycin **1** itself and of hormaomycin analogues. Since

[a] Dr. U. M. Reinscheid, Prof. Dr. C. Griesinger
Max Planck Institute for Biophysical Chemistry
Am Fassberg 11, 37077 Göttingen (Germany)
Fax: (+49) 551-201-2202
E-mail: cigr@nmr.mpibpc.mpg.de

[b] Dr. B. D. Zlatopolskiy, Prof. Dr. A. Zeeck, Prof. Dr. A. de Meijere
Institut für Organische und Biomolekulare Chemie
der Georg-August-Universität Göttingen
Tammannstrasse 2, 37077 Göttingen (Germany)
Fax: (+49) 551-399-475
E-mail: azeeck@gwdg.de
armin.demeijere@chemie.uni-goettingen.de

Supporting information for this article is available on the WWW under http://www.chemeurj.org/ or from the author.

 DOI: 10.1002/chem.200400977

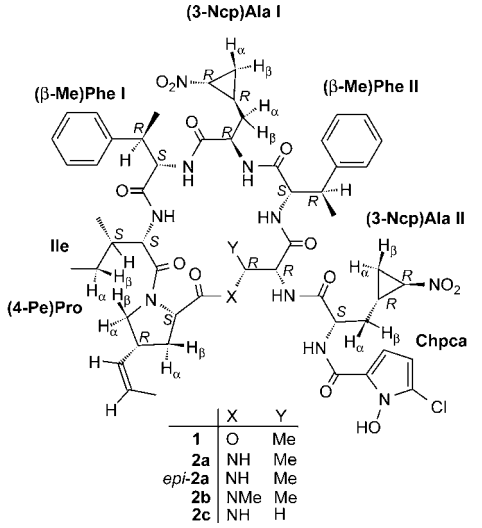

	X	Y
1	O	Me
2a	NH	Me
epi-**2a**	NH	Me
2b	NMe	Me
2c	NH	H

Figure 1. Structural formulas of hormaomycin **1** and its aza-analogues **2a–c** and *epi*-**2a**. Analogue *epi*-**2a** contains an (*R*)-*a*-Ile instead of an Ile moiety.

amide bonds are usually much more stable towards enzymatic cleavage than ester linkages, aza-analogues ought to have longer half-lives in vivo and thereby provide prolonged biological activity. Herewith we present the first chemical syntheses of the hormaomycin analogues **2a–c** and *epi*-**2a** as well as a preliminary evaluation of their biological activities along with a thorough investigation of the three-dimensional structure of hormaomycin **1** and its aza-analogue **2a** in solution by a combination of modern NMR spectroscopic techniques.

Results and Discussion

Synthesis of hormaomycin analogues: At the outset, the appropriate N_α-*p*-methylbenzyloxycarbonyl (MeZ) protected diamino acid methyl esters **7a–c** were synthesized (Scheme 1). The α-azido *tert*-butyl ester **4**, which was prepared according to a published procedure[6] with a Sharpless asymmetric aminohydroxylation as a key step followed by stereoselective azidation, was transformed into the fully protected (2*R*,3*R*)-2,3-diaminobutyric acid (*a*-Dab) derivative **5** as described by Wen et al.[7] The free acid, after simultaneous removal of the *N*-Boc and *O*-*tert*-butyl groups from **5** with trifluoroacetic acid, was esterified with methanol, and the resulting N_β-protected diamino acid methyl ester was acetylated with MeZOSu to give **6** in 69% yield over three steps. Removal of the *N*-Fmoc group just before the next step gave the methyl ester **7a**.

The fully protected diamino acid **10** was synthesized starting from the known *tert*-butyl ester **8**.[8] After removal of the *tert*-butyldimethylsilyl group followed by cleavage of the *tert*-butyl ester, the appropriate *N*-Z-protected isothreonine was esterified with diazomethane to give an intermediate, which was further converted to the corresponding mesylate.

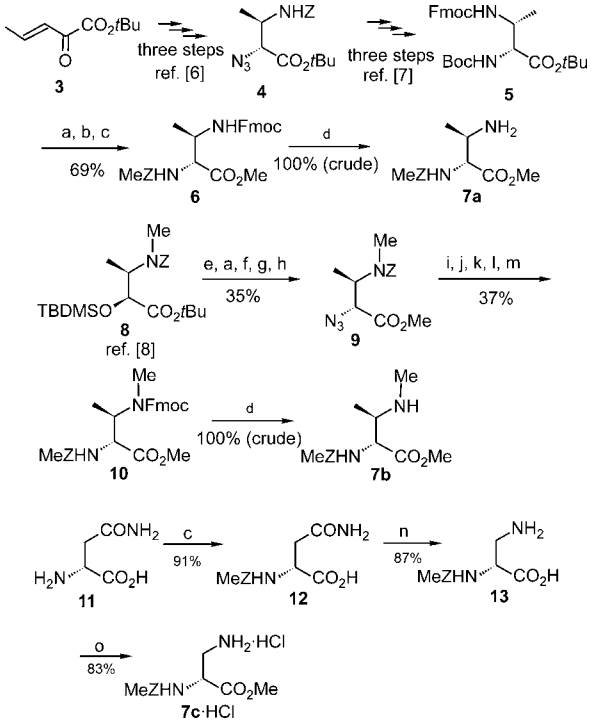

Scheme 1. Syntheses of the suitably protected diamino acids **7a–c**. a) TFA, 20°C, 1 h. b) $SOCl_2$, MeOH, −20 → 50°C, 21 h. c) MeZOSu, $NaHCO_3$, acetone, H_2O, 20°C, 1.5 h. d) 50% Et_2NH in MeCN, 20°C, 40 min. e) 5% aq. HF, MeCN, 0 → 20°C, 4 h. f) CH_2N_2, Et_2O/MeOH, 20°C, 30 min. g) MsCl, Et_3N, CH_2Cl_2, −30 → 20°C, 5 h. h) NaN_3, DMF, 75°C, 15 h. i) Ph_3P, THF/H_2O, 20°C, 24 h, then Boc_2O, 20°C, 24 h. j) H_2, 10% Pd/C, EtOAc, 20°C, 3 h. k) FmocOPfp, HOAt (cat.), TMP, EtOAc, 20°C, 15 h. l) 2M HCl, EtOAc, 20°C, 3 h. m) MeZOSu, DIEA, TMP, MeCN, 20°C, 16 h. n) Iodobenzene bis(trifluoroacetate), pyridine, DMF/H_2O, 20°C, 5 h. o) $SOCl_2$, MeOH, −20 → 20°C, 24 h. MeZOSu = *p*-methylbenzyl-*N*-hydroxysuccinyl carbonate, FmocOPfp = (9-fluorenyl)methyl-pentafluorophenyl carbonate; HOAt = 7-aza-1-hydroxybenzotriazole, TMP = 2,4,6-trimethylpyridine, DIEA = *N*,*N*-diisopropylethylamine, Fmoc = (9-fluorenyl)methyloxycarbonyl, MeZ = *p*-methylbenzyloxycarbonyl, TBDMS = *tert*-butyldimethylsilyl.

This transformation was followed by displacement of the mesylate by an azide group with NaN_3 in DMF to give the azido ester **9**, which was further transformed into the N_α-Boc, N_β-Z protected (2*R*,3*R*)-3-amino-2-methylaminobutyric (*a*-N_βMeDab) acid methyl ester, by treatment first with triphenylphosphine and water, and then with Boc_2O. Subsequent removal of the Z group by hydrogenolysis was followed by introduction of the Fmoc group to give the intermediate N_α-Boc, N_β-Fmoc protected *a*-N_βMeDab methyl ester, which, after removal of the Boc group, was finally acylated with MeZOSu to give **10** in 13% yield over ten steps. The *N*-Fmoc group in **10** was then removed to give **7b**. The latter was immediately used in the peptide coupling step.

The N_α-MeZ protected 2,3-diaminopropionic acid ester **7c** was obtained as a hydrochloride by esterification with methanol of the intermediate **13**, which in turn was prepared in 76% yield over three steps starting from (*R*)-asparagine (**11**) by initial acylation with MeZOSu and subsequent oxi-

dation with iodobenzene bis(trifluoroacetate) in close analogy to a published procedure.[9]

The diamino esters **7a–c** were coupled with the *N*-Boc-protected (2*S*,3*R*)-4-(*Z*)-propenylproline **14**[10] to give the intermediate methyl esters (Scheme 2).[11] Treatment of the latter with tetrabutylammonium hydroxide[12] gave the peptide acids **15a–c** in 71, 68 and 70% yield over two steps, respectively, which were coupled with the *O*-dicyclopropylmethyl (DCPM) protected tetrapeptide **16**[2a] (**15a** and **c**) or with the *O*-(2-trimethylsilyl)ethyl (TMSE) protected tetrapeptide **17**[13] (**15b**), after deprotection of their terminal amino groups, to yield the branched hexapeptides **18a** (80%), **18b** (93%), and **18c** (59%), respectively.

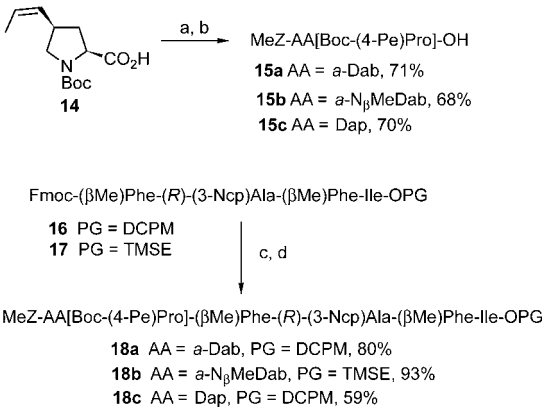

Scheme 2. Syntheses of the linear peptide precursors **18a–c**. a) **7a–c**, EDC, HOAt, TMP, CH_2Cl_2, 0 → 20°C, 16 h. b) 40% aq. $Bu_4N^+OH^-$, THF, 0°C, 45 min. c) 50% Et_2NH in THF, 20°C, 40 min. d) **15a–c**, HATU, HOAt, TMP, CH_2Cl_2, 0 → 20°C, 15 h. EDC = *N*′-(3-dimethylaminopropyl)-*N*-ethylcarbodiimide hydrochloride, HATU = *O*-(7-azabenzotriazole-1-yl)-*N*,*N*,*N*′,*N*′-tetramethyluronium hexafluorophosphate, DCPM = dicyclopropylmethyl, TMSE = 2-trimethylsilyl)ethyl, Dap = 2,3-diaminopropionic acid.

The acidolytic removal of the Boc and DCPM groups from the termini of **18a** and **18c**, as well as the sequential removal first of the TMSE group with tetrabutylammonium fluoride, and then the Boc group with acid from the terminus of **18b** occurred almost quantitatively, and was succeeded by macrocyclization, by using *O*-(7-azabenzotriazole-1-yl)-*N*,*N*,*N*′,*N*′-tetramethyluronium hexafluorophosphate (HATU)[14] in the presence of 7-aza-1-hydroxybenzotriazole (HOAt)[14] under high-dilution conditions (Scheme 3). The cyclization of the hexapeptides, containing *a*-Dab or Dap residues, caused significant epimerization at the α-carbon of the Ile residue (Ile → (*R*)-*a*-Ile)[15] and gave, after HPLC separation, the epimeric macrocycles, **19a** (28%) and *epi*-**19a** (19%), as well as **19c** (34%) and *epi*-**19c** (25%), respectively. In contrast, the cyclization of the *a*-N_βMeDab-containing peptide (similar to the synthesis of the *N*-MeZ protected ring part of hormaomycin **1**)[2a] gave almost exclusively the cyclic peptide **19b** (44%) along with only traces (<2%) of the epimer. Not surprisingly, the epimeric products exhibited features in their ^1H and ^{13}C NMR spectra (chemical shifts, coupling constants and line shapes) as well

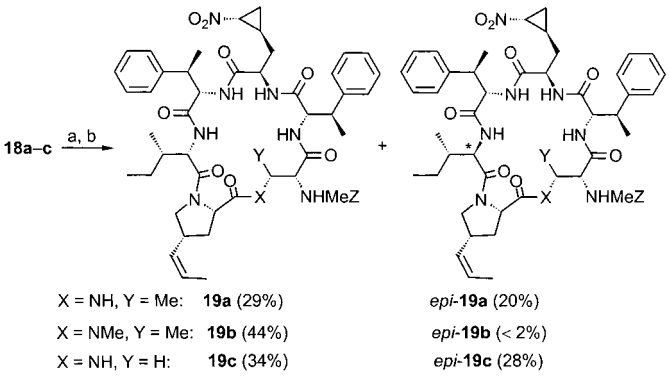

Scheme 3. Cyclization of the linear precursors **18a–c**. a) 2 M HCl, EtOAc, 20°C, 1 h (for **18a** and **18c**) or $Bu_4N^+F^-$, THF, 20 → 55°C, 2 h then 2 M HCl, in EtOAc, 20°C, 1 h (for **18b**). b) HATU, DIEA, TMP, CH_2Cl_2, 0.1 mM, 0 → 20°C, 18–22 h.

as optical rotation values quite different from those of **19a** and **19c** indicating distinctions in their solution structures.

The *N*-MeZ protected cyclohexapeptides were subsequently first deprotected and then coupled with *N*-Teoc-protected (2*S*,1′*R*,2′*R*)-(3-Ncp)Ala-OH[2a] (Scheme 4). Removal of the Teoc group and coupling of the intermediates with *O*-MOM protected Chpca-OH **20**[2a,10] gave the *O*-MOM protected hormaomycin aza-analogues. Finally, removal of the MOM group gave the target compounds **2a–c** and *epi*-**2a**.

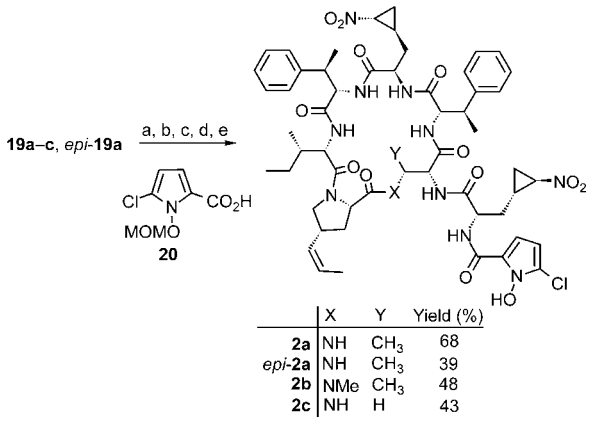

	X	Y	Yield (%)
2a	NH	CH_3	68
epi-**2a**	NH	CH_3	39
2b	NMe	CH_3	48
2c	NH	H	43

Scheme 4. The final steps in the preparation of aza-analogues **2a–c** and *epi*-**2a**. a) Anisole, TFA, 20°C, 2 h. b) Teoc-(2*S*,1′*R*,2′*R*)-(3-Ncp)AlaOH, HATU, HOAt, DIEA, TMP, CH_2Cl_2, 20°C, 15 h. c) TFA, 20°C, 1 h. d) **20**, HATU, HOAt, DIEA, TMP, CH_2Cl_2, 20°C, 4 h. e) $MgBr_2 \cdot Et_2O$, EtSH, CH_2Cl_2, 20°C, 3–4 h. Teoc = (2-trimethylsilylethyl)oxycarbonyl. Analogue *epi*-**2a** contains an (*R*)-*a*-Ile instead of an Ile moiety.

NMR analysis and conformational modelling of hormaomycin 1 and its all-peptide aza-analogue 2a: The conformational analysis of hormaomycin **1** was performed in $CDCl_3$ solution at 293 K. Spin systems were identified by DQF-COSY, TOCSY and ^{13}C-, ^1H-HMBC experiments. Especially useful for the assignment of the aromatic components were the long-range cross peaks between the H_β and the C_{ipso} as

well as the $H_{aromatic}$ and C_β, because they provided the correct assignment of the two phenyl rings of (βMe)Phe I and II.[13,16]

The χ_1 angles of each component were determined by the combined use of coupling constants from P.E. COSY and ^{13}C-HMBC experiments and distance information from ROESY experiments. A two proton example is the χ_1 dihedral angle of *allo*-(*R*)-threonine. In the HMBC spectrum, a strong $^3J_{CH}$ correlation from CO ($\delta = 169.2$ ppm) to the β proton ($\delta = 5.44$ ppm) is visible. This together with a $^3J(H_\alpha,H_\beta)$ value of 5 Hz is consistent with a g$^-$ arrangement of the two protons.

The chemical shift values of the components are shown in Table 1 of the Supporting Information. One-dimensional proton spectra showed one predominant resonance for each amide NH, suggesting either one dominant isomer or fast conformational averaging on the NMR time scale in $CDCl_3$. The coexistence of slowly interconverting conformers could be ruled out by the absence of exchange cross peaks in the ROESY spectra and the correct number of resonances in the 1D-proton spectrum.

The enantiotopic H_β protons of (3-Ncp)Ala I exhibited $\Delta\delta$ values >1.5 ppm indicating a well defined structure. This agrees with the large chemical shift dispersion within the set of NH (6.54–9.13 ppm) and H_α (3.51–5.16 ppm) proton signals. Especially the long-range ROE values between the aromatic protons of Chpca and (βMe)Phe I indicate a compact conformation.[13]

The presence of strong $H_\alpha(i)$–NH(i+1) ROE values and the absence of $H_\alpha(i)$–$H_\alpha(i+1)$ cross peaks confirmed that all the amide bonds are in the *s-trans* conformation.

An *s-trans* conformation with respect to the Ile–Pro peptide bond was assigned according to characteristic ROE cross peaks between the H_α (Ile) and the H_δ [(4-Pe)Pro] as well as the absence of cross peaks between H_α (Ile) and H_α [(4-Pe)Pro]. Additionally, the differences in ^{13}C NMR chemical shifts of C_β–$C_\gamma = -1.7$ ppm [(4-Pe)Pro], are indicative of *trans*-peptide bonds.[17] The difference, directly related to the dihedral angle ψ(Pro), is usually in the range of 2–10 ppm for *cis*-Pro and 0–5 ppm in *trans*-Pro. In (4-Pe)Pro residue of hormaomycin **1**, the (4*R*)-substituent further increases the C_γ chemical shift value.

Cyclic hexapeptides normally adopt an all-*trans*-conformation about the peptide bonds and prefer a conformation with two β turns.[18] The hypothesis that the number of amino acids in cyclopeptides influences the type of secondary structure adopted was later proved in a modified version.[19] However, major influences by the side chains, especially of non-typical amino acids, have not been taken into account. This made predictions of the solution structure of hormaomycin **1** difficult. In fact, hormaomycin **1** combines a cyclic portion with an extended side chain consisting of two components. In addition, the ring contains one ester linkage.

From the restrained MD simulations and energy minimizations, one family of low-energy structures was generated, satisfying the ROE-derived restraints and dihedral angles (Figure 2). No ROE violation greater than 0.5 Å was observed. Further details about the calculation and NMR input data are to be found in the Experimental Section.

The average root mean square deviation (RMSD) of the backbone atoms compared to the average structure was 0.39 Å and for all heavy atoms 0.71 Å.

The propenyl substituent of the (4-Pe)Pro unit of hormaomycin **1** is found antiperiplanar relative to the pyrrolidine nitrogen. It adopts an equatorial position (Figure 2). Allylic 1,3-strain directs the *cis*-propenyl side chain of (4-Pe)Pro into one plane with the γ-hydrogen of the pyrrolidine ring.

The observation of both NH(i)–NH(i+1) and $H_\alpha(i)$–NH(i+1) ROE values indicates that the peptolide backbone exists in a tight turn. A strong ROE between H_α [(βMe)Phe II] and NH [(3-Ncp)Ala I] together with a weak cross peak between H_α [(3-Ncp)Ala I] and NH [(βMe)Phe I] indicate a β turn [(βMe)Phe II, (3-Ncp)Ala I, (βMe)Phe I, Ile]. The CD curves with a positive maximum at 213 nm and a negative maximum around 240 nm already indicated the presence of a β turn.[2b]

The general criterium for the presence of a β turn is that the distance between $C_\alpha(i)$ and $C_\alpha(i+3)$ is less than 7 Å. Type II and type II′ β turns are further differentiated by their dihedral angles of the residues i+1 and i+2 (Table 1). The presence of a CO(i)–HN(i+3) hydrogen bond is possible, but not necessary for a stabilization of the β turn. The structure of hormaomycin **1** exhibits a $C_\alpha(i)$–$C_\alpha(i+3)$ distance of 7 Å for the components Ile and (βMe)Phe II. These two constitute the i and i+3 position (i+3 and i position) of two β turns in the structure of **1**. A γ turn can be excluded because the distances between H_α [(βMe)Phe II]–H_α [(βMe)Phe I] of 6.9 Å and H_α(Ile)–H_β(*a*-Thr) of 6.8 Å are too long.

A type II′ (inverse II) turn is formed with (βMe)Phe II at position i and with (3-Ncp)Ala I and (βMe)Phe I as the central residues (i+1) and (i+2), respectively. The presence of a $H_\alpha(i+1)$–HN(i+2) ROE and the absence of other HN–HN cross peaks differentiates this β turn from the other β turn of hormaomycin **1** which belongs to type II according to the corresponding dihedral angles (Table 1). The type II β turn is formed by Ile at the i position and (4-Pe)Pro and *a*-Thr as the central residues. Proline residues are typically found at the i+1 position of type I and type II β turns.

Table 1. Dihedral angles [°] of ideal β turns of type II and II′ and of the corner components of hormaomycin **1**.

	$\phi(i+1)$	$\psi(i+1)$	$\phi(i+2)$	$\psi(i+2)$
ideal type II	−60	+120	+80	0
ideal type II′	+60	−120	−80	0
(4-Pe)Pro, *a*-Thr	−61	+142	+90	−77
(3-Ncp)Ala I, (βMe)Phe I	+69	−134	−90	−47

Ideal β turns are ten-membered rings when the hydrogen bond is incorporated. In the case of hormaomycin **1**, the type II β turn is composed of (*R*)-*allo*-threonine at the ***i*+2** position and therefore contains the C_β as an additional atom.

Because of the unusual components and the overall structure that appears to be governed by long-range side-chain interactions, the β turns deviate from the ideal values. It is important to underline that the standard distances observed for turns in peptides and proteins containing only (*R*)- or (*S*)-residues cannot be used here.[20]

In general, distances in oligopeptides are strongly influenced by the configurations of the contained amino acids. (*S*)-Xaa-(*R*)-Yaa and (*R*)-Xaa-(*S*)-Yaa dyads have a high tendency to be in the corner positions of type II and type II′ turns, respectively. Indeed, the type II′ β turn in hormaomycin **1** is formed with the residue of (3-Ncp)Ala I [(*R*)-amino acid] in the corner position followed by (βMe)Phe I [(*S*)-amino acid].

With the oxygen of the ester linkage in **1** replaced by an NH in **2a**, the ϕ angle (+90°) of the *i*+2 residue (*a*-Thr) is almost identical with the ideal ϕ angle of a type II turn (+80°). The dihedral angle defined by O-C_α-C_β-CO (taken as $\psi(i+2)$) is substantially different from an ideal type II. It is therefore reasonable to refer to it as "type II-like". The dihedral angles at the *i*+1 position agree with the type II turn ($\phi=-61$ and $\psi=+142°$). The twisted nature of the β turns results in a figure-eight like overall structure for the macrocyclic ring (Figure 3).

Further corroboration of the structure is derived from the detailed analysis of the chemical shifts presented in the Experimental Section and Supporting Information.

The structure of a peptide is not only determined by the backbone conformation, but also the orientation of the side chains. Many conformational studies have shown that the rotamer distribution is the more shifted to a single rotamer, the more "rigid" the backbone is.[21] Hence, the side-chain conformation can be taken as an indicator for the rigidity of the molecule. The two aromatic rings of (βMe)Phe II and Chpca are stacked in-line with each other (Figure 2). The compact overall shape of hormaomycin **1** is dictated by these side-chain interactions which in turn allow only a rigid macrocyclic structure.

The assignments of proton and carbon resonances of the aza-analogue **2a** are compiled in Table 2 of the Supporting Information. Due to signal overlap two dihedral angles (H_α/$H_{3\beta}$ [(4-Pe)Pro] and H_γ/$H_{\delta\alpha}$ [(4-Pe)Pro] could not be determined. All the others, which have been determined for hormaomycin **1**, were also determined for **2a**. An identical range of values was obtained with only one differing dihedral angle in the side chain of isoleucin (C_α-C_β-C_γ-C_δ = +180° for **2a** and −60° for **1**). The side chain is therefore more directed to the solvent. The ROE values measured for **2a** differed only slightly, resulting in the same classification into strong, medium and weak as for hormaomycin **1**. An additional ROESY cross peak was observed between the HN attached to the C_β atom of the *a*-Dab unit and the protons of its methyl group.

The *s-trans*-conformation of all peptide bonds was confirmed by ROE cross peaks as established for hormaomycin **1**. Analogously, the ester linkage of *a*-Thr and (4-Pe)Pro in the calculated structure of hormaomycin **1** takes an *s-trans* orientation which is favored by the anomeric effect.

From the almost identical structural data obtained, one may conclude that the structure of the macrocyclic ring of the aza-analogue **2a** in solution does not differ from that of hormaomycin **1** (see Figure 4).

In general, cyclic peptides in which all the peptide bonds have *s-trans*-conformations lack internal motions in the backbone. This agrees with the present findings, that the modification in the macrocyclic ring from an ester to an amide linkage does not change the overall structure of the macrocycle. In the case of **2a**, the additional peptide bond also adopts an *s-trans*-conformation.

The investigation of the solution structure of the *N*-methyl-aza-analogue **2b** was considered to be useless because of an abundance of slowly equilibrating conformers. As the ^{1}H NMR spectrum of the *des*-methyl-aza-analogue **2c** is very similar to those of hormaomycin **1** and the aza-analogue **2a**, it is quite possible that this peptide in solution also adopts approximately the same overall conformation.

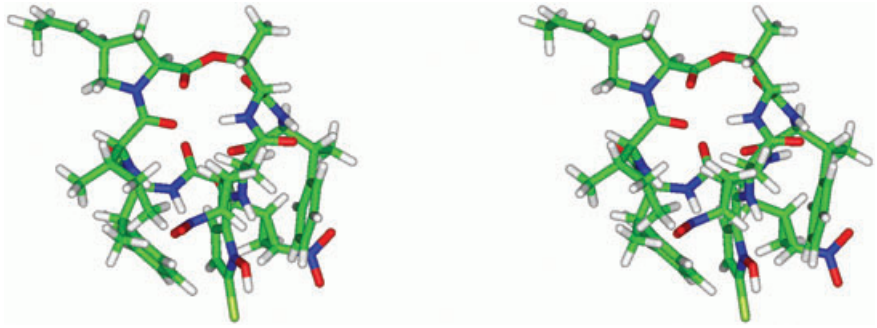

Figure 2. Stereoview of the average structure of hormaomycin **1** in $CDCl_3$.

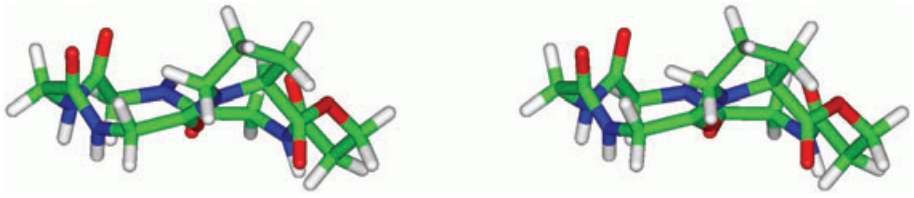

Figure 3. Stereoview of the macrocyclic ring of the average structure of hormaomycin **1** in $CDCl_3$.

Antibacterial activity: As an entry, the antibiotic activity of the new hormaomycin analogues against *Arthrobacter* species was tested (Tables 2, 3).[22]

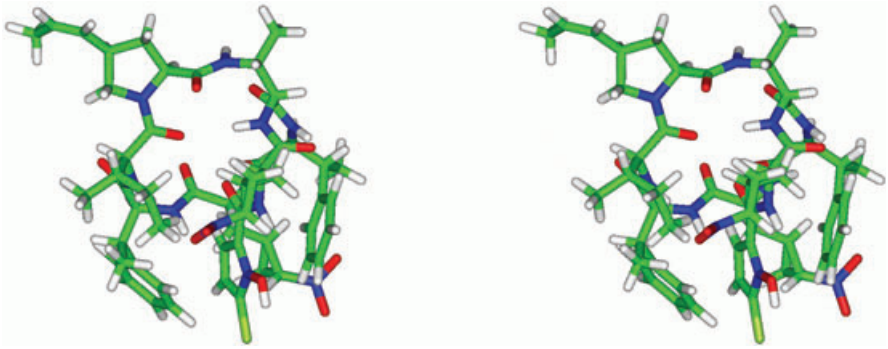

Figure 4. Average structure of the aza-analogous hormaomycin **2a**.

Table 2. Relative antibacterial activities of hormaomycin **1**, aza-analogues **2a** and *epi*-**2a** in serial dilution plate diffusion tests against *Arthrobacter crystallopoites* (strain 20117) (%) (estimated relative to the activity of hormaomycin at 5×10^{-2} mg per 9×0.5 mm plate) 28 °C.

Compound (mg pro plate)	5×10^{-2}	5×10^{-3}	5×10^{-4}	5×10^{-5}
hormaomycin **1**	100	94	71	39
2a	103	90	68	35
epi-**2a**	0	0	–	–

Table 3. Relative antibacterial activities of several compounds in serial dilution plate diffusion tests against *Arthrobacter oxidans* (strain 20119) (%) (estimated relative to the activity of hormaomycin at 1.5×10^{-2} mg per 6×0.65 mm plate) 28 °C.[23]

Compound (mg per plate)	1.5×10^{-2}	1.5×10^{-3}	1.5×10^{-4}
hormaomycin **1**	100	72	44
penicillin G	78	0	0
19a–c, *epi*-**19a**	0	–	–
epi-**19c**	22	0	0
2b	94	72	42
2c	94	83	58

Even these very preliminary biological tests give some information about structure–activity relationships for hormaomycin **1** and its analogues. At least the antibacterial activity of hormaomycin **1** can neither solely be attributed to its macrocyclic part nor to its side chain,[4b] but supposedly is associated with the whole molecule. The weak antibiotic activity of the cyclopeptide *epi*-**19c** may be due to a mode of action on bacteria which is different from that of hormaomycin **1**. The aza-analogues **2a–c** displayed spectral and solubility properties, as well as antibiotic activities very similar to those of the native compound **1**. In contrast, the *epi*-aza-analogue *epi*-**2a**, which exhibits CD and ^{1}H NMR spectra as well as solubility properties quite different from those of hormaomycin **1**, turned out to be totally inactive within the used test system.

Conclusion

We have synthesized several analogues of hormaomycin and investigated the structures of the title compound **1** and its aza-analogue **2a** by solution NMR experiments. The two structures turn out to be virtually identical. Consistent with this finding, **1** and **2a** exhibit similar antibiotic activities. The ^{1}H NMR spectra of *epi*-**2a** substantially differ from those of **1** and **2a** suggesting a different structure. Consistently, *epi*-**2a** is inactive in the antibiotic assay indicating that the conformation of the whole molecule is important for this biological activity.

Experimental Section

General remarks: Synthesis: ^{1}H NMR spectra: Bruker AM 250 (250 MHz), Varian Unity 300 (300 MHz), Varian Inova 600 (600 MHz). ^{1}H chemical shifts are reported in ppm relative to residual peaks of deuterated solvent or tetramethylsilane. Higher order NMR spectra were approximately interpreted as first-order spectra, if possible. The observed signal multiplicities are characterized as follows: s = singlet, d = doublet, t = triplet, q = quartet, quin = quintet, m = multiplet, as well as br = broad, Ar-H = aryl-H. ^{13}C NMR spectra [additional DEPT (Distortionless Enhancement by Polarization Transfer) or APT (Attached Proton Test)]: Bruker AM 250 (62.9 MHz), Varian Unity 300 (75.5 MHz) or Varian Inova 600 (125.7 MHz) instruments. ^{13}C chemical shifts are reported relative to peak of solvent or tetramethylsilane. The following abbreviations were applied: DEPT: + = primary or tertiary (positive signal in DEPT), − = secondary (negative signal in DEPT), C_{quat} = quaternary (no signal in DEPT); APT: + = primary or tertiary (positive signal in APT), − = secondary or quaternary (negative signal in APT); whenever it was necessary and possible HMBC (Heteronuclear Multiple Bond Connectivity) and/or HMQC (Heteronuclear Multiple Quantum Coherence) spectra were also measured. The signals marked with asterisk have been attributed with uncertain reliability. IR spectra: Bruker IFS 66 (FT-IR) spectrometer, samples measured as KBr pellets or oils between KBr plates. The IR spectra of all synthesized peptides showed a broad NH stretch band, arising from the amide moieties, between 3500 and 3250 cm^{-1}. MS: EI-MS: Finnigan MAT 95, 70 eV. High resolution EI-MS spectra with perfluorokerosene as reference substance; pre-selected ion peak matching at $R \geqslant 10000$ to be within ±2 ppm of the exact masses. ESI-MS: Finnigan LCQ. HPLC: pump: Kontron 322 system, detector: Kontron DAD 440, mixer: Kontron HPLC 360, data system: Kontron Kromasystem 200, columns: Knauer Nucleosil-100 C18 (analytical, 5 μm, 3 mm × 250 mm), preparative: A: Kromasil C18 (7 μm, 20 mm × 250 mm), B: Knauer Nucleosil-100 C18 (5 μm, 8 mm × 250 mm). Optical rotations: Perkin–Elmer 241 digital polarimeter, 1 dm cell; optical rotation values are given in 10^{-1} deg cm^2 g^{-1}; concentrations (c) are given in g per 100 mL. Circular dichroism: Jasco J 500 A. Molar ellipticities (Θ) are given in degree cm^2 10^{-1} mol^{-1}. M.p.: Büchi 510 capillary melting point apparatus, uncorrected values. TLC: Macherey–Nagel precoated sheets, 0.25 mm Sil G/UV$_{254}$. The chromatograms were viewed under UV light and/or by treatment with phosphomolybdic acid (10% in ethanol), or ninhydrin (0.2% in ethanol), or Ehrlich's reagent (freshly prepared solution of 1 g of 4-dimethylamino-benzaldehyde in 25 mL of 36% HCl and 75 mL methanol). Column chromatography: Merck silica gel, grade 60, 230–400 mesh and Baker silica gel, 40–140 mesh. Preparative TLC: Macherey–Nagel, silica gel SIL G/UV$_{254}$, layer thickness 0.25 mm (100 × 200 mm or 200 × 200 mm). Elemental analyses: Mikroanalytisches Laboratorium des Instituts für Organische und Biomolekulare Chemie der Universität Göttingen. Starting materials: Anhydrous solvents were pre-

pared according to standard methods by distillation over drying agents and were stored under argon. All other solvents were distilled before use. All reactions were carried out with magnetic stirring and, if air or moisture sensitive, in flame-dried glassware under argon or nitrogen. Organic extracts were dried with anhydrous $MgSO_4$. *tert*-Butyl (2*R*,3*R*)-2-azido-3-(benzyloxycarbonylamino)butyrate (**4**),[6] *tert*-butyl (2*R*,3*R*)-2-*tert*-butyloxycarbonylamino-3-(9-fluorenylmethyloxycarbonylamino)butyrate (**5**),[7] *tert*-butyl (2*S*,3*R*)-2-*tert*-butyldimethylsilyloxy-3-(benzyloxycarbonyl-*N*-methylamino)butyrate (**8**),[8] (2*S*,4*R*)-(N-*tert*-butyloxycarbonyl)-4-(*Z*)-propenylproline (**14**),[10] 1-hydroxy-7-aza-benzotriazole,[24] tetrapeptides **16**[2a] and **17**,[25] (2*S*,1′*S*,2′*R*)-[*N*-(2-trimethylsilyl)ethyloxycarbonyl]-(2′-nitrocyclopropyl)alanine,[2a] 5-chloro-1-methoxymethoxypyrrole-2-carboxylic acid (**20**)[10] were prepared as described elsewhere. Conformational analysis NMR studies: NMR spectra were recorded on Bruker DRX400 and DRX600 spectrometers. The concentration was 5 mM in $CDCl_3$ and measurements were run at 293 K. The assignments were carried out with the help of standard DQF-COSY (Double-Quantum Filtered Correlation Spectroscopy), TOCSY (Total Correlation Spectroscopy), ^{13}C-HSQC, ^{15}N-HSQC and ^{13}C-HMBC experiments. Typically 2 K data points in *F*2 and 512 experiments in *F*1 were acquired. In some cases, additional ROESY experiments were used to confirm the assignments made. The spectra were acquired with 16 transients and a relaxation delay of 2 s except the ROESY experiments with 80 transients. For ROESY experiments, a spinlock field of 3.1 kHz was used with a mixing time of 480 ms.[26] The TOCSY experiments were performed with a spinlock field of 6.25 kHz by using the MLEV17 sequence with mixing times of 40 and 80 ms. The data were zero filled and processed as a 4 K × 1 K matrix. P.E. COSY experiments were processed as an 8 K × 2 K matrix. To obtain the temperature coefficients of the amide proton chemical shifts, TOCSY spectra were recorded between +15 and +45 °C. To determine the χ_1 torsional angle constraints, the H_α–H_β coupling constants ($^3J_{\alpha\beta}$) from the 1D proton and P.E. COSY spectra, the intensity of the intraresidue ROEs (H_α–H_β, NH–H_β) and the intensity of the $^3J_{CH}$ HMBC cross peaks were used. Each amino acid residue was classified with respect to three rotamers, according to the patterns of the $^3J_{HH}$, $^3J_{CH}$ and ROE values. The stereospecific assignments were also established for the β-methylene protons. Assuming that the staggered rotamers are predominantly populated, qualitative considerations together with homonuclear coupling constants[13] are often sufficient for the assignment of diastereotopic methylene protons (Figure 1). The χ_1 angle was set at −60° when both the $^3J(H_\alpha$–$H_{\beta1})$ and the $^3J(H_\alpha$–$H_{\beta2})$ coupling constants are small. If one strong and one weak coupling is observed, χ_1 can be either 60 or 180°. To differentiate between these two cases, stereospecific assignments of the H_β protons are required. This was possible with the help of qualitative heteronuclear *J* couplings (between ^{13}CO and H_β) and ROE cross-peak intensities stemming from the different H_β protons. In this way a set of dihedral angles was obtained and this together with the ROE-derived distances was the input for a molecular modelling (MD) study.[13] *Molecular dynamics*: All molecular mechanics/dynamics simulations were performed with DISCOVER of Insight II (Accelrys) on a Silicon Graphics Octane workstation. The simulations were done using CVFF (Consistent Valence Force Field).[27] A distance-dependent dielectric constant ($\varepsilon = 4.8\,r$) was used. The molecular structure was first minimized. During a 100 ps MD run, 100 structures were sampled which represent starting conformations for the subsequent restrained MD. According to a simulated annealing approach, the resulting starting molecules were heated to 600 K initially, subsequently cooled and finally subjected to an energy minimization using both steepest descent and conjugate gradient methods successively.[28] The final structures were analyzed for similarities by comparing the RMSD deviations.

The distance and torsional angle constraints of Tables 3 and 4 in the Supporting Information were used as restraints in the MD runs as well as the final minimizations. Pseudo-atoms were used for the methyl protons and aromatic protons. Distance restraints derived from ROE-cross peaks, classified empirically as strong, medium and weak, were applied as biharmonic restraints with lower and upper boundaries of 2.0–2.8, 2.0–3.5, 2.0–5.0 Å, respectively. The configurations at the stereogenic carbon atoms were restrained.[13] Likewise, due to the detected *trans*-conformation of all peptide bonds, the ω dihedral angle was restrained to 180°.

Structural validation: The following four interresidual ROEs have not been used in the calculations for cross validation purposes [Chpca 3-H and (βMe)Phe I $H_{aromatic}$, (βMe)Phe II $H_{aromatic}$ and (3-Ncp)Ala I 3′-H_A, (βMe)Phe II $H_{aromatic}$ and (3-Ncp)Ala I 6-H_A, (βMe)Phe II $H_{aromatic}$ and (3-Ncp)Ala I NH]. In the average structure the corresponding distances are 3.8, 4.6, 5.2, and 3.5 Å, respectively, which reasonably agree with the measured ROE values. There is an upfield chemical shift of the β-proton of (βMe)Phe II (3.04 ppm) compared with that of the corresponding proton in (βMe)Phe I (3.72 ppm), which can be explained by the anisotropy effect of the pyrrole ring. This effect requires a specific folding of the two-residue side chain. Additional anisotropy effects are seen for the methyl protons of the Ile residue exerted by the pyrrole ring of Chpca and for the protons of the (3-Ncp)Ala I side chain by the neighboring aromatic ring of (βMe)Phe I. The large downfield shift of the amide proton of (3-Ncp)Ala II (8.14 ppm) compared with NH of (3-Ncp)Ala I may be due to an H-bonding interaction with the oxygen of Chpca. All amide protons of the macrocyclic ring show low temperature chemical shift values (all $< +/-1$ ppb/°C except NH [(βMe)Phe I]: −3 ppb per °C) indicating shielding from solvent or H-bonding. Data have been submitted to PDB (Protein Data Bank) and BMRB (BioMagResBank).

Biological tests were carried out as described elsewhere.[16b]

Deprotection of *N*-Fmoc-protected amino acids 7a and 7b, and peptides 16 and 17—General procedure (GP 1): The protected amino acids or peptides (1 mmol) were taken up with acetonitrile or THF (2 mL), diethylamine (2 mL) was added, and the resulting mixture left at ambient temperature for 40 min. All volatiles were evaporated under reduced pressure, the residue was taken up with toluene (2 × 5 mL), which was evaporated under reduced pressure to remove the last traces of diethylamine. The obtained crude *N*-deprotected amino acids or peptides were directly used in the next condensation step.

Peptide condensation step for the preparation of dipeptide acids 15a–c—General procedure (GP 2): EDC (1.03 mmol) and HOAt (1.05 mmol) were added to a cooled (4 °C) solution of the *N*-Boc-protected 4-(*Z*)-propenylproline **14** (1 mmol) in anhydrous CH_2Cl_2 (3 mL). After 10 min, the solution of the appropriate crude N_β-deprotected diamino ester (0.97 mmol) and TMP (3 mmol) in anhydrous CH_2Cl_2 (1 mL) was added at the same temperature (in the case of **7c**·HCl two additional equivalents of TMP were used). The temperature was allowed to reach 20 °C, and stirring was continued for 6 h. Then the reaction mixture was diluted with Et_2O or EtOAc (30 mL), and the mixture washed with 1 M $KHSO_4$ (3 × 5 mL), water (2 × 5 mL), saturated aqueous solution of $NaHCO_3$ (3 × 5 mL), water (3 × 5 mL), brine (2 × 5 mL), dried and concentrated under reduced pressure. The residue was purified by column chromatography and recrystallization to give the respective dipeptide esters.

Hydrolysis step for the preparation of dipeptide acids 15a–c—General procedure (GP 3): A 40% aqueous solution of tetra-*n*-butylammonium hydroxide (0.15 mmol) was added dropwise to an ice-cold solution of the respective dipeptide ester (0.10 mmol) in THF (0.91 mL) within 3 min, and stirring was continued at the same temperature for an additional 45 min (TLC monitoring to detect complete consuming of the starting material). A 1 M aqueous H_2SO_4 (0.5 mL) was then added, and the mixture was diluted with Et_2O (50 mL). The organic layer was separated and washed with 1 M $KHSO_4$ (2 × 10 mL), water (5 × 10 mL), brine (2 × 5 mL), dried and filtered. The filtrate was concentrated under reduced pressure to give the crude product which was purified by column chromatography or/and recrystallization.

Peptide condensation step for the preparation of the branched hexapeptides 18a–c—General procedure (GP 4): Tetrapeptide **16** or **17** (0.21 mmol) was deprotected according to GP 1, taken up with anhydrous CH_2Cl_2 (5 mL), the respective dipeptide acid (0.23 mmol), HATU (0.25 mmol) and HOAt (0.23 mmol) were added, and the reaction mixture was cooled to 4 °C. After this, a solution of DIEA (29 mg, 0.22 mmol) and TMP (75 mg, 0.62 mmol) in CH_2Cl_2 (2 mL) were added at the same temperature within 5 min. The temperature was allowed to reach 20 °C, and stirring was continued for an additional 15 h. The crude product obtained after aqueous work-up, according to GP 2, was finally purified by recrystallization and/or column chromatography.

Preparation of *N*-MeZ-protected cyclohexapeptides 19a–c, *epi*-19a and *epi*-19c—General procedure (GP 5): 2M HCl in EtOAc (2 mL) was added to the appropriate branched hexapeptide (0.10 mmol); the reaction mixture was stirred at 20°C for 1 h in a dark place, and was then concentrated under reduced pressure at 20°C. The residue was triturated with anhydrous Et_2O (2×5 mL) to give the hydrochloride of the deprotected material as a colorless solid, which was taken up with anhydrous CH_2Cl_2 (1.0 L). The solution was cooled to 4°C (internal temperature), HATU (0.103 mmol) and HOAt (0.10 mmol) were added, and then a solution of DIEA (0.40 mmol) in CH_2Cl_2 (50 mL) was added over 30 min. The cooling bath was removed and stirring continued for an additional 2 h at ambient temperature. Then the reaction mixture was cooled again to 4°C, and a second portion of each, HATU (0.103 mmol) and HOAt (0.10 mmol), was added, and then a solution of DIEA (0.40 mmol) in CH_2Cl_2 (50 mL) was added within 30 min. The temperature was allowed to reach 20°C, and stirring was continued for 15 h. After this, the solvent was removed under reduced pressure, the residue was taken up with Et_2O, and after the usual aqueous work-up (GP 2) and concentration under reduced pressure, the crude product was purified first by column chromatography and then by recrystallization (Et_2O/pentane) to give a mixture of the epimeric cyclopeptides, which was separated by preparative HPLC to give the respective cyclohexapeptides.

Deprotection of *N*-MeZ protected cyclohexapeptides 19a–c and *epi*-19a—General procedure (GP 6): The *N*-MeZ-protected cyclopeptides (18 μmol) were deprotected by treatment with 10% anisole in TFA (1.1 mL) in the dark at ambient temperature for 2 h. All volatiles were removed under reduced pressure (0.05 Torr) at 20°C. The residues were triturated with hexane (6×5 mL) and dried to give the deprotected materials as trifluoroacetates, which were directly used in the next condensation step.

Deprotection of *O*-MOM protected hormaomycin aza-analogues *O*-MOM-2a–c and *epi*-*O*-MOM-2a—General procedure (GP 7): The respective *O*-MOM protected hormaomycin analogue (15 μmol) was deprotected by treatment with $MgBr_2{\cdot}Et_2O$ (0.30 mmol) and EtSH (0.10 mmol) in CH_2Cl_2 (10 mL) at ambient temperature for 3 h. The mixture was taken up with Et_2O (40 mL) and washed with 1N $KHSO_4$ (3×10 mL), water (4×10 mL), brine (2×5 mL), dried, filtered and concentrated under reduced pressure. The residue was recrystallized from CH_2Cl_2/pentane to give the respective hormaomycin analogue, which, if necessary, was further purified by preparative HPLC. The fraction containing the desired product was collected, and its pH value was carefully adjusted to 6.9 (pH meter) with diluted aqueous ammonia, and then it was lyophilized. The residue was dissolved in EtOAc (10 mL), the solution was washed with water (3×5 mL), dried and filtered. Removal of the solvent under reduced pressure gave the pure hormaomycin aza-analogue.

Methyl (2*R*,3*R*)-2-amino-3-(9-fluorenylmethyloxycarbonylamino)butyrate hydrochloride: Boc-*a*-Dab(Fmoc)-O*t*Bu **5** (0.39 g, 0.79 mmol) was deprotected with TFA (5 mL) for 1 h. All volatiles were removed under reduced pressure at 20°C. The solid residue was taken up with 1M HCl (5 mL) and methanol (20 mL) and after 10 min the mixture was concentrated to give the crude H-*a*-Dab(Fmoc)-OH·HCl (0.31 g, 100%), which was dried at 0.02 Torr at ambient temperature for 16 h, and used for the next step without further purification. $SOCl_2$ (0.60 mL, 8.27 mmol) was added dropwise to a solution of the crude amino acid hydrochloride (0.31 g, max 0.79 mmol) in anhydrous methanol (35 mL) at −20°C for 5 min and stirring was continued at the same temperature for an additional 15 min. The mixture was then allowed to warm to 20°C, and, after stirring at this temperature for 1 h, the reaction flask was sealed, and the mixture was heated t 50°C with stirring for an additional 20 h. The reaction mixture was then concentrated under reduced pressure, and the residue was triturated with Et_2O to give the crude title compound (0.29 g, max. 94%) as a colorless solid. R_f=0.30 (MeOH/$CHCl_3$ 1:100); ^{1}H NMR (250 MHz, CD_3OD): δ=1.36 (d, J=7 Hz, 3H, H-4), 3.97 (s, 3H, OMe), 4.16–4.34 (m, 3H, 2-H and 9″-H, 1′-H_a), 4.40–4.59 (m, 2H, 3-H, 1′-H_b), 7.27–7.50 (m, 4H, Ar-H), 7.54 (d, J=6.8 Hz, 1H, NH), 7.70 (d, J=7.3 Hz, 2H, Ar-H), 7.84 (d, J=7.3 Hz, 2H, Ar-H).

MeZ-*a*-Dab(Fmoc)-OMe (6): $NaHCO_3$ (0.156 g, 1.85 mmol) and then a solution of MeZOSu (0.244 g, 0.93 mmol) in acetone (5 mL) were added to a vigorously stirred solution of H-*a*-Dab(Fmoc)-OMe·HCl (0.29 g, max. 0.74 mmol) in water (7 mL), and stirring was continued for 90 min (if a precipitate formed, acetone and/or water was added to obtain a homogeneous solution). The mixture was then concentrated under reduced pressure, diluted with water (40 mL), and the resultant suspension was filtered. The crude product was washed with Et_2O/pentane 1:1 (50 mL), water (100 mL), 3% $NaHCO_3$ (50 mL), water (20 mL), 1M HCl, water (50 mL), pentane (50 mL), dried and finally recrystallized from CH_2Cl_2/hexane to give **6** (0.272 g, 69% over three steps) as a colorless solid. M.p. 167–168°C; $[\alpha]_D^{20}$=8.5 (c=0.40, THF); ^{1}H NMR (250 MHz, $CDCl_3$): δ=1.47 (d, J=6.8 Hz, 3H, 4-H), 2.34 (s, 3H, 1′-H, *MeZ*), 3.77 (s, 3H, OMe), 4.10–4.51 (m, 4H, 3-H and 9′-H, 1-H, *Fmoc*), 4.60 (dd, J=8.1, 3.1 Hz, 1H, 2-H), 5.08 (s, 2H, Bzl-H), 5.32 (d, J=8.0 Hz, 1H, NH), 5.67 (d, J=6.8 Hz, 1H, NH), 7.16 (d, J=7.3 Hz, 2H, Ar-H), 7.21–7.46 (m, 6H, Ar-H), 7.61 (d, J=6.8 Hz, 2H, Ar-H), 7.77 (d, J=7.3 Hz, 2H, Ar-H); ^{13}C NMR (62.9 MHz, $CDCl_3$): δ=16.3 (+, C-4), 21.0 (+, C-1′, *MeZ*), 47.0 (+, C-3), 48.9 (+, C-9′, *Fmoc*), 52.5 (+, OMe), 57.8 (+, C-2), 66.8 (−, Bzl-H, *MeZ*), 67.1 (−, C-1, *Fmoc*), 119.8, 125.0, 126.9, 127.5, 128.3, 129.1 (+, Ar-C), 132.8 (C_{quat}, Ar-C), 137.9 (C_{quat}, Ar-C), 141.1 (C_{quat}, Ar-C), 143.7, 143.9 (C_{quat}, Ar-C), 155.8, 156.4 (C_{quat}, NCO_2), 170.7 (C_{quat}, C-1); IR (KBr): $\tilde{\nu}$=3316, 3067, 2948, 1748, 1691, 1542, 1450, 1338, 1316, 1282, 1231, 1169 cm^{-1}; MS (EI, 70 eV): m/z (%): 502 (1) [M^+], 266 (10) [$C_{14}H_{20}NO_4^+$], 178 (100) [$C_{14}H_{10}^+$], 165 (5), 105 (22) [$C_8H_9^+$], 44 (11) [CO_2^+]; HRMS (EI): m/z: calcd for $C_{29}H_{30}N_2O_6$: 502.2104, correct mass found; elemental analysis calcd (%) for $C_{29}H_{30}N_2O_6$ (502.6): C 69.31, H 6.02, N 5.57; found C 69.08, H 5.88, N 5.38.

Methyl (2*S*,3*R*)-3-(benzyloxycarbonyl-*N*-methylamino)-2-hydroxybutyrate: A solution of the *O*-TBDMS, NMe-Z protected *tert*-butyl ester of (*S*)-isothreonine **8** (0.73 g, 1.67 mmol) in MeCN (38 mL) was treated with 5% aqueous HF (40 mL) at 4°C for 10 min. The mixture was allowed to warm to 20°C, and stirring was continued for an additional 4 h. A saturated aqueous solution of $NaHCO_3$ was then carefully added to adjust the pH value to about 8, and the mixture was extracted with Et_2O (2×50 mL). The organic fraction was washed with water (5×20 mL), brine (2×10 mL), dried, filtered and concentrated under reduced pressure. The resultant crude alcohol was dried at 0.02 Torr for 2 h and then deprotected by treatment with TFA (6 mL). After 1 h, all volatiles were removed under reduced pressure, the residue was dissolved in toluene (2×20 mL), which was distilled off to remove the last traces of TFA to give the crude (2*S*,3*R*)-3-(benzyloxycarbonyl-*N*-methylamino)-2-hydroxybutyric acid (0.42 g, max. 94%). It was dried at 0.02 Torr and ambient temperature for 2 h, then taken up with Et_2O (10 mL; some methanol was added to obtain a homogeneous solution) and the mixture was treated with an excess of an ethereal solution of diazomethane untill a yellow coloration of the reaction mixture persisted. The mixture was then concentrated under reduced pressure, and the residue was purified by column chromatography to give the title compound (0.361 g, 71% over two steps; R_f=0.22, EtOAc/hexane 1:3) as a turbid oil, which was directly used for the next step without any further characterization.

Methyl (2*S*,3*R*)-2-azido-3-(benzyloxycarbonyl-*N*-methylamino)butyrate (9): Mesyl chloride (0.14 mL, 1.81 mmol) was added dropwise to a solution of the NMe-Z protected (*S*)-isothreonine methyl ester (0.36 g, 1.28 mmol) and TEA (0.254 mL, 1.81 mmol) in CH_2Cl_2 (7 mL) at −30°C for 3 min, and stirring was continued at the same temperature for 1 h. The reaction mixture was then allowed to warm to 4°C and stirred at this temperature for an additional 1 h. Finally, the cooling bath was removed, and stirring was continued for an additional 3 h. Saturated aqueous solution of $NaHCO_3$ (3 mL) was then added, and the mixture was taken up with Et_2O (50 mL). After the usual aqueous work-up (GP 2) the organic layer was dried, filtered and concentrated under reduced pressure to give the crude mesylate of NMe-Z protected (*S*)-isothreonine methyl ester (0.46 g, 100%; R_f=0.11, EtOAc/hexane 1:6) as a colorless oil. NaN_3 (0.086 g, 1.32 mmol) was added to a solution of this compound (0.46 g, 1.28 mmol) in DMF (8 mL), and stirring continued at 70°C for 15 h. The mixture was then cooled, concentrated under reduced pressure, and the residue was taken up with Et_2O (50 mL). After the usual aqueous work-up (GP 2) the organic layer was dried, filtered and concentrated under

reduced pressure. The resultant crude product was purified by column chromatography (EtOAc/hexane 1:6, $R_f = 0.19$) to give **9** (0.191 g, 49% over two steps) as a mobile colorless oil, which was directly used for the next step without any further characterization.

Boc-*a*-N$_\beta$Dab(Fmoc)-OMe: Ph_3P (0.262 g, 1.00 mmol) was added to a solution of **9** (0.191 g, 0.62 mmol) in THF/H_2O (20:1) (15.8 mL), the resultant mixture was stirred for 24 h. Boc_2O (0.272 g, 1.25 mmol) was then added, and stirring was continued for an additional 24 h. The mixture was then concentrated, and the residue was purified by column chromatography (twice, hexane 1:4, $R_f = 0.22$) to give the N_β-methylated Boc-*a*-Dab(Z)-OMe (0.135 g, 57%) as a viscous colorless oil. This material (0.135 g, 0.35 mmol) in EtOAc (7 mL) was hydrogenated at ambient pressure of hydrogen over 10% Pd on charcoal (0.07 g) for 3 h. The mixture was then filtered and concentrated under reduced pressure to give the crude Boc-*a*-N$_\beta$MeDab-OMe (90 mg, 100%), which was immediately used for the next step. FmocOPfp (0.159 g, 0.39 mmol) was added to a solution of this material, TMP (43 mg, 0.35 mmol), and HOAt (10 mg, 74 μmol) in EtOAc (5 mL) were added and stirring was continued for 15 h. The mixture was then diluted with Et_2O (50 mL) and subjected to the usual aqueous work-up (GP 2). The organic layer was dried, filtered and concentrated under reduced pressure. The residue was purified by column chromatography (EtOAc/hexane 1:4, $R_f = 0.22$) to give the N_β-methylated Boc-*a*-Dab(Fmoc)-OMe (0.135 g, 81% over two steps) as a colorless oil, which was directly used for the next step without any further characterization.

MeZ-*a*-N$_\beta$Dab(Fmoc)-OMe (10): Boc-*a*-N$_\beta$Dab(Fmoc)-OMe (0.135 g, 0.29 mmol) was deprotected with 2 M HCl in EtOAc (4 mL) for 3 h. The mixture was then concentrated under reduced pressure, and the residue was dissolved in MeCN (4 mL). TMP (45 mg, 0.37 mmol), DIEA (37 mg, 0.29 mmol) and finally MeZOSu (83 mg, 0.32 mmol) were added to this solution, and it was stirred for 16 h. *N*,*N*-Dimethylaminopropylamine (20 mg, 0.20 mmol) was then added, and after 10 min the mixture was concentrated under reduced pressure. The residue was taken up with Et_2O and subjected to the usual aqueous work-up (GP 2). The organic layer was dried, filtered and concentrated under reduced pressure. The resultant crude product was purified by column chromatography (EtOAc/hexane 1:3, $R_f = 0.30$) to give **10** (0.122 g, 13% overall yield over 10 steps from **8**) as a turbid glass. $[\alpha]_D^{20} = 9.2$ ($c = 0.25$, $CHCl_3$); ^{1}H NMR (300 MHz, $CDCl_3$): $\delta = 1.16$, 1.25 (2 × d, $J = 6.9$ Hz, 3H, 4-H), 2.33 (s, 3H, 1′-H, *MeZ*), 2.81 (s, 3H, NMe), 3.66 (s, 3H, OMe), 4.12–4.61 (m, 5H, 2-H, 3-H and 9′-H, 1-H, *Fmoc*), 5.06 (d, $J = 5.1$ Hz, 2H, Bzl-H), 5.31, 5.60 (2 × d, $J = 7.5$ Hz, 1H, NH), 7.15 (d, $J = 7.8$ Hz, 2H, 2-H, *MeZ*), 7.24 (d, $J = 7.8$ Hz, 2H, 3-H, *MeZ*), 7.31 (dd, $J = 7.5$, 7.5 Hz, 2H, 3′-H, *Fmoc*), 7.40 (dd, $J = 7.5$, 7.5 Hz, 2H, 4′-H, *Fmoc*), 7.58–7.64 (m, 2H, 2′-H, *Fmoc*), 7.76 (d, $J = 7.2$ Hz, 5′-H, *Fmoc*); ^{13}C NMR (50.3 MHz, $CDCl_3$): $\delta = 14.3$ (+, C-4), 21.0 (+, C-1′, *MeZ*), 28.9 (+, NMe), 47.1 (+, C-3), 52.4 (+, C-2), 52.9 (+, C-9′, *Fmoc*), 56.6 (+, OMe), 67.0 (−, Bzl-H, *MeZ*), 67.5 (−, C-1, *Fmoc*), 119.8, 124.9, 126.9, 127.5, 128.2, 129.1 (+, Ar-C), 133.0 (C_{quat}, Ar-C), 137.9 (C_{quat}, Ar-C), 141.2 (C_{quat}, Ar-C), 143.8, 143.9 (C_{quat}, Ar-C), 155.9, 156.4 (C_{quat}, NCO_2), 170.9 (C_{quat}, C-1); IR (KBr): $\tilde{\nu} = 2951$, 1751, 1725, 1700, 1521, 1451, 1320, 1273, 1242, 1204, 1018 cm^{-1}; MS (ESI pos.): *m*/*z*: 539 (100) [*M*+Na$^+$].

MeZ-(*R*)-Asn-OH (12): $NaHCO_3$ (0.520 g, 6.18 mmol) and then a solution of MeZOSu (0.775 g, 2.97 mmol) in acetone (7 mL) were added to a vigorously stirred solution of D-aspargine (0.442 g, 2.94 mmol) in water (10 mL), and stirring was continued for 3 h (if a precipitate formed, acetone and/or water was added to obtain a homogeneous solution). The mixture was then concentrated under reduced pressure, diluted with water (40 mL) and washed with CH_2Cl_2 (3 × 10 mL). The pH of the water fraction was adjusted to 1–2 with solid $KHSO_4$, the resulting precipitate was filtered off, washed with H_2O (5 × 20 mL), Et_2O (5 × 20 mL) and dried to give **12** (0.75 g, 91%) as a colorless solid. M.p. 181–183 °C; $[\alpha]_D^{20} = 6.5$ ($c = 1.00$, DMF); ^{1}H NMR (250 MHz, [D$_6$]acetone): $\delta = 2.30$ (s, 3H, 1′-H), 2.50–3.55 (br, 3H, CO_2H, $CONH_2$), 2.65–2.85 (m, 2H, 3-H), 4.39–4.53 (m, 1H, 2-H), 5.03 (s, 2H, Bzl-H), 6.39–6.61 (br, 1H, NH), 7.15 (d, $J = 8.0$ Hz, 2H, Ar-H), 7.26 (d, $J = 8.0$ Hz, 2H, Ar-H); ^{13}C NMR (125.7 MHz, [D$_6$]DMSO): $\delta = 20.7$ (+, C-1′), 36.7 (−, C-3), 50.5 (+, C-2), 65.3 (−, Bzl-H), 127.8 (+, Ar-C), 128.8 (+, Ar-C), 133.8 (C_{quat}, Ar-C), 137.0 (C_{quat}, Ar-C), 155.7 (C_{quat}, NCO_2), 170.7 (C_{quat}, C-1), 173.0 (C_{quat}, C-4); IR (KBr): $\tilde{\nu} = 3419$, 3355, 3214, 3099, 3030, 2989, 2973, 2929, 2827, 2741, 2629, 2533, 1721, 1692, 1645, 1586, 1526, 1346, 1237, 1199, 1183, 1154, 1126 cm^{-1}; MS (EI, 70 eV), *m*/*z* (%): 280 (20) [*M*$^+$], 263 (3) [*M*$^+$ −OH], 159 (8) [$C_5H_7N_2O_4^+$], 122 (46) [$C_8H_{10}O^+$], 105 (100) [$C_8H_9^+$], 87 (16) [$C_3H_7N_2O^+$], 77 (10) [$C_6H_5^+$], 44 (6) [CO_2^+]; elemental analysis calcd (%) for $C_{13}H_{16}N_2O_5$ (280.3): C 55.71, H 5.75, N 9.99; found C 55.97, H 5.73, N 10.08.

MeZ-Dap-OH (13): Iodobenzene bis(trifluoroacetate) (1.46 g, 3.40 mmol) and **12** were suspended by stirring in 50% (*v*/*v*) aqueous DMF (20 mL). After 15 min, pyridine (0.367 g, 4.64 mmol) was added, and the mixture was stirred for an additional 5 h. The emulsion formed was evaporated at 40–45 °C under reduced pressure. The residue was taken up with water (2 × 15 mL), which was evaporated under reduced pressure. The residual oil was taken up in water (50 mL) and washed with chloroform (3 × 10 mL). The aqueous layer was once more concentrated in vacuo, and the residue was dissolved in ethanol (20 mL). The pH value was adjusted to about 7 with pyridine, and the formed suspension was left at 4 °C for 12 h. The precipitate was filtered off and washed with ether (5 × 20 mL) to give, after drying, amino acid **13** (0.51 g, 87%) as a colorless powder. $R_f = 0.32$ (MeCN/AcOH/H_2O 10:1:1); m.p. 210–216 °C (decomp.); $[\alpha]_D^{20} = 38.1$ ($c = 0.31$, 0.1 N HCl); ^{1}H NMR (300 MHz, DCl in D_2O): $\delta = 2.28$ (s, 3H, 1′-H), 3.28 (dd, $J = 12.6$, 9.6 Hz, 1H, 3-H$_a$), 3.49 (dd, $J = 12.6$, 4.5 Hz, 1H, 3-H$_b$), 4.44–4.55 (m, 1H, 2-H), 5.07 (s, 2H, Bzl-H), 7.22 (d, $J = 7.5$ Hz, 2H, Ar-H), 7.28 (d, $J = 7.5$ Hz, 2H, Ar-H); IR (KBr): $\tilde{\nu} = 3303$, 3250–2300, 1695, 1658, 1623, 1592, 1540, 1413, 1273, 1022 cm^{-1}; MS (ESI pos.): *m*/*z*: 275 (86) [*M*+Na$^+$], 253 (12) [*M*+H$^+$]; neg.: *m*/*z*: 251 (10) [*M*−H$^-$]; elemental analysis calcd (%) for $C_{12}H_{16}N_2O_4$ (252.3): C 57.13, H 6.39, N 11.10; found C 56.95, H 6.20, N 10.97.

MeZ-Dap-OMe·HCl (7c·HCl): To a solution of thionyl chloride (0.52 mL, 7.26 mmol) in anhydrous MeOH (10 mL) at −20 °C was added with stirring after 10 min the amino acid **13** (0.50 g, 1.98 mmol). The resulting thick suspension was stirred at 20 °C for 24 h to give a clear solution, which was then left at −28 °C for 16 h. Et_2O (40 mL) was added to complete the precipitation, and the solid was filtered off to give **7c**·HCl (0.47 g, 78%) as long colorless needles. The mother liquor was concentrated, and the residue was recrystallized from MeOH/Et_2O to give a second crop of **7c**·HCl (26 mg, 83% overall yield). M.p. 159–161 °C; $[\alpha]_D^{20} = 32.3$ ($c = 0.86$, DMSO); ^{1}H NMR (250 MHz, [D$_6$]DMSO): $\delta = 2.28$ (s, 3H, 1′-H), 2.98–3.29 (m, 2H, 3-H), 3.66 (s, 3H, OMe), 4.43 (ddddd, $J = 4.3$ Hz, 1H, 2-H), 5.08 (s, 2H, Bzl-H), 7.17 (d, $J = 7.9$ Hz, 2H, Ar-H), 7.25 (d, $J = 7.9$ Hz, 2H, Ar-H), 7.52 (d, $J = 8.3$ Hz,1H, CON*H*), 8.15–8.55 (br, 3H, NH_2·HCl); ^{13}C NMR (125.7 MHz, [D$_6$]DMSO): $\delta = 21.0$ (+, C-1′), 39.2 (−, C-3), 52.0 (+, C-2), 52.8 (+, OMe), 66.0 (−, Bzl-H), 128.2 (+, Ar-C), 129.1 (+, Ar-C), 133.8 (C_{quat}, Ar-C), 137.4 (C_{quat}, Ar-C), 156.3 (C_{quat}, NCO_2), 173.6 (C_{quat}, C-1); IR (KBr): $\tilde{\nu} = 3322$, 3031, 2884, 2621, 1734, 1690, 1597, 1535, 1307, 1264, 1230, 1015 cm^{-1}; MS (ESI pos.): *m*/*z*: 289 (38) [*M*+Na$^+$], 267 (93) [*M*+H$^+$]; elemental analysis calcd (%) for $C_{13}H_{19}N_2O_4Cl$ (302.8): C 51.57, H 6.33, N 9.25; found C 51.29, H 6.48, N 9.11.

MeZ-*a*-Dab[Boc-(4-Pe)Pro]-OMe: Compound **7a** (0.191 g, 0.38 mmol) was deprotected according to GP 1, and the resulting crude N_α-protected diamino ester was coupled with the *N*-Boc protected 4-(*Z*)-propenylproline **14** (0.100 g, 0.39 mmol) by treatment with EDC (77 mg, 0.40 mmol), HOAt (55 mg, 0.41 mmol) and TMP (0.142 g, 1.17 mmol) in CH_2Cl_2 (4 mL) according to GP 2 for 16 h. The crude product obtained after the usual aqueous work-up (GP 2) was finally purified by column chromatography (EtOAc/hexane 1:1.5, $R_f = 0.35$) to give the title compound (0.163 g, 83%) as a turbid oil, which solidified during drying at 60 °C (0.02 Torr) to a colorless solid. M.p. 94–95 °C; $[\alpha]_D^{20} = -41.6$ ($c = 0.32$, $CHCl_3$); ^{1}H NMR (250 MHz, $CDCl_3$): $\delta = 1.04$–1.19 (m, 3H, 4-H, *a-Dab*), 1.41 [s, 9H, C(CH$_3$)$_3$], 1.64 [dd, $J = 7.0$, 1.5 Hz, 3H, 3′-H, (*4-Pe*)*Pro*], 1.72–2.00 [m, 1H, 3-H$_a$, (*4-Pe*)*Pro*], 2.34 (s, 3H, 1′-H, *MeZ*), 2.34–2.54 [m, 1H, 3-H$_b$, (*4-Pe*)*Pro*], 2.92–3.15 [m, 2H, 4-H, 5-H$_a$, (*4-Pe*)*Pro*], 3.76 (s, 3H, OMe), 3.80–3.96 [m, 1H, 5-H$_b$, (*4-Pe*)*Pro*], 4.03–4.22 (m, 1H, 3-H, *a-Dab*), 4.35–4.57 (m, 2H, 2-H), 5.01 (d, $J = 12.3$ Hz, 1H, Bzl-H$_a$), 5.09 (d, $J = 12.3$ Hz, 1H, Bzl-H$_b$), 5.20–5.37 [m, 1H, 1′-H, (*4-Pe*)*Pro*], 5.54 [dq,

J=10.0, 7.0 Hz, 1H, 2′-H, (*4-Pe*)*Pro*], 5.59–5.77, 6.20–6.40 (2×m, 1H, NH), 6.81 (d, J=8.8 Hz, 1H, NH), 7.15 (d, J=7.8 Hz, 2H, Ar-H), 7.25 (d, J=7.8 Hz, 2H, Ar-H); ^{13}C NMR (62.9 MHz, $CDCl_3$): δ=13.0 [+, C-3′, (*4-Pe*)*Pro*], 15.3, 16.8 (+, C-4, *a-Dab*), 21.0 (+, C-1′, *MeZ*), 28.1 [+, $C(CH_3)_3$], 35.8 [+, C-4, (*4-Pe*)*Pro*], 37.8 [−, C-3, (*4-Pe*)*Pro*], 46.6, 47.1 (+, C-3, *a-Dab*), 52.0 [−, C-5, (*4-Pe*)*Pro*], 52.4 (+, OMe), 57.5 (+, C-2, *a-Dab*), 60.9, 61.5 [+, C-2, (*4-Pe*)*Pro*], 66.8, 67.2 (−, Bzl-H, *MeZ*), 80.2 [C_{quat}, $C(CH_3)_3$], 126.4 [+, C-2′, (*4-Pe*)*Pro*], 128.2, 129.0 (+, Ar-C), 129.4 [+, C-1′, (*4-Pe*)*Pro*], 132.7, 137.8 (C_{quat}, Ar-C), 154.2, 156.5 (C_{quat}, NCO_2), 170.2, 171.0 (C_{quat}, C-1), 172.0, 172.3 (C_{quat}, C-1); IR (KBr): $\tilde{\nu}$= 3012, 2978, 2929, 2869, 1728, 1703, 1678, 1541, 1519, 1394, 1368, 1259, 1212, 1162 cm^{-1}; MS (EI, 70 eV): *m/z* (%): 517 (1) [M^+], 444 (3)[$M^+-C_4H_9O$], 416 (6) [$M^+-C_5H_9O_2$], 281 (52) [$C_{15}H_{24}N_2O_3^+$], 238 (15) [$C_{13}H_{20}N_2O_3^+$], 225 (32) [$C_{11}H_{16}N_2O_3^+$], 182 (11), 154 (100) [$C_8H_{12}NO_2^+$], 110 (88) [$C_7H_{12}N^+$], 105 (70) [$C_8H_9^+$], 57 (49) [$C_4H_9^+$], 44 (68) [CO_2^+]; HRMS (EI): *m/z*: calcd for $C_{27}H_{39}N_3O_7$: 517.2788, correct mass found; elemental analysis calcd (%) for $C_{27}H_{39}N_3O_7$ (517.6): C 62.65, H 7.59, N 8.12; found C 62.48, H 7.35, N 7.90.

MeZ-*a*-Dab[Boc-(4-Pe)Pro]-OH (15a): A solution of the dipeptide ester MeZ-*a*-Dab[Boc-(4-Pe)Pro]-OMe (0.145 g, 0.28 mmol) in THF (1.8 mL) was hydrolyzed according to GP 3 by treatment with 40% aqueous solution of tetra-*n*-butylammonium hydroxide (0.545 g, 0.84 mmol). The crude product obtained after the usual aqueous work-up (GP 3) was recrystallized from Et_2O/hexane to give acid **15a** (0.108 g, 76%) as a colorless solid. The mother liquor was concentrated under reduced pressure, and the residue was recrystallized twice from Et_2O/hexane to give a second crop of **15a** (0.012 g, 85% overall yield). R_f=0.06 (EtOAc/hexane 1:2, 1.5% AcOH); ^{1}H NMR (250 MHz, $CDCl_3$): δ=1.13–1.47 (m, 3H, 4-H, *a-Dab*), 1.35, 1.39 [2×s, 9H, $C(CH_3)_3$], 1.64 [d, J=5.8 Hz, 3H, 3′-H, (*4-Pe*)*Pro*], 1.73–2.00 [m, 1H, 3-H_a, (*4-Pe*)*Pro*], 2.33 (s, 3H, 1′-H, *MeZ*), 2.33–2.57 [m, 1H, 3-H_b, (*4-Pe*)*Pro*], 2.87–3.20 [m, 2H, 4-H, 5-H_a, (*4-Pe*)*Pro*], 3.48–3.73, 3.73–3.95 [2×m, 1H, 5-H_b, (*4-Pe*)*Pro*], 4.07–4.29 (m, 1H, 3-H, *a-Dab*), 4.41 (d, J=6.5 Hz, 1H, 2-H), 4.43–4.69 (m, 1H, 2-H), 5.03 (s, 2H, Bzl-H), 5.18–5.33 [m, 1H, 1′-H, (*4-Pe*)*Pro*], 5.53 [dq, J=10.8, 7.0 Hz, 1H, 2′-H, (*4-Pe*)*Pro*], 5.83–6.02, 6.31–6.48 (2×m, 1H, NH), 6.81 (d, J=8.8 Hz, 1H, NH), 7.14 (d, J=8.0 Hz, 2H, Ar-H), 7.21–7.38 (br, 1H, CO_2H), 7.23 (d, J=8.0 Hz, 2H, Ar-H).

MeZ-N$_\beta$Me-*a*-Dab[Boc-(4-Pe)Pro]-OMe: Compound **7b** (0.108 g, 0.21 mmol) was deprotected according to GP 1, and the resultant crude monodeprotected diamino ester was coupled with the *N*-Boc protected 4-(*Z*)-propenylproline **14** (64 mg, 0.25 mmol) by using EDC (48 mg, 0.25 mmol), HOAt (34 mg, 0.25 mmol) and TMP (76 mg, 0.63 mmol) in CH_2Cl_2 (3 mL) according to GP 2 for 16 h. The crude product, obtained after the usual aqueous work-up (GP 2), was finally purified by column chromatography (EtOAc/hexane 1:1.5, R_f=0.35) to give the title compound (0.104 mg, 93%) as a turbid oil. Analytical HPLC: gradient 20 → 90% MeCN in water (0.1% TFA) for 35 min, flow rate=0.5 mL min^{-1}, t_R=26.01 min, purity > 97%; $[\alpha]_D^{20}$=12.0 (c=0.35, $CHCl_3$); ^{1}H NMR (300 MHz, $C_2D_2Cl_4$, 373 K): δ=1.31 (d, J=7.2 Hz, 3H, 4-H, *NMe-a-Dab*), 1.42 [s, 9H, $C(CH_3)_3$], 1.50–1.74 [m, 1H, 3-H_a, (*4-Pe*)*Pro*], 1.67 [dd, J=7.2, 1.8 Hz, 3H, 3′-H, (*4-Pe*)*Pro*], 2.26–2.44 [m, 1H, 3-H_b, (*4-Pe*)*Pro*], 2.36 (s, 3H, 1′-H, *MeZ*), 2.90 (s, 3H, NMe), 3.01–3.21 [m, 2H, 4-H, 5-H_a, (*4-Pe*)*Pro*], 3.23–3.48 [m, 0.5H, 5-H_b, (*4-Pe*)*Pro*], 3.74 (s, 3H, OMe), 4.47 (dd, J=7.8, 7.8 Hz, 1H, 3-H, *NMe-a-Dab*), 4.57 (dd, J=7.8, 7.8 Hz, 1H, 2-H, *NMe-a-Dab*), 4.50–4.95 [m, 1H, C-2, (*4-Pe*)*Pro*], 5.08 (s, 2H, Bzl-H), 5.25–5.36 [m, 1H, 1′-H, (*4-Pe*)*Pro*], 5.50–5.85 (br, 1H, NH), 5.54 [dq, J=11.4, 7.2 Hz, 1H, 2′-H, (*4-Pe*)*Pro*], 7.15 (d, J=7.8 Hz, 2H, Ar-H), 7.23 (d, J=7.8 Hz, 2H, Ar-H); the signal of OMe overlapped with the signal of 0.5H, 5-H_b of the (*4-Pe*)*Pro* moiety; ^{13}C NMR (75.5 MHz, $C_2D_2Cl_4$, 373 K): δ=12.7 [+, C-3′, (*4-Pe*)*Pro*], 14.5 (+, C-4, *NMe-a-Dab*), 20.7 (+, C-1′, *MeZ*), 28.2 (+, $C(CH_3)_3$, NMe), 36.0 [+, C-4, (*4-Pe*)*Pro*], 51.9 [−, C-5, (*4-Pe*)*Pro*], 52.1 (+, C-2, *NMe-a-Dab*), 57.2 (+, OMe), 66.7 (−, Bzl-H, *MeZ*), 79.3 [C_{quat}, $C(CH_3)_3$], 125.8 [+, C-2′, (*4-Pe*)*Pro*], 127.7, 128.8 (+, Ar-C), 130.0 [+, C-1′, (*4-Pe*)*Pro*], 133.3, 137.5 (C_{quat}, Ar-C), 153.5, 155.6 (C_{quat}, NCO_2), 170.6, 173.2 (C_{quat}, C-1); the signals of C-2, C-3 of (*4-Pe*)*Pro* and C-3 of *NMe-a-Dab* were unobservable because of their low intensity; IR (KBr): $\tilde{\nu}$=2977, 1751, 1728, 1700, 1521, 1402, 1281, 1163 cm^{-1}; MS (ESI): pos.: *m/z* (%): 554 (100) [M+Na^+]; elemental analysis calcd (%) for $C_{28}H_{41}N_3O_7$ (531.7): C 63.26, H 7.77, N 7.90; found C 62.95, H 7.70, N 7.70.

MeZ-N$_\beta$Me-*a*-Dab[Boc-(4-Pe)Pro]-OH (15b): A solution of the dipeptide ester MeZ-N$_\beta$Me-*a*-Dab[Boc-(4-Pe)Pro]-OMe (0.128 g, 0.24 mmol) in THF (2.0 mL) was hydrolyzed according to GP 3 by treatment with 40% aqueous solution of tetra-*n*-butylammonium hydroxide (0.24 g, 0.36 mmol). The crude product obtained after the usual aqueous work-up (GP 3) was recrystallized three times from hexane and once from Et_2O/hexane to give **15b** (91 mg, 73%) as an extremely viscous turbid oil (R_f= 0.14, acetone/hexane 2:5). $[\alpha]_D^{20}$=8.9 (c=0.37, $CHCl_3$); MS (ESI): pos.: *m/z* (%): 562 (100) [$M-H^+$+2Na^+], 540 (8) [M+Na^+]; neg.: *m/z* (%): 516 (100) [$M-H^-$].

MeZ-Dap[Boc-(4-Pe)Pro]-OMe: Compound **7c** (0.127 g, 0.42 mmol) was coupled with the *N*-Boc protected (4-propenyl)proline **14** (0.11 g, 0.431 mmol) by treatment with EDC (85 mg, 0.44 mmol), HOAt (60 mg, 0.44 mmol) and TMP (0.314 g, 2.59 mmol) in CH_2Cl_2 (5 mL) according to GP 2 for 16 h. The crude product obtained after the usual aqueous work-up (GP 2) was further purified by column chromatography (acetone/hexane 1:2.5, R_f=0.13) to give an oily residue which was triturated with pentane to furnish the title compound (0.14 g, 66%) as a colorless solid. The mother liquor was cooled to 4°C, and the precipitate was filtered off to give a second crop of the title compound (10 mg, 71% overall yield). M.p. 160–162°C; $[\alpha]_D^{20}$=−41.4 (c=0.35, $CHCl_3$); ^{1}H NMR (300 MHz, $CDCl_3$): δ=1.40 [s, 9H, $C(CH_3)_3$], 1.64 [dd, J=6.9, 1.8 Hz, 3H, 3′-H, (*4-Pe*)*Pro*], 1.78–2.04 [m, 1H, 3-H_a, (*4-Pe*)*Pro*], 2.11–2.57 [m, 1H, 3-H_b, (*4-Pe*)*Pro*], 2.34 (s, 3H, 1′-H, *MeZ*), 2.97–3.15 [m, 1H, 4-H, (*4-Pe*)*Pro*], 2.99 [dd, J=9.3 Hz, 5-H_a, (*4-Pe*)*Pro*], 3.51–3.92 [m, 3H, 3-H, *Dap*, 5-H_b, (*4-Pe*)*Pro*], 3.75 (s, 3H, OMe), 4.12 (dd, J=8.1 Hz, 1H, 2-H, *Dap*), 4.34–4.51 [m, 1H, 2-H, (*4-Pe*)*Pro*], 5.02 (d, J=12.3 Hz, 1H, Bzl-H_a), 5.08 (dq, J=12.3 Hz, 1H, Bzl-H_b), 5.17–5.30 [m, 1H, 1′-H, (*4-Pe*)*Pro*], 5.52 [dq, J=10.5, 6.9 Hz, 1H, 2′-H, (*4-Pe*)*Pro*], 5.74–6.17 (br, 1H, NH), 6.43–6.85 (br, 1H, NH), 7.14 (d, J=8.1 Hz, 2H, Ar-H), 7.33 (d, J=8.1 Hz, 2H, Ar-H); ^{13}C NMR (75.5 MHz, $CDCl_3$): δ=13.2 [+, C-3′, (*4-Pe*)*Pro*], 21.2 (+, C-1′, *MeZ*), 28.3 [+, $C(CH_3)_3$], 36.0 [+, C-4, (*4-Pe*)*Pro*], 38.1 [−, C-3, (*4-Pe*)*Pro*], 40.8, 41.5 (−, C-3, *Dap*), 52.4 [−, C-5, (*4-Pe*)*Pro*], 52.7 (+, OMe), 54.3 (+, C-2, *Dap*), 60.8, 61.4 [+, C-2, (*4-Pe*)*Pro*], 67.0 (−, Bzl-H, *MeZ*), 80.7 [C_{quat}, $C(CH_3)_3$], 126.5 [+, C-2′, (*4-Pe*)*Pro*], 128.3 (+, Ar-C), 129.1 (+, Ar-C), 129.4 [+, C-1′, (*4-Pe*)*Pro*], 133.2 (C_{quat}, Ar-C), 137.9 (C_{quat}, Ar-C), 154.4, 155.1 (C_{quat}, NCO_2), 156.3 (C_{quat}, NCO_2), 170.2, 171.0 (C_{quat}, C-1), 170.9, 173.0 (C_{quat}, C-1); IR (KBr): $\tilde{\nu}$=3013, 2977, 2953, 2876, 1747, 1728, 1521, 1367, 1259, 1209, 1162, 1118 cm^{-1}; MS (EI, 70 eV): *m/z* (%): 503 (4) [M^+], 447 (2) [$M^+-C_4H_8$], 402 (11) [$M^+-C_5H_9O_2$], 210 (15) [$C_{10}H_{14}N_2O_3^+$], 154 (100) [$C_8H_{12}NO_2^+$], 110 (84) [$C_7H_{12}N^+$], 105 (56) [$C_8H_9^+$], 57 (38) [$C_4H_9^+$], 41 (5) [$C_3H_5^+$]; elemental analysis calcd (%) for $C_{26}H_{37}N_3O_7$ (503.6): C 62.01, H 7.41, N 8.34; found C 62.09, H 7.20, N 8.10.

MeZ-Dap[Boc-(4-Pe)Pro]-OH (15c): A solution of the dipeptide ester MeZ-Dap[Boc-(4-Pe)Pro]-OMe (0.13 g, 0.26 mmol) in THF (2.0 mL) was hydrolyzed according to GP 3 by treatment with 40% aqueous solution of tetra-*n*-butylammonium hydroxide (0.20 g, 0.31 mmol). The crude product obtained after the usual aqueous work-up (GP 3) was finally purified by column chromatography [acetone/hexane 4:7 (2% AcOH), R_f= 0.36] to give acid **15c** (0.126 g, 99%) as an extremely viscous turbid oil. ^{1}H NMR (250 MHz, $CDCl_3$): δ=1.31, 1.41 [2×s, 9H, $C(CH_3)_3$], 1.65 [d, J=6.0 Hz, 3H, 3′-H, (*4-Pe*)*Pro*], 1.75–1.98 [m, 1H, 3-H_a, (*4-Pe*)*Pro*], 2.33 (s, 3H, 1′-H, *MeZ*), 2.21–2.53 [m, 1H, 3-H_b, (*4-Pe*)*Pro*], 2.93–3.21 [m, 2H, 4-H, 5-H_a, (*4-Pe*)*Pro*], 3.44–3.60 (m, 2H, 3-H, *Dap*), 3.60–4.03 [m, 1H, 5-H_b, (*4-Pe*)*Pro*], 4.03–4.19 [m, 1H, 2-H, (*4-Pe*)*Pro*], 4.21 (dd, J= 7.5 Hz, 1H, 2-H, *Dap*), 4.30–4.39, 4.41–4.54 (2×br, 1H, NH), 5.04 (s, 2H, Bzl-H), 5.15–5.32 [m, 1H, 1′-H, (*4-Pe*)*Pro*], 5.55 [dq, J=10.8, 7.0 Hz, 1H, 2′-H, (*4-Pe*)*Pro*], 6.25 (d, J=6.5 Hz, 1H, NH), 7.12 (d, J=7.5 Hz, 2H, Ar-H), 7.22 (d, J=7.5 Hz, 2H, Ar-H), 7.42–7.65 (br, 1H, CO_2H); MS (ESI): pos.: *m/z* (%): 534 (100) [$M-H$+2Na^+], 512 (45) [M+Na^+]; neg.: *m/z* (%): 488 (100) [$M-H^-$].

MeZ-*a*-Dab[Boc-(4-Pe)Pro]-(βMe)Phe-(*R*)-(3-Ncp)Ala-(βMe)Phe-Ile-ODCPM (18a): The tetrapeptide **16** (0.172 g, 0.19 mmol), after removal of the Fmoc group according to GP 1, was coupled with the dipeptide acid **15a** (0.104 g, 0.21 mmol) by treatment with HATU (79 mg,

0.21 mmol), HOAt (30 mg, 0.22 mmol) and TMP (75 mg, 0.62 mmol) in CH_2Cl_2 (5 mL) according to GP 4 for 15 h. The mixture was then diluted with Et_2O (50 mL), and subjected to the usual aqueous work-up (GP 2). The organic layer was dried, filtered and concentrated under reduced pressure. The residue was recrystallized from hexane, then purified by column chromatography (EtOAc/hexane 4:3, $R_f = 0.34$) and finally recrystallized from hexane again to give the branched hexapeptide **18a** (0.176 g, 80%) as a colorless solid. M.p. 101–103 °C (decomp.), $[\alpha]_D^{20} = 52.8$ ($c = 0.29$, THF); ^{1}H NMR (600 MHz, $CDCl_3$): $\delta = 0.34$ (dddd, $J = 4.8$, 4.8, 4.8, 4.8 Hz, 1H, 2′-H, *DCPM*), 0.40 (dddd, $J = 4.8$, 4.8, 4.8, 4.8 Hz, 1H, 2′-H, *DCPM*), 0.43 (dddd, $J = 4.8$, 4.8, 4.8, 4.8 Hz, 1H, 2′-H, *DCPM*), 0.45–0.54 (m, 2H, 2′-H, *DCPM*), 0.54–0.59 (m, 2H, 2′-H, *DCPM*), 0.66 (ddddd, $J = 4.2$, 4.2, 4.2, 4.2, 4.2 Hz, 1H, 2′-H, *DCPM*), 0.79 (d, $J = 6.6$ Hz, 3H, 1′-H, *Ile*), 0.84–0.92 [m, 1H, 1′-H, (*3-Ncp*)*Ala*] 0.90 (t, $J = 7.2$ Hz, 3H, 5-H, *Ile*), 1.04 [ddd, $J = 6.0$, 7.2, 7.2 Hz, 1H, 3′-H_a, (*3-Ncp*)*Ala*], 1.06–1.14 (m, 1H, 1′-H_a, *DCPM*), 1.14–1.23 (m, 1H, 1′-H_b, *DCPM*), 1.23 [d, $J = 6.6$ Hz, 3H, 4-H, (β*Me*)*Phe*], 1.25 [d, $J = 6.6$ Hz, 3H, 4-H, (β*Me*)*Phe*], 1.28–1.39 [m, 2H, 3-H, (*3-Ncp*)*Ala*], 1.33 (d, $J = 7.2$ Hz, 3H, 4-H, *a-Dab*), 1.34 [s, 9H, $C(CH_3)_3$], 1.45–1.53 [m, 1H, 3′-H_b, (*3-Ncp*)*Ala*], 1.69 [dd, $J = 6.6$, 1.2 Hz, 3′-H, (*4-Pe*)*Pro*], 1.81 [ddd, $J = 12.0$, 12.0, 12.0 Hz, 1H, 3-H_a, (*4-Pe*)*Pro*], 1.85–1.93 (m, 1H, 3-H, *Ile*), 2.32 (s, 3H, 1′-H, *MeZ*), 2.36 [ddd, $J = 12.0$, 6.0, 6.0 Hz, 3-H_b, (*4-Pe*)*Pro*], 3.12–3.23 [m, 2H, 3-H, (β*Me*)*Phe*, 5-H_a, (*4-Pe*)*Pro*], 3.21–3.30 [m, 2H, 3-H, (β*Me*)*Phe*, 4-H, (*4-Pe*)*Pro*], 3.67 [dd, $J = 9.0$, 7.8 Hz, 1H, 5-H_b, (*4-Pe*)*Pro*], 3.89 [ddd, $J = 7.2$, 3.0, 3.0 Hz, 1H, 2′-H, (*3-Ncp*)*Ala*], 4.14 (t, $J = 7.8$ Hz, 1H, 1-H, *DCPM*), 4.22 [dd, $J = 4.8$, 2.4 Hz, 1H, 2-H, (*4-Pe*)*Pro*], 4.24 (dd, $J = 9.6$, 6.6 Hz, 1H, 2-H, *a-Dab*), 4.30 [dd, $J = 10.8$, 6.0 Hz, 1H, 2-H, (β*Me*)*Phe*], 4.34 (dd, $J = 9.3$, 4.5 Hz, 1H, 2-H, *Ile*), 4.60 [ddd, $J = 10.5$, 5.4, 5.4 Hz, 1H, 2-H, (*3-Ncp*)*Ala*], 4.62–4.70 [m, 2H, 2-H, (β*Me*)*Phe*, 3-H, *a-Dab*], 5.00 (d, $J = 12.0$ Hz, Bzl-H_a), 5.06 (d, $J = 12.0$ Hz, Bzl-H_b), 5.26–5.33 [m, 1H, 1′-H, (*4-Pe*)*Pro*], 5.56 [dq, $J = 11.1$, 6.6 Hz, 1H, 2′-H, (*4-Pe*)*Pro*], 6.61 (d, $J = 6.6$ Hz, 1H, NH), 6.97 (d, $J = 10.2$ Hz, 1H, NH), 7.01 (d, $J = 9.0$ Hz, 1H, NH), 7.10 (d, $J = 8.4$ Hz, 2H, Ar-H), 7.16–7.32 (m, 13H, Ar-H, NH), 7.49 (d, $J = 9.6$ Hz, 1H, NH), 7.60 (d, $J = 9.6$ Hz, 1H, NH); the signal of 4-H of the (β*Me*)*Phe* residue (1.23 ppm) overlapped the signal of 4-H_a of the *Ile* fragment, and the signal of C-(CH_3) overlapped the signal of 4-H_b of the *Ile* moiety; ^{13}C NMR (150.8 MHz, $CDCl_3$): $\delta = 2.5$, 2.79, 2.83, 3.0 (−, C-2′, *DCPM*), 11.6 (+, C-5, *Ile*), 13.2 [+, C-3′, (*4-Pe*)*Pro*], 14.1, 14.6 (+, C-1′, *DCPM*), 15.7 (+, C-1′, *Ile*), 18.5 [+, C-4, (β*Me*)*Phe*], 18.6 [−, C-3′, (*3-Ncp*)*Ala*], 19.7 [+, C-4, (β*Me*)*Phe*], 19.9 (+, C-4, *a-Dab*), 21.1 (+, C-1′, *MeZ*), 21.6 [+, C-1′, (*3-Ncp*)*Ala*], 25.2 (−, C-4, *Ile*), 28.3 [+, $C(CH_3)_3$], 30.8 [−, C-3, (*3-Ncp*)*Ala*], 36.2 [−, C-3, (*4-Pe*)*Pro*], 36.5 (+, C-3, *Ile*), 37.1 [+, C-4, (*4-Pe*)*Pro*], 40.2 [+, C-3, (β*Me*)*Phe*], 41.9 [+, C-3, (β*Me*)*Phe*], 46.3 (+, C-3, *a-Dab*), 50.8 [+, C-2, (*3-Ncp*)*Ala*], 52.5 [−, C-5, (*4-Pe*)*Pro*], 56.6 (+, C-2, *Ile*), 59.5 [+, C-2′, (*3-Ncp*)*Ala*], 60.9 (+, C-2, *a-Dab*), 61.5 [+, C-2, (β*Me*)*Phe*], 63.3 [+, C-2, (*4-Pe*)*Pro*], 63.4 [+, C-2, (β*Me*)*Phe*], 66.7 (−, Bzl-C), 80.2 [C_{quat}, $C(CH_3)_3$], 83.1 (+, C-1, *DCPM*), 126.7(+, Ar-C), 127.0 [+, C-2′, (*4-Pe*)*Pro*], 127.4, 127.6, 127.7, 128.39, 128.43, 128.85, 128.88 (+, Ar-C), 129.2 [+, C-1′, (*4-Pe*)*Pro*], 133.5, 137.7, 141.6, 141.7 (C_{quat}, Ar-C), 154.4, 155.9 (C_{quat}, NCO_2), 169.7, 170.9, 173.56, 173.59, 174.06, 174.11 (C_{quat}, C-1); IR (KBr): $\tilde{\nu} = 3087$, 3010, 2973, 2934, 2876, 1730, 1673, 1545, 1513, 1390, 1368, 1162 cm^{-1}; MS (ESI): pos.: *m*/*z* (%): 1212 (100) [*M*+Na^+]; neg.: *m*/*z* (%): 1188 (100) [*M*−H^-]; elemental analysis calcd (%) for $C_{65}H_{88}N_8O_{13}$ (1189.5): C 65.64, H 7.46, N 9.42; found C 65.63, H 7.22, N 9.26.

MeZ-*a*-N$_\beta$Me-Dab[Boc-(4-Pe)Pro]-(βMe)Phe-(*R*)-(3-Ncp)Ala-(βMe)Phe-Ile-OTMSE (18b): The tetrapeptide **17** (77 mg, 0.081 mmol), after removal of the Fmoc group according to GP 1 by treatment with 50% Et_2NH in THF (2 mL), was coupled with the dipeptide acid **15b** (0.55 mg, 0.106 mmol) by using HATU (40.4 mg, 0.106 mmol), HOAt (14.4 mg, 0.106 mmol) and TMP (64 mg, 0.53 mmol) in CH_2Cl_2 (5 mL) according to GP 4 for 15 h. The mixture was then diluted with Et_2O (50 mL), and subjected to the usual aqueous work-up (GP 2). The organic layer was dried, filtered and concentrated under reduced pressure. The residue was recrystallized from *t*BuOMe/hexane, and then purified by column chromatography (acetone/hexane 1:2, $R_f = 0.32$) to give the branched hexapeptide **18a** (91.0 mg, 93%) as an amorphous colorless solid. $[\alpha]_D^{20} = 10.3$ ($c = 0.31$, $CHCl_3$); ^{1}H NMR (600 MHz, $CDCl_3$): $\delta = 0.09$ [s, 9H, $Si(CH_3)_3$], 0.74 (d, $J = 6.6$ Hz, 3H, 1′-H, *Ile*), 0.90 (t, $J = 7.2$ Hz, 3H, 5-H, *Ile*), 1.04 [ddd, $J = 6.6$, 6.6, 6.6 Hz, 1H, 3′-H_a, (*3-Ncp*)*Ala*], 1.04 (dd, $J = 8.4$, 8.4 Hz, 2H, *TMSE*), 1.09–1.23 [m, 2H, 1′-H, (*3-Ncp*)*Ala*, 4-H_a, *Ile*], 1.26 [d, $J = 6.6$ Hz, 3H, 4-H, (β*Me*)*Phe*], 1.35 [s, 9H, $C(CH_3)_3$], 1.40–1.46 [m, 2H, 3-H_b, 3′-H_b, (*3-Ncp*)*Ala*], 1.49 (d, $J = 7.2$ Hz, 3H, 4-H, *a*-N$_\beta$*Me-Dab*), 1.58 [ddd, $J = 11.4$, 11.4, 11.4 Hz, 1H, 3-H_a, (*4-Pe*)*Pro*], 1.68 [dd, $J = 6.6$, 1.2 Hz, 3′-H, (*4-Pe*)*Pro*], 1.84–1.93 (m, 1H, 3-H, *Ile*), 2.28 [ddd, $J = 11.4$, 6.6, 6.6 Hz, 3-H_b, (*4-Pe*)*Pro*], 2.32 (s, 3H, 1′-H, *MeZ*), 2.93 (s, 3H, NMe, *a*-N$_\beta$*Me-Dab*), 3.15 [dd, $J = 10.5$, 10.5 Hz, 1H, 5-H_a, (*4-Pe*)*Pro*], 3.18–3.28 [m, 1H, 4-H, (*4-Pe*)*Pro*], 3.31–3.40 [m, 2H, 2×H-3, (β*Me*)*Phe*] 3.71 [dd, $J = 10.5$, 7.8 Hz, 1H, 5-H_b, (*4-Pe*)*Pro*], 3.87 [ddd, $J = 6.6$, 3.0, 3.0 Hz, 1H, 2′-H, (*3-Ncp*)*Ala*], 4.12 [dd, $J = 11.4$, 6.6 Hz, 1H, 2-H, (*4-Pe*)*Pro*], 4.19 (d, $J = 4.8$ Hz, 1H, 2-H, *a*-N$_\beta$*Me-Dab*), 4.28 (dd, $J = 8.4$, 8.4, 1-H, *TMSE*), 4.37 [dd, $J = 9.0$, 4.5 Hz, 1H, 2-H, (β*Me*)*Phe*], 4.53 [ddd, $J = 9.6$, 4.8, 4.8 Hz, 1H, 2-H, (*3-Ncp*)*Ala*], 4.65 (dd, $J = 10.5$, 10.5 Hz, 1H, 2-H, *Ile*), 4.75 [dd, $J = 9.9$, 7.5 Hz, 1H, 2-H, (β*Me*)*Phe*], 4.89 (d, $J = 12.0$ Hz, Bzl-H_a), 5.09 (d, $J = 12.0$ Hz, Bzl-H_b), 5.12–5.19 (m, 1H, 3-H, *a*-N$_\beta$*Me-Dab*), 5.22–5.28 [m, 1H, 1′-H, (*4-Pe*)*Pro*], 5.55 [dq, $J = 11.7$, 6.6 Hz, 1H, 2′-H, (*4-Pe*)*Pro*], 6.92 (d, $J = 9.0$ Hz, 1H, NH), 7.10 (d, $J = 8.4$ Hz, 2H, Ar-H, *MeZ*), 7.14–7.28 (m, 11H, Ar-H, NH), 7.22 (d, $J = 8.4$ Hz, 2H, Ar-H, *MeZ*), 7.29 (d, $J = 6.0$ Hz, 1H, NH), 7.61 (d, $J = 9.6$ Hz, 1H, NH), 8.02–8.10 (br, 1H, NH); the signal of 4-H of the (β*Me*)*Phe* (1.30 ppm) residue overlapped the signal of 3-H_a of the (*3-Ncp*)*Ala* moiety, and the signal of $C(CH_3)$ overlapped the signal of 4-H_b of the *Ile* moiety; ^{13}C NMR (150.8 MHz, $CDCl_3$): $\delta = -1.5$ [+, $Si(CH)_3$], 11.7 (+, C-5, *Ile*), 13.2 [+, C-3′, (*4-Pe*)*Pro*], 15.9 (+, C-1′, *Ile*), 16.3 (−, C-2, *TMSE*), 18.3 [−, C-3′, (*3-Ncp*)*Ala*], 18.9 [+, C-4, (β*Me*)*Phe*], 19.6 [+, C-4, (β*Me*)*Phe*], 21.1 (+, C-1′, *MeZ*), 21.8 [+, C-1′, (*3-Ncp*)*Ala*], 25.2 (−, C-4, *Ile*), 28.3 [+, $C(CH_3)_3$], 30.7 (+, NMe, *a*-N$_\beta$*Me-Dab*), 31.3 [−, C-3, (*3-Ncp*)*Ala*], 35.4 [−, C-3, (*4-Pe*)*Pro*], 36.3 [+, C-4, (*4-Pe*)*Pro*], 37.3 (+, C-3, *Ile*), 40.0 [+, C-3, (β*Me*)*Phe*], 41.9 [+, C-3, (β*Me*)*Phe*], 50.3 (+, C-3, *a*-N$_\beta$*Me-Dab*), 50.5 [+, C-2, (*3-Ncp*)*Ala*], 52.3 [−, C-5, (*4-Pe*)*Pro*], 56.2 [+, C-2, (β*Me*)*Phe*], 57.5 [+, C-2, (β*Me*)*Phe*], 59.6 [+, C-2′, (*3-Ncp*)*Ala*], 61.2 (+, C-2, *Ile*), 62.6 [+, C-2, (*4-Pe*)*Pro*], 63.6 (+, C-2, *a*-N$_\beta$*Me-Dab*), 63.9 (−, C-1, *TMSE*), 66.5 (−, Bzl-C), 79.8 [C_{quat}, $C(CH_3)_3$], 126.8 [+, C-2′, (*4-Pe*)*Pro*], 127.05, 127.08, 127.6, 127.9, 128.5, 128.6, 128.7, 128.9, (+, Ar-C), 129.2 [+, C-1′, (*4-Pe*)*Pro*], 133.4, 137.7, 141.2, 142.3 (C_{quat}, Ar-C), 154.1, 155.9 (C_{quat}, NCO_2), 170.2, 170.73, 170.79, 173.0, 174.0, 175.5, (C_{quat}, C-1); IR (KBr): $\tilde{\nu} = 3059$, 2970, 2879, 1660, 1638, 1543, 1400, 1367, 1164 cm^{-1}; MS (ESI): pos.: *m*/*z* (%): 1232 (100) [*M*+Na^+]; neg.: *m*/*z* (%): 1207 (20) [*M*−H^-]; HRMS (ESI): *m*/*z*: calcd for [$C_{64}H_{82}N_8O_{13}SiNa^+$]: 1231.6445; found 1231.6444.

MeZ-Dap[Boc-(4-Pe)Pro]-(βMe)Phe-(*R*)-(3-Ncp)Ala-(βMe)Phe-Ile-ODCPM (18c): The tetrapeptide **16** (0.203 g, 0.22 mmol), after removal of the Fmoc group according to GP 1, was coupled with the dipeptide acid **15c** (0.120 g, 0.25 mmol) by treatment with HATU (93 mg, 0.25 mmol), HOAt (33 mg, 0.25 mmol) and TMP (0.119 g, 0.98 mmol) in CH_2Cl_2 (5 mL) according to GP 4 for 15 h. The mixture was then diluted with Et_2O (50 mL), and subjected to the usual aqueous work-up (GP 2). The organic layer was dried, filtered and concentrated under reduced pressure. The oily residue was purified by column chromatography (acetone/hexane 5:2, $R_f = 0.22$, three times) and finally recrystallized twice from Et_2O/hexane to give the branched hexapeptide **18c** (0.151 g, 59%) as a colorless solid. M.p. 102–103 °C, $[\alpha]_D^{20} = 88.9$ ($c = 0.46$, $CHCl_3$); ^{1}H NMR (600 MHz, $CDCl_3$): $\delta = 0.33$ (dddd, $J = 4.8$, 4.8, 4.8, 4.8 Hz, 1H, 2′-H, *DCPM*), 0.38 (dddd, $J = 4.8$, 4.8, 4.8, 4.8 Hz, 1H, 2′-H, *DCPM*), 0.41 (dddd, $J = 4.8$, 4.8, 4.8, 4.8 Hz, 1H, 2′-H, *DCPM*), 0.47–0.61 (m, 2H, 2′-H, *DCPM*), 0.54–0.59 (m, 2H, 2′-H, *DCPM*), 0.66 (dddddd, $J = 4.8$, 4.8, 4.8, 4.8, 4.8, 4.8 Hz, 1H, 2′-H, *DCPM*), 0.81 (d, $J = 6.6$ Hz, 3H, 1′-H, *Ile*), 0.91 (t, $J = 7.2$ Hz, 3H, 5-H, *Ile*), 0.92–0.97 [m, 1H, 1′-H, (*3-Ncp*)*Ala*] 1.00 [ddd, $J = 7.2$, 7.2, 7.2 Hz, 1H, 3′-H_a, (*3-Ncp*)*Ala*], 1.04–1.12 (m, 1H, 1′-H_a, *DCPM*), 1.12–1.17 (m, 1H, 1′-H_b, *DCPM*), 1.17–1.22 (m, 1H, 4-H_a, *Ile*), 1.23–1.27 [m, 1H, 3-H_a, (*3-Ncp*)*Ala*], 1.27 [d, $J = 6.6$ Hz, 3H, 4-H, (β*Me*)*Phe*], 1.34 [s, 9H, $C(CH_3)_3$], 1.47–1.54 [m, 1H, 3′-H_b, (*3-Ncp*)*Ala*], 1.68 [dd, $J = 6.6$, 1.2 Hz, 3′-H, (*4-Pe*)*Pro*], 1.81 [ddd, $J = 12.0$, 12.0, 12.0 Hz, 1H, 3-H_a, (*4-Pe*)*Pro*], 1.84–1.92 (m, 1H, 3-H, *Ile*), 2.33 (s, 3H, 1′-H, *MeZ*), 2.35 [ddd, $J = 12.0$, 6.0, 6.0 Hz, 3-H_b, (*4-Pe*)*Pro*], 3.04 (ddd, $J = 13.8$, 2.8, 2.8 Hz, 3-H_a, *Dap*), 3.12–3.21 [m, 2H, 3-H, (β*Me*)*Phe*, 5-H_a, (*4-Pe*)*Pro*], 3.21–3.29 [m, 1H, 4-H, (*4-Pe*)*Pro*], 3.32 [dq, $J = 10.2$, 6.6 Hz,

1-H, 3-H, (βMe)*Phe*], 3.67 [dd, J=8.4, 7.2 Hz, 1H, 5-H_b, (*4-Pe*)*Pro*], 3.86 [ddd, J=7.2, 3.0, 3.0 Hz, 1H, 2′-H, (*3-Ncp*)*Ala*], 4.04 (t, J=7.8 Hz, 1H, 1-H, *DCPM*), 4.23–4.31 [m, 3H, C-2, (*4-Pe*)*Pro*, (βMe)*Phe*, *Dap*], 4.32 (ddd, J=13.8, 2.8, 2.8 Hz, 1H, 3-H_b, *Dap*), 4.37 (dd, J=9.0, 4.2 Hz, 1H, 2-H, *Ile*), 4.53 [ddd, J=10.8, 6.0, 6.0 Hz, 1H, 2-H, (*3-Ncp*)*Ala*], 4.58 [dd, J=10.2, 10.2 Hz, 1H, 2-H, (βMe)*Phe*], 5.00 (d, J=12.3 Hz, Bzl-H_a), 5.08 (d, J=12.3 Hz, Bzl-H_b), 5.26–5.33 [m, 1H, 1′-H, (*4-Pe*)*Pro*], 5.56 [dq, J=10.2, 6.6 Hz, 1H, 2′-H, (*4-Pe*)*Pro*], 6.59 (d, J=6.0 Hz, 1H, NH), 6.83 (d, J=9.0 Hz, 1H, NH), 6.2 (d, J=9.6 Hz, 1H, NH), 7.12 (d, J=8.4 Hz, 2H, Ar-H, *MeZ*), 7.16–7.20 (m, 2H, Ar-H), 7.21–7.27 (m, 7H, Ar-H), 7.28–7.37 (m, 3H, Ar-H), 7.50 (d, J=9.0 Hz, 1H, NH), 7.78 (dd, J=10.2, 2.4 Hz, 1H, NH), 8.20 (d, J=6.0 Hz, 1H, NH); the signal of C(CH_3) overlapped the signals of 4-H_b of the *Ile* moiety, 4-H of (βMe)*Phe* residue and 3-H_b of the (*3-Ncp*)*Ala* fragment; ^{13}C NMR (150.8 MHz, $CDCl_3$): δ= 2.6, 2.87, 2.96, 3.0 (−, C-2′, *DCPM*), 11.7 (+, C-5, *Ile*), 13.2 [+, C-3′, (*4-Pe*)*Pro*], 14.2, 14.6 (+, C-1′, *DCPM*), 15.6 (+, C-1′, *Ile*), 18.4 [−, C-3′, (*3-Ncp*)*Ala*], 18.8 [+, C-4, (βMe)*Phe*], 19.8 [+, C-4, (βMe)*Phe*], 21.1 (+, C-1′, *MeZ*), 21.8 [+, C-1′, (*3-Ncp*)*Ala*], 25.2 (−, C-4, *Ile*), 28.3 [+, C-(CH_3)$_3$], 31.1 [−, C-3, (*3-Ncp*)*Ala*], 36.2 [+, C-4, (*4-Pe*)*Pro*], 36.4 [−, C-3, (*4-Pe*)*Pro*], 37.6 (+, C-3, *Ile*), 40.3 [+, C-3, (βMe)*Phe*], 40.8 (−, C-3, *Dap*), 41.7 [+, C-3, (βMe)*Phe*], 51.0 [+, C-2, (*3-Ncp*)*Ala*], 52.4 [−, C-5, (*4-Pe*)*Pro*], 56.5 (+, C-2, *Ile*), 59.2 (+, C-2, *Dap*), 59.5 [+, C-2′, (*3-Ncp*)*Ala*], 60.7 [+, C-2, (*4-Pe*)*Pro*], 61.0 [+, C-2, (βMe)*Phe*], 63.4 [+, C-2, (βMe)*Phe*], 66.7 (−, Bzl-C), 80.2 [C_{quat}, C(CH_3)$_3$], 83.5 (+, C-1, *DCPM*), 126.7 [+, C-2′, (*4-Pe*)*Pro*], 127.0, 127.4, 127.6, 127.7, 128.47, 128.50, 128.93 (? 2) (+, Ar-C), 129.3 [+, C-1′, (*4-Pe*)*Pro*], 133.4, 137.7, 141.8, 141.9 (C_{quat}, Ar-C), 154.4, 156.1 (C_{quat}, NCO_2), 169.7, 170.8, 173.1, 173.4, 174.7, 175.4 (C_{quat}, C-1); IR (KBr): $\tilde{\nu}$=3089, 3062, 3010, 2972, 2933, 2877, 1725, 1667, 1542, 1454, 1416, 1392, 1368, 1258, 1216, 1162 cm^{-1}; MS (ESI): pos.: *m/z* (%): 1197 (100) [M+Na^+]; neg.: *m/z* (%): 1173 (100) [M−H^-]; elemental analysis calcd (%) for $C_{64}H_{86}N_8O_{13}$ (1175.4): C 65.40, H 7.37, N 9.53; found C 65.17, H 7.13, N 9.34.

MeZ-Protected branched cyclohexapeptide (19a) and its epimer (*epi*-19a): The branched hexapeptide **18a** (0.188 g, 0.165 mmol) was deprotected according to GP 5 by treatment with the freshly prepared 2 M HCl in EtOAc (3 mL) to give the hydrochloride of the deprotected peptide as a colorless solid [0.145 g; MS (ESI): pos.: *m/z* (%): 996 (100) [M+H^+]; neg.: *m/z* (%): 994 (100) [M−H^-], which was taken up with anhydrous CH_2Cl_2 (1.5 L) and cyclized by treatment with HATU (2×61 mg, 2×0.160 mmol) and HOAt (2×18 mg, 2×0.133 mmol) and solution of DIEA (2×55 mg, 2×0.426 mmol) in CH_2Cl_2 (2×20 mL) according to GP 2 for 18 h. After this, the solvent was removed under reduced pressure, the residue was taken up with Et_2O (50 mL), and after the usual aqueous work-up (GP 5), drying and filtration, the organic layer was concentrated under reduced pressure. The residue was purified first by column chromatography (acetone/hexane 1:1.75, R_f=0.29), and then by recrystallization (Et_2O/pentane) to give a crude product (81.0 mg), which contained two components according to analytical HPLC. The mixture was separated by preparative HPLC to give cyclodepsipeptide **19a** (41 mg, 28% over two steps) and its epimer *epi*-**19a** (28 mg, 19% over two steps) as colorless solids. Preparative HPLC: column A, isocratic, 85% MeCN in H_2O (0.07% TFA), flow rate 2.5 mL min^{-1}.

Compound 19a: analytical HPLC: isocratic, 60% MeCN in H_2O (0.1% TFA), flow rate=0.5 mL min^{-1}, t_R=20.18 min, purity > 99%; $[\alpha]_D^{20}$=8.6 (c=0.21, $CHCl_3$); ^{1}H NMR (600 MHz, $CDCl_3$): δ=0.15–0.31 [m, 1H, 3′-H_a, (*3-Ncp*)*Ala*], 0.32–0.47 [m, 1H, 3-H_a, (*3-Ncp*)*Ala*], 0.78 (t, J=7.2 Hz, 3H, 5-H, *Ile*), 0.84 (d, J=6.6 Hz, 3H, 1′-H, *Ile*), 0.88–0.97 [m, 1H, 1′-H, (*3-Ncp*)*Ala*], 0.97–1.06 (m, 1H, 4-H_a, *Ile*), 1.08–1.25 [m, 1H, 3-H_b, (*3-Ncp*)*Ala*], 1.25 [d, J=7.2 Hz, 3H, 4-H, (βMe)*Phe*], 1.26–1.34 (m, 1H, 4-H_b, *Ile*), 1.29 [d, J=7.2 Hz, 3H, 4-H, (βMe)*Phe*], 1.34–1.44 [m, 1H, 3′-H_b, (*3-Ncp*)*Ala*], 1.40 (d, J=7.2 Hz, 3H, 4-H, *a-Dab*), 1.63–1.73 (m, 1H, 3-H, *Ile*), 1.66 [d, J=6.6 Hz, 3′-H, (*4-Pe*)*Pro*], 1.87 [ddd, J=11.4, 11.4, 11.4 Hz, 1H, 3-H_a, (*4-Pe*)*Pro*], 2.18 [ddd, J=11.4, 6.0, 6.0 Hz, 1H, 3-H_b, (*4-Pe*)*Pro*], 2.38 (s, 3H, 1′-H, *MeZ*), 3.01 [dddd, J=1.2, 7.2 Hz, 1H, 3-H, (βMe)*Phe*], 3.07–3.19 [m, 1H, 4-H, (*4-Pe*)*Pro*], 3.23 [dd, J=9.8, 9.8 Hz, 1H, 5-H_a, (*4-Pe*)*Pro*], 3.40–3.51 [m, 1H, 2′-H, (*3-Ncp*)*Ala*], 3.64–3.71 [m, 1H, 3-H, (βMe)*Phe*], 3.71–3.79 [m, 1H, 2-H, (*3-Ncp*)*Ala*], 3.78–3.85 [m, 1H, 2-H, (*4-Pe*)*Pro*], 3.86–3.94 [m, 1H, 5-H_b, (*4-Pe*)*Pro*], 4.28–4.34 [m, 2H, 3-H, *a-Dab*, 2-H, (βMe)*Phe*], 4.34–4.50 (m, 1H, 2-H, *a-Dab*), 4.50–4.60 [m, 2H, 2-H, *Ile*, 2-H, (βMe)*Phe*], 4.97 (d, J=12.0 Hz, Bzl-H_a), 5.19 (d, J=12.0 Hz, Bzl-H_b), 5.25 [dd, J=9.6, 9.6 Hz, 1H, 1′-H, (*4-Pe*)*Pro*], 5.58 [dq, J=9.6, 7.2 Hz, 1H, 2′-H, (*4-Pe*)*Pro*], 5.63–5.80 (br, 1H, NH), 6.04–6.37 (br, 1H, NH), 6.51–6.67 (br, 1H, NH), 6.86–7.02 (br, 1H, NH), 7.02–7.12 (m, 1H, NH), 7.14–7.31 (m, 15H, Ar-H, NH); ^{13}C NMR (150.8 MHz, $CDCl_3$): δ=10.5 (+, C-5, *Ile*), 13.2 [+, C-3′, (*4-Pe*)*Pro*], 13.5 [+, C-4, (βMe)*Phe*], 14.9 (+, C-1′, *Ile*), 17.8 [−, C-3′, (*3-Ncp*)*Ala*], 18.0 [+, C-4, (βMe)*Phe*], 18.7 (+, C-4, *a-Dab*), 21.0 [+, C-1′, (*3-Ncp*)*Ala*], 21.1 (+, C-1′, *MeZ*), 24.3 (−, C-4, *Ile*), 32.7 [−, C-3, (*3-Ncp*)*Ala*], 35.2 [−, C-3, (*4-Pe*)*Pro*], 36.6 [+, C-4, (*4-Pe*)*Pro*], 37.3 (+, C-3, *Ile*), 38.8 [+, C-3, (βMe)*Phe*], 43.6 [+, C-3, (βMe)*Phe*], 47.5 (+, C-3, *a-Dab*), 52.5 [+, C-2, (*3-Ncp*)*Ala*], 52.7 [−, C-5, (*4-Pe*)*Pro*], 54.5 (+, C-2, *Ile*), 58.9 [+, C-2′, (*3-Ncp*)*Ala*], 59.30 [+, 2 ? C-2, *a-Dab*, (βMe)*Phe*], 59.5 [+, C-2, (βMe)*Phe*], 62.3 [+, C-2, (*4-Pe*)*Pro*], 67.0 (−, Bzl-C), 126.8, 127.1, 127.2, 127.5 (+, Ar-C), 127.7 [C-2′, (*4-Pe*)*Pro*], 128.0 (+, Ar-C), 128.4 [C-1′, (*4-Pe*)*Pro*], 128.5, 128.6, 129.1 (+, Ar-C), 133.4, 137.8, 141.4, 142.3 (C_{quat}, Ar-C), 157.3 (C_{quat}, NCO_2), 169.1, 170.49 (× 2), 170.90 (× 2), 172.0 (C_{quat}, C-1); IR (KBr): $\tilde{\nu}$=3060, 3029, 2969, 2936, 2877, 1670, 1634, 1542, 1517, 1452, 1369, 1205 cm^{-1}; MS (ESI): pos.: *m/z* (%): 1000 (100) [M+Na^+]; neg.: *m/z* (%): 976 (100) [M−H^-]; HRMS (ESI): *m/z*: calcd for [$C_{53}H_{68}N_8O_{10}Na^+$]: 999.4951; found 999.4951.

***epi*-19a**: analytical HPLC 1: isocratic, 60% MeCN in H_2O (0.1% TFA), flow rate=0.5 mL min^{-1}, t_R=17.25 min, purity > 97%; $[\alpha]_D^{20}$=−42.68 (c=0.27, $CHCl_3$); ^{1}H NMR (600 MHz, $CDCl_3$): δ=0.65–0.73 (m, 3H, 1′-H, *a-Ile*), 0.84 (t, J=7.2 Hz, 3H, 5-H, *a-Ile*), 0.89 [ddd, J=5.4, 5.4, 5.4 Hz, 1H, 3′-H_a, (*3-Ncp*)*Ala*], 1.10 [d, J=5.4 Hz, 3H, 4-H, (βMe)*Phe*], 1.10–1.15 [m, 1H, 3-H_a*, (*3-Ncp*)*Ala*], 1.17–1.26 [m, 4H, 4-H, (βMe)*Phe*, 4-H_a*, *a-Ile*], 1.40–1.48 [m, 1H, 3-H_b*, (*3-Ncp*)*Ala*], 1.44 (d, J=7.8 Hz, 3H, 4-H, *a-Dab*), 1.50–1.59 [m, 1H, 1′-H, (*3-Ncp*)*Ala*], 1.59–1.63 [m, 2H, 3′-H_b, (*3-Ncp*)*Ala*, 3-H, *a-Ile*], 1.63 [d, J=6.6 Hz, 3′-H, (*4-Pe*)*Pro*], 2.08–2.22 [m, 1H, 3-H_a, (*4-Pe*)*Pro*], 2.28 (s, 3H, 1′-H, *MeZ*), 2.25–2.33 [m, 1H, 3-H_b, (*4-Pe*)*Pro*], 3.06 [ddddd, J=7.8, 7.8, 7.8, 7.8, 7.8 Hz, 1H, 4-H, (*4-Pe*)*Pro*], 3.17–3.30 [m, 2H, 5-H_a, (*4-Pe*)*Pro*, 3-H*, (βMe)*Phe*], 3.31–3.44 [m, 2H, 2′-H*, (*3-Ncp*)*Ala*, 3-H, (βMe)*Phe*], 3.74 [dd, J=7.8, 7.8 Hz, 1H, 5-H_b, (*4-Pe*)*Pro*], 3.74–3.84 (m, 1H, 2-H), 4.08–4.20 (m, 1H, 3-H, *a-Dab*), 4.31–4.84 (m, 2H, 2-H), 4.48–4.62 (m, 2H, 2-H), 4.73 (dd, J=7.8, 7.8 Hz, 1H, 2-H), 4.98 (d, J=12.0 Hz, Bzl-H_a), 5.09 (d, J=12.0 Hz, Bzl-H_b), 5.29 [dd, J=10.2, 10.2 Hz, 1H, 1′-H, (*4-Pe*)*Pro*], 5.52 [dq, J=10.2, 6.6 Hz, 1H, 2′-H, (*4-Pe*)*Pro*], 5.92–6.04 (br, 1H, NH), 6.74 (d, J=7.2 Hz, 1H, NH), 7.05–7.12 (br, 1H, NH), 7.07 (d, J=7.8 Hz, 2H, Ar-H), 7.16–7.29 (m, 10H, Ar-H, NH), 7.30–7.36 (m, 4H, Ar-H, NH), 7.44–7.51 (br, 1H, NH); the absorption of 4-H_b, *a-Ile* is masked by the signal of 3′-H, (*4-Pe*)*Pro*; ^{13}C NMR (150.8 MHz, $CDCl_3$): δ=11.7 (+, C-5, *a-Ile*), 13.2 [+, C-3′, (*4-Pe*)*Pro*], 14.0 (+, C-1′, *a-Ile*), 17.3 [+, C-4, (βMe)*Phe*], 17.5 (+, C-4, *a-Dab*), 17.6 [−, C-3′, (*3-Ncp*)*Ala*], 17.6 [+, C-4, (βMe)*Phe*], 21.1 (+, C-1′, *MeZ*), 21.9 [+, C-1′, (*3-Ncp*)*Ala*], 26.3 (−, C-4, *a-Ile*), 31.8 [−, C-3, (*3-Ncp*)*Ala*], 34.2 [−, C-3, (*4-Pe*)*Pro*], 36.1 [+, C-4, (*4-Pe*)*Pro*], 36.9 (+, C-3, *a-Ile*), 40.43 [+, 2×C-3, (βMe)*Phe*], 49.3 (+, C-3, *a-Dab*), 51.0 (+, C-2), 52.9 [−, C-5, (*4-Pe*)*Pro*], 54.1 (+, C-2), 58.8 [+, C-2′*, (*3-Ncp*)*Ala*], 59.3 (+, C-2*), 59.4 (+, C-2*), 60.34 (+, 2×C-2), 67.2 (−, Bzl-C), 126.7, 127.0, 127.6, 127.7, 128.2, 128.3, 128.5, 128.7, 129.0, 129.1 [+, Ar-C, C-1′, C-2′, (*4-Pe*)*Pro*], 132.8, 138.0, 142.0, 142.6 (C_{quat}, Ar-C), 156.2 (C_{quat}, NCO_2), 170.33 (× 2), 170.82 (× 2), 170.9, 171.0 (C_{quat}, C-1); IR (KBr): $\tilde{\nu}$= 3061, 3030, 2969, 2934, 2877, 1654, 1540, 1453, 1369, 1270 cm^{-1}; MS (ESI): pos.: *m/z* (%): 1000 (100) [M+Na^+]; neg.: *m/z* (%): 976 (100) [M−H^-].

MeZ-*a*-N$_\beta$Me-Dab[Boc-(4-Pe)Pro]-(βMe)Phe-(*R*)-(3-Ncp)Ala-(βMe)Phe-Ile-OH: $(Bu)_4N^-F^+$ (70.0 mg, 0.22 mmol) was added to a stirred solution of the ester **18b** (88.0 mg, 72.8 μmol) in MeCN (2.0 mL), and the mixture was stirred at 20 °C for an additional 1 h. As TLC showed the presence of the starting material the mixture was carefully heated at 55 °C with a heat-gun and then was stirred for another 1 h. 1 N H_2SO_4 (1 mL) was added, and the reaction mixture was then diluted with Et_2O (40 mL), washed with 1 M $KHSO_4$ (3×10 mL), water (3×10 mL), brine (2×10 mL), dried, filtered and concentrated under reduced pressure. The residue was recrystallized from Et_2O/pentane to give the title compound (79.0 mg, 98%) as a colorless solid which was used for the next step without additional purification. R_f=0.36, acetone/hexane 4:7

(3% AcOH); MS (ESI): pos.: *m/z* (%): 1153 (78) [*M*−H+2Na$^+$], 1131 (100) [*M*+Na$^+$]; neg.: *m/z* (%): 1107 (100) [*M*−H$^-$].

MeZ-Protected branched cyclohexapeptide (19b): The branched hexapeptide acid MeZ-*a*-N$_\beta$Me-Dab[Boc-(4-Pe)Pro]-(βMe)Phe-(*R*)-(3-Ncp)Ala-(βMe)Phe-Ile-OH (79.0 mg, 71.2 μmol) was deprotected according to GP 5 by treatment with 2 M HCl in EtOAc (2 mL) to give the hydrochloride of the deprotected material as a colorless solid (80 mg), which was taken up with anhydrous CH_2Cl_2 (1.1 L) and cyclized by treatment with HATU (2×28.0 mg, 2×73.3 μmol) and HOAt (2×9.6 mg, 2×73.3 μmol) and solution of DIEA (2×37 mg, 2×0.285 mmol) in CH_2Cl_2 (2×50 mL) according to GP 2 for 22 h. After this, the solvent was removed under reduced pressure, the residue was taken up with Et_2O (50 mL), and after the usual aqueous work-up (GP 5), drying and filtration, the organic layer was concentrated under reduced pressure. The residue was purified first by column chromatography (acetone/hexane 1:2, R_f=0.32) to give a crude product (43.0 mg), which was finally purified by preparative HPLC to give cyclodepsipeptide **19b** (31.6 mg, 44% over three steps) and a small amount of its epimer *epi*-**19b** (1.4 mg, 2% over three steps) as colorless solids. Preparative HPLC: column B, isocratic, 65% MeCN in H_2O (0.1% TFA), flow rate 2.7 mL min^{-1}.

Compound 19b: analytical HPLC: isocratic, 75% MeCN in H_2O (0.1% TFA), flow rate = 0.5 mL min^{-1}, t_R = 10.64 min, purity > 99%; gradient 55 → 100% MeCN in H_2O (0.1% TFA) for 15 min, flow rate = 0.5 mL min^{-1}, t_R = 14.65 min, purity > 99%; $[\alpha]_D^{20}$ = 37.8 (*c* = 0.33, $CHCl_3$); ^{1}H NMR (600 MHz, $CDCl_3$): δ = 0.69–0.77 [m, 1H, 3-H$_a$, (*3-Ncp*)*Ala*], 0.77 (t, *J* = 7.2 Hz, 3H, 5-H, *Ile*), 0.79 (d, *J* = 7.2 Hz, 3H, 1′-H, *Ile*), 0.85 [ddd, *J* = 7.2, 7.2, 7.2 Hz, 1H, 3′-H$_a$, (*3-Ncp*)*Ala*], 1.11 (ddq, *J* = 7.8, 6.6, 6.6 Hz, 1H, 4-H$_a$, *Ile*), 1.34 [d, *J* = 6.6 Hz, 3H, 4-H, (β*Me*)*Phe*], 1.32–1.41 [m, 2H, 4-H$_b$, *Ile*, 1′-H, (*3-Ncp*)*Ala*], 1.42 [d, *J* = 6.6 Hz, 3H, 4-H, (β*Me*)*Phe*], 1.34–1.44 [m, 1H, 3′-H$_b$, (*3-Ncp*)*Ala*], 1.58 (d, *J* = 7.2 Hz, 3H, 4-H, *a*-N$_\beta$*Me-Dab*), 1.59–1.64 [m, 3H, 3-H, *Ile*, 3-H$_b$, 3′-H$_b$, (*3-Ncp*)*Ala*], 1.66 [dd, *J* = 7.2, 1.8 Hz, 3′-H, (*4-Pe*)*Pro*], 1.73 [ddd, *J* = 12.0, 12.0, 12.0 Hz, 1H, 3-H$_a$, (*4-Pe*)*Pro*], 2.13 [ddd, *J* = 12.0, 6.0, 6.0 Hz, 1H, 3-H$_b$, (*4-Pe*)*Pro*], 2.35 (s, 3H, 1′-H, *MeZ*), 2.92 (s, 3H, NMe, *a*-N$_\beta$*Me-Dab*), 2.99 [dq, *J* = 6.6, 7.5 Hz, 1H, 3-H, (β*Me*)*Phe*], 3.17–3.30 [m, 2H, 4-H, 5-H$_a$, (*4-Pe*)*Pro*], 3.48 [dq, *J* = 6.6, 6.6 Hz, 1H, 3-H, (β*Me*)*Phe*], 3.62–3.72 [m, 1H, 2-H, (*3-Ncp*)*Ala*], 3.84 [ddd, *J* = 7.2, 3.0, 3.0 Hz, 1H, 2′-H, (*3-Ncp*)*Ala*], 4.01–4.10 [m, 1H, 5-H$_b$, (*4-Pe*)*Pro*], 4.29 (d, *J* = 7.2 Hz, 1H, 2-H, *a*-N$_\beta$*Me-Dab*), 4.45 [dd, *J* = 10.2, 6.6 Hz, 1H, 2-H, (β*Me*)*Phe*], 4.45–4.54 [m, 2H, 2-H, *Ile*, 2-H, (*4-Pe*)*Pro*], 4.34–4.50 (m, 1H, 2-H, *a-Dab*), 4.71 [dd, *J* = 7.5, 7.5 Hz, 1H, 2-H, (β*Me*)*Phe*], 4.99 (dd, *J* = 7.2, 7.2 Hz, 3-H, *a*-N$_\beta$*Me-Dab*), 5.09 (s, 2H, Bzl), 5.17–5.27 [dd, *J* = 9.6, 9.6 Hz, 1H, 1′-H, (*4-Pe*)*Pro*], 5.57 [dq, *J* = 9.6, 7.2 Hz, 1H, 2′-H, (*4-Pe*)*Pro*], 6.11 (d, *J* = 6.0 Hz, 1H, NH), 6.23–6.37 (br, 2H, 2×NH), 6.51–6.67 (br, 1H, NH), 7.01 (d, *J* = 6.0 Hz, 1H, NH), 7.09–7.21 (m, 6H, Ar-H), 7.22–7.27 (m, 4H, Ar-H), 7.28 (dd, *J* = 7.2 Hz, Ar-H), 7.35 (dd, *J* = 7.8, 7.8 Hz, Ar-H), 7.43 (d, *J* = 8.4 Hz, NH); ^{13}C NMR (150.8 MHz, $CDCl_3$): δ = 10.1 (+, C-5, *Ile*), 13.4 [+, C-3′, (*4-Pe*)*Pro*], 14.7 (+, C-1′, *Ile*), 15.3 [+, C-4, (β*Me*)*Phe*], 17.04 (+, C-4, *a*-N$_\beta$*Me-Dab*), 17.2 [−, C-3′, (*3-Ncp*)*Ala*], 18.2 [+, C-4, (β*Me*)*Phe*], 21.2 (+, C-1′, *MeZ*), 21.4 [+, C-1′, (*3-Ncp*)*Ala*], 24.7 (−, C-4, *Ile*), 31.2 (+, NMe, *a*-N$_\beta$*Me-Dab*), 32.2 [−, C-3, (*3-Ncp*)*Ala*], 35.0 [−, C-3, (*4-Pe*)*Pro*], 36.3 (+, C-3, *Ile*), 36.9 [+, C-4, (*4-Pe*)*Pro*], 39.6 [+, C-3, (β*Me*)*Phe*], 45.5 [+, C-3, (β*Me*)*Phe*], 52.0 (+, C-3, *a*-N$_\beta$*Me-Dab*), 52.6 [−, C-5, (*4-Pe*)*Pro*], 53.8 [+, C-2, (*3-Ncp*)*Ala*], 54.6 (+, C-2, *Ile*), 57.5 [+, C-2, (β*Me*)*Phe*], 58.9 [+, C-2, (β*Me*)*Phe*], 59.0 [+, C-2′, (*3-Ncp*)*Ala*], 60.3 [+, C-2, (*4-Pe*)*Pro*], 61.6 (+, C-2, *a*-N$_\beta$*Me-Dab*), 67.0 (−, Bzl-C), 127.1, 127.3, 127.57, 127.62 (+, Ar-C), 127.7 [+, C-2′, (*4-Pe*)*Pro*], 128.1 [+, C-1′, (*4-Pe*)*Pro*], 128.3, 128.6, 128.8, 129.1 (+, Ar-C), 133.3, 137.9, 140.8, 142.5 (C_{quat}, Ar-C), 156.6 (C_{quat}, NCO_2), 170.2, 170.4, 170.7, 170.8, 171.0, 174.8 (C_{quat}, C-1); IR (KBr): $\tilde{\nu}$ = 2971, 2936, 2878, 1720, 1633, 1541, 1506, 1453, 1369, 1209, 1032 cm^{-1}; MS (ESI): pos.: *m/z* (%): 1013 (100) [*M*+Na$^+$]; neg.: *m/z* (%): 989 (100) [*M*−H$^-$]; HRMS (ESI): *m/z*: calcd for [$C_{54}H_{71}N_8O_{10}^+$]: 991.5288; found 991.5291.

***epi*-19b**: analytical HPLC: isocratic, 75% MeCN in H_2O (0.1% TFA), flow rate = 0.5 mL min^{-1}, t_R = 9.61 min, purity > 95%; gradient 55 → 100% MeCN in H_2O (0.1% TFA) for 15 min, flow rate = 0.5 mL min^{-1}, t_R = 14.15 min, purity > 95%; MS (ESI): pos.: *m/z* (%): 1013 (100) [*M*+Na$^+$]; neg.: *m/z* (%): 989 (100) [*M*−H$^-$].

MeZ-Protected branched cyclohexapeptide (19c) and its epimer (*epi*-19c): The branched hexapeptide **18c** (0.134 g, 0.114 mmol) was deprotected according to GP 5 by treatment with a freshly prepared 2 M HCl in EtOAc (2.5 mL) to give the hydrochloride of the deprotected peptide as a colorless solid, which was taken up with anhydrous CH_2Cl_2 (1.3 L) and cyclized by treatment with HATU (2×44.6 mg, 2×0.117 mmol), HOAt (2×15.9 mg, 2×0.117 mmol) and a solution of DIEA (2×59 mg, 2×0.456 mmol) in CH_2Cl_2 (2×50 mL) according to GP 2 for 18 h. After this, the solvent was removed under reduced pressure, the residue was taken up with Et_2O (50 mL), and after the usual aqueous work-up (GP 5), drying and filtration, the organic layer was concentrated under reduced pressure. The residue was purified by column chromatography (acetone/hexane 1:1.5, R_f=0.31) to give a crude product (90.0 mg), which contained two components according to analytical HPLC. The mixture was separated by preparative HPLC to give cyclodepsipeptide **19c** (37.7 mg, 34% over two steps) and its epimer *epi*-**19a** (27.9 mg, 25% over two steps) as colorless solids. Preparative HPLC: column B, isocratic, 69% MeCN in H_2O (0.1% TFA), flow rate 2.5 mL min^{-1}.

Compound 19c: analytical HPLC: isocratic, 70% MeCN in H_2O (0.1% TFA), flow rate = 0.5 mL min^{-1}, t_R = 12.00 min, purity > 99%; $[\alpha]_D^{20}$ = 16.0 (*c* = 0.77, $CHCl_3$); ^{1}H NMR (600 MHz, $CDCl_3$): δ = 0.40–0.54 [m, 1H, 3-H$_a$, (*3-Ncp*)*Ala*], 0.58–0.69 [m, 1H, 3′-H$_a$, (*3-Ncp*)*Ala*], 0.76 (t, *J* = 7.2 Hz, 3H, 5-H, *Ile*), 0.88 (d, *J* = 6.0 Hz, 3H, 1′-H, *Ile*), 1.00–1.17 [m, 2H, 1′-H, (*3-Ncp*)*Ala*, 1H, 4-H$_a$, *Ile*], 1.26 [d, *J* = 6.6 Hz, 3H, 4-H, (β*Me*)*Phe*], 1.26–1.34 [m, 1H, 3-H$_b$, (*3-Ncp*)*Ala*], 1.34 [d, *J* = 7.2 Hz, 3H, 4-H, (β*Me*)*Phe*], 1.42–1.49 [m, 1H, 3′-H$_b$, (*3-Ncp*)*Ala*], 1.59 [d, *J* = 6.6 Hz, 3′-H, (*4-Pe*)*Pro*], 1.69–1.79 (m, 1H, 3-H, *Ile*), 1.81 [ddd, *J* = 12.0, 12.0, 12.0 Hz, 1H, 3-H$_a$, (*4-Pe*)*Pro*], 2.16 [ddd, *J* = 12.0, 6.0, 6.0 Hz, 1H, 3-H$_b$, (*4-Pe*)*Pro*], 2.35 (s, 3H, 1′-H, *MeZ*), 2.90 [dq, *J* = 6.0, 6.0 Hz, 1H, 3-H, (β*Me*)*Phe*], 3.03–3.15 [m, 1H, 4-H, (*4-Pe*)*Pro*], 3.23 [dd, *J* = 9.2, 9.2 Hz, 1H, 5-H$_a$, (*4-Pe*)*Pro*], 3.43–3.58 [m, 2H, 2-H, (*3-Ncp*)*Ala*, 3-H$_a$, *Dap*], 3.62–3.72 [m, 2H, 3-H, (β*Me*)*Phe*, 2′-H, (*3-Ncp*)*Ala*], 3.84–3.93 [m, 1H, 3-H$_b$, *Dap*], 3.94 [dd, *J* = 9.2, 9.2 Hz, 1H, 5-H$_b$, (*4-Pe*)*Pro*], 4.03–4.12 [m, 1H, 2-H, (*4-Pe*)*Pro*], 4.41–4.48 (m, 1H, *Dap*), 4.50–4.55 [m, 1H, 2-H, (β*Me*)*Phe*], 4.59 (dd, *J* = 8.7, 8.7 Hz, 1H, 2-H, *Ile*), 4.64 [dd, *J* = 7.8, 7.8 Hz, 1H, 2-H, (β*Me*)*Phe*], 5.06 (d, *J* = 12.0 Hz, Bzl-H$_a$), 5.13 (d, *J* = 12.0 Hz, Bzl-H$_b$), 5.22 [dd, *J* = 10.2, 10.2 Hz, 1H, 1′-H, (*4-Pe*)*Pro*], 5.57 [dq, *J* = 10.2, 6.6 Hz, 1H, 2′-H, (*4-Pe*)*Pro*], 6.06–6.23 (br, 1H, NH), 6.71–6.90 (br, 2H, 2×NH), 6.98–7.09 (br, 1H, NH), 7.11–7.18 (m, 3H, Ar-H), 7.18–7.22 (m, 2H, Ar-H), 7.22–7.28 (m, 7H, Ar-H), 7.28–7.34 (m, 2H, Ar-H), 7.34–7.57 (br, 1H, NH), 7.59–7.84 (br, 1H, NH); the signal of 4-H of the (β*Me*)*Phe* residue (1.34 ppm) overlapped the signal of 4-H$_b$ of the *Ile* moiety; ^{13}C NMR (150.8 MHz, $CDCl_3$): δ = 10.6 (+, C-5, *Ile*), 13.3 [+, C-3′, (*4-Pe*)*Pro*], 13.9 [+, C-4, (β*Me*)*Phe*], 15.0 (+, C-1′, *Ile*), 17.3 [−, C-3′, (*3-Ncp*)*Ala*], 17.9 [+, C-4, (β*Me*)*Phe*], 21.25 (+, C-1′, *MeZ*), 21.33 [+, C-1′, (*3-Ncp*)*Ala*], 24.6 (−, C-4, *Ile*), 32.0 [−, C-3, (*3-Ncp*)*Ala*], 35.2 [−, C-3, (*4-Pe*)*Pro*], 36.9 [+, C-4, (*4-Pe*)*Pro*], 37.3 (+, C-3, *Ile*), 39.1 [+, C-3, (β*Me*)*Phe*], 40.6 (−, C-3, *Dap*), 45.0 [+, C-3, (β*Me*)*Phe*], 53.0 [−, C-5, (*4-Pe*)*Pro*], 53.7 [+, C-2, (*3-Ncp*)*Ala*], 54.6 (+, C-2, *Ile*), 57.8 (+, C-2, *Dap*), 58.8 [+, C-2, (β*Me*)*Phe*], 59.1 [+, C-2′, (*3-Ncp*)*Ala*], 59.5 [+, C-2, (β*Me*)*Phe*], 61.5 [+, C-2, (*4-Pe*)*Pro*], 67.2 (−, Bzl-C), 127.08, 127.12, 127.4, 127.7 [C-2′, (*4-Pe*)*Pro*], 128.0 [C-1′, (*4-Pe*)*Pro*], 128.3, 128.6, 128.8, 129.17 (×2) (+, Ar-C), 133.3, 137.9, 141.3, 142.1 (C_{quat}, Ar-C), 157.3 (C_{quat}, NCO_2), 169.2, 170.9 (×2), 171.4, 172.0, 174.2 (C_{quat}, C-1); IR (KBr): $\tilde{\nu}$ = 3060, 3029, 2972, 2936, 2879, 1725, 1667, 1638, 1543, 1513, 1453, 1369, 1204 cm^{-1}; MS (ESI): pos.: *m/z* (%): 986 (100) [*M*+Na$^+$]; neg.: *m/z* (%): 962 (100) [*M*−H$^-$]; HRMS (ESI): *m/z*: calcd for [$C_{52}H_{66}N_8O_{10}Na^+$]: 985.4794; found 985.4797.

***epi*-19c**: analytical HPLC 1: isocratic, 60% MeCN in H_2O (0.1% TFA), flow rate = 0.5 mL min^{-1}, t_R = 9.44 min, purity > 99%; $[\alpha]_D^{20}$ = −43.1 (*c* = 0.42, $CHCl_3$); ^{1}H NMR (600 MHz, $C_2D_2Cl_4$, 353.1 K): δ = 0.67 (d, *J* = 6.0 Hz, 3H, 1′-H, *a-Ile*), 0.82 (t, *J* = 7.2 Hz, 3H, 5-H, *a-Ile*), 0.93 [ddd, *J* = 6.6, 6.6, 6.6 Hz, 1H, 3′-H$_a$, (*3-Ncp*)*Ala*], 0.93–0.99 (m, 1H, 4-H$_a$, *a-Ile*), 1.05–1.15 (m, 1H, 4-H$_b$, *a-Ile*), 1.24 [d, *J* = 6.6 Hz, 3H, 4-H, (β*Me*)*Phe*], 1.37 [d, *J* = 6.6 Hz, 3H, 4-H, (β*Me*)*Phe*], 1.37–1.45 [m, 1H, 3-H$_a$, (*3-Ncp*)*Ala*], 1.54–1.63 [m, 2H, 3-H$_b$, (*3-Ncp*)*Ala*, 3-H, *a-Ile*], 1.66 [d, *J* = 6.0 Hz, 3′-H, (*4-Pe*)*Pro*], 1.67–1.76 [m, 1H, 1′-H, (*3-Ncp*)*Ala*], 1.84 [ddd, *J* = 10.2, 10.2, 10.2 Hz, 1H, 3-H$_a$, (*4-Pe*)*Pro*], 2.34 (s, 3H, 1′-H, *MeZ*), 2.35–2.44 [m, 1H, 3-H$_b$, (*4-Pe*)*Pro*], 3.07 [m, 1H, 4-H, (*4-Pe*)*Pro*], 3.27

[dd, $J=9.2$, 9.2 Hz, 1H, 5-H_a, (*4-Pe*)*Pro*], 3.31–3.40 [m, 2H, 2 ? 3-H, (β*Me*)*Phe*], 3.48–3.66 (m, 1H, 3-H, *Dap*), 3.74 [dd, $J=9.2$, 9.2 Hz, 1H, 5-H_b, (*4-Pe*)*Pro*], 3.85–3.92 [m, 1H, 2′-H, (*3-Ncp*)*Ala*], 4.29–4.40 [m, 3H, 2-H, *a-Ile*, 2 ? 2-H, (β*Me*)*Phe*], 4.41–4.47 [m, 1H, 2-H, (*3-Ncp*)*Ala*], 4.47–4.54 [m, 1H, 2-H, (*4-Pe*)*Pro*], 4.61 (dd, $J=8.4$, 8.4 Hz, 1H, 2-H, *Dap*), 5.10 (d, $J=12.0$ Hz, Bzl-H_a), 5.14 (d, $J=12.0$ Hz, Bzl-H_b), 5.27–5.35 [dd, $J=10.2$, 10.2 Hz, 1H, 1′-H, (*4-Pe*)*Pro*], 5.61 [dq, $J=10.2$, 6.0 Hz, 1H, 2′-H, (*4-Pe*)*Pro*], 6.55–6.69 (br, 2H, NH), 6.89–7.01 (br, 2H, NH), 7.15 (d, $J=7.2$ Hz, 2H, Ar-H, *MeZ*), 7.18–7.22 (m, 1H, Ar-H), 7.22–7.29 (m, 11H, Ar-H), 7.29–7.36 (m, 3H, Ar-H), 7.39–7.48 (br, 2H, NH); the absorption of 3′-H_b, (*3-Ncp*)*Ala* is masked by the signal of 3′-H, (*4-Pe*)*Pro*; ^{13}C NMR (150.8 MHz, $C_2D_2Cl_4$, 353.1 K): $\delta=11.4$ (+, C-5, *a-Ile*), 12.8 [+, C-3′, (*4-Pe*)*Pro*], 13.6 (+, C-1′, *a-Ile*), 16.9 [+, C-4, (β*Me*)*Phe*], 17.2 [+, C-4, (β*Me*)*Phe*], 17.4 [−, C-3′, (*3-Ncp*)*Ala*], 20.8 (+, C-1′, *MeZ*), 21.9 [+, C-1′, (*3-Ncp*)*Ala*], 26.2 (−, C-4, *a-Ile*), 32.1 [−, C-3, (*3-Ncp*)*Ala*], 35.4 [−, C-3, (*4-Pe*)*Pro*], 36.0 (+, C-3, *a-Ile*), 36.3 [+, C-4, (*4-Pe*)*Pro*], 39.9 [+, C-3, (β*Me*)*Phe*], 41.1 [+, C-3, (β*Me*)*Phe*], 42.4 (−, C-3, *Dap*), 51.5 [+, C-2, (*3-Ncp*)*Ala*], 52.2 [−, C-5, (*4-Pe*)*Pro*], 54.3 (+, C-2, *a-Ile*), 55.8 [+, C-2, (*4-Pe*)*Pro*], 58.8 (+, C-2, *Dap*), 59.3 [+, C-2′, (*3-Ncp*)*Ala*], 60.0 [+, C-2, (β*Me*)*Phe*], 60.4 [+, C-2, (β*Me*)*Phe*], 67.0 (−, Bzl-C), 126.5, 126.8 (+, Ar-C), 127.1 [+, C-2′, (*4-Pe*)*Pro*], 127.4, 127.5, 128.0, 128.3, 128.4 (+, Ar-C), 128.6 [+, C-1′, (*4-Pe*)*Pro*], 129.0 (+, Ar-C), 132.9, 137.8, 142.3, 142.5 (C_{quat}, Ar-C), 156.3 (C_{quat}, NCO_2), 170.2, 170.3, 170.6, 170.8, 171.3, 173.2 (C_{quat}, C-1); IR (KBr): $\tilde{\nu}=3034$, 2969, 2871, 1659, 1541, 1453, 1369, 1256, 1206, 1065 cm^{-1}; MS (ESI): pos.: *m/z* (%): 985 (100) [*M*+Na^+]; neg.: *m/z* (%): 961 (100) [*M*−H^-]; HRMS (ESI): *m/z*: calcd for [$C_{52}H_{66}N_8O_{10}Na^+$]: 985.4794; found 985.4793.

[*a*-Dab^1]-Hormaomycin (2a): A solution of the CHA salt of Teoc-(2*S*,1′*R*,2′*R*)-(3-Ncp)AlaOH (26.6 mg, 63.75 μmol) in Et_2O (50 mL) was washed with 1 M H_2SO_4 (3×5 mL), 1 M $KHSO_4$ (2×5 mL), water (3×5 mL), brine (2×5 mL), dried, filtered and concentrated under reduced pressure. The resulting *N*-protected amino acid was dried at 0.02 Torr for 2 h and then coupled with the depsipeptide, obtained after deprotection of **19a** (19.5 mg, 19.96 μmol) by treatment with 10% anisole in TFA (1.1 mL) according to GP 6 for 2 h, applying HATU (22.8 mg, 59.96 μmol), HOAt (8.1 mg, 59.94 μmol), DIEA (2.57 mg, 19.88 μmol) and TMP (21.8 mg, 179.00 μmol) in CH_2Cl_2 (3 mL) according to GP 4 for 15 h. The mixture was then diluted with Et_2O (40 mL), and the crude product obtained after the usual aqueous work-up (GP 2) was purified by preparative TLC (200×200 mm, acetone/hexane 1:2.7) to give the respective Teoc-(*S*)-(3-Ncp)Ala-cyclohexapeptide (21.6 mg, 96%; $R_f=0.18$, acetone/hexane 1:2.5) as a colorless glass which was used for the next step without any characterization. This substance (21.6 mg, 19.13 μmol) was deprotected by treatment with TFA (2.0 mL) for 1 h. The mixture was concentrated under reduced pressure at 20 °C and then taken up with toluene (3×15 mL), which was distilled off to remove the last traces of TFA. The resulting deprotected branched peptide was coupled with Chpca(MOM)-OH **20** (7.0 mg, 34.04 μmol) by treatment with HATU (12.9 mg, 33.93 μmol), DIEA (2.47 mg, 19.13 μmol) and TMP (12.37 mg, 102.08 μmol) in CH_2Cl_2 (3 mL) according to GP 4 for 5 h. The mixture was then diluted with Et_2O (40 mL) and the crude product obtained after the usual aqueous work-up (GP 2) was purified by preparative TLC (200×200 mm, acetone/hexane 1:2.7, two fold development) and finally by recrystallization from Et_2O/hexane to give the *O*-MOM protected [*a*-Dab^1]-hormaomycin (20.2 mg, 90%; $R_f=0.09$, acetone/hexane 1:3) as a colorless solid which was used for the next step without any characterization. MOM-**2a** (19.1 mg, 16.92 μmol) was deprotected appling $MgBr_2$•Et_2O (164 mg, 633.89 μmol) and EtSH (0.018 mL, 243.07 μmol) in CH_2Cl_2 (10 mL) according to GP 7 for 3 h. The mixture was diluted with Et_2O (50 mL), and the crude product obtained after the usual aqueous work-up (GP 7) was recrystallized from Et_2O/pentane and then from CH_2Cl_2/pentane to give **2a** (15.4 mg, 84%, 68% over five steps from **19a**) as a colorless solid. $R_f=0.14$, acetone/hexane 1:2.5; analytical HPLC: gradient 25 → 85% MeCN in 0.15% ammonium acetate buffer (pH 5.5) for 25 min, flow rate = 0.5 mL min^{-1}, $t_R=21.72$ min, purity > 99%; $[\alpha]_D^{20}=23.0$ ($c=0.1$, $CHCl_3$); ^{1}H NMR (600 MHz, $CDCl_3$): $\delta=-0.69$ [ddd, $J=6.6$, 6.6, 6.6 Hz, 1H, 3′-H_a, (*3-Ncp*)*Ala*], −0.17–0.07 [m, 1H, 3-H_a, (*3-Ncp*)*Ala*], 0.20–0.27 [m, 1H, 1′-H, (*3-Ncp*)*Ala*], 0.54 [ddd, $J=14.4$, 4.8, 4.8 Hz, 1H, 3-H_b, (*3-Ncp*)*Ala*], 0.90 (t, $J=7.2$ Hz, 3H, 5-H, *Ile*), 0.98–1.05 [m, 1H, 3′-H_b, (*3-Ncp*)*Ala*], 1.03 [ddd, $J=7.2$, 7.2, 7.2 Hz, 1H, 3′-H_a, (*3-Ncp*)*Ala*], 1.07 (d, $J=7.2$ Hz, 3H, 1′-H, *Ile*), 1.32 [d, $J=7.2$ Hz, 3H, 4-H, (β*Me*)*Phe*], 1.35 [d, $J=7.2$ Hz, 3H, 4-H, (β*Me*)*Phe*], 1.41 (d, $J=7.8$ Hz, 3H, *a-Dab*), 1.53–1.59 (m, 1H, 4-H_b, *Ile*), 1.63–1.75 [m, 2H, 3-H, (*3-Ncp*)*Ala*], 1.69 [dd, $J=7.2$, 1.8 Hz, 3H, 3′-H, (*4-Pe*)*Pro*], 1.84–1.95 [m, 3H, 3′-H_b, (*3-Ncp*)*Ala*, 3-H, *Ile*, 3-H_a, (*4-Pe*)*Pro*], 1.95–2.01 [m, 1H, 3-H_a, (*4-Pe*)*Pro*], 2.27 [ddd, $J=12.0$, 6.0, 6.0 Hz, 1H, 4-H_b, (*4-Pe*)*Pro*], 2.85 [ddd, $J=6.6$, 4.8, 4.8 Hz, 1H, 2′-H, (*3-Ncp*)*Ala*], 3.02 [dq, $J=11.4$, 7.2 Hz, 1H, 3-H, (β*Me*)*Phe*], 3.22–3.32 [m, 2H, 4-H, 5-H_a, (*4-Pe*)*Pro*], 3.46–3.52 [m, 1H, 2-H, (*3-Ncp*)*Ala*], 3.70 [dq, $J=3.6$, 7.2 Hz, 1H, 3-H, (β*Me*)*Phe*], 3.92 [dd, $J=11.4$, 5.4 Hz, 2-H, (*4-Pe*)*Pro*], 3.95–3.99 [m, 1H, 5-H_b, (*4-Pe*)*Pro*], 4.03 [ddd, $J=7.2$, 3.6, 3.6 Hz, 1H, 2′-H, (*3-Ncp*)*Ala*], 4.35 (dd, $J=10.8$, 10.8 Hz, 1H, 2-H), 4.42–4.48 (m, 1H, 3-H, *a-Dab*), 4.45 (dd, $J=10.2$, 4.2 Hz, 1H, 2-H), 4.50 (dd, $J=9.0$, 3.0 Hz, 1H, 2-H), 4.66 (dd, $J=9.0$, 9.0 Hz, 1H, 2-H), 5.11–5.16 [m, 1H, 2-H, (*3-Ncp*)*Ala*], 5.26–5.31 [m, 1H, 1′-H, (*4-Pe*)*Pro*], 5.63 [dq, $J=10.8$, 6.6 Hz, 1H, 2′-H, (*4-Pe*)*Pro*], 6.15 (d, $J=4.2$ Hz, 1H, 4-H, *Chpca*), 6.43 (d, $J=7.8$ Hz, 1H, NH), 6.77–6.86 (br, 1H, NH), 6.85 (d, $J=4.2$ Hz, 1H, 3-H, *Chpca*), 7.02–7.06 (m, 2H, Ar-H), 7.12–7.19 (m, 6H, Ar-H, NH), 7.21–7.30 (m, 4H, Ar-H, NH), 7.44 (d, $J=10.8$ Hz, 1H, NH), 8.87 (d, $J=9.0$ Hz, 1H, NH), 10.70–11.00 (br, 1H, OH); the signal of 4-H_a, *Ile* was masked by absorption of 4-H, (β*Me*)*Phe* (1.35 ppm); ^{13}C NMR (150.8 MHz, $CDCl_3$): $\delta=10.4$ (+, C-5, *Ile*), 13.1 [+, C-3′, (*4-Pe*)*Pro*], 13.3 (+, C-4, *a-Dab*), 14.9 (+, C-1′, *Ile*), 17.0 [−, C-3′, (*3-Ncp*)*Ala*], 17.2 [−, C-3′, (*3-Ncp*)*Ala*], 17.6 [+, C-4, (β*Me*)*Phe*], 17.7 [+, C-4, (β*Me*)*Phe*], 20.0 [+, C-1′, (*3-Ncp*)*Ala*], 21.7 [+, C-1′, (*3-Ncp*)*Ala*], 25.1 (−, C-4, *Ile*), 32.8 [−, C-3, (*3-Ncp*)*Ala*], 35.2 [−, C-3, (*3-Ncp*)*Ala*], 35.9 [−, C-3, (*4-Pe*)*Pro*], 36.4 [+, C-4, (*4-Pe*)*Pro*], 38.0 (+, C-3, *Ile*), 39.2 [+, C-3, (β*Me*)*Phe*], 41.2 [+, C-3, (β*Me*)*Phe*], 45.3 (+, C-3, *a-Dab*), 51.0 [+, C-2, (*3-Ncp*)*Ala*], 51.8 [+, C-2, (*3-Ncp*)*Ala*], 53.1 [−, C-5, (*4-Pe*)*Pro*], 54.6 (+, C-2), 55.2 (+, C-2), 58.1 [+, C-2′, (*3-Ncp*)*Ala*], 59.3 [+, C-2′, (*3-Ncp*)*Ala*], 59.8 (+, C-2), 60.0 (+, C-2), 63.8 [+, C-2, (*4-Pe*)*Pro*], 103.6 (+, C-4, *Chpca*), 109.9 (+, C-3, *Chpca*), 119.9 (C_{quat}, C-2, *Chpca*), 121.7 (C_{quat}, C-5, *Chpca*), 126.9, 127.3, 127.4, 127.6 (+, Ar-C), 127.87 [+, C-1′, (*4-Pe*)*Pro*], 127.92 [+, C-2′, (*4-Pe*)*Pro*], 128.5, 128.7 (+, Ar-C), 141.3, 142.2 (C_{quat}, Ar-C), 159.3 (C_{quat}, C-1, *Chpca*), 168.3, 169.6, 170.0, 170.2, 171.60, 171.62, 171.9 (C_{quat}, C-1); IR (KBr): $\tilde{\nu}=3383$, 2968, 2933, 2879, 1747, 1651, 1626, 1548, 1452, 1372, 1321, 1182 cm^{-1}; UV (MeOH): neutral: $\lambda_{max}(\varepsilon)=277$ (1.6×10^4) nm; basic: 281 (1.5×10^4), 205 (7.0×10^4) nm; acidic: 272 (1.4×10^4) nm; CD (MeOH): $\lambda_{max}[\Theta]=280.2$ (2.01×10^4); 276.5 (2.05×10^4), 225.6 (-4.55×10^4), 221.5 (-5.06×10^4) nm ($c=1.45\times10^{-5}$ M); MS (ESI): pos.: *m/z* (%): 1151 (100) [*M*+Na^+]; neg.: *m/z* (%): 1127 (100) [*M*−H^-]; HRMS (ESI): *m/z*: calcd for [$C_{55}H_{71}N_{11}O_{13}Cl^+$]: 1128.4916; found 1128.4921.

[*a*-Dab^1,*a*-Ile^5]-Hormaomycin (*epi*-2a): A solution (50 mL) of the CHA salt of Teoc-(2*S*,1′*R*,2′*R*)-(3-Ncp)AlaOH (27.3 mg, 65.39 μmol) in Et_2O (50 mL) was washed with 1 M H_2SO_4 (3×5 mL), 1 M $KHSO_4$ (2×5 mL), water (3×5 mL), brine (2×5 mL), dried, filtered and concentrated under reduced pressure. The resulting *N*-protected amino acid was dried at 0.02 Torr for 2 h and then coupled with the depsipeptide, obtained after deprotection of *epi*-**19a** (20.0 mg, 20.47 μmol) by treatment with 10% anisole in TFA (1.1 mL) according to GP 6 for 2 h, applying HATU (23.4 mg, 61.54 μmol), HOAt (8.3 mg, 61.42 μmol), DIEA (2.64 mg, 20.39 μmol) and TMP (22.36 mg, 183.6 μmol) in CH_2Cl_2 (3 mL) according to GP 4 for 15 h. The mixture was then diluted with Et_2O (40 mL), and the crude product obtained after the usual aqueous work-up (GP 2) was purified by two crystallizations from Et_2O/hexane to give the respective Teoc-(*S*)-(3-Ncp)Ala-*epi*-cyclohexapeptide (17.0 mg, 74%; $R_f=0.19$, acetone/hexane 1:2.5) as a colorless glass which was used for the next step without any characterization. This substance (17.0 mg, 14.50 μmol) was deprotected by treatment with TFA (2.0 mL) for 1 h. The mixture was concentrated under reduced pressure at 20 °C, and then taken up with toluene (3×15 mL) which was distilled off to remove the last traces of TFA. The resulting deprotected branched peptide was coupled with Chpca(MOM)-OH **20** (5.5 mg, 26.74 μmol) applying HATU (10.15 mg, 26.69 μmol), DIEA (1.95 mg, 15.09 μmol) and TMP (12.37 mg, 102.08 μmol) in CH_2Cl_2 (3 mL) according to GP 4 for 5 h. The mixture was then diluted with Et_2O (40 mL), and the crude product obtained after the usual aqueous work-up (GP 2) was recrystallized twice from CH_2Cl_2/hexane to give the *O*-MOM protected [*a*-Dab^1,*a*-Ile^5]-hormaomy-

cin (14.2 mg, 80%; R_f=0.11, acetone/hexane 1:3) as a colorless solid which was used for the next step without any characterization. MOM-*epi*-**2a** (14.2 mg, 12.11 μmol) was deprotected applying $MgBr_2{\cdot}Et_2O$ (110 mg, 425.17 μmol) and EtSH (0.018 mL, 243.07 μmol) in CH_2Cl_2 (10 mL) according to GP 7 for 3 h. The mixture was taken up with Et_2O (50 mL), and the crude product obtained after the usual aqueous work-up (GP 7) was recrystallized from Et_2O/pentane and then from CH_2Cl_2/pentane to give the crude product (13.1 mg), which was finally purified by preparative HPLC to give *epi*-**2a** (9.0 mg, 39% over five steps from *epi*-**19a**) as a colorless solid, which was insoluble in $CHCl_3$. R_f=0.14, acetone/hexane 1:2.5; preparative HPLC: column B, 62% MeCN in H_2O (0.07% TFA), flow rate=2.5 mL min^{-1}; analytical HPLC: the same column, the same conditions, t_R=17.72 min, purity > 99%; ^{1}H NMR (600 MHz, CD_3OD): δ=0.69 (t, J=7.2 Hz, 3H, 5-H, *a-Ile*), 0.72 (d, J=7.2 Hz, 3H, 1′-H, *a-Ile*), 0.82–0.92 (m, 1H, 4-H$_a$, *a-Ile*), 0.95 (ddd, J=7.2, 7.2, 7.2 Hz, 1H, 4-H$_b$, *Ile*), 1.00 [ddd, J=6.0, 6.0, 6.0 Hz, 1H, 3′-H$_a$, (*3-Ncp*)*Ala*], 1.07 [ddd, J=6.6, 6.6, 6.6 Hz, 1H, 3′-H$_a$, (*3-Ncp*)*Ala*], 1.14 [d, J=6.6 Hz, 3H, 4-H, (β*Me*)*Phe*], 1.25 [d, J=7.2 Hz, 3H, 4-H, (β*Me*)*Phe*], 1.31 (d, J=7.2 Hz, 3H, *a-Dab*), 1.34–1.41 [m, 1H, 3-H$_a$, (*3-Ncp*)*Ala*], 1.44–1.52 [m, 1H, 3-H$_a$, (*3-Ncp*)*Ala*], 1.54–1.60 [m, 1H, 3′-H$_b$, (*3-Ncp*)*Ala*], 1.65 [dd, J=7.2, 1.8 Hz, 3H, 3′-H, (*4-Pe*)*Pro*], 1.82 [ddd, J=7.8, 7.8, 7.8 Hz, 1H, 3-H$_a$, (*4-Pe*)*Pro*], 1.93–2.01 [m, 2H, 3-H$_b$, 1′-H, (*3-Ncp*)*Ala*], 2.03–2.15 [m, 2H, 3-H$_b$, (*3-Ncp*)*Ala*, 3-H$_b$, (*4-Pe*)*Pro*], 2.98 [dd, J=10.8, 10.8 Hz, 1H, 5-H$_a$, (*4-Pe*)*Pro*], 3.07 [m, 1H, 4-H, (*4-Pe*)*Pro*], 3.13–3.24 [m, 2H, 2×3-H, (β*Me*)*Phe*], 3.69 [dd, J=10.8, 7.2 Hz, 1H, 5-H$_b$, (*4-Pe*)*Pro*], 4.08 [ddd, J=6.6, 3.0, 3.0 Hz, 1H, 2′-H, (*3-Ncp*)*Ala*], 4.10–4.14 (m, 1H, 2-H, *a-Ile*), 4.19–4.29 [m, 3H, 3-H, *a-Dab*, 2-H, 2′-H, (*3-Ncp*)*Ala*], 4.40 [d, J=10.8 Hz, 2-H, (β*Me*)*Phe*], 4.49 (d, J=3.6 Hz, 1H, 2-H, *a-Dab*), 4.51 [dd, J=7.8, 7.8 Hz, 1H, 2-H, (*4-Pe*)*Pro*], 4.77 [d, J=11.4 Hz, 1H, 2-H, (β*Me*)*Phe*], 4.79–4.82 [m, 1H, 2-H, (*3-Ncp*)*Ala*], 5.38–5.44 [m, 1H, 1′-H, (*4-Pe*)*Pro*], 5.59 [dq, J=10.2, 7.2 Hz, 1H, 2′-H, (*4-Pe*)*Pro*], 6.00 (d, J=4.5 Hz, 1H, 4-H, *Chpca*), 6.73 (d, J=4.5 Hz, 1H, 3-H, *Chpca*), 7.01–7.15 (m, 1H, Ar-H), 7.17–7.25 (m, 3H, Ar-H), 7.25–7.31 (m, 6H, Ar-H), 7.41–7.49 (br, 1H, NH), 7.80–7.84 (br, 1H, NH); the signal of 1′-H, (*3-Ncp*)*Ala* was masked by absorption of 4-H, *a-Dab* and the signals of 3-H, *a-Ile* and 3′-H$_b$, (*3-Ncp*)*Ala* were masked by absorption of 3′-H, (*4-Pe*)*Pro*; ^{13}C NMR (150.8 MHz, CD_3OD): δ=12.2 (+, C-5, *a-Ile*), 13.3 [+, C-3′, (*4-Pe*)*Pro*], 14.6 (+, C-1′, *a-Ile*), 17.9 [−, C-3′, (*3-Ncp*)*Ala*], 18.0 [+, C-4, (β*Me*)*Phe*], 18.9 [−, C-3′, (*3-Ncp*)*Ala*], 19.1 (+, C-4, *a-Dab*), 19.4 [+, C-4, (β*Me*)*Phe*], 23.6 [+, C-1′, (*3-Ncp*)*Ala*], 23.8 [+, C-1′, (*3-Ncp*)*Ala*], 27.3 (−, C-4, *a-Ile*), 34.06 [−, C-3, (*3-Ncp*)*Ala*], 34.15 [−, C-3, (*3-Ncp*)*Ala*], 34.18 [−, C-3, (*4-Pe*)*Pro*], 36.5 (+, C-3, *a-Ile*), 37.7 [+, C-4, (*4-Pe*)*Pro*], 41.6 [+, C-3, (β*Me*)*Phe*], 43.4 [+, C-3, (β*Me*)*Phe*], 48.9 (+, C-3, *a-Dab*), 51.0 [+, C-2, (*3-Ncp*)*Ala*], 53.2 [−, C-5, (*4-Pe*)*Pro*], 53.3 [+, C-2′, (*3-Ncp*)*Ala*], 53.9 [+, C-2, (*3-Ncp*)*Ala*], 55.9 (+, C-2, *a-Ile*), 58.4 (+, C-2, *a-Dab*), 59.5 [+, C-2, (β*Me*)*Phe*], 60.2 [+, C-2, (*3-Ncp*)*Ala*], 60.3 [+, C-2′, (*3-Ncp*)*Ala*], 61.3 [+, C-2, (*4-Pe*)*Pro*], 62.0 [+, C-2, (β*Me*)*Phe*], 104.0 (+, C-4, *Chpca*), 111.1 (+, C-3, *Chpca*), 119.2 (C_{quat}, C-2, *Chpca*), 122.1 (C_{quat}, C-5, *Chpca*), 127.5 [+, C-2′, (*4-Pe*)*Pro*], 127.8, 128.2, 128.95, 128.99, 129.59, 129.67 (+, Ar-C), 130.8 [+, C-1′, (*4-Pe*)*Pro*], 143.6, 144.5 (C_{quat}, Ar-C), 161.7 (C_{quat}, C-1, *Chpca*), 171.3, 172.0, 172.2, 172.7, 172.87, 172.90, 174.3 (C_{quat}, C-1); IR (KBr): $\tilde{\nu}$=3445, 2926, 2850, 1653, 1558, 1543, 1458, 1383, 1321, 1020 cm^{-1}; UV (MeOH): neutral: $\lambda_{max}(\varepsilon)$=279 ($8.3\times10^3$) nm; basic: 283 ($8.0\times10^3$), 209 ($2.3\times10^4$) nm; acidic: 271 ($8.7\times10^3$) nm; CD (MeOH): $\lambda_{max}[\Theta]$=279.6 (1.15×10^4); 275.7 (1.08×10^4), 225.3 (-3.85×10^4) nm ($c=1.26\times10^{-5}$ M); MS (ESI): pos.: *m/z* (%): 1151 (100) [M+Na$^+$], 1129 (52) [M+H$^+$]; neg.: *m/z* (%): 1127 (100) [M−H$^-$].

[*a*-N$_\beta$Me-Dab^1]-Hormaomycin (2b): A solution of the CHA salt of Teoc-(2*S*,1′*R*,2′*R*)-(3-Ncp)AlaOH (40.3 mg, 96.5 μmol) in Et_2O (50 mL) was washed with 1 M H_2SO_4 (3×5 mL), 1 M $KHSO_4$ (2×5 mL), water (3×5 mL), brine (2×5 mL), dried, filtered and concentrated under reduced pressure. The resulting *N*-protected amino acid was dried at 0.02 Torr for 2 h and then coupled with the peptolide, obtained after deprotection of **19b** (29.0 mg, 29.3 μmol) by treatment with 10% anisole in TFA (1.5 mL) according to GP 6 for 2 h, applying HATU (33.3 mg, 87.8 μmol), HOAt (13.0 mg, 96.5 μmol), DIEA (3.78 mg, 29.3 μmol) and TMP (31.9 mg, 263.3 μmol) in CH_2Cl_2 (3 mL) according to GP 4 for 15 h. The mixture was then diluted with Et_2O (40 mL), and the crude product obtained after the usual aqueous work-up (GP 2) was purified by crystallization first from CH_2Cl_2/pentane and then from Et_2O/pentane to give the respective Teoc-(*S*)-(3-Ncp)Ala-cyclohexapeptide (32.5 mg, 97%; R_f=0.22, acetone/hexane 4:7) as a colorless solid, which was used for the next step without any characterization. This substance (32.5 mg, 28.4 μmol) was deprotected by treatment with TFA (2.0 mL) for 1 h. The mixture was concentrated under reduced pressure at 20 °C and then taken up with toluene (3×15 mL) which was distilled off to remove the last traces of TFA. The resulting deprotected branched peptide was coupled with Chpca(MOM)-OH **20** (14.6 mg, 71.1 μmol) applying HATU (25.9 mg, 68.2 μmol), DIEA (3.67 mg, 28.4 μmol) and TMP (26.0 mg, 213.0 μmol) in CH_2Cl_2 (3 mL) according to GP 4 for 5 h. The mixture was then diluted with Et_2O (40 mL), and the crude product obtained after the usual aqueous work-up (GP 2) was purified by chromatography (R_f=0.39, acetone/hexane 1:1.5) to give the *O*-MOM protected [*a*-N$_\beta$Me-Dab^1]-hormaomycin (25.0 mg, 74%) as a colorless solid, which was used for the next step without any characterization. MOM-**2b** (25.0 mg, 21.1 μmol) was deprotected by treatment with $MgBr_2{\cdot}Et_2O$ (150 mg, 579.7 μmol) and EtSH (0.015 mL, 202.6 μmol) in CH_2Cl_2 (10 mL) according to GP 7 for 3.5 h. The mixture was diluted Et_2O (50 mL), and the crude product obtained after the usual aqueous work-up (GP 7) was recrystallized from CH_2Cl_2/pentane to give a crude product (22.0 mg), which was finally purified by preparative HPLC to give **2b** (16.0 mg, 48% over five steps) as a colorless solid. Preparative HPLC: column B, 69% MeCN in H_2O (0.1% TFA), flow rate=2.5 mL min^{-1}; analytical HPLC: 70% MeCN in H_2O (0.1% TFA), flow rate=0.5 mL min^{-1}, t_R=10.00 min, purity > 99%; R_f=0.24, acetone/hexane 1:1.5; $[\alpha]_D^{20}$=75.0 (c=0.15, MeOH); ^{1}H NMR (600 MHz, $CDCl_3$): δ=−0.01–0.16 [m, 2H, 3-H$_a$, 3′-H$_a$, (*3-Ncp*)*Ala*], 0.64–0.76 [m, 1H, 1′-H, (*3-Ncp*)*Ala*], 0.81 (t, J=7.2 Hz, 3H, 5-H, *Ile*), 1.03 (d, J=6.6 Hz, 3H, 1′-H, *Ile*), 1.15–1.25 (m, 1H, 4-H$_a$, *Ile*), 1.26 [d, J=6.6 Hz, 3H, 4-H, (β*Me*)*Phe*], 1.37 [d, J=7.2 Hz, 3H, 4-H, (β*Me*)*Phe*], 1.45–1.53 (m, 1H, 4-H$_b$, *Ile*), 1.55 (d, J=7.2 Hz, 3H, *a-N*$_\beta$*Me-Dab*), 1.66 [dd, J=6.6, 1.2 Hz, 3H, 3′-H, (*4-Pe*)*Pro*], 1.70–1.79 [m, 3H, 3-H, (*3-Ncp*)*Ala*, 3-H$_a$, (*4-Pe*)*Pro*], 1.83–1.88 [m, 1H, 3′-H$_b$, (*3-Ncp*)*Ala*], 1.94–2.02 [m, 1H, 3-H, *Ile*], 2.03–2.10 [m, 1H, 1′-H, (*3-Ncp*)*Ala*], 2.17–2.23 [m, 1H, 4-H$_b$, (*4-Pe*)*Pro*], 2.85 [dq, J=9.6, 6.6 Hz, 1H, 3-H, (β*Me*)*Phe*], 3.10 (s, 3H, NMe, *a-N*$_\beta$*Me-Dab*), 3.20–3.34 [m, 3H, 4-H, 5-H$_a$, (*4-Pe*)*Pro*, 2′-H, (*3-Ncp*)*Ala*], 3.54–3.60 [m, 1H, 2-H, (*3-Ncp*)*Ala*], 3.70 [dq, J=5.2, 7.2 Hz, 1H, 3-H, (β*Me*)*Phe*], 4.02 [dd, J=7.2, 7.2 Hz, 1H, 5-H$_b$, (*4-Pe*)*Pro*], 4.19–4.24 [m, 1H, 2′-H, (*3-Ncp*)*Ala*], 4.50 [dd, J=9.6 Hz, 1H, 2-H, (β*Me*)*Phe*], 4.52 [dd, J=12.0, 5.2 Hz, 1H, 2-H, (β*Me*)*Phe*], 4.59–4.64 [m, 4H, 2-H, *Ile*, 2-H, 3-H, *a-N*$_\beta$*Me-Dab*, 2-H, (*4-Pe*)*Pro*], 4.98–5.02 [m, 1H, 2-H, (*3-Ncp*)*Ala*], 5.24–5.29 [m, 1H, 1′-H, (*4-Pe*)*Pro*], 5.60 [dq, J=11.2, 6.6 Hz, 1H, 2′-H, (*4-Pe*)*Pro*], 5.98–6.01 (m, 1H, 4-H, *Chpca*), 6.60–6.67 (m, 1H, 3-H, *Chpca*), 6.64–6.71 (br, 1H, NH), 7.02–7.08 (m, 2H, Ar-H), 7.10–7.19 (m, 4H, Ar-H, NH), 7.16–7.20 (m, 2H, Ar-H), 7.22–7.28 (m, 4H, Ar-H, NH), 7.34–7.40 (br, 1H, NH), 7.40–7.47 (br, 1H, NH), 7.98–8.10 (br, 1H, NH), 8.52–8.62 (br, 1H, NH), 12.0–13.2 (br, 1H, OH); the signals of 3-H$_b$, (*3-Ncp*)*Ala* and 3′-H$_b$, (*3-Ncp*)*Ala* was masked by absorption of 1′-H, *Ile* and the signal of 3′-H$_b$, (*3-Ncp*)*Ala* by absorption of 4-H, (β*Me*)*Phe* (1.26 ppm); ^{13}C NMR (150.8 MHz, $CDCl_3$): δ=10.4 (+, C-5, *Ile*), 13.26 [+, C-4, (β*Me*)*Phe*], 13.31 [+, C-3′, (*4-Pe*)*Pro*], 15.4 (+, C-1′, *Ile*), 16.6 (+, C-4, *a-N*$_\beta$*Me-Dab*), 17.0 [−, C-3′, (*3-Ncp*)*Ala*], 17.2 [−, C-3′, (*3-Ncp*)*Ala*], 18.0 [+, C-4, (β*Me*)*Phe*], 20.7 [+, C-1′, (*3-Ncp*)*Ala*], 21.9 [+, C-1′, (*3-Ncp*)*Ala*], 24.7 (−, C-4, *Ile*), 32.4 (+, NMe, *a-N*$_\beta$*Me-Dab*), 32.6 [−, C-3, (*3-Ncp*)*Ala*], 33.5 [−, C-3, (*3-Ncp*)*Ala*], 34.8 [−, C-3, (*4-Pe*)*Pro*], 36.6 (+, C-3, *Ile*), 36.8 [+, C-4, (*4-Pe*)*Pro*], 39.1 [+, C-3, (β*Me*)*Phe*], 43.7 [+, C-3, (β*Me*)*Phe*], 50.6 [+, C-2, (*3-Ncp*)*Ala*], 52.3 (+, C-3, *a-N*$_\beta$*Me-Dab*), 52.60 [+, C-2, (*3-Ncp*)*Ala*], 52.65 [−, C-5, (*4-Pe*)*Pro*], 54.9 (+, C-2, *Ile*), 58.6 [+, C-2′, (*3-Ncp*)*Ala*], 58.8 (+, C-2, *a-N*$_\beta$*Me-Dab*), 58.9 [+, C-2, (β*Me*)*Phe*], 59.4 [+, C-2′, (*3-Ncp*)*Ala*], 59.5 [+, C-2, (β*Me*)*Phe*], 59.6 [+, C-2, (*4-Pe*)*Pro*], 103.1 (+, C-4, *Chpca*), 108.5 (+, C-3, *Chpca*), 117.7 (C_{quat}, C-2, *Chpca*), 119.0 (C_{quat}, C-5, *Chpca*), 126.8, 127.0, 127.3, 127.6 (+, Ar-C), 127.8 [+, C-1′, (*4-Pe*)*Pro*], 128.0 [+, C-2′, (*4-Pe*)*Pro*], 128.44 (×2) (+, Ar-C), 141.9, 142.3 (C_{quat}, Ar-C), 160.1 (C_{quat}, C-1, *Chpca*), 169.8, 170.0, 170.2, 170.7, 170.8, 171.2, 174.2 (C_{quat}, C-1); IR (KBr): $\tilde{\nu}$=3383, 2968, 2935, 2877, 1634, 1543, 1440, 1368, 1311, 1263, 1212, 1129 cm^{-1}; UV (MeOH): neutral: $\lambda_{max}(\varepsilon)$=277 ($1.5\times10^4$) nm; basic: 281 ($1.3\times10^4$), 205

(7.0×10^4) nm; acidic: 273 (1.6×10^4) nm; CD (MeOH): $\lambda_{max}[\Theta]=278.8$ (3.4×10^4); 229.0 (-2.54×10^4) nm ($c=2.1\times10^{-5}$ M); MS (ESI): pos.: *m*/*z* (%): 1165 (100) [*M*+Na$^+$]; neg.: *m*/*z* (%): 1141 (100) [*M*−H$^-$]; HRMS (ESI): *m*/*z*: calcd for [$C_{56}H_{73}N_{11}O_{13}Cl^+$]: 1142.5072; found 1142.5072.

[Dap^1]-Hormaomycin (2c): A solution of the CHA salt of Teoc-(2*S*,1′*R*,2′*R*)-(3-Ncp)AlaOH (40.6 mg, 97.3 μmol) in Et_2O (50 mL) was washed with 1 M H_2SO_4 (3×5 mL), 1 M $KHSO_4$ (2×5 mL), water (3×5 mL), brine (2×5 mL), dried, filtered and concentrated under reduced pressure. The resulting *N*-protected amino acid was dried at 0.02 Torr for 2 h and then coupled with the peptolide, obtained after deprotection of **19c** (28.4 mg, 29.5 μmol) by treatment with 10% anisole in TFA (1.5 mL) according to GP 6 for 2 h, applying HATU (33.6 mg, 88.5 μmol), HOAt (13.2 mg, 97.3 μmol), DIEA (3.81 mg, 29.5 μmol) and TMP (32.2 mg, 265.4 μmol) in CH_2Cl_2 (3 mL) according to GP 4 for 15 h. The mixture was then diluted with Et_2O (40 mL), and the crude product obtained after the usual aqueous work-up (GP 2) was purified by crystallization first from CH_2Cl_2/pentane and then from Et_2O/pentane to give the respective Teoc-(*S*)-(3-Ncp)Ala-cyclohexapeptide (30.2 mg, 92%; $R_f=0.25$, acetone/hexane 4:7) as a colorless solid, which was used for the next step without any characterization. This substance (30.2 mg, 27.1 μmol) was deprotected by treatment with TFA (2.0 mL) for 1 h. The mixture was concentrated under reduced pressure at 20 °C and then taken up with toluene (3×15 mL), which was distilled off to remove the last traces of TFA. The resultant deprotected branched peptide was coupled with Chpca-(MOM)-OH **20** (13.9 mg, 67.7 μmol) applying HATU (23.7 mg, 62.3 μmol), DIEA (3.50 mg, 27.1 μmol) and TMP (25.0 mg, 203.1 μmol) in CH_2Cl_2 (3 mL) according to GP 4 for 5 h. The mixture was then diluted with Et_2O (40 mL), and the crude product obtained after the usual aqueous work-up (GP 2) was purified by chromatography (acetone/hexane 1:1.5) to give the *O*-MOM protected [Dap^1]-hormaomycin (22.0 mg, 70%; $R_f=0.10$, acetone/hexane 4:7) as a colorless solid, which was used for the next step without any characterization. MOM-**2c** (22.0 mg, 21.1 μmol) was deprotected by treatment with $MgBr_2\cdot Et_2O$ (150 mg, 579.7 μmol) and EtSH (0.015 mL, 202.6 μmol) in CH_2Cl_2 (10 mL) according to GP 7 for 3.5 h. The mixture was diluted Et_2O (50 mL), and the crude product obtained after the usual aqueous work-up (GP 7) was recrystallized from CH_2Cl_2/pentane to give a crude product (21.5 mg), which was finally purified by preparative HPLC to give **2c** (14.2 mg, 43% over five steps) as a colorless solid. Preparative HPLC: column B, 70% MeCN in H_2O (0.1% TFA), flow rate = 2.5 mL min^{-1}; analytical HPLC: 70% MeCN in H_2O (0.1% TFA), flow rate = 0.5 mL min^{-1}, $t_R=9.27$ min, purity > 99%; $R_f=0.10$ (acetone/hexane 4:7); $[\alpha]_D^{20}=61.0$ ($c=0.10$, MeOH); ^{1}H NMR (600 MHz, $CDCl_3$): $\delta=-0.60$ [ddd, $J=6.6$, 6.6, 6.6 Hz, 1H, 3′-H$_a$, (*3-Ncp*)*Ala*], −0.20–0.02 [m, 1H, 3-H$_a$, (*3-Ncp*)*Ala*], 0.25–0.31 [m, 1H, 1′-H, (*3-Ncp*)*Ala*], 0.52 [ddd, $J=13.8$, 4.8, 4.8 Hz, 1H, 3-H$_b$, (*3-Ncp*)*Ala*], 0.89 (t, $J=7.2$ Hz, 3H, 5-H, *Ile*), 0.98–1.05 [m, 2H, 3′-H$_a$, 3′-H$_b$, (*3-Ncp*)*Ala*], 1.07 (d, $J=7.2$ Hz, 3H, 1′-H, *Ile*), 1.30 [d, $J=7.2$ Hz, 3H, 4-H, (β*Me*)*Phe*], 1.40 [d, $J=7.2$ Hz, 3H, 4-H, (β*Me*)*Phe*], 1.54–1.60 (m, 1H, 4-H$_b$, *Ile*), 1.67 [dd, $J=6.6$ Hz, 3H, 3′-H, (*4-Pe*)*Pro*], 1.67–1.75 [m, 2H, 3-H, (*3-Ncp*)*Ala*], 1.84–1.93 [m, 3H, 3′-H$_b$, (*3-Ncp*)*Ala*, 3-H, *Ile*, 3-H$_a$, (*4-Pe*)*Pro*], 1.95–2.01 [m, 1H, 3-H$_a$, (*4-Pe*)*Pro*], 2.23 [ddd, $J=12.0$, 6.0, 6.0 Hz, 1H, 4-H$_b$, (*4-Pe*)*Pro*], 2.87 [ddd, $J=6.6$, 3.0, 3.0 Hz, 1H, 2′-H, (*3-Ncp*)*Ala*], 3.04 [dq, $J=10.5$, 7.2 Hz, 1H, 3-H, (β*Me*)*Phe*], 3.18–3.30 [m, 2H, 4-H, 5-H$_a$, (*4-Pe*)*Pro*], 3.33 (d, $J=13.8$ Hz, 1H, 3-H$_a$, *Dap*), 3.49 [ddd, $J=7.2$, 3.6 Hz, 1H, 2-H, (*3-Ncp*)*Ala*], 3.68 [dq, $J=4.8$, 7.2 Hz, 1H, 3-H, (β*Me*)*Phe*], 3.93 [dd, $J=12.0$, 5.4 Hz, 2-H, (*4-Pe*)*Pro*], 3.94–3.98 [m, 1H, 5-H$_b$, (*4-Pe*)*Pro*], 4.04 [ddd, $J=7.2$, 3.6, 3.6 Hz, 1H, 2′-H, (*3-Ncp*)*Ala*], 4.16 (dddd, $J=13.8$, 10.8, 3.0, 3.0 Hz, 1H, 3-H$_b$, *Dap*), 4.33 [dd, $J=10.5$, 10.5 Hz, 1H, 2-H, (β*Me*)*Phe*], 4.47 [dd, $J=9.6$, 4.8 Hz, 1H, 2-H, (β*Me*)*Phe*], 4.50 (dd, $J=9.0$, 3.0 Hz, 1H, 2-H), 4.60–4.68 (m, 2H, 2-H, *Ile*, 2-H, *Dap*), 5.14–5.20 [m, 1H, 2-H, (*3-Ncp*)*Ala*], 5.24–5.30 [m, 1H, 1′-H, (*4-Pe*)*Pro*], 5.61 [dq, $J=10.8$, 6.6 Hz, 1H, 2′-H, (*4-Pe*)*Pro*], 6.15 (d, $J=4.8$ Hz, 1H, 4-H, *Chpca*), 6.46 (d, $J=6.6$ Hz, 1H, NH), 6.78–6.83 (br, 1H, NH), 6.83 (d, $J=4.8$ Hz, 1H, 3-H, *Chpca*), 7.02–7.06 (m, 2H, Ar-H), 7.10–7.19 (m, 6H, Ar-H, NH), 7.20–7.24 (m, 5H, Ar-H, NH), 7.32 (d, $J=9.0$ Hz, 1H, NH), 8.17 (d, $J=7.8$ Hz, 1H, NH), 8.75 (d, $J=8.4$ Hz, 1H, NH), 10.75–11.15 (br, 1H, OH); The signal of 4-H$_a$, *Ile* was masked by absorption of C-4, (β*Me*)*Phe* (1.30 ppm); ^{13}C NMR (150.8 MHz, $CDCl_3$): $\delta=10.3$ (+, C-5, *Ile*), 13.2 [+, C-4, (β*Me*)*Phe*], 13.3 [+, C-3′, (*4-Pe*)*Pro*], 14.8 (+, C-1′, *Ile*), 16.9 [−, C-3′, (*3-Ncp*)*Ala*], 17.1 [−, C-3′, (*3-Ncp*)*Ala*], 17.5 [+, C-4, (β*Me*)*Phe*], 20.0 [+, C-1′, (*3-Ncp*)*Ala*], 21.6 [+, C-1′, (*3-Ncp*)*Ala*], 25.1 (−, C-4, *Ile*), 32.9 [−, C-3, (*3-Ncp*)*Ala*], 35.0 [−, C-3, (*3-Ncp*)*Ala*], 35.7 [−, C-3, (*4-Pe*)*Pro*], 36.3 [+, C-4, (*4-Pe*)*Pro*], 37.8 (+, C-3, *Ile*), 38.0 (−, C-3, *Dap*), 39.1 [+, C-3, (β*Me*)*Phe*], 41.6 [+, C-3, (β*Me*)*Phe*], 50.9 [+, C-2, (*3-Ncp*)*Ala*], 51.8 (+, C-2, *Dap*), 52.0 [+, C-2, (*3-Ncp*)*Ala*], 53.0 [−, C-5, (*4-Pe*)*Pro*], 54.5 (+, C-2, *Ile*), 58.0 [+, C-2′, (*3-Ncp*)*Ala*], 59.2 [+, C-2′, (*3-Ncp*)*Ala*], 60.0 [+, C-2, (β*Me*)*Phe*], 60.3 [+, C-2, (β*Me*)*Phe*], 63.5 [+, C-2, (*4-Pe*)*Pro*], 103.6 (+, C-4, *Chpca*), 109.8 (+, C-3, *Chpca*), 119.9 (C_{quat}, C-2, *Chpca*), 121.6 (C_{quat}, C-5, *Chpca*), 126.9, 127.3, 127.4, 127.6 (+, Ar-C), 127.8 [+, C-1′, (*4-Pe*)*Pro*], 127.9 [+, C-2′, (*4-Pe*)*Pro*], 128.5, 128.6 (+, Ar-C), 141.3, 142.1 (C_{quat}, Ar-C), 159.2 (C_{quat}, C-1, *Chpca*), 168.4, 169.5, 170.3, 170.8, 171.7, 172.4, 172.5 (C_{quat}, C-1); IR (KBr): $\tilde{\nu}=3347$, 2968, 2933, 2877, 1625, 1544, 1428, 1368, 1260, 1210 cm^{-1}; UV (MeOH): neutral: $\lambda_{max}(\varepsilon)=277$ (1.6×10^4), 209 (5.6×10^4) nm; basic: 280 (1.7×10^4), 211 (5.6×10^4) nm; acidic: 273 (1.6×10^4), 208 (5.6×10^4) nm; CD (MeOH): $\lambda_{max}[\Theta]=276.0$ (3.31×10^4); 222.6 (-3.47×10^4), 210.8 (-5.67×10^3) nm ($c=2.9\times10^{-5}$ M); MS (ESI): pos.: *m*/*z* (%): 1137 (100) [*M*+Na$^+$], 1115 (32) [*M*+H$^+$]; neg.: *m*/*z* (%): 1113 (72) [*M*−H$^-$]; HRMS (ESI): *m*/*z*: calcd for [$C_{54}H_{69}N_{11}O_{13}Cl^+$]: 1114.4759; found 1114.4760.

Acknowledgements

This work was supported by the Deutsche Forschungsgemeinschaft (SFB-416, Projects A3, B5 and ZS), the Max-Planck-Gesellschaft and the Fonds der Chemischen Industrie. The authors are indebted to Dr. H. Frauendorf (Göttingen) for performing the HPLC/MS experiments, to Mr. H.-P. Kroll (Göttingen) for excellent technical assistance and to Dr. B. Knieriem (Göttingen) for his careful proofreading of the final manuscript.

[1] a) N. Andres, H. Wolf, H. Zähner, E. Rössner, A. Zeeck, W. A. König, V. Sinnwell, *Helv. Chim. Acta* **1989**, *72*, 426–437; b) E. Rössner, A. Zeeck, W. A. König, *Angew. Chem.* **1990**, *102*, 84–85; *Angew. Chem. Int. Ed. Engl.* **1990**, *29*, 64–65.

[2] For the final elucidation of the structure of hormaomycin **1**, see: a) B. D. Zlatopolskiy, K. Loscha, P. Alvermann, S. I. Kozhushkov, S. V. Nikolaev, A. Zeeck, A. de Meijere, *Chem. Eur. J.* **2004**, *10*, 4708–4717; for its total synthesis see: b) B. D. Zlatopolskiy, A. de Meijere, *Chem. Eur. J.* **2004**, *10*, 4718–4727. The formula **1** as presented here depicts the correct absolute configuration in the (*S*)-isoleucine (Ile) moiety. The formulas in our recently published corrigendum in *Chem. Eur. J.* **2004**, *10*, 5568, were indeed erroneous in this respect.

[3] K. Otoguro, H. Ui, A. Ishiyama, N. Arai, M. Kobayashi, Y. Takahashi, R. Masuma, K. Shiomi, H. Yamada, S. Omura, *J. Antibiot.* **2003**, *56*, 322–324.

[4] a) M. Brandl, S. I. Kozhushkov, B. D. Zlatopolskiy, B. Geers, P. Alvermann, A. Zeeck, A. de Meijere, *Eur. J. Org. Chem.* **2005**, 123–125; b) S. I. Kozhushkov, B. D. Zlatopolskiy, M. Brandl, M. Radzom, B. Geers, P. Alvermann, A. Zeeck, A. de Meijere, *Eur. J. Org. Chem.* **2005**, in press; c) B. D. Zlatopolskiy, M. Radzom, A. Zeeck, A. de Meijere, unpublished results.

[5] P. Alvermann, *PhD Thesis*, Universität Göttingen, **2001**.

[6] H. Han, J. Yoon, K. D. Janda, *J. Org. Chem.* **1998**, *63*, 2045–2048.

[7] K. Wen, H. Han, T. Z. Hoffman, K. D. Janda, L. E. Orgel, *Bioorg. Med. Chem. Lett.* **2001**, *11*, 689–692.

[8] D. D. Hennings, R. M. Williams, *Synthesis* **2000**, 1310–1314.

[9] V. V. Sokolov, S. I. Kozhushkov, S. Nikolskaya, V. N. Belov, M. Es-Sayed, A. de Meijere, *Eur. J. Org. Chem.* **1998**, 777–783.

[10] B. D. Zlatopolskiy, H.-P. Kroll, E. Melotto, A. de Meijere, *Eur. J. Org. Chem.* **2004**, 4492–4502.

[11] It is noteworthy that the NMR spectra measured in $CDCl_3$ and $C_2D_2Cl_4$ of the acid **15b** (as well as of the corresponding methyl ester) showed the presence of at least four conformers instead of the usual two as in the case of the peptides **15a**, **15c**, MeZ-*a*-Thr-[Boc-(4-Pe)Pro-OH] (and of the corresponding methyl esters) due to the hindered rotation around the tertiary urethane bond of Boc-(4-Pe)Pro. This is presumed to be attributable to the additionally hindered rotation around the tertiary amide bond between (4-Pe)Pro and *a*-N_βMe-Dab fragments. A complicated temperature dependence for the spectra measured in $C_2D_2Cl_4$ was also observed. On heating up to 100 °C, the coalescence point was almost reached, but spectra measured at 125 °C again showed the presence of several conformers; as already at this temperature the compound started to decompose, no attempts were made to measure spectra at higher temperatures.
[12] See: A. F. Abdel-Magid, J. H. Cohen, C. A. Maryanoff, R. D. Shah, F. J. Villani, F. Zhang, *Tetrahedron Lett.* **1998**, *39*, 3391–3394.
[13] See Supporting Information for details.
[14] L. A. Carpino, *J. Am. Chem. Soc.* **1993**, *115*, 4397–4398.
[15] Determined according to the advanced Marfey method (cf.: K. Fujii, Y. Ikai, T. Mayumi, H. Oka, M. Suzuki, K. Harada, *Anal. Chem.* **1997**, *69*, 3346–3352; Y. Suzuki, M. Ojika, Y. Sakagami, K. Kaida, R. Fudou, T. Kameyama, *J. Antibiot.* **2001**, *54*, 22–28) after acidic hydrolysis of the appropriate peptides. See Supporting Information for details.
[16] For preliminary assignments of ^1H and ^{13}C NMR spectra of **1**, see: a) P. Henne, *Dissertation*, Universität Göttingen, **1994**; b) B. Geers, *Dissertation*, Universität Göttingen, **1998**.
[17] D. E. Dorman, F. A. Bovey, *J. Org. Chem.* **1973**, *38*, 2379–2383.
[18] a) R. Schwyzer, J. P. Garrión, B. Gorup, H. Nolting, A. Tun-Kyi, *Helv. Chim. Acta* **1964**, *47*, 441–464; b) H. Kessler, *Angew. Chem.* **1982**, *94*, 509–520; *Angew. Chem. Int. Ed. Engl.* **1982**, *21*, 512–523.
[19] A. C. Gibbs, L. H. Kondejewski, W. Gronwald, A. M. Nip, R. S. Hodges, B. D. Sykes, D. S. Wishart, *Nat. Struct. Mol. Biol.* **1998**, *5*, 284–288.
[20] G. D. Rose, L. M. Gierasch, J. A. Smith, *Adv. Protein Chem.* **1985**, *38*, 1–109.
[21] H. Kessler, J. W. Bats, C. Griesinger, S. Koll, M. Will, K. Wagner, *J. Am. Chem. Soc.* **1988**, *110*, 1033–1049.
[22] Some hormaomycin analogues show interesting shifts of their antibiotic activities.[4c] Consequently, the antibiotic activities of all synthesized hormaomycin analogues against *E. coli*, *B. subtilis*, *S. aureus*, *C. albicans* were also tested. Analogue **2c** was more active against *S. aureus* species than hormaomycin **1**. Nevertheless, its activity was lower than that of penicillin G.
[23] Cyclopeptides obtained after deprotection of **19a–c**, *epi*-**19a** and *epi*-**19c** as well as the *N*-MeZ protected ring part of hormaomycin **1** were also tested (as trifluoroacetates), but were all totally inactive.
[24] L. A. Carpino, Patent US 5 580 981, **1996**.
[25] a) B. D. Zlatopolski, *Dissertation*, Universität Göttingen, **2003**; b) Supporting Information.
[26] T. L. Hwang, A. J. Shaka, *J. Am. Chem. Soc.* **1992**, *114*, 3157–3159.
[27] P. Dauber-Osguthorpe, V. A. Roberts, D. J. Osguthorpe, J. Wolff, M. Genest, A. T. Hagler, *Proteins Struct. Funct. Genet.* **1988**, *4*, 31–47.
[28] M. Nilges, G. M. Clore, A. M. Gronenborn, *FEBS Lett.* **1988**, *229*, 317–324.

Received: September 24, 2004
Published online: March 7, 2005

CHEMISTRY
A EUROPEAN JOURNAL

Supporting Information

The Structure of Hormaomycin and One of Its All-Peptide Aza-Analogues in Solution – Syntheses and Biological Activities of New Hormaomycin Analogues

U. M. Reinscheid,[a] B. D. Zlatopolskiy,[b] A. Zeeck,[b]* C. Griesinger,[a]* and A. de Meijere[b]*

[a] Dr. Uwe M. Reinscheid, Prof. Dr. Christian Griesinger
Max Planck Institute for Biophysical Chemistry, Am Faßberg 11, D-37077, Göttingen, Germany
Fax: (internat.) + 49 (0)551/2012202
E-mail: cigr@nmr.mpibpc.mpg.de

[b] Dr. Boris D. Zlatopolskiy, Prof. Dr. Axel Zeeck, Prof. Dr. Armin de Meijere
Institut für Organische und Biomolekulare Chemie der Georg-August-Universität Göttingen,
Tammannstrasse 2, D-37077 Göttingen, Germany
Fax: (internat.) + 49-(0)551/399475
E-mail: Armin.deMeijere@chemie.uni-goettingen.de
E-mail: Azeeck@gwdg.de

General remarks. Synthesis: ^{1}H NMR spectra: Bruker AM 250 (250 MHz). Proton chemical shifts are reported in ppm relative to residual peaks of deuterated solvents. Higher order NMR spectra were approximately interpreted as first-order spectra, if possible. ^{13}C-NMR spectra and additional DEPT (Distortionless Enhancement by Polarization transfer): Bruker AM 250 (62.9 MHz) instrument. ^{13}C chemical shifts are reported relative to peaks of solvent or to dioxane in D_2O (δ = 67.19 ppm). IR spectra: Bruker IFS 66 (FT-IR) spectrometer as KBr pellets or oils between KBr plates. MS: EI-MS: Finnigan MAT 95, 70 eV, high resolution EI-MS spectra with perfluorokerosene as reference substance; ESI-MS: Finnigan LCQ. HPLC-MS: pump: Flux Instruments Rheos 4000; degasser: Flux Instruments ERC 3415α; detector: Linear UVIS-205; data system: Flux Instruments Janeiro; ESI: Finnigan LCQ, positive and

negative mode; data system: Finnigan LCQ Xcalibur; column: Crom Superspher 100 RP-18 endcapped (4 μm, 2 × 100 mm); HPLC conditions: eluent A: H_2O (0.05% HCOOH), eluent B: 90% MeCN (0.05% HCOOH), 30 → 70% B for 30 min, flow rate: 300 μL/min. Optical rotations: Perkin-Elmer 241 digital polarimeter, 1-dm cell. M.p.: Büchi 510 capillary melting point apparatus, uncorrected values. TLC: Macherey-Nagel precoated sheets, 0.25 mm Sil G/UV_{254}. Column chromatography: Merck silica gel, grade 60, 230–400 mesh and Baker silica gel, 40–140 mesh. Starting materials: Anhydrous diethyl ether and THF were obtained by distillation from sodium benzophenone ketyl, CH_2Cl_2 and DMF from molecular sieves 4 Å. All other chemicals were used as commercially available (Merck, Acrõs, BASF, Bayer, Aldrich, Fluka, Hoechst, Degussa AG). (2*S*,3*R*)-(*N*-9-Fluorenylmethyloxycarbonyl)-β-methylphenylalanine,[1] *N*-Fmoc-3-(2*R*,1'*R*,2'*R*)-(*trans*-2'-Nitrocyclopropyl)alanine[2] were prepared as described elsewhere. Organic extracts were dried over anhydrous $MgSO_4$. NMR conformational studies: NMR spectra were recorded on Bruker Avance 400 and DRX600 spectrometers. The concentration was 5 mM in $CDCl_3$ and measurements were run at 293 K. The assignments were carried out with the help of standard DQF-COSY, TOCSY, ^{13}C-HSQC, ^{15}N-HSQC and ^{13}C-HMBC experiments. Typically 2K data points in F2 and 512 experiments in F1 were acquired. In some cases, additional ROESY experiments were used to confirm the assignments made. The spectra were acquired with 16 transients and a relaxation delay of 2s except the ROESY experiments with 80 transients. For ROESY experiments, a spinlock field of 3.1 kHz was used with a mixing time of 480 ms.[3] The TOCSY experiments were performed with a spinlock field of 6.25 kHz using the MLEV17 sequence with mixing times of 40 ms and 80 ms. The data were zero filled and processed as 4K × 1K matrix. P.E. COSY experiments were processed as 8K × 2K matrix. To obtain the temperature coefficients of the amide proton chemical shifts, TOCSY spectra were recorded between +15 °C and +45 °C. To determine the χ_1 torsion angle constraints, the H_α–H_β coupling constants ($^3J_{\alpha\beta}$) from the 1D

proton and P.E. COSY spectra, the intensity of the intraresidue ROEs (H_α–H_β, NH–H_β) and the intensity of the $^3J_{CH}$ HMBC cross peaks were used. Each component was classified to three rotamers, according to the patterns of the $^3J_{\alpha\beta}$, $^3J_{CH}$ and ROE values. The stereospecific assignments were also established for the β-methylene protons.

Table 1. Chemical shift assignments for the components of hormaomycin **1**.

Position	δ_H (ppm)	δ_C (ppm)
	Chpca	
1	–	159.7
2	–	120.2
3	6.83	110.3
4	6.21	104.1
5	–	122.1
OH	10.84	–
	(3-Ncp)Ala II	
1	–	172.2
2	5.16	51.4
3	1.62 (H_a), 1.85 (H_b)	35.43
1'	1.95	22.2
2'	4.07	59.5
3'	1.06 (H_a), 1.93 (H_b)	17.84
NH	8.08	–
	***a*-Thr**	
1	–	169.2
2	4.60	55.3
3	5.44	69.3
4	1.57	17.3
NH	9.13	–
	(4-Pe)Pro	
1	–	171.5
2	4.30	61.7
3	1.84 (H_a), 2.41 (H_b)	35.43
4	3.32	37.1
5	3.31 (H_a), 4.00 (H_b)	53.1
1'	5.31	127.8
2'	5.66	128.8
3'	1.72	13.8
	Ile	
1	–	171.6
2	4.70	54.9

3	1.92	38.4
4	1.36 (H_a), 1.60 (H_b)	25.3
5	0.92	10.8
1'	1.06	15.3
NH	7.28	–
	(b**Me)Phe I**	
1	–	170.2
2	4.47	60.00
3	3.72	39.6
4	1.43	13.6
1'	–	142.5
2'	7.26	128.9
3'	7.26	127.5
4'	7.22	127.1
NH	6.79	–
	(3-Ncp)Ala I	
1	–	168.4
2	3.51	52.1
3	–0.12 (H_a), 0.58 (H_b)	33.1
1'	0.29	20.3
2'	2.93	58.5
3'	–0.66 (H_a), 1.02 (H_b)	17.80
NH	6.54	–
	(b**Me)Phe II**	
1	–	171.1
2	4.41	60.04
3	3.00	42.1
4	1.32	17.9
1'	–	141.9
2'	7.25	129.1
3'	7.25	127.7
4'	7.04	127.4
NH	6.83	–

Table 2. Chemical shift assignments for the components of the aza-analogue **2a**.

Position	δ_H (ppm)	δ_C (ppm)
	Chpca	
1	–	160.0
2	–	120.4
3	6.89	110.3
4	6.19	104.0
5		122.1

OH	10.78	–
	(3-Ncp)Ala II	
1	–	172.2
2	5.15	51.5
3	1.64 (H_a), 1.76 (H_b)	35.6
1'	1.95	22.0
2'	4.06	59.7
3'	1.04 (H_a), 1.96 (H_b)	17.6
NH	8.18	–
	***a*-Dab**	
1	–	172.0
2	4.52	55.5
3	4.48	45.6
4	1.39	17.9
2-NH	8.91	–
3-NH	7.46	–
	(4-Pe)Pro	
1	–	170.3
2	3.94	64.1
3	1.94 (H_a), 2.29 (H_b)	36.2
4	3.31	36.8
5	3.31 (H_a), 4.00 (H_b)	53.5
1'	5.31	128.2
2'	5.66	128.2
3'	1.72	13.6
	Ile	
1	–	170.4
2	4.69	55.0
3	1.94	38.3
4	1.38 (H_a), 1.61 (H_b)	25.4
5	0.93	10.8
1'	1.10	15.2
NH	7.28	–
	(b**Me)Phe I**	
1	–	170.0
2	4.47	60.5
3	3.73	39.5
4	1.45	13.5
1'	–	142.8
2'	7.27	127.8
3'	7.27	128.9
4'	7.22	127.4
NH	6.78	–
	(3-Ncp)Ala I	
1	–	168.6

2	3.47	52.3
3	–0.14 (H_a), 0.65 (H_b)	32.9
1'	0.25	20.1
2'	2.87	58.4
3'	–0.75 (H_a), 1.00 (H_b)	17.2
NH	6.44	–
	(bMe)Phe II	
1	–	170.6
2	4.38	60.2
3	3.12	41.5
4	1.37	18.0
1'	–	141.6
2'	7.17	128.1
3'	7.17	129.0
4'	7.04	127.6
NH	7.06	–

Peptide condensation step for the preparation of peptides. – General procedure (GP 1): EDC (1.03 mmol) and HOAt (1.05 mmol) were added to a cooled (4 °C) solution of the respective *N*-protected amino acid (1 mmol) in anhydrous CH_2Cl_2 (3 mL). After 10 min, a solution of the respective crude *N*-deprotected peptide (0.97 mmol) and TMP (3 mmol) in anhydrous CH_2Cl_2 (1 mL) was added at the same temperature. The temperature was allowed to reach 20 °C, and stirring was continued for 15 h. Then the reaction mixture was diluted with Et_2O or EtOAc (30 mL) and washed with 1 M $KHSO_4$ (3 × 5 mL), water (2 × 5 mL), 3% aq. solution of $NaHCO_3$ (3 × 5 mL), water (3 × 5 mL), brine (2 × 5 mL), dried and concentrated under reduced pressure. The residue was purified by column chromatography or recrystallization.

Deprotection of *N*-Fmoc-protected peptides. – General procedure (GP 2): The protected peptides (1 mmol) were taken up with acetonitrile or THF (2 mL), diethylamine (2 mL) was added, and the resulting mixture left at ambient temperature for 30 min. All volatiles were evaporated under reduced pressure, the residue was taken up with toluene (2 × 5 mL), which

was evaporated under reduced pressure to remove the last traces of diethylamine. The obtained crude *N*-deprotected peptides were directly used in the next condensation step.

***N*-Boc-3-(2*S*,3*R*)Methylphenylalanine:** A solution of Boc_2O (0.607 g, 2.78 mmol) in acetone (5 mL) was added to a solution of 3-(*2S,3R*)-methylphenylalanine hydrochloride (0.50 g, 2.32 mmol) in 1 M NaOH (4.7 mL), and the resulting mixture was stirred for 15 h. The mixture was then concentrated to ca. 5 mL under reduced pressure, diluted with water (20 mL) and extracted with Et_2O (3 × 5 mL). The pH of the aqueous layer was adjusted to 2 with solid $NaHSO_4$, and the emulsion obtained was extracted with Et_2O (40 mL). The organic layer was washed with 1 M aqueous $NaHSO_4$ (3 × 10 mL), water (3 × 10 mL), brine (2 × 5 mL), dried, filtered and concentrated under reduced pressure to give a crude product which was recrystallized from hexane to give the title compound (0.53 g, 82%) as a colorless solid. $[\alpha]_D^{20}$ = 18.6 (*c* = 1.73, $CHCl_3$) [lit.:[4] $[\alpha]_D^{20}$ = 17.0 (*c* = 1.70, $CHCl_3$]; ^{1}H NMR (250 MHz, $CDCl_3$): δ = 1.19 (m, 3 H, CH_3), 1.39 [s, 9 H, $C(CH_3)_3$], 3.33 (dq, *J* = 6.3, 5.0 Hz, 1 H, 3-H), 4.36–4.50 (m, 0.3 H, 2-H), 4.45 (dd, *J* = 5.0, 9.8 Hz, 0.7 H, 2-H), 5.04 (d, *J* = 8.3 Hz, 0.7 H, NH), 6.42 (d, *J* = 8.3 Hz, 0.3 H, NH), 7.18–7.39 (m, 5H, Ph-H), 11.10–12.00 (br, 1H, CO_2H).

Boc-(b**Me)Phe-Ile-OTMSE**: To a solution of Boc-Ile-OH (0.50 g, 2.16 mmol), 2-trimethylsilylethanol (0.256 g, 2.16 mmol) and DMAP (53 mg, 0.43 mmol) in CH_2Cl_2 (5 mL) was added at –10 °C EDC (0.427 g, 2.23 mmol), and the mixture was then allowed to warm to 20 °C and was stirred for 3h. The reaction mixture was then diluted with Et_2O (50 mL) and after the usual aqueous work-up (GP 1) concentrated to give, after prolonged drying at 5 Torr crude Boc-Ile-OTMSE (0.47 g, 66% crude yield) as a colorless oil, which was used without purification for the next step. A solution of this material (0.47 g, 1.42 mmol) and *p*TsOH·H_2O

(0.297 g, 1.56 mmol) in anhydrous benzene (15 mL) was heated under reflux for 1.5 h. The mixture was concentrated under reduced pressure, and the residue was recrystallized from EtOAc/hexane to give TsOH·H_2N-Ile-OTMSE (0.505 g, 88% crude yield) as a white solid which was used without further purification for the next step. A solution of this tosylate (0.283 g, 0.70 mmol) in Et_2O (40 mL) was washed with saturated aqueous $NaHCO_3$ (3 × 5 mL), brine (2 × 5 mL), dried and filtered. The solution was concentrated under reduced pressure to leave H_2N-Ile-OTMSE (0.150 g, 93% crude yield) as a colorless oil, which was directly used for the peptide condensation in CH_2Cl_2 (5 mL) according to GP 1 with the *N*-Boc protected β-methylphenylalanine (0.193 g, 0.69 mmol) using EDC (0.127 g, 0.66 mmol), HOAt (0.089 g, 0.66 mmol) and TMP (0.089 g, 0.73 mmol). The organic layer, after aqueous work-up (GP 1), was concentrated under reduced pressure to give the title compound (0.275 g, 80%; 43% over 4 steps) as a colorless glass. R_f = 0.38, EtOAc/hexane 1:4; $[\alpha]_D^{20}$ = –3.3 (*c* = 0.4, $CHCl_3$); ^{1}H NMR (250 MHz, $CDCl_3$): δ = 0.04 [s, 9 H, $Si(CH_3)_3$], 0.79 (d, *J* = 6.8 Hz, 3 H, 1'-H, *Ile*), 0.86 (d, *J* = 7.4 Hz, 3 H, 5-H, *Ile*), 0.82–0.95 (m, 2 H, 2-H, *TMSE*), 0.95–1.15 (m, 1 H, 4-H_a, *Ile*), 1.31 [d, *J* = 7.3 Hz, 3 H, 4-H, *(bMe)Phe*], 1.40 [s, 9 H, $C(CH_3)_3$], 1.73–1.82 (m, 1 H, 3-H, *Ile*), 3.16 [quint, *J* = 6.9 Hz, 1 H, 3-H, *(bMe)Phe*], 3.95–4.19 (m, 2 H, 1-H, *TMSE*), 4.20–4.36 [m, 2 H, 2-H, *Ile* and 2-H, *(bMe)Phe*], 5.15 (d, *J* = 8.8 Hz, 1 H, NH), 6.17 (d, *J* = 8.3 Hz, 1 H, NH), 7.01–7.33 (m, 5 H, Ar-H); the peaks of $C(CH_3)_3$ and 4-H of the *(bMe)Phe* moiety masked the absorption for 4-H_b of *Ile* residue; ^{13}C NMR (62.9 MHz, $CDCl_3$): δ = –1.79 [+, $Si(CH_3)_3$], 11.3 (+, C-5, *Ile*), 15.0 (+, C-1', *Ile*), 16.9 [+, C-4, *(bMe)Phe*], 17.1 (–, C-2, *TMSE*), 24.9 (–, C-4, *Ile*), 28.0 [+, $C(CH_3)_3$], 37.7 (+, C-3, *Ile*), 42.1 [+, C-3, *(bMe)Phe*], 56.2 (+, C-2, *Ile*), 60.0 [+, C-2, *(bMe)Phe*], 63.0 (–, C-1, *TMSE*), 79.4 [C_{quat}, $C(CH_3)_3$], 126.5, 127.4, 128.2 (+, Ar-C), 142.3 (C_{quat}, Ar-C), 155.5 (C_{quat}, NCO_2), 170.6 (C_{quat}, C-1, *Ile*), 170.8 [C_{quat}, C-1, *(bMe)Phe*]; IR (film): nu(tilde) = 3500–2500 cm^{-1}, 3066, 2953, 1720, 1542, 1478, 1369, 1234, 1106, 1078; MS (EI, 70 eV), *m/z* (%) = 492 (7)

[M^+], 436 (4) [$M^+ - C_4H_8$], 375 (8) [$M^+ - C_5H_{13}OSi$], 259 (38), 178 (52), 134 (58), 73 (40), 57 (100) [$C_4H_9^+$]; HRMS (EI): calcd for $C_{26}H_{44}N_2O_5Si$: 492.3020; found 492.3020.

Fmoc-(3-Ncp)Ala-(b**Me)Phe-Ile-OTMSE:** The dipeptide Boc-(βMe)Phe-Ile-OTMSE (0.268 g, 0.54 mmol) was deprotected by treatment with 3.9 M HCl in dioxane (4 mL) for 1 h. The mixture was then concentrated under reduced pressure and the residue was taken up with Et_2O (40 mL) and washed with saturated aqueous $NaHCO_3$ (3 × 10 mL), brine (2 × 5 mL), dried, filtered and concentrated under reduced pressure to give H-(βMe)Phe-Ile-OTMSE (0.167 g, 78%) as a colorless oil, which was directly coupled with the *N*-Fmoc protected (3-Ncp)Ala (0.178 g, 0.45 mmol) in CH_2Cl_2 (4 mL) according to GP 1 employing EDC (89 mg, 0.46 mmol), HOAt (61 mg, 0.45 mmol) and TMP (54 mg, 0.45 mmol) to give after the usual aqueous work-up (GP 1) a crude product, which was crystallized twice from CH_2Cl_2/hexane and finally purified by column chromatography ($CHCl_3$/EtOAc 7:1) to give the title compound (0.240 g, 57% over two steps) as a colorless solid. R_f = 0.28, EtOAc/hexane 1:2; $[\alpha]_D^{20} = -7.5$ (*c* = 0.12, $CHCl_3$); ^{1}H NMR (250 MHz, $CDCl_3$): δ = 0.04 [s, 9 H, $Si(CH_3)_3$], 0.79 (d, *J* = 7.0 Hz, 3 H, 1'-H, *Ile*), 0.86 (t, *J* = 7.6 Hz, 3 H, 5-H, *Ile*), 0.87–1.14 [m, 4 H, 2-H, *TMSE*, 3'-H_a, *(3-Ncp)Ala*, 4-H_a, *Ile*], 1.24–1.41 (m, 1 H, 4-H_b, *Ile*), 1.31 [d, *J* = 7.0 Hz, 3 H, 4-H, *(bMe)Phe*], 1.49–1.67 [m, 1 H, 3'-H_b, *(3-Ncp)Ala*], 1.67–1.82 [m, 2 H, 3-H, *Ile*, 1'-H, *(3-Ncp)Ala*], 1.82–2.03 [m, 2 H, 3-H, *(3-Ncp)Ala*], 3.21 [quint, *J* = 7.5 Hz, 1 H, 3-H, *(bMe)Phe*], 3.97–4.15 (m, 3 H, 1-H, *TMSE*, 2-H), 4.16–4.54 (m, 5 H, 2 × 2-H and 1'-H, 9''-H, *Fmoc*), 4.62 [ddd, *J* = 8.5 Hz, 1 H, 2'-H, *(3-Ncp)Ala*], 5.49–5.83 (br, 1 H, NH), 6.00–6.34 (br, 1 H, NH), 7.08–7.46 (m, 9 H, Ar-H), 7.52–7.66 (m, 2 H, Ar-H), 7.77 (d, *J* = 7.3 Hz, 2 H, Ar-H); ^{13}C NMR (62.9 MHz, $CDCl_3$): δ = –1.79 [+, $Si(CH_3)_3$], 11.3 (+, C-5, *Ile*), 15.0 (+, C-1', *Ile*), 17.1 [+, C-4, *(bMe)Phe*], 17.2 (–, C-2, *TMSE*), 17.9 [–, C-3', *(3-Ncp)Ala*], 22.2 [+, C-1', *(3-Ncp)Ala*], 25.0 (–, C-4, *Ile*), 34.0 [–, C-3, *(3-Ncp)Ala*], 37.9 (+, C-3, *Ile*), 41.9 [+, C-3,

(bMe)Phe], 46.9 (+, C-9', *Fmoc*), 54.0 [+, C-2, *(3-Ncp)Ala*], 56.3 (+, C-2, *Ile*), 58.7 [+, C-2, *(bMe)Phe*], 58.9 [+, C-2', *(3-Ncp)Ala*], 63.3 (–, C-1, *TMSE*), 67.0 (–, C-1, *Fmoc*), 112.3 (+, Ar-C), 124.9 (+, Ar-C), 126.8 (+, Ar-C), 126.9 (+, Ar-C), 127.0 (+, Ar-C), 127.6 (+, Ar-C), 128.3 (+, Ar-C), 141.09, 141.12 (C_{quat}, Ar-C), 141.7 (C_{quat}, Ar-C), 143.5, 143.7 (C_{quat}, Ar-C), 156.0 (C_{quat}, NCO_2), 170.2, 171.2, 171.4 (C_{quat}, C-1); IR (KBr): nu(tilde) = 3341 cm^{-1}, 3261, 3068, 2964, 2877, 1732, 1712 1642, 1544, 1368, 1251, 1228; MS (ESI), positive *m/z* (%) = 794 (30) [M + Na^+], 1564 (100) [2M + Na^+]; negative *m/z* (%) = 805 (20) [M + Cl^-].

Fmoc-(b**Me)Phe-(3-Ncp)Ala-(**b**Me)Phe-Ile-OTMSE (17):** The *N*-Fmoc protected (βMe)Phe (0.132 g, 0.33 mmol) was coupled according to GP 1 with the tripeptide obtained after deprotection of Fmoc-(3-Ncp)Ala-(βMe)Phe-Ile-OTMSE (0.230 g, 0.30 mmol) according to GP 2 in CH_2Cl_2/DMF 3:1 (3 mL) employing EDC (65 mg, 0.34 mmol), HOAt (46 mg, 0.34 mmol) and TMP (41 mg, 0.34 mmol). The mi xture was then taken up with EtOAc (30 mL), and concentrated after usual aqueous work-up (GP 1) to give a crude product, which was triturated with Et_2O/hexane 1:1 and then recrystallized from THF/hexane to give **17** (0.248 g, 89%) as an off-white solid. R_f = 0.21, EtOAc/$CHCl_3$ 2:9; $[\alpha]_D^{20}$ = –7.5 (*c* = 0.12, $CHCl_3$); ^{1}H NMR (250 MHz, [D_8]THF): δ = 0.03 [s, 9 H, $Si(CH_3)_3$], 0.78 (q, *J* = 7.1 Hz, 6 H, 5-H, 1'-H, *Ile*), 0.91 (dd, *J* = 8.6, 8.6 Hz, 2 H, 2-H, *TMSE*), 0.98–1.17 [m, 2 H, 3'-H_a, *(3-Ncp)Ala*, 4-H_a, *Ile*], 1.20 [d, *J* = 7 Hz, 3 H, 4-H, *(bMe)Phe*], 1.30–1.51 [m, 4 H, 1'-H, 3'-H_b, *(3-Ncp)Ala*, 3-H, 4-H_b, *Ile*], 1.33 [d, *J* = 7.0 Hz, 3 H, 4-H, *(bMe)Phe*], 1.54–1.79 [m, 2 H, 3-H, *(3-Ncp)Ala*], 3.10 [m, 1 H, 3-H, *(bMe)Phe*], 3.24 [t, *J* = 7.3 Hz, 1 H, 3-H, *(bMe)Phe*], 3.91–4.08 (m, 3 H, 1-H, *TMSE*, 2-H), 4.19–4.48 [m, 6 H, 2 × 2-H, 1-H, 9'-H, *Fmoc*, 2'-H, *(3-Ncp)Ala*], 4.55 (dd, *J* = 8.5, 8.5 Hz, 1 H, 2-H), 7.02–7.38 (m, 16 H, Ar-H), 7.52 (d, *J* = 9.0 Hz, 1 H, NH), 7.57 (d, *J* = 8.3 Hz, 1 H, NH), 7.64 (d, *J* = 7.5 Hz, 1 H, NH), 7.68 (d, *J* = 7.3 Hz, 1 H, NH), 7.77 (d, *J* = 7.3 Hz, 2 H, Ar-H); ^{13}C NMR (62.9 MHz, [D_8]THF): δ = –1.3 [+, $Si(CH_3)_3$], 11.9 (+, C-5,

Ile), 15.9 (+, C-1', *Ile*), 18.0 [+, C-4, *(bMe)Phe*], 18.2 (–, C-2, *TMSE*), 18.7 [+, C-4, *(bMe)Phe*], 18.7 [–, C-3', *(3-Ncp)Ala*], 23.1 [+, C-1', *(3-Ncp)Ala*], 26.0 (–,C-4, *Ile*), 34.8 [–, C-3, *(3-Ncp)Ala*], 38.8 (+, C-3, *Ile*), 42.8 [+, C-3, *(bMe)Phe*], 44.1 [+, C-3, *(bMe)Phe*], 48.4 (+, C-9', *Fmoc*), 52.7 (+, C-2), 57.1 (+, C-2), 59.5 (+, C-2), 60.1 (+, C-2), 62.0 [+, C-2', *(3-Ncp)Ala*], 63.5 (–, C-1, *TMSE*), 67.8 (–, C-1, *Fmoc*), 120.7 (+, Ar-C), 126.3 (+, Ar-C), 127.4 (+, Ar-C), 127.6 (+, Ar-C), 128.0 (+, Ar-C), 128.5 (+, Ar-C), 129.0 (+, Ar-C), 129.1 (+, Ar-C), 129.2 (+, Ar-C), 129.3 (+, Ar-C), 142.4 (2 × C_{quat}, Ar-C), 143.9, 144.3 (C_{quat}, Ar-C), 145.3, 145.5 (C_{quat}, Ar-C), 157.7 (C_{quat}, NCO_2), 171.2, 171.4, 172.0, 172.1 (C_{quat}, C-1); IR (KBr): nu(tilde) = 3276 cm^{-1}, 3064, 2965, 1710, 1668, 1637, 1543, 1452, 1369, 1249; MS (ESI), positive *m/z* (%) = 1886 (80) [2M + Na^+], 955 (90) [M + Na^+]; negative *m/z* (%) = 966 (22) [M + Cl^-].

Total hydrolysis of peptides 19a, 19c, *epi*-19a and *epi*-19c (GP 3): The respective peptide was hydrolyzed with 6 M HCl/AcOH (1:1, 0.5 mL per 1 mg of peptide) in sealed tubes at 105 °C within 24 h. The solvent was then removed under reduced pressure, and the residue was used for further derivatization.

Derivatization of the amino acids or the hydrolysates of peptides with (*S*)-FDVA (GP 4): The pH of a solution of 0.4 mg of the respective sample in 0.5 mL of H_2O was adjusted to 9 with 1 M $NaHCO_3$, and a 1% solution of (*S*)-FDVA [N_α-2,4-dinitro-5-fluorophenyl-(*S*)-valine amide] in acetone (0.1 mL) was added. The reaction mixture was stirred at 40 °C for 1 h, and then the pH was adjusted to 6–7 with 0.1 M HCl. After this, the reaction mixture was diluted with 1 mL of MeCN and was directly used for HPLC/MS experiments.

Preparation and HPLC behavior of (*S*)-FDVA-derivatives of the constituents of hormaomycin and analogs: A mixture of H-(*S*)-(3-Ncp)Ala-OH, H-(2*S*,3*R*)-(βMe)Phe-OH, H-(*S*)-Ile, H-(2*S*,4*R*)-(Pe)Pro-OH, H-(*R*)-*a*-Thr-OH (ca. 0.4 mg each) was divided into two equal portions, one of each was directly transformed into a mixture of the (*S*)-FDVA derivatives (GP 4), and the second one was dissolved in water (0.2 mL) and treated with Et_3N (0.08 mL) and Ac_2O (0.08 mL). The mixture was then heated at 60 °C for 1 h, concentrated under reduced pressure to give a residue, which was finally hydrolyzed according to GP 3 within 12 h to give a mixture of pairs of corresponding epimers at C-2 which was also further transformed into a mixture of the appropriate (*S*)-FDVA derivatives (GP 3). Also [(*S*)-FDVA]$_2$-(*R*)-*a*-Dab-OH and [(*S*)-FDVA]$_2$-(*R*)-Dap-OH were prepared. Detection: UV: 340 nm; ESI-MS, positive, *m/z*: 454.7–455.7 [(3-Ncp)Ala], 434.7–435.7 [(4-PE)Pro], 459.7–460.7 [(βMe)Phe], 411.7–412.7 (Ile), 399.7–400.7 (*a*-Thr), 678.7–679.7 (*a*-Dab), 663.7–664.7 (Dap); ESI-MS, negative, *m/z*: 452.6–453.6 [(3-Ncp)Ala], 433.6–434.6 [(4-PE)Pro], 457.6–458.6 [(βMe)Phe], 409.6–410.6 (Ile), 397.6–398.6 (*a*-Thr), 676.7–677.7 (*a*-Dab), 661.7–662.7 (Dap); retention times: (3-Ncpa)Ala: (2*S*,1'*R*,2'*R*)-isomer – t_R = 8.96 min, (2*S*,1'*R*,2'*R*)-isomer – t_R = 11.44 min; (4-Pe)Pro: (2*S*,4*R*)-isomer – t_R = 13.08 min; the concentration of this amino acid after hydrolysis (GP 3) and derivatization was usually lower then detection limit; (βMe)Phe: (2*S*,3*R*)-isomer – t_R = 13.75 min; (2*R*,3*R*)-isomer – t_R = 18.53 min; Ile: (*S*)-isomer – t_R = 11.69 min; (*R*)-*a*-isomer – t_R = 17.25 min; *a*-Thr: (*R*)-isomer – t_R = 5.56 min; this amino acid did not epimerize under conditions applied; *a*-Dab: (2*R*,3*R*)-isomer – t_R = 20.21 min; Dap: (*R*)-isomer – t_R = 16.27 min; (*S*)-isomer – t_R = 15.74 min.

Comparison of the amino acid composition of cyclopeptides 19a and *epi*-19a and 19c and *epi*-19c, respectively: Aliquots of **19a,** *epi*-**19a**, **19c** and *epi*-**19c** (0.5 mg each) were hydrolyzed according to GP 3, and the resulting hydrolysates, after concentration under reduced pressure, were treated with (*S*)-FDVA according to GP 4 and analyzed by HPLC/MS

using the mixtures of (*S*)-FDVA derivatives of synthetic amino acids as standards. These experiments showed the only difference between two pairs of these substances: cyclopeptides **19a** and **19c** contained an Ile moiety, and *epi*-**19a** and *epi*-**19c** contained an (*R*)-*a*-Ile residue.

Table 3. Vicinal proton-proton coupling constants for hormaomycin **1** in $CDCl_3$.[5]

Proton	Component	^3J (Hz)
1	Chpca 3-H	4.7
2	Chpca 4-H	
20	Ala-Ncp II 3-HA	8.5
22	Ala-Ncp II 4-H	
20	Ala-Ncp II 3-HA	14.0
64	Ala-Ncp II 2-H	
21	Ala-Ncp II 3-HB	4.7
64	Ala-Ncp II 2-H	
22	Ala-Ncp II 4-H	9.0
23	Ala-Ncp II 5-H	
23	Ala-Ncp II 5-H	9.5
25	Ala-Ncp II 6-HA	
26	Ala-Ncp II NH	9.4
64	Ala-Ncp II 2-H	
34	a-Thr 2-H	5.0
35	a-Thr 3-H	
19	a-Thr NH	9.5
34	a-Thr 2-H	
35	a-Thr 3-H	7.0
63	a-Thr 4-H_3	
36	4-Pe Pro 2-H	6.0
38	4-Pe Pro 3-HA	
36	4-Pe Pro 2-H	11.5
37	4-Pe Pro 3-HB	
37	4-Pe Pro 3-HB	13.5

41	4-Pe Pro 4-H	
41	4-Pe Pro 4-H	8.0
65	4-Pe Pro 6-H	
65	4-Pe Pro 6-H	18
66	4-Pe Pro 7-H	
66	4-Pe Pro 7-H	7.0
69	4-Pe Pro 8-H_3	
40	4-Pe Pro 5-HB	14.0
41	4-Pe Pro 4-H	
42	Ile 3-H	7.0
45	Ile 6-H_3	
28	Ile 2-H	8.0
42	Ile 3-H	
3	Ile NH	9.0
28	Ile 2-H	
51	Phe-Me I 3-H	7.0
54	Phe-Me I 10-H_3	
29	Phe-Me I 2-H	4.5
51	Phe-Me I 3-H	
4	Phe-Me I NH	9.5
29	Phe-Me I 2-H	
55	Ala-Ncp I 4-H	18.0
56	Ala-Ncp I 6-HB	
32	Ala-Ncp I 3-HB	9.4
55	Ala-Ncp I 4-H	
30	Ala-Ncp I 2-H	4.7
32	Ala-Ncp I 3-HB	
30	Ala-Ncp I 2-H	11.7
31	Ala-Ncp I 3-HA	
13	Ala-Ncp I 5-H	14.0
55	Ala-Ncp I 4-H	
12	Ala-Ncp I 6-HA	11.7

55	Ala-Ncp I 4-H	
12	Ala-Ncp I 6-HA	9.4
13	Ala-Ncp I 5-H	
5	Ala-Ncp I NH	7.0
30	Ala-Ncp I 2-H	
57	Phe-Me II 3-H	7.0
60	Phe-Me II 10-H_3	
33	Phe-Me II 2-H	13.0
57	Phe-Me II 3-H	
6	Phe-Me II NH	10.0
33	Phe-Me II 2-H	

Table 4. ROE cross peaks for hormaomycin **1** in $CDCl_3$.

293 K: ROESY with 480 ms mixing time
reference peaks: H31–H32 AlaNcpI (–0.17 / 0.53) geminal protons: 178 pm 480 ms:
integral: 88

Classified intensities:

weak	medium	strong
w	m	s

Pseudoatoms:

al1: H22/H24

pe1: H39/H41
pe2: H67/H68/H69

ile1: H48/H49/H50

pm11: H52/H53/H54
pm12: H7/H8/H10/H11

pm21: H58/H59/H60
pm22: H14/H15/H17/H18

classification:
intra (within the component)
seq (connecting neighboured components)

lr (long range)

Proton 1	Proton 2	intensity	classification
31 AlaNcpI	12 AlaNcpI	w	intra
55 AlaNcpI	56 AlaNcpI	m	intra
55 AlaNcpI	31 AlaNcpI	w	intra
32 AlaNcpI	55 AlaNcpI	w	intra
13 AlaNcpI	31 AlaNcpI	w	intra
13 AlaNcpI	32 AlaNcpI	w	intra
30 AlaNcpI	32 AlaNcpI	m	intra
30 AlaNcpI	31 AlaNcpI	m	intra
5 AlaNcpI	30 AlaNcpI	w	intra
5 AlaNcpI	13 AlaNcpI	w	intra
5 AlaNcpI	33 PheMeII	s	seq
26 AlaNcpII	1 Chpca	w	lr
26 AlaNcpII	H22/H24 AlaNcpII (al1)	w	intra
26 AlaNcpII	20 AlaNcpII	w	intra
26 AlaNcpII	64 AlaNcpII	w	intra
24 or 22 (al1) AlaNcpII	64 AlaNcpII	s	intra
20 AlaNcpII	64 AlaNcpII	w	intra
20 AlaNcpII	23 AlaNcpII	w	intra
39 or 41 (pe1) 4PePro	42 Ile	m	seq
39 or 41 (pe1) 4PePro	43 Ile	m	seq
39 or 41 (pe1) 4PePro	67 (pe2) 4PePro	m	intra
39 or 41 (pe1) 4PePro	65 4PePro	m	intra
36 4PePro	37 4PePro	m	intra
38 4PePro	65 4PePro	s	intra
65 4PePro	66 4PePro	s	intra
34 Thr	31 AlaNcpI	w	lr
34 Thr	61 Thr	m	intra
34 Thr	51 PheMeI	w	lr
19 Thr	35 Thr	w	intra
19 Thr	64 AlaNcpII	s	seq
19 Thr	34 Thr	m	intra
35 Thr	34 Thr	s	intra
35 Thr	22/24 AlaNcpII (al1)	w	seq
28 Ile	40 4PePro	s	seq
28 Ile	47 Ile	w	intra

28 Ile	46 Ile	w	intra
28 Ile	42 Ile	w	intra
28 Ile	43 Ile	m	intra
28 Ile	48 Ile	w	intra
3 Ile	4 PheMeI	w	seq
3 Ile	42 Ile 3H	w	intra
3 Ile	28 Ile	m	intra
2 Chpca	7 PheMeI	w	lr
2 Chpca	13 AlaNcpI	w	lr
2 Chpca	23 AlaNcpI	w	lr
2 Chpca	31 AlaNcpI	w	lr
1 Chpca	PheMeI (pm12)	m	lr
1 Chpca	PheMeI (pm11)	w	lr
1 Chpca	31 AlaNcpI 3HA	w	lr
6 PheMeII	58 (pm21) PheMeII	w	intra
6 PheMeII	34 Thr	m	seq
6 PheMeII	57 PheMeII	m	intra
6 PheMeII	29 PheMeI 2H	w	lr
6 PheMeII	30 AlaNcpI 2H	m	seq
14 (pm22) PheMeII	12 AlaNcpI 6HA	w	seq
14 (pm22) PheMeII	31 AlaNcpI 3HA	w	seq
14 (pm22) PheMeII	5 AlaNcpI	w	seq
14 PheMeII (pm22)	33 PheMeII	m	intra
14 PheMeII (pm22)	50 Ile	w	lr
14 PheMeII (pm22)	57 PheMeII	s	intra
14 PheMeII (pm22)	58 PheMeII (pm21)	m	intra
14 PheMeII (pm22)	55 AlaNcpI	w	seq
33 PheMeII	57 PheMeII	w	intra
33 PheMeII	58 (pm21) PheMeII	w	intra
29 PheMeI	52 PheMeI	w	intra
29 PheMeI	51 PheMeI	s	intra
7 PheMeI (pm12)	31 AlaNcpI	w	seq
7 PheMeI (pm12)	29 PheMeI	m	intra
7 PheMeI (pm12)	51 PheMeI	s	intra
7 PheMeI (pm12)	52 PheMeI (pm11)	s	intra
7 PheMeI (pm12)	56 AlaNcpI	w	seq
7 PheMeI (pm12)	12 AlaNcpI	w	seq
4 PheMeI	51 PheMeI 3H	m	intra
4 PheMeI	30 AlaNcpI 2H	m	seq
4 PheMeI	52 PheMeI (pm11)	w	intra

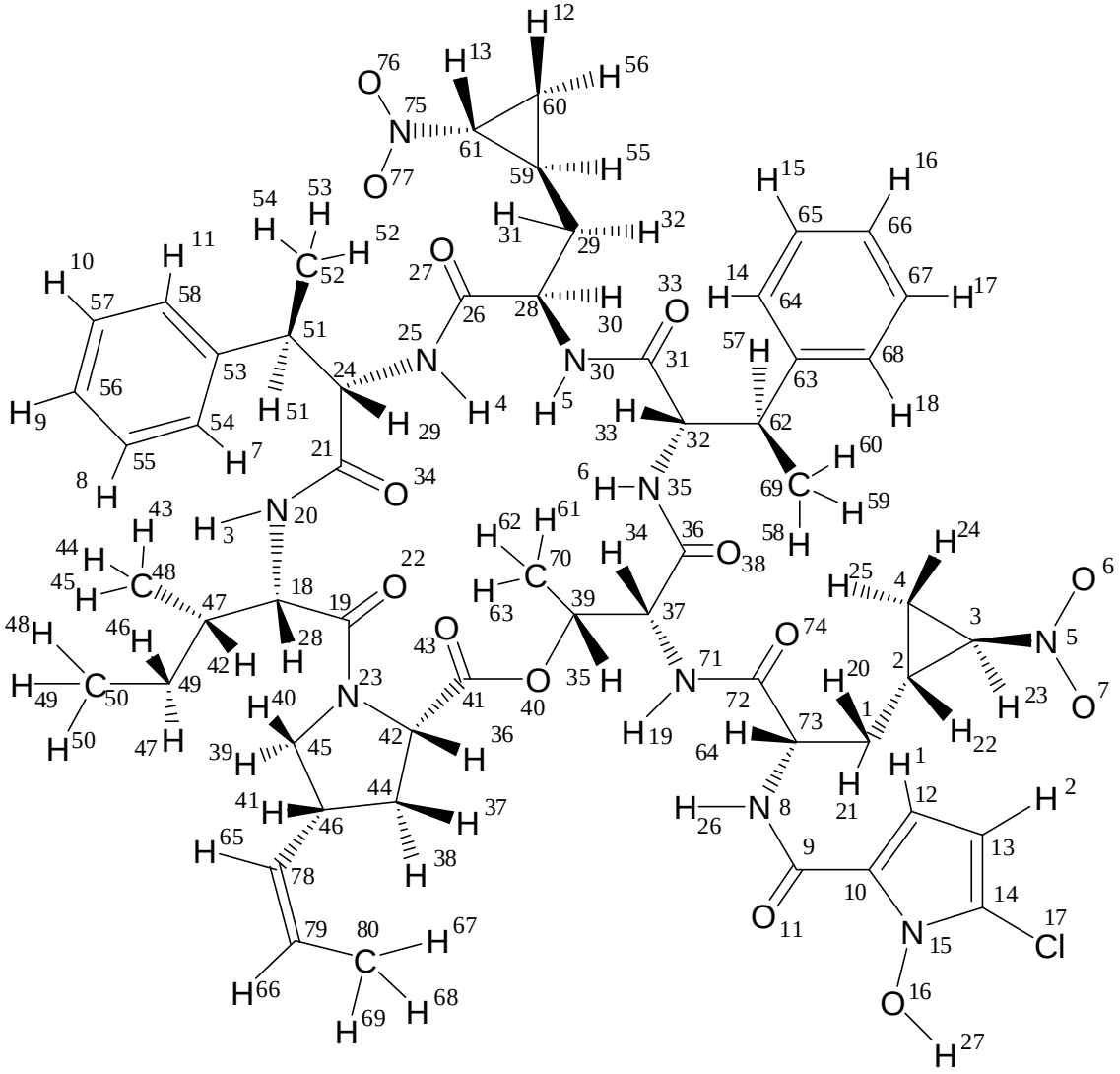

Figure 1. The structure and atom numbering of hormaomycin **1**.

Table 5. Restraints input file for Discover.

```
!BIOSYM restraint 1
!
#chiral
1:MON_1:C73 S
1:MON_1:C2 R
1:MON_1:C3 R
1:MON_1:C37 R
1:MON_1:C32 S
1:MON_1:C62 R
1:MON_1:C28 R
1:MON_1:C59 R
1:MON_1:C61 R
1:MON_1:C24 S
1:MON_1:C51 R
1:MON_1:C18 S
1:MON_1:C47 S
```

```
1:MON_1:C46 R
1:MON_1:C42 S
1:MON_1:C39 R
!
#distance
1:MON_1:H31      1:MON_1:H12  2.0     5.0     10.00  10.00  50.0
1:MON_1:H20      1:MON_1:H23  2.0     5.0     10.00  10.00  50.0
1:MON_1:H38      1:MON_1:H65  2.0     2.8     10.00  10.00  50.0
1:MON_1:AL1      1:MON_1:H64  2.0     2.8     10.00  10.00  50.0
1:MON_1:H13      1:MON_1:H31  2.0     5.0     10.00  10.00  50.0
1:MON_1:H13      1:MON_1:H32  2.0     5.0     10.00  10.00  50.0
1:MON_1:PE1      1:MON_1:H42  2.0     5.0     10.00  10.00  50.0
1:MON_1:PE1      1:MON_1:H43  2.0     5.0     10.00  10.00  50.0
1:MON_1:PE1      1:MON_1:PE2  2.0     3.5     10.00  10.00  50.0
1:MON_1:H34      1:MON_1:H31  2.0     5.0     10.00  10.00  50.0
1:MON_1:H34      1:MON_1:H51  2.0     5.0     10.00  10.00  50.0
1:MON_1:H28      1:MON_1:H40  2.0     2.8     10.00  10.00  50.0
1:MON_1:H28      1:MON_1:H47  2.0     5.0     10.00  10.00  50.0
1:MON_1:H28      1:MON_1:H46  2.0     5.0     10.00  10.00  50.0
1:MON_1:H28      1:MON_1:H48  2.0     5.0     10.00  10.00  50.0

1:MON_1:H35      1:MON_1:AL1  2.0     5.0     10.00  10.00  50.0
1:MON_1:H2       1:MON_1:H7   2.0     5.0     10.00  10.00  50.0
1:MON_1:H2       1:MON_1:H13  2.0     5.0     10.00  10.00  50.0
1:MON_1:H2       1:MON_1:H51  2.0     5.0     10.00  10.00  50.0
1:MON_1:H2       1:MON_1:H31  2.0     5.0     10.00  10.00  50.0

1:MON_1:H5       1:MON_1:H13  2.0     5.0     10.00  10.00  50.0
1:MON_1:H6       1:MON_1:PM21 2.0     5.0     10.00  10.00  50.0
1:MON_1:H6       1:MON_1:H57  2.0     3.5     10.00  10.00  50.0

1:MON_1:H1       1:MON_1:PM11 2.0     5.0     10.00  10.00  50.0
1:MON_1:H1       1:MON_1:H31  2.0     5.0     10.00  10.00  50.0


1:MON_1:H4       1:MON_1:PM11 2.0     5.0     10.00  10.00  50.0
1:MON_1:H4       1:MON_1:H51  2.0     3.5     10.00  10.00  50.0


1:MON_1:PM22     1:MON_1:H33      2.0     5.0     10.00  10.00  50.0
1:MON_1:PM22     1:MON_1:H50      2.0     5.0     10.00  10.00  50.0

1:MON_1:PM22     1:MON_1:H55      2.0     5.0     10.00  10.00  50.0
1:MON_1:PM12     1:MON_1:H31      2.0     5.0     10.00  10.00  50.0

1:MON_1:PM12     1:MON_1:H29      2.0     5.0     10.00  10.00  50.0
1:MON_1:PM12     1:MON_1:H56      2.0     5.0     10.00  10.00  50.0
1:MON_1:H26      1:MON_1:AL1  2.0     5.0     10.00  10.00  50.0
1:MON_1:H26      1:MON_1:H20  2.0     5.0     10.00  10.00  50.0
1:MON_1:H19      1:MON_1:H35  2.0     5.0     10.00  10.00  50.0
```

!
#NMR_dihedral

! 4-Pe Pro
1:MON_1:H36 1:MON_1:C42 1:MON_1:C44 1:MON_1:H37 -20 20
30 30 500
1:MON_1:H39 1:MON_1:C45 1:MON_1:C46 1:MON_1:H41 160 -160
10 10 500

! Ala-Ncp I
1:MON_1:H32 1:MON_1:C29 1:MON_1:C59 1:MON_1:H55 160 -160
30 30 500
1:MON_1:H30 1:MON_1:C28 1:MON_1:C29 1:MON_1:H31 160 -160
100 100 500

! Ile
1:MON_1:H28 1:MON_1:C18 1:MON_1:C47 1:MON_1:C49 160 -160
30 30 500
1:MON_1:H46 1:MON_1:C49 1:MON_1:C47 1:MON_1:C18 160 -160
30 30 500

! a-Thr
1:MON_1:H34 1:MON_1:C37 1:MON_1:C39 1:MON_1:H35 -80 -40
30 30 500

! Ala-Ncp II
1:MON_1:H20 1:MON_1:C1 1:MON_1:C2 1:MON_1:H22 160 -160
30 30 500
1:MON_1:H20 1:MON_1:C1 1:MON_1:C73 1:MON_1:H64 160 -160
30 30 500

! Phe-Me I
1:MON_1:H29 1:MON_1:C24 1:MON_1:C51 1:MON_1:H51 -80 -40
50 50 500

! Phe-Me II
1:MON_1:H33 1:MON_1:C32 1:MON_1:C62 1:MON_1:H57 170 -170
50 50 500

! trans
1:MON_1:C42 1:MON_1:N23 1:MON_1:C19 1:MON_1:C18 170 -170
100 100 500
1:MON_1:C28 1:MON_1:N30 1:MON_1:C31 1:MON_1:C32 170 -170
100 100 500

```
1:MON_1:C18     1:MON_1:N20     1:MON_1:C21     1:MON_1:C24     170    -170
        100   100    500

1:MON_1:C24     1:MON_1:N25     1:MON_1:C26     1:MON_1:C28     170    -170
        100   100    500
1:MON_1:C32     1:MON_1:N35     1:MON_1:C36     1:MON_1:C37     170    -170
        100   100    500
1:MON_1:C37     1:MON_1:N71     1:MON_1:C72     1:MON_1:C73     170    -170
        100   100    500
! 4-Pe Pro propenyl configuration cis
1:MON_1:H65     1:MON_1:C78     1:MON_1:C79     1:MON_1:H66     -20     20
        100   100    500
```

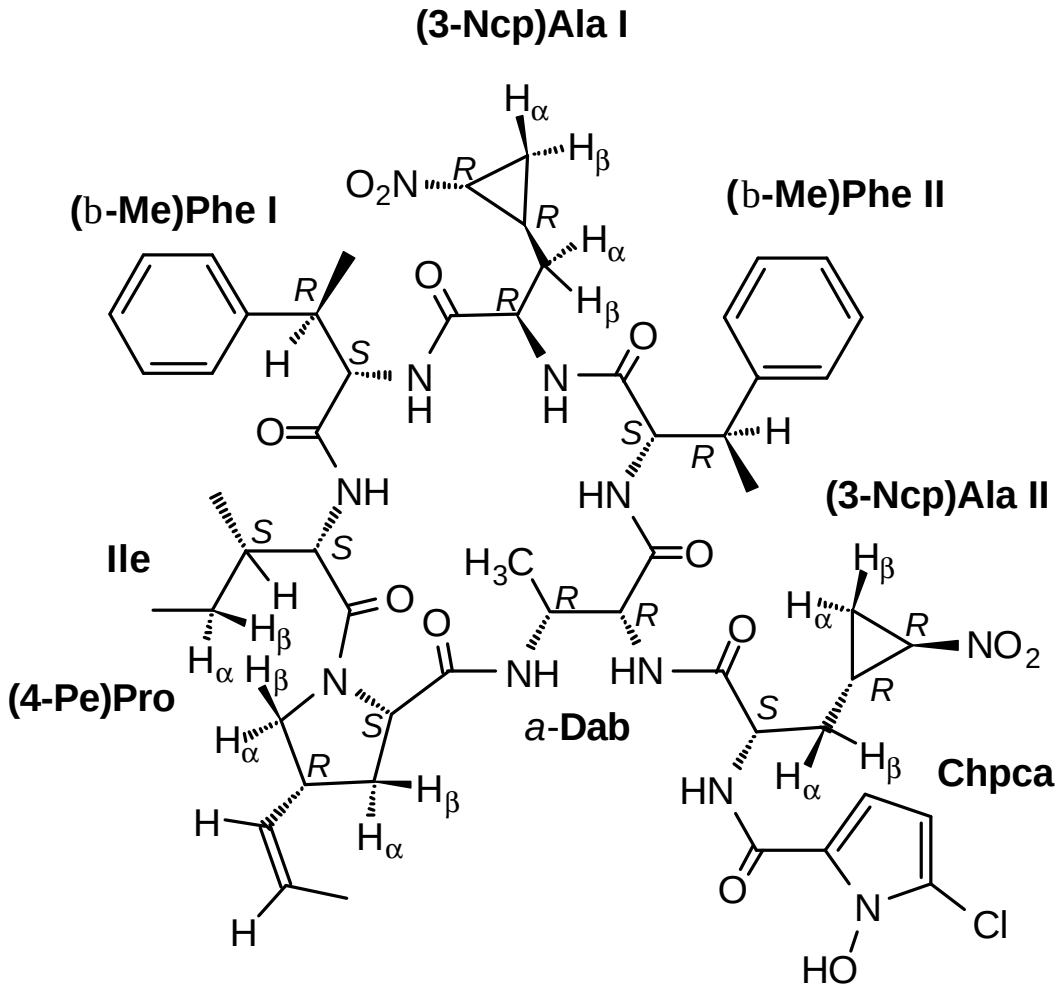

Figure 2. Structural formula of the all-peptide aza-analog **2a**.

---

[1] D. M. Birney, D. C. Cole, C. E. Crosson, B. F. Kahl, B. W. Neff, T. W. Reid, K. Ren, R. D. Walkup, *J. Med. Chem.* **1995**, *38*, 2478–2482.

[2] B. D. Zlatopolskiy, A. de Meijere, *Chem. Eur. J.* **2004**, *10*, 4718–4727.

[3] T. L. Hwang, A. J. Shaka, *J. Am. Chem. Soc.* **1992**, *114*, 3157–3159.

[4] M. Pasto, A. Moyano, M. A. Pericas, A. Riera, *J. Org. Chem.* **1997**, *62*, 8425–8431.

[5] For the numbering of atoms see Figure 1.

DOI: 10.1002/cbic.200500277

Effect of the Solvent on the Conformation of a Depsipeptide: NMR-Derived Solution Structure of Hormaomycin in DMSO from Residual Dipolar Couplings in a Novel DMSO-Compatible Alignment Medium

Uwe M. Reinscheid,[a] Jonathan Farjon,[a] Markus Radzom,[c] Peter Haberz,[a] Axel Zeeck,[c] Martin Blackledge,*[b] and Christian Griesinger*[a]

The macrocyclic compound hormaomycin has been investigated by NMR spectroscopy and by restrained molecular-dynamics simulations. Measurement of residual dipolar couplings induced by dissolving the depsipeptide in a polyacrylamide gel compatible with DMSO and their incorporation into the structure calculation of the title compound improved the precision of the family of structures. In DMSO the macrocyclic ring shows two β-turns, whose positions in the sequence differ from those found in the $CDCl_3$ solution structure and in the crystal structure obtained from hexylene glycol/H_2O (50:50). The bulky side chain consisting of a 3-(2-nitrocyclopropyl)alanine and a chlorinated N*-hydroxypyrrole moiety is flexible in DMSO.*

Introduction

Hormaomycin is a secondary metabolite produced by *Streptomyces griseoflavus* (strain W-384).[1] This depsipeptide contains (*S*)-isoleucine [(*S*)-Ile] as the only proteinogenic amino acid, along with two units of (2*S*,3*R*)-3-methylphenylalanine [(β-Me)Phe], one of (*R*)-*allo*-threonine [*a*-Thr], as well as two (1′*R*,2′*R*)-3-(2-nitrocyclopropyl)alanine [(3-Ncp)Ala] moieties [the (2*S*,1′*R*,2′*R*) diastereomer in the bulky side chain and the (2*R*,1′*R*,2′*R*) diastereomer in the macrocyclic ring of the molecule] and one (2*S*,4*R*)-4-(*Z*)-propenylproline [(4-Pe)Pro] residue (Figure 1). The bulky side chain of hormaomycin is terminated by an amide-bound 5-chloro-1-hydroxypyrrole-2-carboxylic acid [Chpca] moiety. The last three components have never been found in any natural product before. Besides its challenging structural features, hormaomycin also possesses an interesting spectrum of biological activities, including a marked influence on secondary metabolite production by other streptomycetes, an exceptionally selective antibiotic activity against coryneforme bacteria[1] and antimalarial activity.[2]

Its total synthesis became feasible once the correct absolute configurations of all its stereocentres—especially those of the two (3-Ncp)Ala moieties—had been established.[3] We have recently published a structure of hormaomycin in $CDCl_3$,[4] whilst a crystal structure (50:50 mixture of hexylene glycol/H_2O buffered at pH 8.0 with the addition of 0.1 M $MgCl_2$) has also recently been obtained.[5]

Since the conformation of the depsipeptide differs significantly in solution and in the crystal, its solvent dependence has been investigated here. DMSO was chosen as solvent because its solvent properties lie in-between those of the crystallization medium and those of chloroform. In addition, the impact of measuring additional residual dipolar couplings (RDCs) on the structural precision was evaluated. RDCs were induced by dissolving the title compound in a recently reported polyacrylamide gel that contains sulfonic acid groups and therefore also swells in aprotic solvents such as DMSO.[6] It can be shown that the incorporation of RDCs into the structure calculation protocol improves the precision of the derived solution structures in a similar manner to that shown previously for proteins and nucleic acids.[7–10]

[a] *Dr. U. M. Reinscheid, Dr. J. Farjon, P. Haberz, Prof. C. Griesinger*
Max Planck-Institute for Biophysical Chemistry
Am Faßberg 11, 37077 Göttingen (Germany)
Fax: (+49) 551-2012-202
E-mail: cigr@nmr.mpibpc.mpg.de

[b] *Dr. M. Blackledge*
Institut de Biologie Structurale
41, rue Jules Horowitz, 38027 Grenoble (France)
Fax: (+33) 4-38-78-54-94
E-mail: martin.blackledge@ibs.fr

[c] *M. Radzom, Prof. A. Zeeck*
Institut für Organische und Biomolekulare Chemie
Georg-August-Universität Göttingen
Tammanstrasse 2, 37077 Göttingen (Germany)

Supporting information for this article is available on the WWW under http://www.chembiochem.org or from the author: molecular formula with atom numbering, distance information, a list of restraints for molecular modelling, a NOE table and fitting plots of experimentally derived RDCs, together with calculated ones from the chloroform and crystal structures.

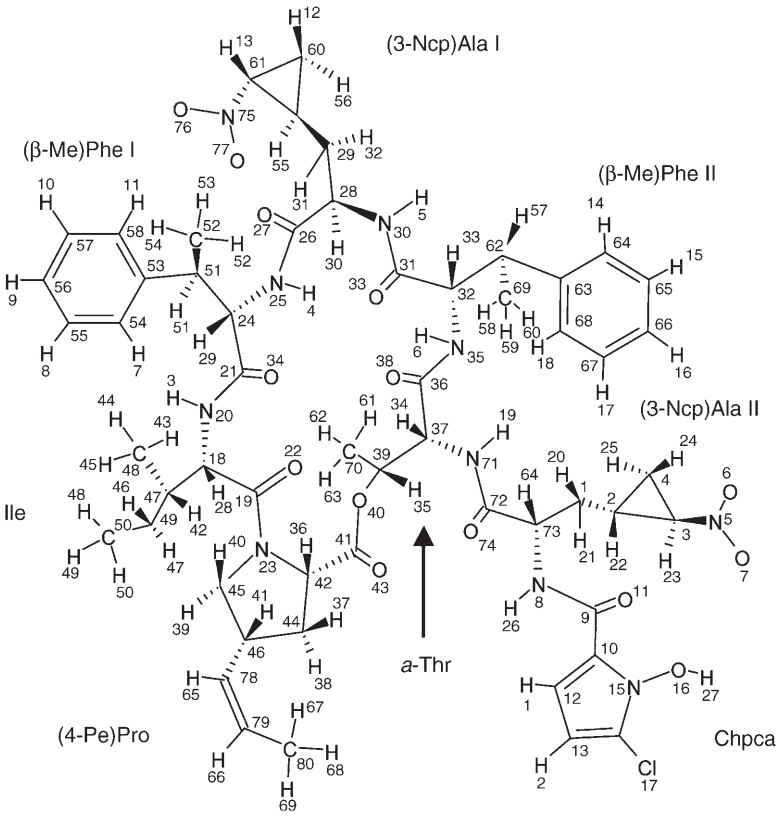

Figure 1. Molecular formula of hormaomycin with numbering used for calculations.

Results and Discussion

The molecular formula of hormaomycin is shown in Figure 1. Spin systems were identified by DQF-COSY, TOCSY and $^{1}H,^{13}C$-HMBC experiments (Table 1). Smaller chemical shift dispersions within the sets of HN (7.18–8.45 ppm) and H_α (3.95–4.91 ppm) protons than observed for hormaomycin in $CDCl_3$ (HN: 6.54–9.13 ppm, H_a: 3.51–5.16 ppm) indicate a less rigid structure. In particular, the missing long-range NOEs between the aromatic protons of the distal Chpca and (β-Me)Phe I components further support this finding. A second conformation (with the same batch the ratios between minor and major resonances differed in $CDCl_3$ and in DMSO) could be detected when the depsipeptide was dissolved in DMSO independently of whether the sample was in the isotropic or anisotropic phase. The concentration of this minor conformer did not exceed 8% relative to the major conformer and it was not considered further.

NOE- and *J* coupling-refined structures of hormaomycin

A total of 85 NOEs, together with eight dihedral angle restraints, were used for structure calculations. Nine hundred structures were calculated with use only of the NOE- and ^{3}J-derived restraints, by using protocol 2 in the Experimental Section, starting from 900 different structures calculated without restraints (protocol 1). The resultant NJ ensemble comprises the 40 structures of lowest experimentally determined energy (total experimentally determined NOE and *J* coupling energy term < 17.5 kcal mol^{-1} Å^{-2}, minimum energy 13.3 kcal mol^{-1} Å^{-2}, 5.4 ± 0.9 restraint violations beyond 0.15 Å and 1.1 ± 0.2 beyond 0.3 Å). Two families (representatives of which are shown in blue and red in Figure 2A and 2B) can be resolved in this ensemble: the NJa family, comprising 23 structures, and the NJb family, comprising 17 structures. The NJa family forms a tighter bundle (0.1 ± 0.1 Å RMSD).

The average pairwise RMSD over all atoms between members of the two different groups is 3.63 Å, while the average intrafamily values are 1.34 Å for NJa and 2.94 Å for NJb. For the macrocyclic ring atoms these numbers fall to 0.2 Å for NJa and 0.7 Å for NJb, and 1.4 Å average pairwise RMSD between members of the two different families. We can conclude that, although both families are in agreement with the NOEs and *J* couplings to essentially the same extent, the structures of the macrocyclic rings are significantly different. This structural difference arises around the ψ dihedral angle of (β-Me)Phe II (Figure 3).

There are therefore two conformations of the macrocycle that are essentially in equal agreement with the NOE and *J* coupling restraints. This is not necessarily due to molecular flexibility, it is much more likely that the experimental data are not sufficient to define a single conformation of the macrocycle. In order to refine this structural ambiguity further, we introduced RDCs into the structure calculation. The orientational information present in these restraints is complementary to the distance and dihedral angle restraints used for the NJ ensemble. In order to facilitate the use of RDCs in structure calculation it is useful to have some initial idea of the molecular alignment tensor resulting from the partial alignment of the molecule. As this is difficult to predict without a known structure we used the extensive conformational sampling present in the NOE/*J* coupling (NJ) and the restraint-free (RF) ensembles to represent the available conformational sampling for the molecule, and attempted to identify the alignment tensor that would fit best to members of this ensemble of 900 structures. If the conformational sampling of this ensemble is sufficiently large this procedure should simultaneously identify the best-fitting conformers with respect to the RDCs and also determine the most appropriate alignment tensor. As the side chains are potentially more flexible than the macrocyclic ring, we restricted this analysis to the 16 RDCs present in the ring.

The entire NOE-/*J* coupling-refined NJ ensemble (both families) was also used in the initial RDC analysis. Each of the 900 structures was used to fit the RDCs from the macrocyclic ring (four NH RDCs and 12 CH RDCs). Although there is a very broad spectrum of fit quality, illustrating the diversity of the entire ensemble, a family of structures do actually fit these RDCs quite well (Figures 4 and 5). The 40 structures that best fit the macrocyclic ring RDCs all give very similar alignment tensor parameters ($A_a = (8.71 \pm 0.03) \times 10^{-4}$, $A_r = (5.69 \pm 0.03) \times 10^{-4}$),[10] and are in fact very similar with respect to their RMSD. This sub-ensemble contains only members of family NJb, and

Table 1. Chemical shift assignments of hormaomycin in [D_6]DMSO.

Carbon, proton or group	δ_H [ppm]	δ_C [ppm]	Carbon, proton or group	δ_H [ppm]	δ_C [ppm]
Chpca					
C9	–	158.2	C10	–	116.2
C12–H1	6.70	108.5	C13–H2	6.10	102.1
C14	–	121.1	OH	n.d.	–
(3-Ncp)Ala II					
C72	–	170.0	C73–H64	4.51	51.8
C1–H21/H20	1.80 (pro*S*), 1.85 (pro*R*)	32.3	C2–H22	1.98	22.6
C3–H23	4.52	58.6	C4–H25/H24	1.25 (pro*S*), 1.93 (pro*R*)	17.6
H26	8.23	-			
a-Thr					
C36	–	167.4	C37–H34	4.50	57.8
C39–H35	5.00	70.7	C70–H61/H62/H63	1.21	16.9
H19	8.40	–			
(4-Pe)Pro					
C41	–	170.7	C42–H36	3.95	59.0
C44–H38/H37	1.51 (pro*R*), 2.27 (pro*S*)	34.4	C46–H41	3.24	36.1
C45–H39/H40	3.16 (pro*S*), 3.90 (pro*R*)	51.1	C78–H65	5.33	128.5
C79–H66	5.54	126.6	C80–H67/H68/H69	1.65	12.8
Ile					
C19	–	169.8	C18–H28	4.49	53.9
C47–H42	1.89	35.5	C49–H47/H46	0.99 (pro*R*), 1.42 (pro*S*)	22.5
C50–H48/H49/H50	0.84	10.7	C48/H43/H44/H45	0.92	15.4
H3	7.18	-			
(β-Me)Phe I					
C21	–	169.5	C24–H29	4.20	58.9
C51–H51	3.55	38.4	C52–H52/H53/H54	1.23	13.3
C53	–	142.6	C58–H11 and C54/H7	7.23	127.3
C57–H10 and C55/H8	7.16	126.1	C56–H9	7.02	127.5
H4	8.42	-			
(3-Ncp)Ala I					
C26	–	170.9	C28–H30	4.51	50.4
C29–H31/H32	0.68 (pro*S*), 0.88 (pro*R*)	33.1	C59–H55	1.21	21.9
C61–H13	4.00	58.2	C60–H56/H12	0.28 (pro*R*), 1.28 (pro*S*)	18.2
H5	8.45	-			
(β-Me)Phe II					
C31	–	169.2	C32–H33	4.91	56.0
C62–H57	2.89	43.8	C69–H58/H59/H60	1.01	18.1
C63	–	142.5	C64–H14 and C68–H18	7.12	127.6
C65–H15 and C67/H17	7.07	127.5	C66–H16	6.95	125.6
H35	7.81	–			

none from family NJa, and therefore already demonstrates the power of RDCs to resolve structural ambiguity resulting from NOE-based analysis. The estimate of the alignment tensor coincides with the best-fit tensor found from a similar analysis of the 900 structures determined without restraints (ensemble RF, data not shown) and these estimated eigenvalues were subsequently used in the RDC refinement process. This stage of fitting RDC values over the structures obtained by NOE and *J* analysis thus allows the NJa family to be excluded.

Refining the structure of hormaomycin with RDCs

The RDC-derived structure of hormaomycin was determined by a protocol identical to that used for the NJ ensemble, but with additional steps allowing for the initial determination of the optimal orientation of the alignment tensor for the respective structure through the use of the 16 macrocyclic ring RDCs. The eigenvalues A_a and A_r were tethered to the values determined as described above and the orientation was allowed to evolve freely throughout the calculation (protocol 3 in the Experimental Section). During the 80 ps sampling period, 42 RDCs (excepting those measured in the aromatic and methyl groups) were used with equal weighting. Again, the 40 structures with the lowest combined experimentally determined energy terms were taken to form the final NJR ensemble (Figure 2C and D). Not surprisingly, the average RMSD of the macrocyclic ring coordinates of this ensemble is lower than those measured for the NJ ensemble (1.9 ± 0.3 Å for heavy atoms, compared to 2.6 ± 0.7 Å, and 0.32 ± 0.16 Å for the macrocyclic ring atoms, compared to 0.60 ± 0.22 Å).

The refinement procedure results in a structural ensemble (NJR) in which the macrocycle ring conformation strongly resembles that in the NJb family determined from the NOE/*J* coupling data only (Table 2A and B). This is not surprising, as the NJa family was found to agree less well with the RDCs than the NJb family. It therefore appears that the structural ambiguity present in the NJ ensemble was indeed due to a lack of sufficient restraints, and that the RDCs have provided

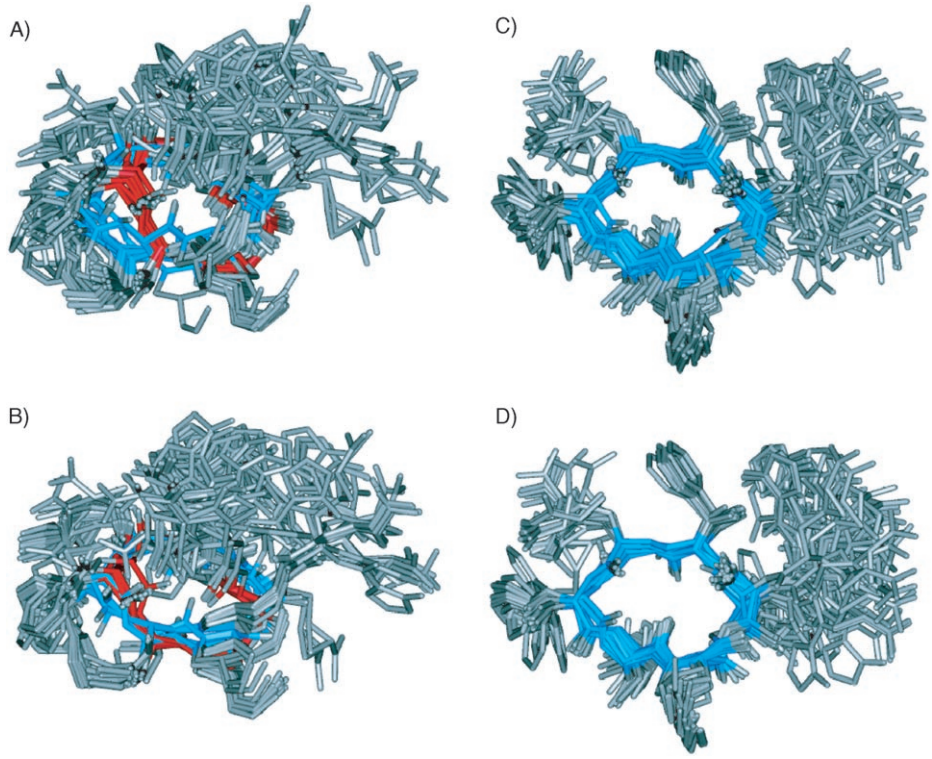

Figure 2. Comparison of the ensembles refined from NOE and *J* coupling only (NJ) and from NOE/*J* coupling and RDC (NJR). A) 40 lowest-energy structures from the NJ ensemble (all-atom superposition). The two families of macrocyclic ring conformations are coloured red and blue. B) 40 lowest-energy structures from the NJ ensemble (macrocyclic ring superposition). C) 40 lowest-energy structures from the NJR ensemble (all-atom superposition). D) 40 lowest energy structures from the NJR ensemble (macrocyclic ring superposition).

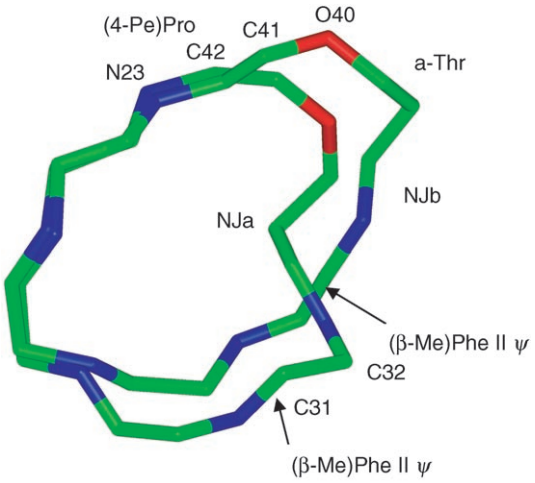

Figure 3. Representation of the two major families in the NOE/*J* coupling ensemble (NJ). Lowest-energy members of the two families show major differences about the (β-Me)Phe II ψ dihedral angle.

the complementary orientational information necessary to distinguish clearly between the two families. The average pairwise RMSD of the macrocyclic ring conformations of the NJR ensemble is 1.2 Å with respect to the NJa family and only 0.75 Å with respect to the NJb family.

From the reduction of the RMSD, it is evident that the RDCs have defined both backbone and side chain conformations significantly.

In this case, the average number of NOE violations above 0.15 Å is 9.1 ± 0.9, with 1.4 ± 0.6 beyond 0.3 Å. The total experimentally obtained NOE and *J* coupling energy term is 19.6 ± 2.4 kcal mol^{-1} Å^{-2} (minimum energy 15.8 kcal mol^{-1} Å^{-2}). Although the NJR ensemble is in slightly worse agreement with the NOE and *J* couplings, this effect is quite small and apparently not significant.

Comparison of refined structures

The pairwise RMSDs of representative structures of the ensembles (NJ, NJR and the A family of the NJ ensemble) are listed in Table 2A and 2B. Except for the closely defined NJa family (RMSD of NJ19–NJ1 = 0.60 Å), the RMSD for the whole molecule is higher than 1.5 Å; this can be explained by the different side chain conformations. In contrast, the RMSD of the macrocyclic ring is similar for the structure pairs between the NJR ensemble and the NJb family.

Two structures of the NJb ensemble (NJ1 and NJ19) were analysed by comparing the RDCs calculated from the structure and the experimentally measured ones. The 16 backbone RDCs are in good agreement ($R = 0.96$, Table 3, Figure 5A and B) with the back-calculated ones from these structures. However all 42 experimentally measured RDCs (excluding methyl groups and the aromatic *ortho* and *meta* RDCs) fit poorly with those calculated from the NOE structures (Table 3 and Figure 5E).

In order to show the benefit of using RDCs for structural refinement, the experimentally obtained RDCs were compared with the back-calculated values by use of representative structures from the NJR ensemble (NJR1 and NJR19). For both structure NJR1 and NJR19, the fitting factor *R* is close to 1 when the 16 backbone RDCs are used, which indicates a perfect fit between the calculated structure and the RDC values that had been used to refine the structure (Table 3). Moreover, the fitting factors with 42 RDCs are again very good: $R = 0.99$ (Table 3, Figure 5C and 5D), even if the side chains have different conformations. A similar fitting factor was obtained for the other structures of the NJR ensemble (data not shown).

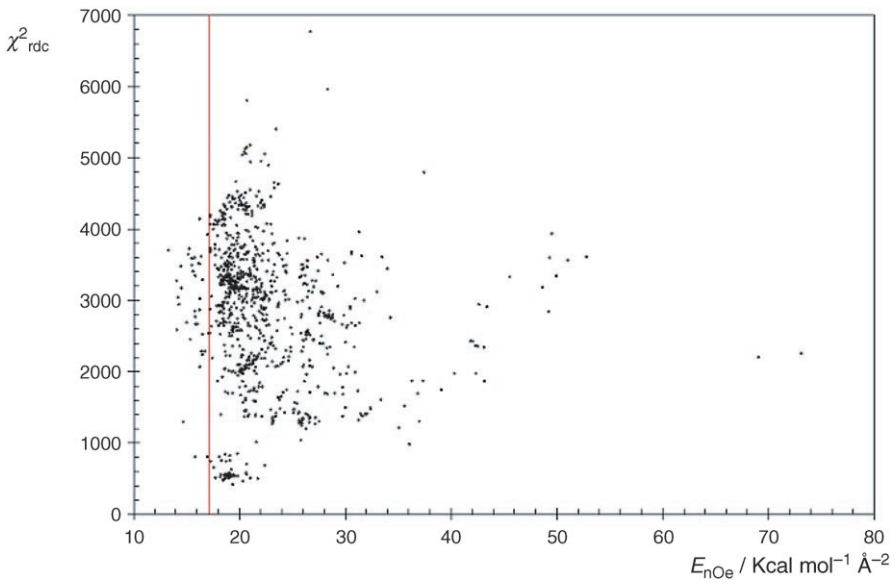

Figure 4. Structure selection to create the NJ ensemble based on NOE/*J* coupling terms with respect to the RDC fitting. Only RDCs originating from the macrocyclic core structure are used in the fitting procedure . Structures with experimental energies $E_{NOE} < 17$ kcal mol^{-1} Å^{-2} were selected for inclusion in the ensemble NJ. Note that conformers that fulfil the NOE/*J* coupling restraints to similar extents reproduce the macrocycle ring RDCs to very different degrees.

Flexibility of hormaomycin in DMSO

Within the NJR ensemble, the most prominent structural differences are found in the bulky side chain starting at C_α of *a*-Thr. Because of severe overlap only a limited number of ^3J couplings and NOE signals for this part of the molecule could be extracted unambiguously. Comparison with the NMR structure in $CDCl_3$ indicated a more disordered conformation ensemble, because long-range NOEs of the pyrrole ring protons are missing. A detailed analysis using the RDC structures NJR1 and NJR19 as representatives was undertaken. In the bulky side chain, four dihedrals differ, two of them substantially (N-CO-C-N in Chpca and N-C_α-C_β-C_γ in (3-Ncp)Ala II (Table 4). The first dihedral amounts to a value of 165° in the NJR1 structure and to −17° in NJR19, which constitutes a pyrrole ring flip. Both positions can be stabilized by a hydrogen bond (Chpca (O)H and Chpca (C)O or (3-Ncp)Ala II (N)H and Chpca O(H)). The measured NOE between Chpca 3-H and (3-Ncp)Ala II NH (see Table S2 of the Supporting Information) is intermediate between the distances in the two structures (NJR1: 2.0 Å, NJR19: 4.4 Å). The same holds for all proton pairs for which a reliable NOE could be measured and which have different distances in the two structures. The spatial proximity between the NH of (3-Ncp)Ala II and the NH of (β-Me)Phe II indicated by the measured NOE integrals is achieved through different sets of dihedrals in the two structures NJR19 and NJR1 (Table 4). In the two structures there are two combinations of the ϕ dihedral of *a*-Thr and the ψ of (3-Ncp)Ala II, which in both cases direct the NH of (3-Ncp)Ala II into the vicinity of the NH of the (β-Me)-Phe II component. We therefore conclude that the bulky side chain of hormaomycin is sampling the conformational space with concomitant change in several dihedral angles. Potentially, the ensemble of structures could be restricted by recording more dipolar couplings, which is outside the scope of this article.

Structural characterization of the macrocyclic ring of the RDC structure NJR19

The structure of hormaomycin exhibits one type II′ and one type III β-turn (Figure 3). The III β-turn comprises the four amino acids Ile (*i*), (4-Pe)Pro (*i*+1), *a*-Thr (*i*+2) and (β-Me)Phe II (*i*+3), while the II′ β-turn comprises the amino acids (β-Me)Phe II (*i*), (3-Ncp)Ala I (*i*+1), (β-Me)Phe I (*i*+2) and Ile (*i*+3). For the two β-turns a $C_\alpha(i)$–$C_\alpha(i+3)$ distance of 6.5 Å is found for the components Ile and (β-Me)Phe II. Assignment of the turns to their respective types was achieved from the values of the observed dihedral angles of the residues *i*+1 and *i*+2 (Table 5).

These are indicative of type II′ and III β-turns. For the identification of the two β-turns we took the general criterion that the distance between $C_\alpha(i)$ and $C_\alpha(i+3)$ be less than 7 Å.[11] There is no hydrogen bond between CO (Ile) and NH (*a*-Thr), in accordance with the observation that a CO(*i*)–HN(*i*+3) hydrogen bond is not necessary for stabilization of a β-turn.

Backbone chirality plays an important role in defining the conformational space for β-turn formation.[12] L-Xaa- D-Yaa and D -Xaa-L-Yaa dyads have strong tendencies to occupy the corner positions of type II and type II′ turns, respectively. Indeed, the type II′ β-turn in hormaomycin is formed with the D diastereomer of (3-Ncp)Ala I in the corner position, followed by the L diastereomer of (β-Me)Me I. In an idealised type III and type II′ β-turn all four C_α atoms lie within one plane, whilst in hormaomycin both turns are twisted in relation to the ideal structures of type III and II′ β-turns.

Comparison of the NMR solution structures of hormaomycin in $CDCl_3$ and DMSO and of the crystal structure from hexylene glycol/H_2O (50:50)

β-Turns of the macrocyclic ring

The structures in the three solvents are each characterized by two β-turns, which in DMSO and $CDCl_3$ are formed by the same amino acids, supporting the observation that β-turns are rather stable.[11] Comparison of the dihedral angles of the macrocyclic ring clearly shows considerable similarities between the three structures (Table 6; Figure 6). Nevertheless, the RMSD for the macrocyclic ring between the DMSO structure and the crystal structure is high (2.3 Å), in contrast to a low value between the DMSO and the $CDCl_3$ structures (0.66 Å).

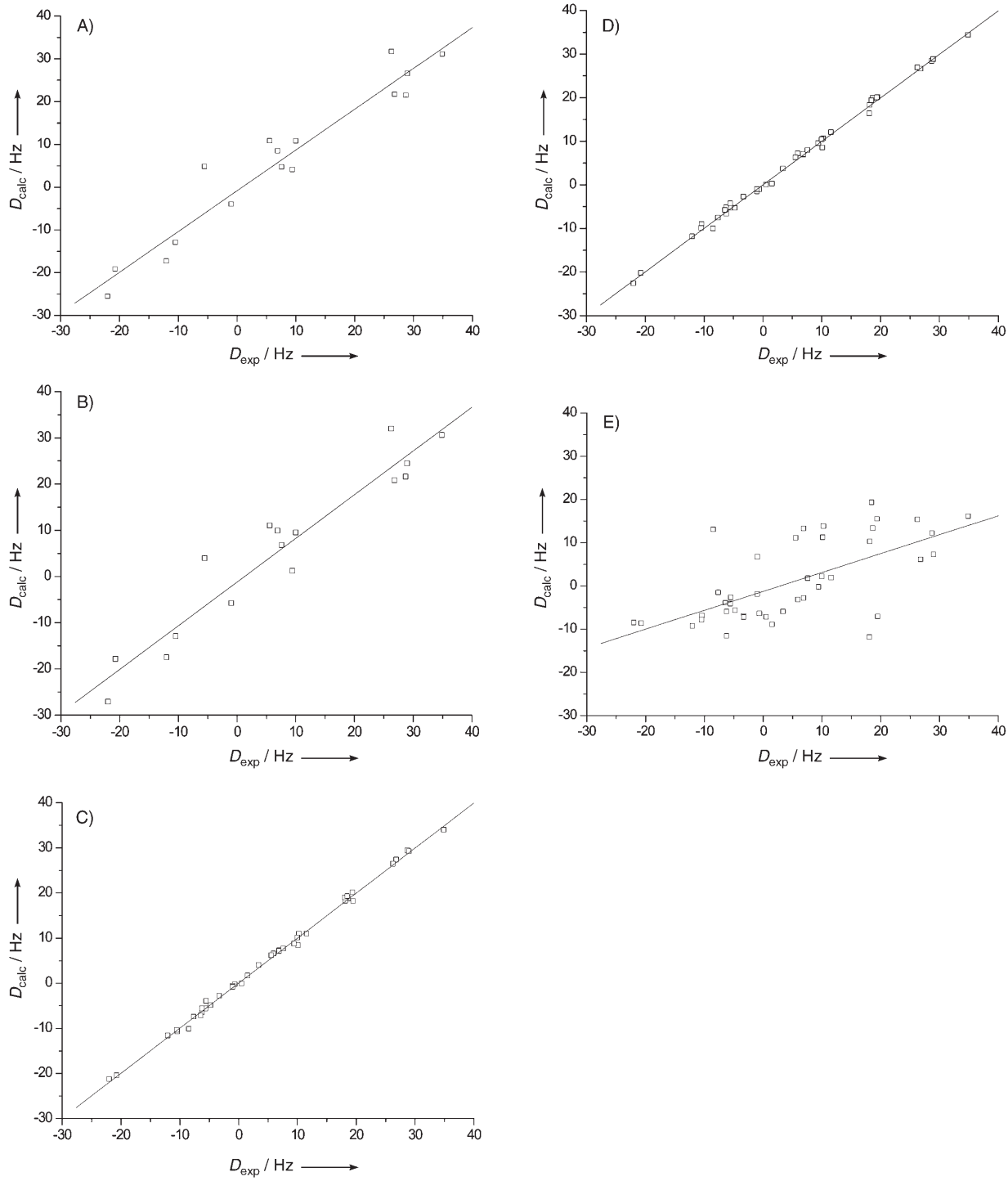

Figure 5. Experimentally observed versus back-calculated RDCs for NJ1, NJ19 and NJR19. In a comparison of the 16 RDCs of the macrocyclic ring for NJ1 (A) the equation of the fitting curve is $D_{calc}=0.95\,D_{exp}-0.85$ whilst for NJ19 (B), $D_{calc}=0.95\,D_{exp}-1.2$. With the 42 RDCs for NJR19 (C), $D_{calc}=0.99\,D_{exp}-0.04$, whilst for NJR1 (D), $D_{calc}=0.99\,D_{exp}-0.02$ and for NJ19 (E), $D_{calc}=0.44\,D_{exp}-1.26$.

The pairs of β-turns in the DMSO and $CDCl_3$ structures are formed from the same components, resulting in the low RMSD for the macrocyclic ring. One of the turns is classified in both cases as type II′, while the other is different: type III in DMSO and type II in $CDCl_3$. This is confirmed by an average fitting factor $R=0.80$ between the back-calculated RDCs from the chloroform structure and the experimentally measured ones (Table 7 and Figure S1 A in the Supporting Information). Nevertheless, a poor fit ($R=0.40$) is obtained with 42 RDCs calculated from the $CDCl_3$ structure compared to the experimental RDCs obtained in DMSO. (Table 7 and Figure S1 B in the Supporting Information).

In the crystal structure, the amino acids in positions *i* and *i*+3 are (3-Ncp)Ala I and (4-Pe)Pro, which corresponds to a ro-

Table 2. Pairwise RMSDs of superimposed structures.

	NJ1	NJ19	NJR1	NJR19
A) whole molecule				
NJR19	2.75	2.68	2.28	
NJR1	1.58	1.48		
NJ19	0.60			
Structure number 1 of family NJa	5.54	5.54	4.36	4.36
Structure number 19 of family NJa	5.69	5.66	4.49	4.49
B) macrocyclic ring)				
NJR19	0.53	0.53	0.38	
NJR1	0.31	0.31		
NJ19	0.05			
Structure 1 of family NJa	1.37	1.36	1.22	0.98
Structure 19 of family NJa	1.38	1.37	1.23	0.99

Table 3. R and Q factors defined by Cornilescu et al.[25] for different structures of hormaomycin comparing the RDCs both of the macrocyclic ring and of the side chains with the experimentally observed values.

Refined structures	R backbone[a]	R all[b]	Q backbone[a]	Q all[b]
NJR1	0.99	0.99	0.01	0.02
NJR19	0.99	0.99	0.02	0.02
NJ1	0.96	0.6	0.17	0.81
NJ19	0.96	0.64	0.16	0.84

[a] 16 RDCs used, [b] 42 RDCs used

Table 4. The most different dihedral angles in the bulky side chains of the two RDC structures NJR1 and NJR19.

	NJR1	NJR19
NH (3-Ncp)Ala II)–H_α (a-Thr)	137°	−174°
ψ of (3-Ncp)Ala II	41°	−27°
N-CO-C-N (Chpca)	165°	−17°
N-C_α-C_β-C_γ (3-Ncp)Ala II	61°	−89°

Table 5. Dihedral angles of ideal β-turns of types III and II′ and of the components of NJR19.

	$\phi(i+1)$	$\psi(i+1)$	$\phi(i+2)$	$\psi(i+2)$
ideal type III	−60°	−30°	−60°	−30°
ideal type II′	+60°	−120°	−80°	0°
ideal type II	−60°	120°	80°	0°
(4-Pe)Pro, *a*-Thr	−66°	+41°	−68°	−80°
(3-Ncp)Ala I, (β-Me)Phe I	+116°	−133°	−83°	−7°

tation of the secondary structure by one residue in relation to the secondary structure found in $CDCl_3$ and DMSO (Scheme 1). The corresponding distance between $C_{\alpha,i}$ and $C_{\alpha,i+3}$ is 6.7 Å. If the same secondary structure as in $CDCl_3$ and DMSO were assumed in the crystal, the $C_{\alpha,i}$ and $C_{\alpha,i+3}$ distance would be 7.3 Å, which is beyond the "allowed" distance for a β-turn, so the secondary structure is indeed rotated in the crystal in relation to that in $CDCl_3$ and DMSO. Because of this rotation the pairwise RMSD of the crystal structure with both NMR structures is very large. Not surprisingly, for the same reason, the RDCs calculated from the crystal structure are in poor agreement (Table 7 and Figure S2 A and B in the Supporting Information) with the experimentally obtained RDCs.

These structural dissimilarities could be explicable in terms of the different ε values and different hydrogen bond characteristics of the three solvents: $CDCl_3$ is a weak donor and acceptor, DMSO is a strong acceptor, and hexylene glycol/H_2O is a strong donor and acceptor.

Overall structure including the bulky side chain

In $CDCl_3$ the conformation of the side chain is very well defined by long-range NOEs between Chpca/(β-Me)Phe I and Chpca/(3-Ncp)Ala I.[4] The pyrrole ring of Chpca participates in an stacking interaction with the phenyl ring of (β-Me)Phe II. This type of interaction does not occur in the DMSO structures, indicating a flexible and/or under-determined bulky side chain. The crystal structure of the monomer should give rise to the observation of ROEs between Chpca and (β-Me)Phe II, which are not visible either in DMSO or in $CDCl_3$ (see Supporting Information). Furthermore, the ROE signals observed in $CDCl_3$ between Chpca/(β-Me)Phe I and Chpca/(3-Ncp)Ala I also could not occur in the crystal structure, which shows too long distances (see Supporting Information).

Consequently, the RMSDs seen between the RDC structure NJR19 and the crystal structure and the NMR structure in $CDCl_3$ are substantial: 6.91 Å and 4.10 Å, respectively. The RMSD between the DMSO and $CDCl_3$ structures reflects the higher flexibility of the bulky side chain, whereas the further increased value with the crystal structure indicates a substantial influence of the solvent and/or a methodological component.

Data are accessible in BMRB under accession code 6887.

Conclusion

We have shown that the structure of hormaomycin in DMSO differs from the NMR structures determined in $CDCl_3$ and the crystal structure. In particular, the bulky side chain is flexible in DMSO, while this not the case in chloroform. The secondary structure of hormaomycin, with the adoption of two β-turns, is identical in DMSO and chloroform, but differs from that in the crystal structure obtained from ethanol, in which the two β-turns are rotated by one residue. The structure in DMSO could be refined by using residual dipolar couplings obtained from a recently developed DMSO-compatible compressible gel. Without RDC refinement, two major conformations for the macrocyclic ring were derived, whereas after refinement with RDCs from the backbone and the side chains, only one of the two macrocyclic ring conformations remained valid. Since there is a strong dependence of the adopted conformation on the solvent system, it remains unclear, in the absence of knowledge about interaction partners, what the biologically active conformation may be.

Table 6. Dihedral angles of the macrocyclic ring in the NJR19 structure (DMSO), the structure derived from NOEs in $CDCl_3$ and the structure derived from crystals. Values are marked in bold when there is a value for the same angle that deviates by less than 20° in another structure.

	ϕ			ψ			ω Ile to (β-Me)Phe I		
	DMSO	$CDCl_3$	crystal	DMSO	$CDCl_3$	crystal	DMSO	$CDCl_3$	crystal
(β-Me)Phe I (βII′)	**−83**	**−90**	**−80**	**−7**	−47	**−15**	**180**	**173**	**173**
(3-Ncp)Ala I (βII′)	**116**	69	**131**	**−133**	**−135**	−163	**178**	**−168**	**−179**
(β-Me)Phe II	**−98**	−67	**−103**	**126**	180	**133**	**170**	**166**	**172**
a-Thr (βIII) (OCCαCβO)	−80	**43**	**54**				**−173**	**170**	**180**
a-Thr (βIII) (HNCOCαCβ)				−57	170	−89			
Ester (βIII) (CaCbOCO)				−68	90	158			
Ester (βIII) (CβOCOCα)							143	**−173**	**168**
(4-Pe)Pro	**−66**	**−61**	**−58**				**174**	**−176**	**179**
(4-Pe)Pro (OCOCαN)				41	**143**	**152**			
Ile	**−128**	**−93**	**−110**	**160**	**152**	**167**			

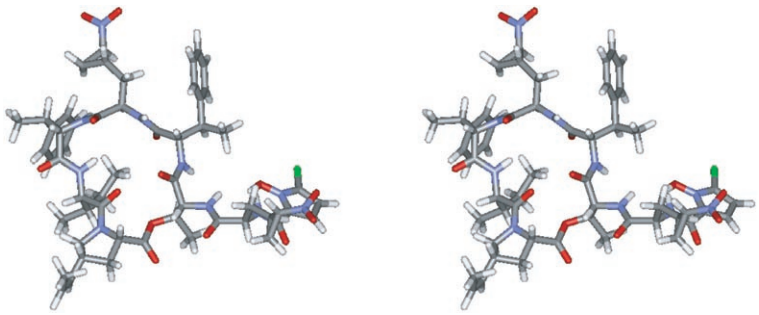

Figure 6. Stereoview of the RDC structure NJR19.

Table 7. *R* factors for different structures of hormaomycin, comparing the calculated RDCs of the macrocyclic ring alone and of the ring plus the side chains with the values determined experimentally in DMSO.

Structures	*R*	
	backbone[a]	all[b]
chloroform	0.80	0.41
crystal	0.74	0.52

[a] 16 RDCs used, [b] 42 RDCs used

Experimental Section

Isotropic solution NMR: NMR spectra were recorded on Bruker 400, 600 and 700 MHz (for TOCSY and NOESY) spectrometers. For the isotropic measurements the concentration was 20 mM in [D_6]DMSO. All measurements were run at 298 K.

The assignments were carried out with the aid of DQF-COSY, P.E. COSY, TOCSY, $^1H,^{13}C$-HSQC, $^1H,^{15}N$-HSQC and $^1H,^{13}C$-HMBC experiments. Typically, 4096 complex data points in t_2 and 512 experiments in t_1 were acquired. The stereochemistry of four diastereoisotopic protons could be assigned by use of distance and ^3J coupling information. The spectra were acquired with 16 scans and a relaxation delay of 2 s, except in the case of the NOESY experiments (32 scans and a mixing time of 800 ms). For ROESY experiments, a spinlock field of 3.1 kHz was used with a mixing time of 600 ms and 40 scans. The TOCSY experiments were performed with a spinlock field of 6.25 kHz and a mixing time of 80 ms. The data were zero-filled and processed as 4096×1024 complex matrix. P.E. COSY experiments were processed resulting in 4096×1024 hypercomplex matrices, meaning that each of the four matrices is 4096×1024.

Assignment: The *a*-Thr component (Figure 1), with a unique COSY cross peak between H_α and H_β at low field (4.50 and 5.00 ppm, respectively), served as starting point for the resonance assignment of the macrocyclic ring. The two (β-Me)Phe moieties could easily be identified due to their aromatic side chains. The identification of the (3-Ncp)Ala I spin system allowed assignment of the NMR resonances of all atoms in the molecule.

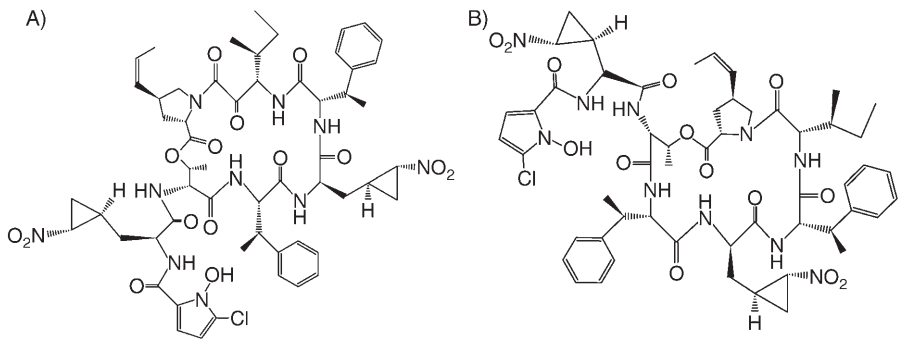

Scheme 1. β-Turns in the NMR solution structures (A; chloroform and DMSO) and in the crystal (B).

The presence of $H_\alpha(i)$–$NH(i+1)$ NOEs and the absence of $H_\alpha(i)$–$H_\alpha(i+1)$ cross peaks confirmed that all the amide bonds exist in the *trans* conformation. A *trans* conformation with respect to the Xxx–Pro peptide bond was indicated by characteristic NOE cross peaks from H_α (Ile) to the H_δ ((4-Pe)Pro) and the absence of cross peaks from H_α (Ile) to H_α ((4-Pe)Pro). Additionally, the difference of −1.7 ppm in the ^{13}C chemical shifts of C_β and C_γ ((4-Pe)Pro) is in-

dicative of a *trans* peptide bond.[13] The propenyl substituent must contain a *cis* C=C bond because of the strong NOE cross peak between the two olefinic protons, which indicates a distance of < 2.5 Å.

To determine the torsional restraints, the proton–proton coupling constants ($^3J_{HH}$) from the 1D proton and P.E. COSY spectra, the intensity of intraresidual NOEs and the intensity of the $^3J_{CH}$ HMBC cross peaks were used.

DMSO-gel NMR: Polyacrylamide gels were originally introduced as aligning media in high-resolution NMR for study of biomolecules in water by Tycko et al.[14] and Meier et al.[15] The NMR sample was prepared by the method described previously.[6] The charged gel is compressed, due to the restraints of the glass wall of the NMR tube. The alignment of hormaomycin resulting from the gel compression along the NMR tube is confirmed by the deuterium quadrupolar splitting of the solvent (of 3.5 Hz). The hormaomycin concentration was 50 mM in gel/DMSO (gel concentration 12% (*w/v*)). NMR spectra were recorded on a Bruker 600 MHz spectrometer fitted with a HCN cryoprobe. For the measurement of X,H (X: ^{13}C,^{15}N) residual dipolar couplings, ^{1}H,^{13}C-HSQC and ^{1}H,^{15}N-HSQC experiments without decoupling during acquisition[16] and with sensitivity enhancement[17–19] were recorded in the DMSO and gel/DMSO media.

The ω_2-coupled HSQC requires shorter acquisition times than the ω_1-coupled HSQC and allows RDCs to be measured with higher accuracy.[20] Furthermore, it also facilitates individual measurements of RDCs for both protons of CH_2 groups.[21]

For ^{1}H,^{13}C-HSQC, 4096 complex data points in t_2 (TD2) and 1024 (TD1) experiments in t_1 were acquired with 24 scans and 8 scans for the isotropic and the gel sample, respectively. The 2D matrices were zero-filled to 8192×2048 and Fourier transformed in both time domains. For ^{1}H-^{15}N-HSQC, 2048 complex data points in t_2 and 64 experiments in t_1 were acquired with 32 scans and 16 scans for the isotropic and the gel sample, respectively. The 2D matrices were zero-filled to 8192×512 and Fourier transformed in both time domains. In total, 54 RDCs were extracted (6 NH and 48 CH for directly bonded nuclei), 16 of them belonging to the macrocyclic ring (Table 8). The stereochemistry of the 14 diastereoisotopic protons was assigned with the aid of the RDCs; incorrect assignments would have resulted in worse Pearson's factors (R) in comparison of the experimentally observed RDCs and the calculated ones (data not shown).

The extraction of direct RDCs ($^1D_{X,H}$) was achieved by directly measuring the $^1D_{X,H}$ from the averaged frequency differences of the equivalent submultiplets in the isotropic and anisotropic ω_2 traces of each proton of the molecule. This procedure was used in order to reduce possible inaccuracies of measurements and due to strong coupling effects.[6]

Restrained molecular dynamics calculations: All molecular mechanics/dynamics simulations were performed either with DISCOVER[22] or with the program SCULPTOR[23] (structure calculation using long-range, paramagnetic, tensorial and orientational restraints), developed from the DISCOVER of the Insight II (Accelrys) package to deal with this kind of restraint. Calculations were performed either on a Silicon Graphics Octane workstation or on a Linux PC. Simulations were all carried out with use of the consistent valence force field (CVFF). A distance-dependent dielectric constant ($\varepsilon^{DMSO} = 46.7\,r$) was used.

Table 8. Direct residual dipolar couplings of hormaomycin in gel/[D_6]DMSO. The inaccuracies of the RDCs are indicated in brackets and the RDCs of the macrocyclic ring backbone are in bold italic.

Atom couple	D(NH) ± 0.5 [Hz]	Atom couple	D(NH) ± 0.5 [Hz]
N8–H26	−5.5	N25–H4	***−20.6***
N20–H3	***7.0***	N71–H19	−7.6
N35–H6	***−10.4***	N30–H5	***−11.9***
Group	**D(CH) ± 0.5 [Hz]**	**Group**	**D(CH) ± 0.5 [Hz]**
C50–H48/49/50	−1.7	C80–H67/68/69	−2.6
C52–H52/53/54	−8.7	C48–H43/44/45	5.6
C70–H61/62/63	3.9	C4–H24	−8.4
C4–H25	10.2	C69–H58/59/60	−1.1
C60–H12	19.5	C60–H56	−6.1
C59–H55 *R*	6	C49–H46	−4.7
C49–H47	1.6	C2–H22 *R*	18.7
C1–H20	−3.2	C1–H21	10.3
C29–H31	−0.5	C29–H32	18.2
C44–H37	***5.6***	C44–H38	***−5.5***
C47–H42 *S*	−6.1	C46–H41 *R*	***10.1***
C51–H51 *R*	−6.3	C62–H57 *R*	19.4
C28–H30 *R*	***28.8***	C45–H40	***−21.9***
C45–H39	***7.7***	C73–H64 *S*	0.6
C18–H28 *S*	***−0.9***	C32–H33 *S*	***26.3***
C37–H34 *R*	***26.9***	C61–H13 *R*	18.2
C3–H23 *R*	7	C24–H29 *S*	***35.0***
C42–H36 *S*	***9.5***	C39–H35 *R*	***29.0***
C13–H1	3.5	C12–H2	−0.9
C66–H16	−3.2	C79–H66	−10.3
C54–H7	9.5	C58–H11	9.5
C56–H9	18.5	C65–H15	18.5
C67–H17	18.5	C64–H14	17.5
C68–H18	17.5	C78–H65	11.6

NOE-, *J* coupling- and RDC-based refinement protocols using SCULPTOR

1. Restraint-free ensemble (RF): In this protocol no experimental restraints were used. An initial molecular model was first minimized with a gradient criterion of less than 0.5 kcal mol^{-1}. The molecule is then heated to a temperature of 1000 K over a period of 5 ps, in steps of 1 fs. The molecule evolves at this temperature for 80 ps (80000 steps), thus sampling conformational space extensively. This is followed by a 3 ps cooling period to 100 K and energy minimisation. This protocol was repeated 500 times and the resulting conformers were placed in the RF (restraint-free) ensemble.

2. NOE- and J coupling-refined ensemble (NJ): The protocol using NOE-derived distance restraints and dihedral restraints from ^3J coupling data is described below:

The distance and torsional angle restraints of Table S1 (Supporting Information) were used in both the minimization and the MD runs. Pseudo-atoms were used for the methyl protons and unresolved methylene protons. Distance restraints derived from NOE cross peak integrals were applied as biharmonic restraints with lower and upper bounds of 2.0–2.5, 2.0–2.8, 2.0–3.5, 2.0–4.0 and 2.0–5.0 Å, respectively. The timing of this protocol is identical to that described for protocol 1. The only difference is that during the 80 ps (80000 steps) sampling period, NOE- and *J* coupling-derived dihedral angle terms are raised from their initial weighting (0.2 kcal mol^{-1} Å^{-2} and 1.0 kcal mol^{-1} deg^{-2}) to their final weighting of 20.0 kcal mol^{-1} Å^{-2} and 1000 kcal mol^{-1} deg^{-2}, respectively. This protocol was repeated 900 times and the resulting lowest-energy conformers were placed in the NJ (NOE/*J* coupling) ensemble,

which consists of two families: NJa and NJb. For further characterization two structures of the NJb family were arbitrarily chosen and designated NJ1 and NJ19. We always checked that the other structures in the same ensemble would have shown the same behaviour as these two representative structures

3. NOE/J coupling/RDC ensemble (NJR) using tethered alignment tensor eigenvalues: The determination of molecular structures with the aid of RDC restraints applied the following protocols required to optimize the treatment of the alignment tensor. The parameters A_a and A_r are restrained to be close to predetermined values by use of a harmonic potential function. Starting structures are taken from the NJ ensemble derived from step 2. The molecular coordinates are initially fixed, while the orientation of the alignment tensor evolves under the influence of RDCs measured from sites present in the macrocyclic ring of hormaomycin. This step is composed of a sampling period of 4 ps at 300 K, followed by 3 ps at 200 K and conjugate gradient minimization. For each structure, the most appropriate orientation for the tensor is thus defined. The molecule is then released, and the tensor orientation and molecular structure evolve under the influence of 42 RDC restraints. Remaining parameters are identical to those described in protocols 2 and 3. This protocol was repeated 900 times and the resulting lowest-energy conformers were placed in the NJR (NOE/*J* coupling/RDC) ensemble. For further characterization two representatives structures (structures NJR1 and NJR19) were arbitrarily selected and, similarly to the NJ structures, all the conclusions were found to be independent of this selection.

RDCs calculations: Back-calculated RDCs were obtained by use of the SVD module in the PALES program.[24]

Acknowledgements

This work was supported by the Max Planck Gesellschaft, the Deutsche Forschungsgemeinschaft (SFB-416, Projects B5 and ZS) and the Fonds der Chemischen Industrie (to C.G.). J.F. was supported by a grant from the DAAD.

Keywords: conformation analysis · hormaomycin · natural products · NMR spectroscopy · residual dipolar couplings

[1] E. Rössner, W. A. Zeeck, W. König, *Angew. Chem.* **1990**, *102*, 84–85; *Angew. Chem. Int. Ed. Engl.* **1990**, *29*, 64–65.
[2] K. Otoguro, H. Ui, A. Ishigama, N. Arai, M. Kobayashi, Y. Takahashi, R. Masuma, K. Shiomi, H. Yamada, S. Omura, *J. Antibiot.* **2003**, 56, 322–324.
[3] a) B. D. Zlatopolskiy, K. Loscha, P. Alvermann, S. I. Kozhushkov, S. V. Nikolaev, A. Zeeck, A. de Meijere, *Chem. Eur. J.* **2004**, *10*, 4708–4717; b) B. D. Zlatopolskiy, A. de Meijere, *Chem. Eur. J.* **2004**, *10*, 4718–4727.
[4] U. M. Reinscheid, B. D. Zlatopolskiy, C. Griesinger, A. Zeeck, A. de Meijere, *Chem. Eur. J.* **2005**, *11*, 2929–2945.
[5] G. M. Sheldrick, personal communication.
[6] P. Haberz, J. Farjon, C. Griesinger, *Angew. Chem.* **2005**, *117*, 431–433; *Angew. Chem. Int. Ed.* **2005**, *44*, 427–429.
[7] E. de Alba, N. Tjandra, *Prog. Nucl. Magn. Reson. Spectrosc.* **2002**, *40*, 175–197.
[8] A. Annila, P. Permi, *Concepts Magn. Reson. Part A* **2004**, *23A*, 22–37.
[9] J. H. Prestegard, *Methods Enzymol.* **2005**, 394, 175–209.
[10] M. Blackledge, *Prog. Nucl. Magn. Reson. Spectrosc.* **2005**, *46*, 23–61.
[11] G. D. Rose, L. M. Gierasch, J. A. Smith, *Adv. Protein Chem.* **1985**, *37*, 1–109.
[12] A. C. Gibbs, T. C. Bjorndahl, R. S. Hodges, D. S. Wishart, *J. Am. Chem. Soc.* **2002**, *124*, 1203–1213.
[13] D. E. Dorman, F. A. Bovey, *J. Org. Chem.* **1973**, *38*, 2379–2383.
[14] R. Tycko, F. J. Blanco, Y. Ishii, *J. Am. Chem. Soc.* **2000**, *122*, 9340–9341.
[15] S. Meier, D. Häussinger, S. Grzesiek, *J. Biomol. NMR* **2002**, 24, 351–356.
[16] G. Bodenhausen, D. J. Ruben, *Chem. Phys. Lett.* **1980**, *69*, 185–189.
[17] J. Cavanagh, A. G. Palmer, P. E. Wright, M. Rance, *J. Magn. Reson.* **1991**, 91, 429–436.
[18] L. E. Kay, P. Keifer, T. Saarinen, *J. Am. Chem. Soc.* 1992, 114, 10663–10665.
[19] J. Schleucher, M. Sattler, C. Griesinger, *Angew. Chem.* **1993**, *105*, 1518–1521; *Angew. Chem. Int. Ed. Engl.* **1993**, *32*, 1489–1491.
[20] V. M. Marathias, I. Goljer, A. C. Bach II, *Magn. Reson. Chem.* **2005**, *43*, 512–519.
[21] L. Verdier, P. Sakhaii, M. Zweckstetter, C. Griesinger, *J. Magn. Reson.* **2003**, *163*, 353–359.
[22] P. Dauber-Osguthorpe, V. A. Roberts, D. J. Osguthorpe, J. Wolff, M. Genest, A. T. Hagler, *Proteins Struct. Funct. Genet.* **1988**, 4, 31–47.
[23] J.-C. Hus, D. Marion, M. Blackledge, *J. Mol. Biol.* **2000**, *298*, 927–936.
[24] M. Zweckstetter, A. Bax, *J. Am. Chem. Soc.* **2000**, *122*, 3791–3792.
[25] G. Cornilescu, J. L. Marquardt, M. Ottinger, A. Bax, *J. Am. Chem. Soc.* **1998**, *120*, 6836–6837.

Received: July 1, 2005
Published online on January 17, 2006

CHEMBIOCHEM

Supporting Information

CHEMBIOCHEM

Supporting Information

for

Effect of the Solvent on the Conformation of a Depsipeptide: NMR-Derived Solution Structure of Hormaomycin in DMSO by Using Residual Dipolar Couplings in a Novel DMSO-Compatible Alignment Medium

Uwe M. Reinscheid, Jonathan Farjon, Markus Radzom, Peter Haberz, Axel Zeeck, Martin Blackledge*, and Prof. Christian Griesinger*

Spatial differences between hormaomycin structures in different solvents compared with ROE values

The crystal structure of the monomer would lead to the observation of ROEs between the Chpca component and (β-Me)Phe II, which are not visible.

Distances between protons of Chpca with protons of (β-Me)Phe II (in Å):

H1-H57: 2.44
H1-H14/H18: 2.34
H1- H58/59/60: 4.26
H2-H57: 4.54
H2-H14/H18: 3.65
H2-H58/59/60: 5.97

The observed ROE signals in $CDCl_3$ between Chpca / (β-Me)Phe I and Chpca / (3-Ncp)Ala I are not visible in DMSO. This complies with the crystal structure which shows too long distances to observe ROEs.

Distances in crystal structure for proton pairs that show ROE signals in $CDCl_3$ in Å:

Chpca with (β-Me)Phe I

H2-H51: 13.7
H1-aromatic protons: 11
H1-CH3: 11.5

Chpca with (3-Ncp)Ala I

H2-H13: 8.7
H2-H31: 8.5
H1-H31: 7.1

Table S1: Restraint file for DISCOVER: dipolar coupling, distances, dihedrals

19: Lys5:N	19: Lys5:HN	3.8	0.5	1.00	0
19: Ile6:N	19: Ile6:HN	-1.3	0.5	1.00	0
19: Thr7:N	19: Thr7:HN	-0.3	0.5	1.00	0
19: Cys14:N	19: Cys14:HN	0.1	0.5	1.00	0
19: Ala15:N	19: Ala15:HN	1.4	0.5	1.00	0
19: Ala16:N	19: Ala16:HN	-2.7	0.5	1.00	0
19: His17:N	19: His17:HN	-1.1	0.5	1.00	0
19: Val18:N	19: Val18:HN	-1.3	0.5	1.00	0
19: Lys19: N	19: Lys19: HN	0.6	0.5	1.00	0
19: Glu20:N	19: Glu20:HN	-4.1	0.5	1.00	0
19: Leu22:N	19: Leu22:HN	-0.8	0.5	1.00	0
19: Ala31:N	19: Ala31:HN	13.7	0.5	1.00	0
19: Leu32:N	19: Leu32:HN	14.1	0.5	1.00	0
19: Val33:N	19: Val33:HN	15.1	0.5	1.00	0
19: Ala40:N	19: Ala40:HN	14.4	0.5	1.00	0
19: Gln41:N	19: Gln41:HN	12.6	0.5	1.00	0
19: Ile44:N	19: Ile44:HN	7.1	0.5	1.00	0
19: Asp51:N	19: Asp51:HN	-0.2	0.5	1.00	0
19: Ala52:N	19: Ala52:HN	-8.1	0.5	1.00	0
19: Leu53:N	19: Leu53:HN	7.3	0.5	1.00	0
19: Thr54:N	19: Thr54:HN	6.4	0.5	1.00	0
19: Ala55:N	19: Ala55:HN	-3.1	0.5	1.00	0
19: Ala56:N	19: Ala56:HN	-5.0	0.5	1.00	0
19: Val57:N	19: Val57:HN	6.7	0.5	1.00	0
19: Ala58:N	19: Ala58:HN	-0.5	0.5	1.00	0
19: Lys63:N	19: Lys63:HN	-1.4	0.5	1.00	0
19: Ala64:N	19: Ala64:HN	-0.4	0.5	1.00	0
19: Leu4:C	19: Lys5:HN	-0.4	0.5	1.00	0
19: Lys5:C	19: Ile6:HN	-2.2	0.5	1.00	0
19: Ile6:C	19: Thr7:HN	2.2	0.5	1.00	0
19: Cys14:C	19: Ala15:HN	1.4	0.5	1.00	0
19: Ala15:C	19: Ala16:HN	-3.4	0.5	1.00	0
19: Ala16:C	19: His17:HN	7.2	0.5	1.00	0
19: His17:C	19: Val18:HN	-0.6	0.5	1.00	0
19: Val18:C	19: Lys19: HN	-1.3	0.5	1.00	0
19: Lys19: C	19: Glu20:HN	-0.8	0.5	1.00	0

19: Ala21:C	19: Leu22:HN	1.0	0.5	1.00	0
19: Leu22:C	19: Glu23:HN	-3.6	0.5	1.00	0
19: Ala31:C	19: Leu32:HN	-4.8	0.5	1.00	0
19: Leu32:C	19: Val33:HN	-3.4	0.5	1.00	0
19: Val33:C	19: Ser34:HN	-3.8	0.5	1.00	0
19: Ala40:C	19: Gln41:HN	-2.0	0.5	1.00	0
19: Ala43:C	19: Ile44:HN	-3.4	0.5	1.00	0
19: Pro50:C	19: Asp51:HN	-1.2	0.5	1.00	0
19: Asp51:C	19: Ala52:HN	3.9	0.5	1.00	0
19: Ala52:C	19: Leu53:HN	-0.8	0.5	1.00	0
19: Leu53:C	19: Thr54:HN	-4.4	0.5	1.00	0
19: Thr54:C	19: Ala55:HN	0.5	0.5	1.00	0
19: Ala55:C	19: Ala56:HN	5.1	0.5	1.00	0
19: Ala56:C	19: Val57:HN	-2.9	0.5	1.00	0
19: Val57:C	19: Ala58:HN	-2.7	0.5	1.00	0
19: Tyr62:C	19: Lys63:HN	-0.4	0.5	1.00	0
19: Lys63:C	19: Ala64:HN	-0.3	0.5	1.00	0

1:MON_1:C73 S
1:MON_1:C2 R
1:MON_1:C3 R
1:MON_1:C37 R
1:MON_1:C32 S
1:MON_1:C62 R
1:MON_1:C28 R
1:MON_1:C59 R
1:MON_1:C61 R
1:MON_1:C24 S
1:MON_1:C51 R
1:MON_1:C18 S
1:MON_1:C47 S
1:MON_1:C46 R
1:MON_1:C42 S
1:MON_1:C39 R

1:MON_1:H26	1:MON_1:H6	2.0	4.0	20.00	20.00	50.0
1:MON_1:H26	1:MON_1:H1	2.0	4.0	20.00	20.00	50.0
1:MON_1:H26	1:MON_1:H22	2.0	4.0	20.00	20.00	50.0
1:MON_1:H26	1:MON_1:H20	2.0	3.5	20.00	20.00	50.0
1:MON_1:H6	1:MON_1:PM21	2.0	5.0	20.00	20.00	50.0
1:MON_1:H6	1:MON_1:H35	2.0	2.8	20.00	20.00	50.0
1:MON_1:H6	1:MON_1:H33	2.0	4.0	20.00	20.00	50.0
1:MON_1:H6	1:MON_1:H57	2.0	3.5	20.00	20.00	50.0
1:MON_1:PM11	1:MON_1:H29	2.0	3.8	20.00	20.00	50.0
1:MON_1:PM11	1:MON_1:H13	2.0	5.0	20.00	20.00	50.0
1:MON_1:PM11	1:MON_1:H51	2.0	3.5	20.00	20.00	50.0
1:MON_1:PM21	1:MON_1:H33	2.0	3.8	20.00	20.00	50.0
1:MON_1:H66	1:MON_1:H65	2.0	2.5	20.00	20.00	50.0
1:MON_1:H66	1:MON_1:H39	2.0	5.0	20.00	20.00	50.0
1:MON_1:H66	1:MON_1:H41	2.0	5.0	20.00	20.00	50.0
1:MON_1:H66	1:MON_1:H40	2.0	5.0	20.00	20.00	50.0

1:MON_1:H66	1:MON_1:H37	2.0	5.0	20.00	20.00	50.0
1:MON_1:H66	1:MON_1:H38	2.0	4.0	20.00	20.00	50.0
1:MON_1:H65	1:MON_1:H39	2.0	3.5	20.00	20.00	50.0
1:MON_1:H65	1:MON_1:H41	2.0	3.5	20.00	20.00	50.0
1:MON_1:H65	1:MON_1:H40	2.0	3.5	20.00	20.00	50.0
1:MON_1:H65	1:MON_1:H37	2.0	3.5	20.00	20.00	50.0
1:MON_1:H65	1:MON_1:PE3	2.0	4.5	20.00	20.00	50.0
1:MON_1:H65	1:MON_1:H38	2.0	2.5	20.00	20.00	50.0
1:MON_1:H35	1:MON_1:H57	2.0	5.0	20.00	20.00	50.0
1:MON_1:H33	1:MON_1:H57	2.0	3.5	20.00	20.00	50.0
1:MON_1:H29	1:MON_1:H51	2.0	2.5	20.00	20.00	50.0
1:MON_1:H29	1:MON_1:AL11	2.0	5.5	20.00	20.00	50.0
1:MON_1:H13	1:MON_1:AL11	2.0	4.5	20.00	20.00	50.0
1:MON_1:H13	1:MON_1:AL12	2.0	4.5	20.00	20.00	50.0
1:MON_1:H13	1:MON_1:AL11	2.0	4.0	20.00	20.00	50.0
1:MON_1:H36	1:MON_1:H41	2.0	2.8	20.00	20.00	50.0
1:MON_1:H36	1:MON_1:H40	2.0	5.0	20.00	20.00	50.0
1:MON_1:H36	1:MON_1:H37	2.0	2.5	20.00	20.00	50.0
1:MON_1:H36	1:MON_1:PE3	2.0	4.5	20.00	20.00	50.0
1:MON_1:H36	1:MON_1:H38	2.0	3.5	20.00	20.00	50.0
1:MON_1:H36	1:MON_1:ILE1	2.0	5.5	20.00	20.00	50.0
1:MON_1:H39	1:MON_1:H41	2.0	2.8	20.00	20.00	50.0
1:MON_1:H39	1:MON_1:H37	2.0	5.0	20.00	20.00	50.0
1:MON_1:H39	1:MON_1:H42	2.0	4.0	20.00	20.00	50.0
1:MON_1:H39	1:MON_1:PE3	2.0	5.5	20.00	20.00	50.0
1:MON_1:H39	1:MON_1:H38	2.0	4.0	20.00	20.00	50.0
1:MON_1:H39	1:MON_1:ILE1	2.0	4.5	20.00	20.00	50.0
1:MON_1:H41	1:MON_1:H40	2.0	2.5	20.00	20.00	50.0
1:MON_1:H41	1:MON_1:H37	2.0	2.8	20.00	20.00	50.0
1:MON_1:H41	1:MON_1:PE3	2.0	4.0	20.00	20.00	50.0
1:MON_1:H41	1:MON_1:H38	2.0	4.0	20.00	20.00	50.0
1:MON_1:H40	1:MON_1:H37	2.0	4.0	20.00	20.00	50.0
1:MON_1:H40	1:MON_1:H42	2.0	4.0	20.00	20.00	50.0
1:MON_1:H40	1:MON_1:PE3	2.0	5.5	20.00	20.00	50.0
1:MON_1:H40	1:MON_1:H38	2.0	4.0	20.00	20.00	50.0
1:MON_1:H40	1:MON_1:ILE1	2.0	4.5	20.00	20.00	50.0
1:MON_1:H37	1:MON_1:PE3	2.0	4.5	20.00	20.00	50.0
1:MON_1:H22	1:MON_1:H21	2.0	3.5	20.00	20.00	50.0
1:MON_1:H22	1:MON_1:H20	2.0	4.0	20.00	20.00	50.0
1:MON_1:H42	1:MON_1:ILE3	2.0	4.0	20.00	20.00	50.0
1:MON_1:ILE1	1:MON_1:ILE3	2.0	4.8	20.00	20.00	50.0
1:MON_1:H6	1:MON_1:H5	2.0	4.0	20.00	20.00	50.0
1:MON_1:H4	1:MON_1:H3	2.0	4.0	20.00	20.00	50.0
1:MON_1:H19	1:MON_1:H6	2.0	2.5	20.00	20.00	50.0
1:MON_1:H26	1:MON_1:H19	2.0	4.0	20.00	20.00	50.0

1:MON_1:H6	1:MON_1:H34	2.0	3.5	20.00	20.00	50.0
1:MON_1:H5	1:MON_1:H33	2.0	2.5	20.00	20.00	50.0
1:MON_1:H3	1:MON_1:H29	2.0	4.0	20.00	20.00	50.0
1:MON_1:H19	1:MON_1:H35	2.0	2.8	20.00	20.00	50.0
1:MON_1:H26	1:MON_1:H20	2.0	4.0	20.00	20.00	50.0
1:MON_1:H26	1:MON_1:H21	2.0	4.0	20.00	20.00	50.0
1:MON_1:H3	1:MON_1:H28	2.0	2.8	20.00	20.00	50.0
1:MON_1:H3	1:MON_1:H42	2.0	4.0	20.00	20.00	50.0
1:MON_1:H4	1:MON_1:H29	2.0	3.5	20.00	20.00	50.0
1:MON_1:H4	1:MON_1:H51	2.0	4.0	20.00	20.00	50.0
1:MON_1:H5	1:MON_1:H30	2.0	3.5	20.00	20.00	50.0
1:MON_1:H5	1:MON_1:AL12	2.0	5.0	20.00	20.00	50.0
1:MON_1:H57	1:MON_1:H6	2.0	3.5	20.00	20.00	50.0
1:MON_1:H33	1:MON_1:H6	2.0	4.0	20.00	20.00	50.0

NMR_dihedral

1:MON_1:H20	1:MON_1:C1	1:MON_1:C2	1:MON_1:H22	-80	-40	50	50	500
1:MON_1:H42	1:MON_1:C47	1:MON_1:C18	1:MON_1:C19	40	80	50	50	500
1:MON_1:H29	1:MON_1:C24	1:MON_1:C51	1:MON_1:H51	40	80	50	50	500
1:MON_1:H34	1:MON_1:C37	1:MON_1:C39	1:MON_1:H35	170	-170	100	100	500
1:MON_1:H33	1:MON_1:C32	1:MON_1:C62	1:MON_1:H57	120	-120	50	50	500
1:MON_1:H36	1:MON_1:C42	1:MON_1:C44	1:MON_1:H37	-50	-10	50	50	500
1:MON_1:H36	1:MON_1:C42	1:MON_1:C44	1:MON_1:H38	-179	-140	50	50	500
1:MON_1:H42	1:MON_1:C47	1:MON_1:C49	1:MON_1:C50	120	-120	50	50	500

trans

1:MON_1:C42	1:MON_1:N23	1:MON_1:C19	1:MON_1:C18	170	-170	100	100	500
1:MON_1:C28	1:MON_1:N30	1:MON_1:C31	1:MON_1:C32	170	-170	100	100	500
1:MON_1:C18	1:MON_1:N20	1:MON_1:C21	1:MON_1:C24	170	-170	100	100	500
1:MON_1:C24	1:MON_1:N25	1:MON_1:C26	1:MON_1:C28	170	-170	100	100	500
1:MON_1:C32	1:MON_1:N35	1:MON_1:C36	1:MON_1:C37	170	-170	100	100	500
1:MON_1:C37	1:MON_1:N71	1:MON_1:C72	1:MON_1:C73	170	-170	100	100	500

4-Pe Pro propenyl configuration *cis*

1:MON_1:H65	1:MON_1:C78	1:MON_1:C79	1:MON_1:H66	-20	20	100	100	500

Ala-Ncp I ring configuration: *cis* H12-H13

1:MON_1:H12	1:MON_1:C60	1:MON_1:C61	1:MON_1:H13	-20	20	100	100	500

Ala-Ncp II ring configuration: *cis* H23-H25

1:MON_1:H23	1:MON_1:C3	1:MON_1:C4	1:MON_1:H25	-20	20	100	100	500

ring Phe Me I

1:MON_1:C53	1:MON_1:C58	1:MON_1:C57	1:MON_1:H10	180	180	500	500	500
1:MON_1:H11	1:MON_1:C58	1:MON_1:C57	1:MON_1:H10	0	0	500	500	500
1:MON_1:C58	1:MON_1:C57	1:MON_1:C56	1:MON_1:H9	180	180	500	500	500
1:MON_1:C57	1:MON_1:C56	1:MON_1:C55	1:MON_1:H8	180	180	500	500	500
1:MON_1:C56	1:MON_1:C55	1:MON_1:C54	1:MON_1:H7	180	180	500	500	500
1:MON_1:H8	1:MON_1:C55	1:MON_1:C54	1:MON_1:H7	0	0	500	500	500
1:MON_1:H7	1:MON_1:C54	1:MON_1:C53	1:MON_1:C58	180	180	500	500	500

1:MON_1:H7	1:MON_1:C54	1:MON_1:C53	1:MON_1:C51	0	0	500	500	500
1:MON_1:H11	1:MON_1:C58	1:MON_1:C53	1:MON_1:C51	0	0	500	500	500

ring Phe Me II

1:MON_1:C68	1:MON_1:C67	1:MON_1:C66	1:MON_1:H16	180	180	500	500	500
1:MON_1:C67	1:MON_1:C68	1:MON_1:C63	1:MON_1:C62	180	180	500	500	500
1:MON_1:C62	1:MON_1:C63	1:MON_1:C64	1:MON_1:C65	180	180	500	500	500
1:MON_1:C63	1:MON_1:C64	1:MON_1:C65	1:MON_1:C66	0	0	500	500	500
1:MON_1:C64	1:MON_1:C65	1:MON_1:C66	1:MON_1:H16	180	180	500	500	500
1:MON_1:C62	1:MON_1:C63	1:MON_1:C64	1:MON_1:H14	0	0	500	500	500
1:MON_1:H14	1:MON_1:C64	1:MON_1:C65	1:MON_1:C66	180	180	500	500	500

ring Chpca

1:MON_1:C13	1:MON_1:C12	1:MON_1:C10	1:MON_1:C9	180	180	500	500	500
1:MON_1:H1	1:MON_1:C12	1:MON_1:C13	1:MON_1:H2	0	0	500	500	500
1:MON_1:C10	1:MON_1:C12	1:MON_1:C13	1:MON_1:H2	180	180	500	500	500
1:MON_1:C14	1:MON_1:C13	1:MON_1:C12	1:MON_1:H1	180	180	500	500	500
1:MON_1:C13	1:MON_1:C14	1:MON_1:N15	1:MON_1:C10	0	0	500	500	500
1:MON_1:CL17	1:MON_1:C14	1:MON_1:N15	1:MON_1:O16	0	0	500	500	500
1:MON_1:CL17	1:MON_1:C14	1:MON_1:C13	1:MON_1:C12	180	180	500	500	500
1:MON_1:CL17	1:MON_1:C14	1:MON_1:N15	1:MON_1:C10	180	180	500	500	500

Table S2. Distances and NOE intensities of proton pairs of the *bulky side chain* of NJR1 and NJR19 (in bold are the restraints that have been used)

	NJR1	NJR19	NOE-derived distance
H1-H26	2.0	4.4	**<4.0**
H1-H6	3.7	8.1	no NOE measured
H26-H6	3.9	4.1	**<4.0**
H26-H22	3.5	3.7	**<4.0**
H26-H24	3.2	5.8	<5.0
H26-H25	2.0	5.9	<5.0
H26-H19	3.0	2.1	<4.0
H26-H20 (overlay)	3.8	2.8	**<3.5**
H26-H64	3.1	3.1	<3.5
H26-H58/59/60	4.2	3.0	<4.0
H19-H6	2.7	2.4	<2.8

A)

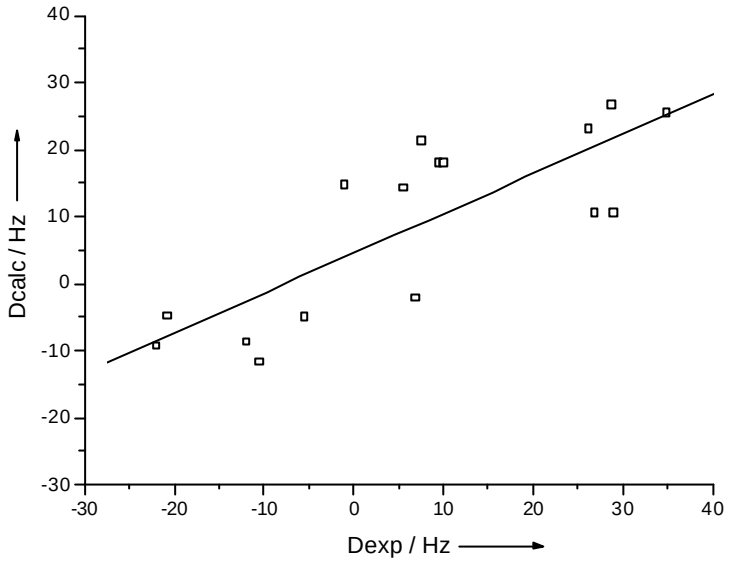

B)

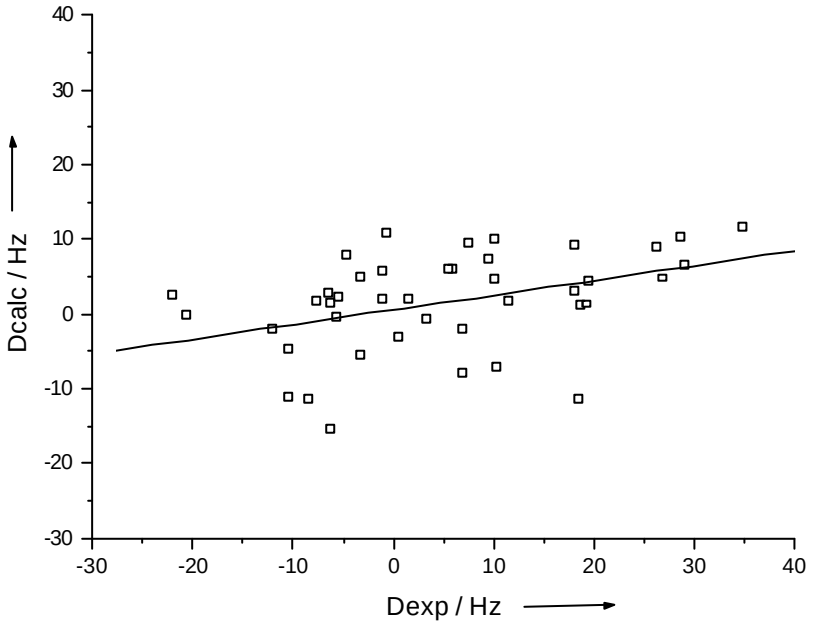

Figure S1. Fitting between experimental RDCs and the ones calculated from the chloroform structure of hormaomycin. A) RDCs from the backbone of the macrocyclic ring are used. The equation of the fitting curve is $D_{calc} = 0.59\, D_{exp} + 4.50$ B) when 42 RDCs are used: $D_{calc} = 0.20\, D_{exp} + 0.54$

A)

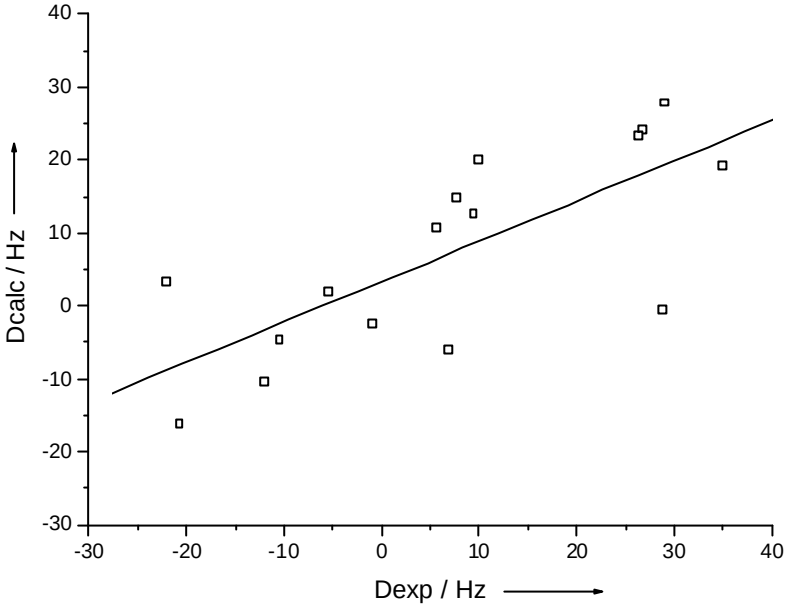

B)

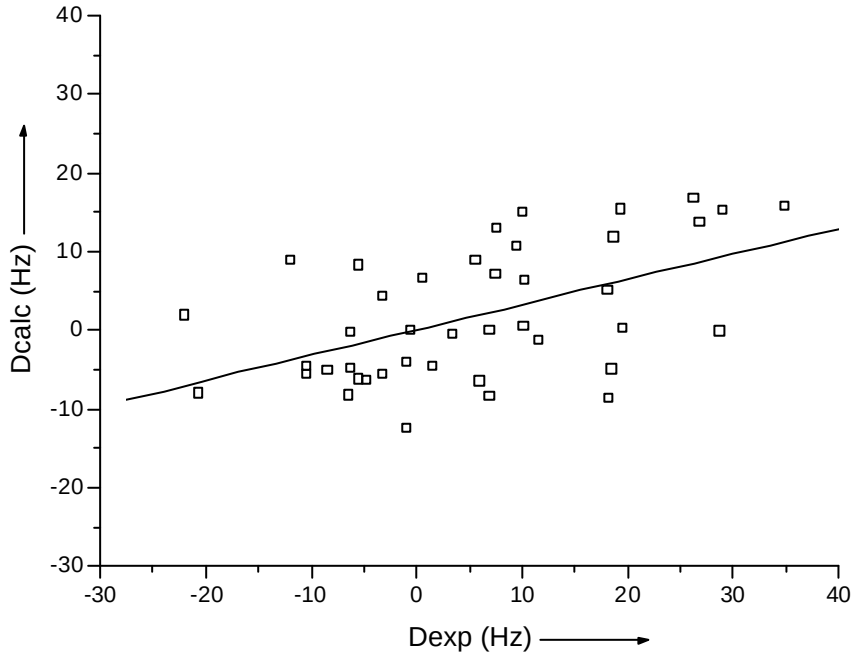

Figure S2. Fitting between experimental RDCs and the ones calculated from the crystal structure of hormaomycin. A) D_{calc} = 0.55 D_{exp} + 3.32 is obtained with RDCs from the back-one of the macrocyclic ring. B) D_{calc} = 0.32 D_{exp} + 0.03 is obtained with 42 RDCs.

DOI: 10.1002/chem.200600144

Synthesis and Structural Model of an α(2,6)-Sialyl-T Glycosylated MUC1 Eicosapeptide under Physiological Conditions

Sebastian Dziadek,[a, c] Christian Griesinger,*[b] Horst Kunz,*[a] and Uwe M. Reinscheid[b, c]

Abstract: To study the effect of O-glycosylation on the conformational propensities of a peptide backbone, a 20-residue peptide (GSTAPPAHGVTSAPDTRPAP) representing the full length tandem repeat sequence of the human mucin MUC1 and its analogue glycosylated with the (2,6)-sialyl-T antigen on Thr11, were prepared and investigated by NMR and molecular modeling. The peptides contain both the GVTSAP sequence, which is an effective substrate for GalNAc transferases, and the PDTRP fragment, a known epitope recognized by several anti-MUC1 monoclonal antibodies. It has been shown that glycosylation of threonine in the GVTSAP sequence is a prerequisite for subsequent glycosylation of the serine at GVTSAP. Furthermore, carbohydrates serve as additional epitopes for MUC1 antibodies. Investigation of the solution structure of the sialyl-T glycoeicosapeptide in a H_2O/D_2O mixture (9:1) under physiological conditions (25 °C and pH 6.5) revealed that the attachment of the saccharide side-chain affects the conformational equilibrium of the peptide backbone near the glycosylated Thr11 residue. For the GVTSA region, an extended, rod-like secondary structure was found by restrained molecular dynamics simulation. The APDTR region formed a turn structure which is more flexibly organized. Taken together, the joined sequence GVTSAPDTR represents the largest structural model of MUC1 derived glycopeptides analyzed so far.

Keywords: antigens · conformation analysis · glycopeptides · solid-phase synthesis

Introduction

Tumor immunotherapy utilizing the remarkable specificity of the human immune system for a selective attack on malignant cells would be a highly attractive approach for the treatment of cancer.[1–3] An essential requirement for the development of a functional antitumor vaccine is to focus the highly specific immune reactions on tumor cells ideally without affecting healthy tissue. It is therefore necessary to identify suitable structural elements that clearly distinguish a tumor cell from a normal cell. Such important cancer-selective structural information is observed in the tumor-associated mucin MUC1 which is a heavily O-glycosylated membrane glycoprotein present at the interface between many epithelia and their extracellular environments.[4–6] The extracellular domain of MUC1 consists of tandem repeats comprising 20 amino acids of the sequence GSTAPPAHGVTSAPDTRPAP containing five O-glycosylation sites. In epithelial tumor cells the expression of MUC1 is drastically increased. This MUC1 over-expression is accompanied by the downregulation of a glucosaminyltransferase (C-2GnT-1) and the concomitant over-expression of different sialyltransferases resulting in the formation of short, prematurely sialylated glycan side-chains such as the sialyl-T_N, α(2,3)-sialyl-T, and α(2,6)-sialyl-T saccharide antigens.[7] Moreover, the incomplete glycosylation in tumor cells is supposed to lead to a changed conformation of the protein backbone[8] and to the exposure of peptide epitopes, which are masked in normal cells. A variety of monoclonal antibodies recognize these epitopes and specifically bind to malignant but not normal epithelial cells. Most antibodies are

[a] Dr. S. Dziadek, Prof. Dr. H. Kunz
Institut für Organische Chemie der Universität Mainz
Duesbergweg 10–14, 55099 Mainz (Germany)
Fax: (+49) 6131-39-24786
E-mail: hokunz@uni-mainz.de

[b] Prof. Dr. C. Griesinger, Dr. U. M. Reinscheid
Max-Planck Institute for Biophysical Chemistry
Am Fassberg 11, 37077 Göttingen (Germany)
Fax: (+49) 551-201-2202
E-mail: cigr@nmr.mpibpc.mpg.de

[c] Dr. S. Dziadek, Dr. U. M. Reinscheid
S. Dziadek and U. M. Reinscheid contributed equally to this work.

Supporting information for this article is available on the WWW under http://www.chemeurj.org/ or from the author: Complete list of ROE values used for the structure calculation of the sialyl-T glycoeicosapeptide **13**.

directed to the immunodominant PDTRPAP motif on the MUC1 tandem repeat.[9] These tumor-associated structure alterations render glycopeptide partial structures from MUC1 valuable target molecules for the generation of immunostimulating antigens.

Immunizations of mice with a vaccine construct consisting of a glycopeptide sequence from the MUC1 tandem repeat carrying a sialyl-T_N side-chain conjugated via a flexible spacer with a specific T_H-cell epitope from ovalbumin lead to the induction of a strong, highly specific humoral immune response against the tumor-associated MUC1 glycopeptide.[10] The isolated antibodies from the mouse sera exclusively recognized a combination of saccharide as well as peptide structural elements as determined by a neutralization experiment.[10] In contrast, neither the unglycosylated MUC1 peptide sequence alone nor the sialyl-T_N saccharide antigen attached to a different peptide chain from MUC4 were capable of binding to and hence neutralizing the antibody. These significant results prompted our interest in investigating the structural propensities of tumor-associated MUC1 glycopeptides, in particular the influence of the O-glycans on the conformation of the peptide chain, under nearly physiological conditions in aqueous solution. We herein propose a valuable structural model of the immunogenically relevant parts of the MUC1 peptide core.

Results and Discussion

Syntheses of MUC1-derived glycopeptides: To allow detailed NMR based structural elucidation, eicosapeptides and glycopeptides representing the full length tandem repeat sequence of the mucin MUC1 were synthesized according to an efficient convergent strategy. In order to be able to study the effect of O-glycosylation on the conformational propensities of the underlying peptide backbone, in addition to the glycoeicosapeptide carrying the complex tumor-associated α(2,6)-sialyl-T antigen the unglycosylated MUC1 eicosapeptide was assembled on a solid support. The glycopeptide structure was accessible by incorporating a pre-formed O-glycosyl amino acid into the sequential glycopeptide synthesis.

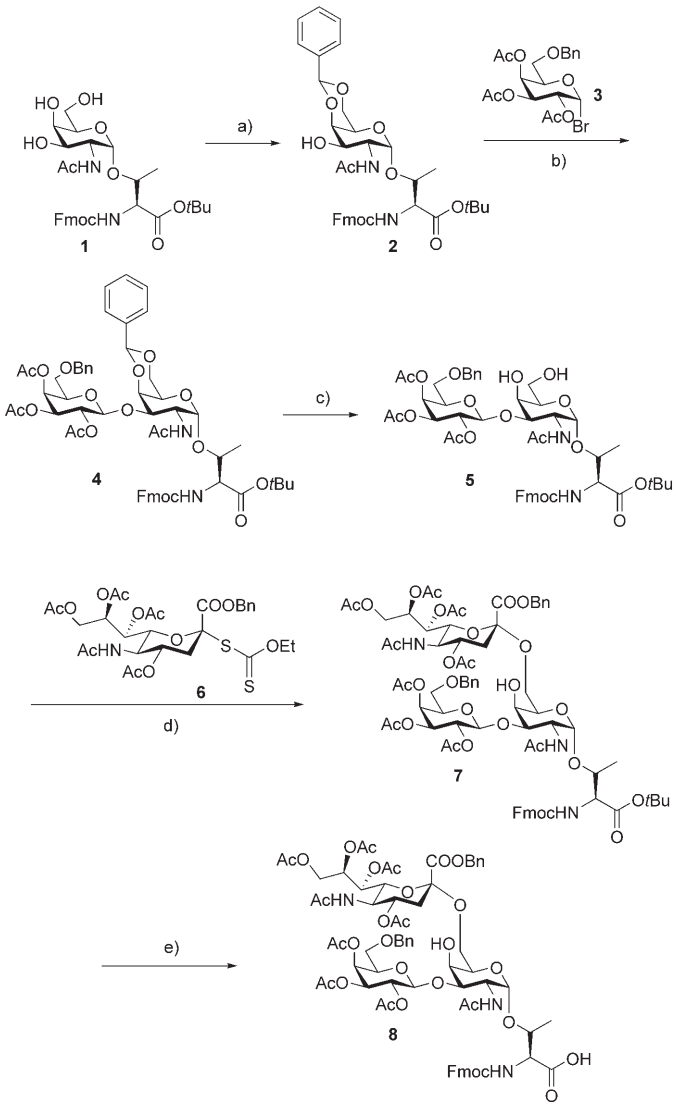

Scheme 1. a) MeCN, α,α-dimethoxytoluene, cat. PTSA, RT, 15 h, 75%. b) $Hg(CN)_2$, CH_3NO_2/CH_2Cl_2 3:2, 4 Å MS, 18 h, 93%. c) 80% AcOH, 80°C, 1 h, 82%. d) MeSBr, AgOTf, 3 Å MS, CH_3CN/CH_2Cl_2 2:1, 4 h, −65°C, 61% α-anomer, 12% β-anomer. e) TFA, anisole, 85%. DTBP = di-*tert*-butylpyridine; PTSA = *p*-toluenesulfonic acid; TFA = trifluoroacetic acid.

Biomimetic synthesis of the O-glycosyl amino acid building block: The preparation of the α(2,6)-sialyl-T threonine building blocks for solid-phase glycopeptide synthesis according to a linear synthetic approach[11] mimicking the glycan biosynthesis in tumor cells is outlined in Scheme 1.

The N-Fmoc and *tert*-butyl ester protected T_N-antigen threonine derivative **1**[12,13] served as synthon for the assembly of the (2,6)-sialyl-T-antigen. It was converted to the 4,6-benzylidene acetal **2** using α,α-dimethoxytoluene in the presence of catalytic *p*-toluenesulfonic acid in acetonitrile. The subsequent stereoselective β-galactosylation to form the blocked disaccharide **4**[11] was accomplished employing the 6-*O*-benzyl protected galactosyl bromide **3**[14] activated with mercury(II) cyanide under Helferich[15] conditions. Selective removal of the benzylidene acetal with aqueous acetic acid at 80°C furnished a suitable sialyl acceptor **5**. For the regio- and stereoselective sialylation of the 6-OH group in **5**, the xanthate[16,17] **6** of the *N*-acetyl neuraminic acid benzyl ester activated with methylsulfenyl triflate[18] as a promoter proved to be an efficient donor. Using a mixture of acetonitrile[19] and dichloromethane for the glycosylation reaction, the desired α(2,6)-sialyl-T-threonine derivative **7** was obtained in a yield of 61% after preparative RP-HPLC. Subsequent acidolysis of the *tert*-butyl ester with trifluoroacetic acid and anisole (10:1) yielded the N-Fmoc protected (2,6)-sialyl-T-threonine building block **8** which was incorporated into the sequential solid-phase synthesis without O-acetylation of the sterically hindered 4-OH group.

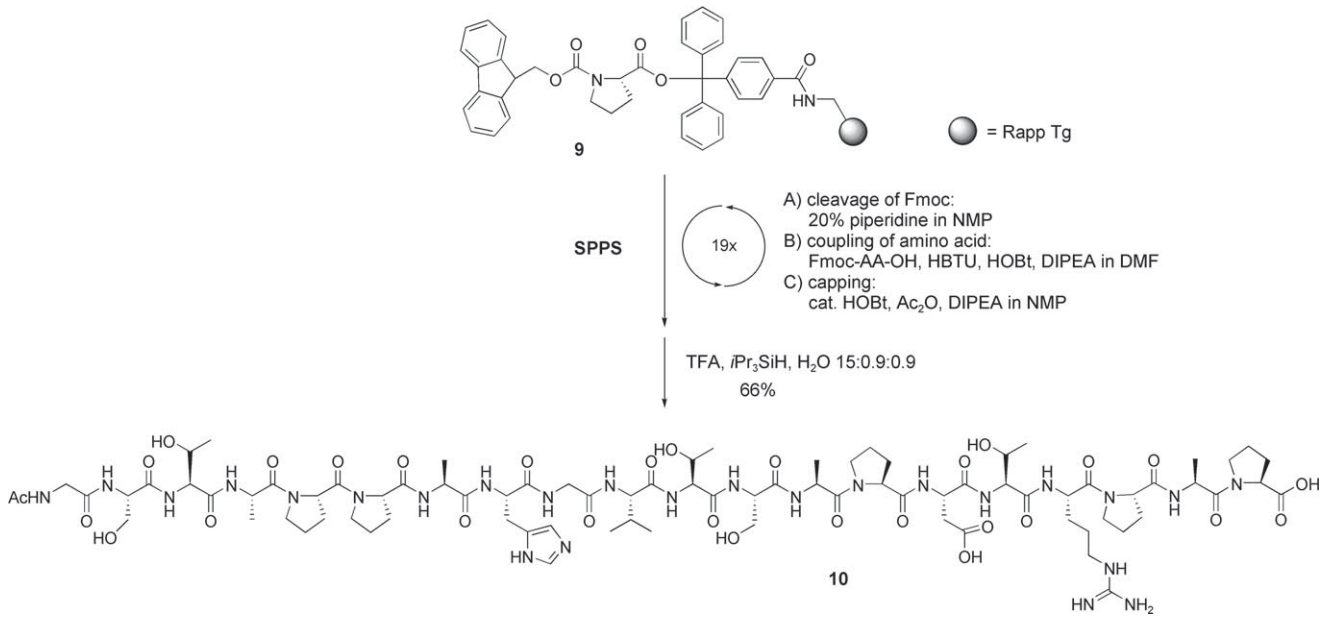

Scheme 2. Solid-phase peptide synthesis of MUC1 eicosapeptide **10**.

Solid-phase glycopeptide synthesis: Prior to the synthesis of different glycoeicosapeptides, the unglycosylated full length tandem repeat sequence of MUC1 was assembled by condensing N-Fmoc[20] and side-chain protected amino acids (10 equiv) on Tentagel resin[21] **9** functionalized with Fmoc-proline via the trityl linker (Scheme 2).

Couplings were achieved by activating the amino acid building blocks with *O*-(1*H*-benzotriazol-1-yl)-*N*,*N*,*N*′,*N*′-tetramethyluronium hexafluorophosphate (HBTU)[22]/*N*-hydroxybenzotriazole (HOBt)[23] and DIPEA. Following each coupling step, unreacted amino components were capped with acetic anhydride/HOBt and DIPEA. After completion of the MUC1 consensus sequence and acetylation of the amino terminus, the peptide was liberated from the resin by acidolysis of the trityl linker under simultaneous removal of all acid-labile side-chain protecting groups. Purification by preparative HPLC and subsequent lyophilization furnished the target structure **10** in a yield of 66%.

To generate suitable model structures for conformational analyses, the threonine residue at position-11, that is, outside the immunodominant PDTRP domain, was chosen for the attachment of the tumor-associated saccharide side chains. For this purpose, the protected resin-bound nonapeptide **11** representing the C-terminal segment of the MUC1 tandem repeat was prepared according to the Fmoc protocol[20] (Scheme 3).

For the synthesis of the (2,6)-sialyl-T glycoeicosapeptide one part of the functionalized resin **11** was employed, which was liberated from the Fmoc group by treatment with piperidine (20%) in NMP. Subsequently, the glycosylated threonine derivative **8** (Scheme 1) was coupled manually to the resin-bound peptide fragment employing an excess of only 1.7 equivalents of the precious building block activated with a combination of the coupling reagents *O*-(7-azabenzotriazole-1-yl)-*N*,*N*,*N*′,*N*′-tetramethyluronium hexafluorophosphate (HATU) and *N*-hydroxy-7-azabenzotriazole (HOAt).[24] Following the coupling reaction and capping of unreacted amino groups, the MUC1 sequence was completed by standard condensations of Fmoc-amino acids and final acetylation of the amino terminus. Simultaneous detachment of the glycopeptide from the polymeric support and cleavage of the acid-labile amino acid side-chain protecting groups was achieved by treatment with a mixture of trifluoroacetic acid, triisopropylsilane and water. The resulting partially deblocked MUC1 glycopeptide **12** was purified by preparative RP-HPLC and isolated in a yield of 44% based on the proline loaded resin **9a**. Final deprotection of the glycan portion by hydrogenolysis of the benzyl groups and O-deacetylation under Zemplén[25] conditions furnished the target structure **13** which was obtained in 55% yield after purification by RP-HPLC.

NMR analysis of the eicosapeptide from MUC1 and its glycosylated analogue: A number of NMR studies have been undertaken to elucidate the structural effects of glycosylation on peptides in general and on MUC1-derived peptides in particular.[8,26] The drawback of "insufficient structure" under physiological conditions was circumvented by lowering the temperature, and/or addition of solvents and adjustment of pH to low values.[27–31] As an example, Kirnarsky et al.[32,33] studied glycosylated 15-mers of MUC1 at low temperatures (5 and 10°C) in water, and 9-mers in DMSO.

We were able to study structural effects of complex carbohydrates on MUC1 derived peptides consisting of the full length tandem repeat in a phosphate buffer of pH 6.5 at 25°C. Using NMR restrained molecular dynamics structured areas could be derived of a full length repeat substituted by complex carbohydrates under physiological conditions. Con-

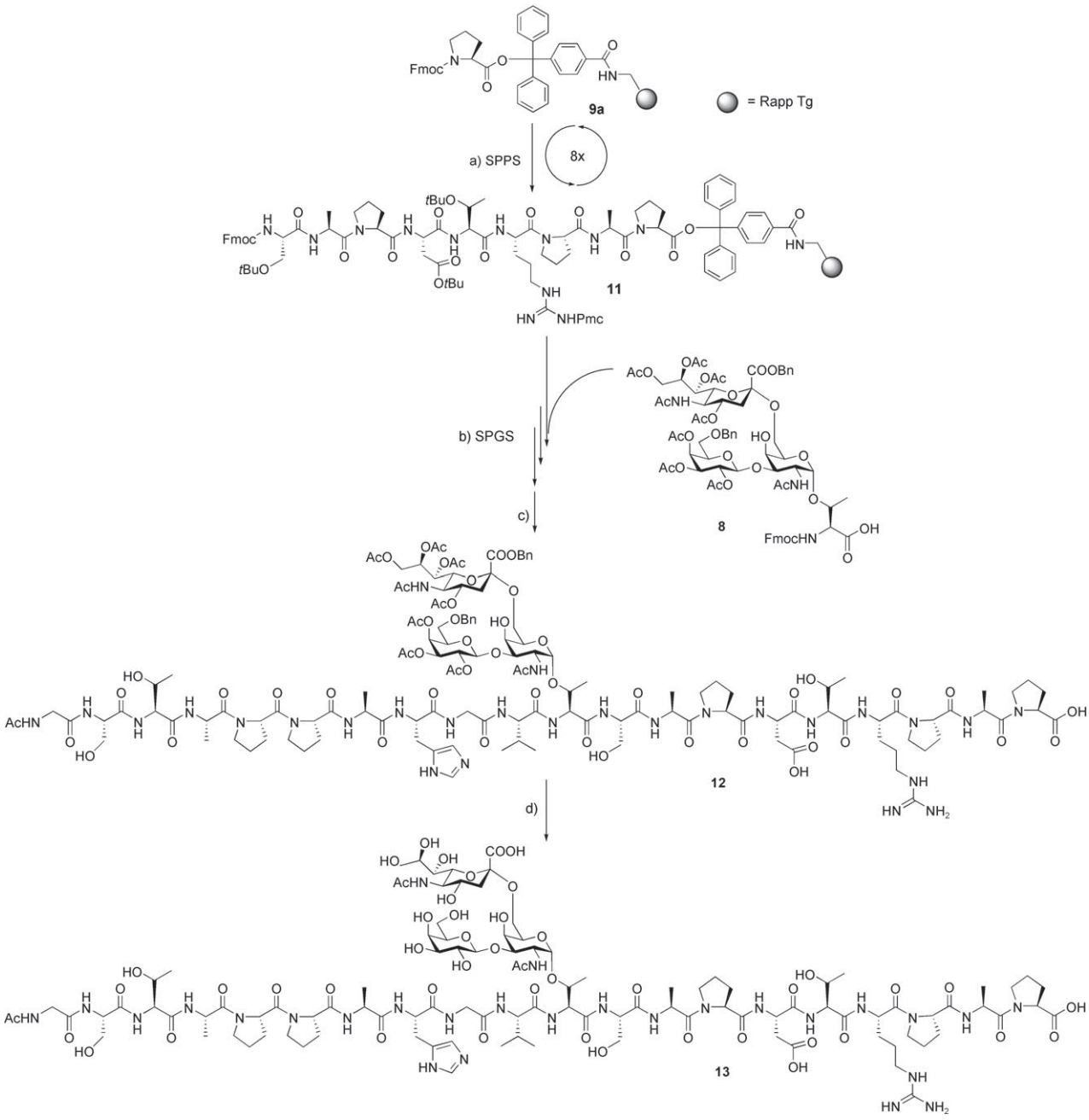

Scheme 3. a) Solid-phase peptide synthesis (SPPS): Fmoc removal (20% piperidine/NMP); coupling (steps 1–8: 1 mmol Fmoc-AA-OH, HBTU/HOBt/DIPEA, DMF; capping: Ac_2O, DIPEA, HOBt 4:1:0.12. Synthesis of (2,6)-sialyl-T glycoeicosapeptide **13** from MUC1: b) solid-phase glycopeptide synthesis (SPGS): Fmoc removal (20% piperidine/NMP); coupling step 9: 1.7 equiv **8**, HATU/HOAt/NMM, DMF, 4 h; steps 10–19: 1 mmol Fmoc-AA-OH, HBTU/HOBt/DIPEA, DMF; capping: Ac_2O, DIPEA, HOBt 4:1:0.12; c) TFA/TIS/H_2O 15:0.9:0.9, 2 h, 44% based on the pre-loaded resin **9a**); d) i) H_2, 5% Pd/C, MeOH, 20 h, ii) NaOMe/methanol, pH 9.5, 55% over two steps. HATU = *O*-(7-aza-benzotriazole-1-yl)-*N*,*N*,*N*′,*N*′-tetramethyluronium hexafluorophosphate, HBTU = *O*-(1*H*-benzotriazol-1-yl)-*N*,*N*,*N*′,*N*′-tetramethyluronium hexafluorophosphate, HOAt = *N*-hydroxy-7-azabenzotriazole, HOBt = *N*-hydroxybenzotriazole; NMM = *N*-methylmorpholine; TIS = triisopropylsilane; Pmc = 2,2,5,7,8-pentamethylchroman-6-sulfonyl.

sequently, direct comparisons with earlier results[8,26–34] have to be treated cautiously.

Proton and ^{13}C NMR resonances were assigned for two MUC1 derived peptides: the unglycosylated full length tandem repeat sequence **10** and the glycosylated peptide **13** (Tables 1–3).

One-dimensional proton NMR spectra showed one predominant resonance for each amide NH suggesting either one dominant isomer or fast conformational averaging on the NMR time scale in phosphate buffer. The coexistence of slowly interconverting conformers could be ruled out by the absence of exchange cross peaks in the ROESY spectra and

Table 1. Chemical shifts (in ppm) of the MUC1 peptide **10** in H_2O/D_2O (9:1, pH 6.5) at 298 K.[a]

	NH	Hα	Cα	Hβ	Cβ	Hγ	Cγ	Hδ	Cδ
G1	8.212	3.893	42.45	–	–	–	–	–	–
S2	8.276	4.457	55.50	a: 3.78, b: 3.818	61.12	–	–	–	–
T3	8.143	4.270	58.83	4.155	67.07	1.114	18.74	–	–
A4	8.148	4.51	47.82	1.249	15.36	–	–	–	–
P5	–	4.61	58.72	a: 2.263, b: 1.794	27.98	1.948	24.7	a: 3.742, b: 3.528	47.6
P6	–	4.291	nd	a: 2.18, b: 1.762	29.28	1.931	24.6	a: 3.724, b: 3.578	47.5
A7	8.316	4.15	49.7	1.241	16.4	–	–	–	–
H8	8.384	4.615	nd	a: 3.207, b: 3.11	26.34	H4: 7.228	C4: 117.425	H2: 8.516	C2: 133.67
G9	8.347	a: 3.871, b: 3.915	nd	–	–	–	–	–	–
V10	8.056	4.140	59.57	2.02	30.18	a: 0.862, b: 0.852	a: 18.39, b: 17.61	–	–
T11	8.245	4.327	58.97	4.137	67.07	1.116	18.74	–	–
S12	8.219	4.371	55.32	a: 3.75, b: 3.891	61.25	–	–	–	–
A13	8.268	4.521	47.85	1.281	15.38	–	–	–	–
P14	–	4.323	nd	a: 2.19, b: 1.829	29.29	1.945	24.5	a: 3.716, b: 3.525	nd
D15	8.505	4.64	50.33	a: 2.874, b: 2.792	35.19	–	–	–	–
T16	7.965	4.236	58.99	4.132	67.07	1.095	18.83	–	–
R17	8.174	4.558	51.19	a: 1.76, b: 1.66	27.46	1.58	23.98	3.127	40.611
P18	–	4.325	nd	a: 2.19, b: 1.796	29.28	1.93	24.5	a: 3.728, b: 3.525	nd
A19	8.326	4.481	47.65	1.284	15.16	–	–	–	–
P20	–	4.305	nd	a: 2.22, b: 1.92	28.88	1.945	24.5	a: 3.693, b: 3.580	nd

[a] nd: not determined.

Table 2. Chemical shifts (in ppm) of the (2,6)-sialyl-T glycoeicosapeptide **13** in H_2O/D_2O (9:1, pH 6.5) at 298 K.

	NH	^{15}N	Hα	Cα	Hβ	Cβ	Hγ	Cγ	Hδ	Cδ
G1	8.216	114.16	3.890	42.52	–	–	–	–	–	–
S2	8.280	115.37	4.454	55.49	a: 3.816, b: 3.777	61.04	–	–	–	–
T3	8.149	115.73	4.267	58.87	4.144	66.95	1.110	18.65	–	–
A4	8.152	127.99	4.505	47.68	1.248	15.21	–	–		
P5	–	–	4.607	58.57	a: 2.260, b: 1.795	27.82	1.944	24.50	a: 3.732, b: 3.527	47.8
P6	–	–	4.290	60.05	a: 2.178, b: 1.754	29.11	1.920	24.50	a: 3.724, b: 3.532	47.6
A7	8.316	124.35	4.142	48.20	1.242	16.28	–	–	–	–
H8	8.328	117.14	4.588	52.49	a: 3.187, b: 3.100	26.59	H4: 7.186	117.63	H2: 8.38	134.15
G9	8.328	120.09	a: 3.838, b: 3.912	43.05	–	–	–	–	–	–
V10	8.016	120.03	4.244	59.28	2.006	30.13	a: 0.890, b: 0.870	a: 18.42, b: 17.67	–	–
T11*	8.660	117.02	4.562	57.11	4.216	77.44	1.216	18.27	–	–
S12	8.450	116.23	4.387	54.96	a: 3.760, b: 3.685	61.50	–	–	–	–
A13	8.432	126.18	4.367	47.75	1.300	14.96	–	–	–	–
P14		–	4.310	60.20	a: 2.215, b: 1.835	29.19	1.958	24.50	a: 3.722, b: 3.556	47.7
D15	8.383	110.10	4.517	51.40	a: 2.64, b: 2.567	38.08	–	–	–	–
T16	7.948	114.16	4.230	58.88	4.143	66.95	1.095	18.70	–	–
R17	8.184	124.69	4.524	51.38	a: 1.751, b: 1.676	29.11	1.594	23.81	3.125	40.56
P18	–	–	4.314	60.30	a: 2.186, b: 1.808	29.22	1.908	24.49	a: 3.730, b: 3.528	47.6
A19	8.240	126.12	4.483	47.46	1.284	15.13	–	–	–	–
P20	–	–	4.136	61.89	a: 2.124, b: 1.810	29.19	1.890	24.39	a: 3.653, b: 3.543	47.4

Table 3. Chemical shifts (in ppm) of the (2,6)-sialyl-T glycoeicosapeptide **13** in H_2O/D_2O (9:1, pH 6.5) at 298 K.

GalNAc				Gal				NeuNAc			
H1:	4.860	C1:	99.31	H1′:	4.325	C1′:	104.70	$H3_{eq}''$:	2.580	C3″:	40.15
H2:	4.125	C2:	48.26	H2′:	3.408	C2′:	70.65	$H3_{ax}''$:	1.543		
H3:	3.900	C3:	77.16	H3′:	3.495	C3′:	72.63	H4″:	3.564	C4″:	68.26
H4:	4.095	C4:	68.99	H4′:	3.800	C4′:	68.64	H5″:	3.727	C5″:	51.85
H5:	4.007	C5:	69.63	H5′:	3.530	C5′:	74.91	H6″:	3.600	C6″:	72.49
H6a:	3.830	C6:	63.85	H6a′:	3.675	C6′:	61.05	H7″:	3.790	C7″:	71.77
H6b:	3.478			H6b′:	3.627			H8″:	3.484	C8″:	68.26
NH:	7.445	^{15}N:	121.68					H9a″:	3.777	C9″	62.65
AcNH:	1.917	C_{Ac}:	22.03					H9b″:	3.550		
								NH:	7.954	^{15}N:	123.04
								AcNH:	1.935	C_{Ac}:	21.90

the correct number of resonances in the 1D proton spectrum. The presence of strong $H_\alpha(i)$–NH(i+1) ROE signals and the absence of $H_\alpha(i)$–$H_\alpha(i+1)$ cross peaks confirmed that all amide bonds were in the *trans* configuration. A *trans* configuration with respect to the X-Pro peptide bonds was indicated by characteristic ROE cross peaks from the H_α (X) to the H_δ (Pro), the absence of cross peaks from H_α (X) to H_α (Pro) and a chemical shift difference of around 31 ppm between C_α and C_β.[35] Additionally, the differences in ^{13}C chemical shifts of C_β–C_γ were around 4.5 ppm which indicated *trans*-peptide bonds.[36,37]

In contrast, Schuman et al.[28] observed two sets of resonances in a MUC1 derived 9-mer suggesting that *cis*/*trans* isomerization occurred at one of the X-Pro peptide bonds. A population ratio of 5:1 was inferred under the experimental conditions (5 °C, pH 5.1). The low signal to noise ratio of the *cis* isomer precluded further structural analysis. In contrast to our results, glycosylation of the 9-mer shifted the *cis*/*trans* equilibrium toward the *trans* isomer for residues at the C-terminal side of the glycosylation. These differing observations might be correlated to different experimental conditions concerning the peptide (sequence, length), the carbohydrates (type, complexity) and the environmental parameters (temperature, pH, solvent system).

A number of side-chain methylene proton pairs exhibited a spectral dispersion that indicated conformational preferences even in the unglycosylated MUC1 peptide. The H_β protons of Ser12 in the unglycosylated peptide **10** showed a $\Delta\delta$ value of 0.15 ppm indicating a non-averaged conformation of the χ_1 dihedral. Upon glycosylation, large chemical shift dispersion was measured within the pair of NH protons of the two Thr residues Thr11 and Thr16, the first of them being glycosylated in **13**. In this glycopeptide the difference increased to more than 0.7 ppm. Conversely, Grinstead et al.[38] observed for a MUC1 hexadecapeptide degenerate H_β resonances of Ser which changed into well resolved peaks only after glycosylation. Again, the experimental conditions may explain these differences.

Chemical shift deviation: Generally, H_α chemical shift deviations (CSD, $\Delta\delta_{H\alpha \text{ or } C\alpha} = \delta_{observed} - \delta_{random\ coil}$) exhibit a mean shift of −0.39 ppm when the residue is placed in a helical conformation while a mean shift of +0.37 ppm is observed when the residue is found in an extended conformation.[35,39] The CSD values, δH_α and δC_α, for the unglycosylated MUC1 derived 20-mer peptide **10** were close to random coil ($\Delta\delta_{H\alpha} \pm 0.02$ ppm and $\Delta\delta_{C\alpha} \pm 0.4$ ppm) for all residues except Ala4 and Pro5 at the N-terminus, and Ala13, Arg17 and Ala19 at the C-terminus. In addition, the H_α resonances for residues near the site of glycosylation in the glycosylated peptide **13** (Figure 1) showed significant downfield shifts for Val10 and Thr11 (+0.104 and +0.235 ppm) whereas Ala13 and Asp15 H_α resonances were shifted upfield by −0.154 and −0.123 ppm, respectively. This is in agreement with an increase in the population of extended structures in the GVTSA region and an ordering effect of the glycan for the PDTR region. The influence of the position of glycosylation

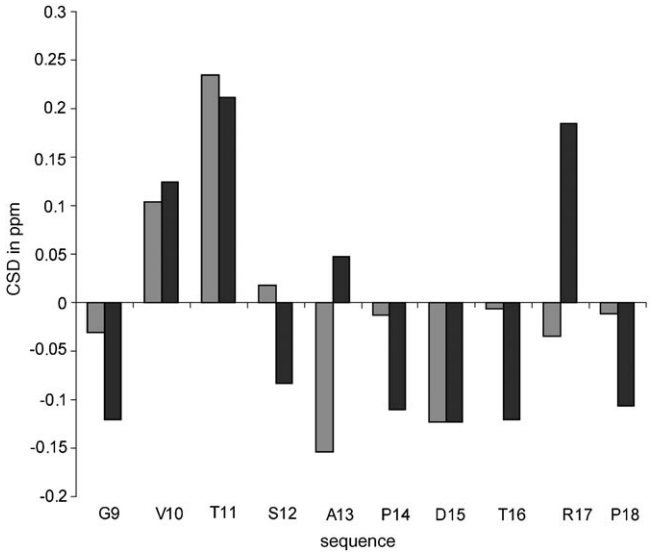

Figure 1. Chemical shift deviations (CSD) of H_α for the glycopeptide **13**. The CSD relative to the values of the unglycosylated peptide **10** is shown in bright grey, while the dark gray color represents the CSD relative to random coil values (helical: −0.39 ppm, extended: +0.37 ppm).

at Thr11 is clearly seen when the differences between the chemical shifts of **13** and **10** are displayed (Figure 1). The comparison with random coil values (δ(**13**)−δ(random coil)) shows a deviation at Ala13, Pro14, Thr16 and Arg17 which can be explained by sequence effects for instance induced by the proline residues Pro14 and Pro18.

Temperature coefficients: The temperature dependence of the NH proton chemical shifts in partially folded peptides is a function of at least two variables: the temperature dependent equilibrium between the folded and random coil states, and the degree of structuring of the folded state at the lower temperature.[40] For unfolded regions, temperature coefficients ($\Delta\delta/\Delta T$) are expected to be between 6 and 10 ppb per K, indicating that the backbone is freely solvated by water and that no hydrogen bonds are present which would protect the backbone amides from proton exchange. In glycopeptide **13** the values of the temperature coefficients were below 5 ppb K^{-1} between residues Val10 and Arg17, suggesting at least partial shielding from solvent and/or hydrogen bonding (Figure 2). The negative $\Delta\delta/\Delta T$ value observed for Thr11 correlated with a downfield shift of the HN resonance of Thr11 in the glycosylated peptide when compared with the non-glycosylated peptide which could be interpreted as a hydrogen bond effect.

Coupling constants: β Turns are characterized by a dihedral angle of $\phi_{i+1} = -60°$, which is consistent with a coupling constant of $^3J_{N\alpha}$ between 4 and 5 Hz, assuming a β turn that is 100% populated. Inverse γ turns show a ϕ_{i+2} of approximately −80° with a coupling constant between 6 and 8 Hz. Because unstructured regions also display values within this range, inverse γ turns cannot be distinguished from random coil on the basis of this coupling constant alone.[41] The high

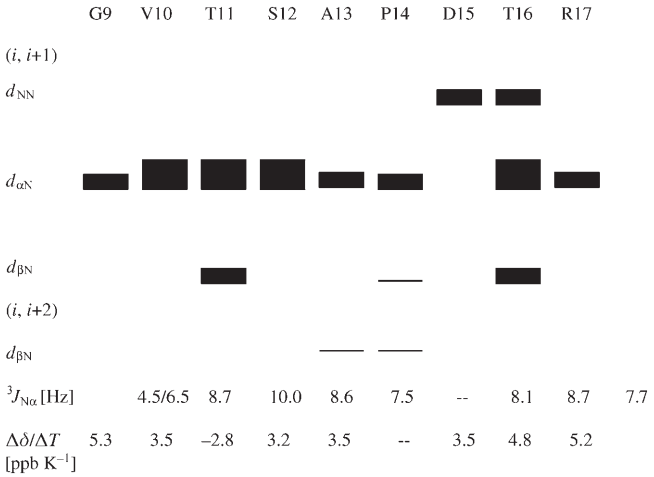

Figure 2. ROE connectivities, $^3J_{N\alpha}$ and temperature coefficients for glycopeptide **13**. The line thickness corresponds to the ROE intensity. In the case of proline, NH refers to δ protons.

value of 10.0 Hz observed for Thr11 in **13** defined a restrained dihedral at the site of glycosylation (Figure 2). The sequence from Val10 to Arg17 exhibited values above 7.5 Hz which indicates either the presence of possibly interconverting turn structures and/or the presence of extended conformations.[38] Considering together the CSD, *J* coupling and temperature coefficients, it appears that the four residues in **13** around the site of glycosylation (Val10, Thr11, Ser12, Ala13) and the neighboured sequence PDTR have a high propensity for an extended and turn structure.

ROE cross peaks: The ROE connectivities were found to be very similar for both peptides except for the glycosylated region in **13**, in which significant differences were observed. In this area, a large number of strong consecutive $d_{\alpha N}(i,i+1)$ connectivities indicated the predominance of extended backbone conformations.[42] The important observation of ROE signals between GalNAc and Gal that clearly indicate the rigidity of the carbohydrate substituent in **13**, prompted us to further investigate this glycopeptide in detail. For this structure, exclusively interresidual ROE contacts are depicted in Figure 3. A significant number of peptide–saccharide ROE signals near the glycosylation site was detected. They include ROE signals between the backbone NH proton of Thr11 and the methyl as well as NH protons of the N-acetyl group of GalNAc, and ROE signals between the β proton and γ proton of Thr11 and the anomeric H1 proton of GalNAc. These ROE interactions suggested that rotation about the α-glycosidic linkage is hindered.

Similar peptide–sugar connectivities have been observed in other NMR studies of α-GalNAc O-glycosylated peptides.[27,32,43] All ROE values used for structure calculation are listed in Table S1 of the Supporting Information.

Conformational analysis of the (2,6)-sialyl-T glycoeicosapeptide 13 by restrained MD calculations: A total of 107 ROE signals were collected for the (2,6)-sialyl-T glycoeicosapeptide **13** and classified into four groups according to their integrated intensities. These distance information in combination with peptide bonds restrained in the *trans* conformation were used as input for a restrained MD simulation. After energy minimization, a final set of eight low energy structures (< 15 kcal mol^{-1}, < 0.05 nm distance restraint violation) was selected.

Two overlapping peptide fragments, GVTSA and APDTR comprising the glycosylated Thr11 with flanking residues, and the immunodominant region PDTR of MUC1, were selected for cluster analysis to determine structural effects of glycosylation. For the GVTSA segment the mean pairwise RMSD for the heavy atoms of these conformers and the corresponding average structure was equal to 0.78 Å. The structural model of **13** exhibits a clearly defined extended, rod-like conformation for the sequence GVTSA (Figure 4).

The directly *O*-linked GalNAc is positioned along one side of an extended β strand formed by the sequence GVTSA. Such positioning is consistent with strong contacts between the *N*-acetyl NH proton of the GalNAc moiety and the amide proton of the glycosylated Thr11 residue and between the methyl group of GalNAc and the H_α and H_β protons of Ala13. Coltart et al.[30] found a similar methyl group association in their study of the glycosylated N-terminal fragment STTAV of the cell surface glycoprotein CD43.

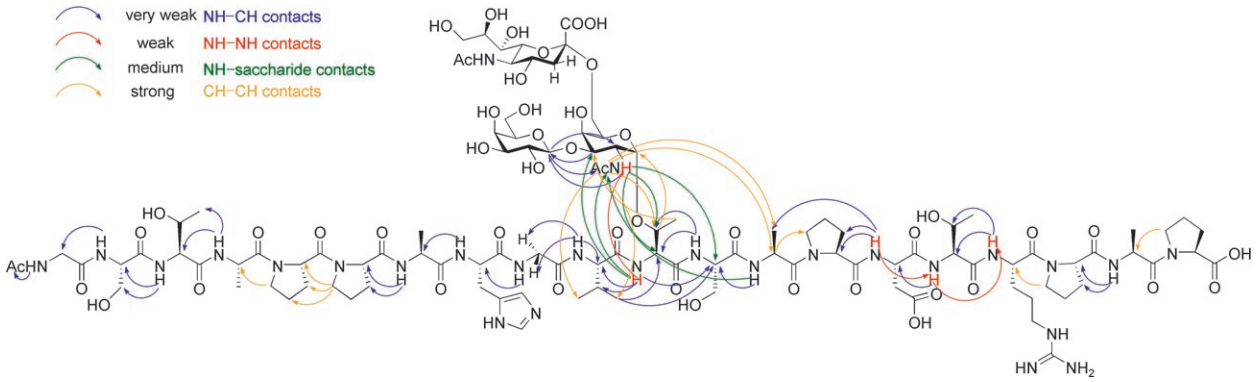

Figure 3. ROE contacts of the glycopeptide **13**.

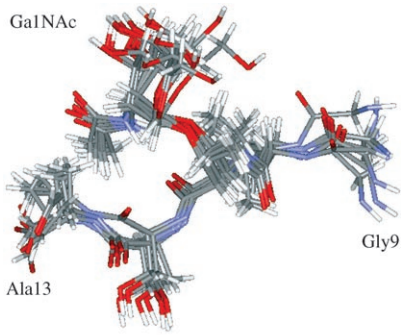

Figure 4. GVTSA sequence of glycopeptide **13** exhibits a rod-like secondary structure. Of the trisaccharide, only GalNAc is shown.

It was suggested by Kirnarsky et al.[32] that the N-acetyl group of the GalNAc moiety interacts directly with the peptide backbone, possibly through hydrogen bonding. An intramolecular hydrogen bonding between the amide proton of GalNAc and the carbonyl oxygen of the O-linked threonine residue was also proposed by Naganagowda et al.[44] as the key stabilizing element, opposed to the O-linked serine analogue for which this interaction seemed to be missing. Our model based on ROE cross peaks clearly indicates a hydrogen bond between the amide proton of GalNAc and the carbonyl oxygen of Thr11 (N–O distance below 2.5 Å, NHO angle $>$ 120°) [ROEs between the NH proton of GalNAc und H_α of Ser12 (medium intensity), H_α of Thr11 (weak intensity) and H_β of Thr11 (weak intensity)].

The structuring effect of the carbohydrates could be explained by the observation that β-branched amino acids favor extended conformations, due to both steric clashes with neighboring side chains and steric clashes with main-chain atoms.[45] Similarly, the attached carbohydrates on Thr11 could act as extremely bulky side chains and influence conformational equilibria of side chain as well as main-chain dihedrals. Schuman et al.[46] concluded in their study of serine trimers substituted by sialyl α(2,6) GalNAc that clustering of more complex carbohydrates shift the conformational equilibrium of the underlying peptide backbone toward a more extended and rigid state.

The analysis of solely monoglycosylated peptides might explain the differing results from Kirnarsky et al.[47] In a recent study on a 21-mer glycosylated with GalNAc, they identified several structural clusters for the GVTSAP sequence by NMR-based molecular modeling comprising turn-like and extended conformations. In a previous report they demonstrated a mostly extended structural shape, termed "γ-turn-like" to indicate that this turn does not fold the peptide chain back.

The significance of our rod-like model of a complex glycopeptide lies in the observation that the inclusion of the tumor-associated Tn carbohydrates at Thr3 and Ser4 upstream from the PDTRP core peptide epitope increased B27.29 antibody binding affinity through direct carbohydrate–antibody interactions.[48] Additionally, Takeuchi et al.[49] showed that the affinity of a sialylated glycopeptide to the anti-MUC1 antibody MY.1E12 was higher than for the analogous glycopeptide without sialylic acid substitution. The latter two findings clearly advocate using complex sugars as epitope-relevant structures.

For the second immunogenically important domain, PDTR, several structural models have been proposed: a type I β turn formed by the residues PDTR[8] and a type II β turn formed by residues APDT were proposed as key element of a knob-like structure.[38,50] The data presented by Kinarsky et al.[32] did not provide direct NMR evidences supporting the existence of either type I or type II β turn. These authors proposed that the PDTR sequence adopts two overlapping inverse γ turns, the first spanning Pro-Asp-Thr and the second Asp-Thr-Arg suggesting a S-shaped bend for the PDTR fragment rather than a knob-like motif.

The strong $d_{NN}(i,i+1)$ connectivities observed by Schuman et al.[28] in their study of 9-residue peptides argued against the existence of two overlapping inverse γ turns, as this arrangement would give rise to only weak $d_{NN}(i,i+1)$ cross peaks between Asp and Thr and between Thr and Arg, corresponding to distances of 3.8 Å in each γ turn. In contrast, the observed NOEs were diagnostic of a type I β turn spanning Pro-Asp-Thr-Arg within the PDTRP peptide epitope region.

With our experimental data obtained under typical bioassay conditions we calculated turn-like structures for the PDTR sequence of **13** (Figure 5). The RMSD of 2.2 Å supports the view of a well-ordered secondary structure in close vicinity to the extended, rod-like conformation of GVTSA.

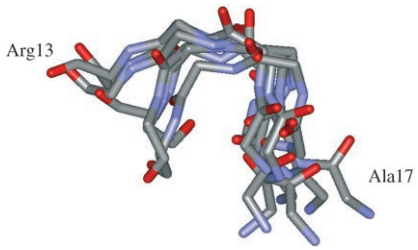

Figure 5. APDTR sequence of glycopeptide **13** exhibits a turn-like structure.

A clear indication of a β-turn structure according to the 7 Å criterion[41] is the $ProC_\alpha$–$ArgC_\alpha$ distance of 5.3 Å in a representative structure of **13**. Although the dihedrals for the $i+1$ and $i+2$ residues of an ideal β turn are not fulfilled [$Asp(\phi_{i+1}) = +66°$, $Asp(\psi_{i+1}) = -84$, $Thr(\phi_{i+1}) = -123°$, $Thr(\psi_{i+1}) = +107$], which correlates to the equatorial position of both side chains in contrast to an axial position for residue $i+2$ in an ideal β turn, the short distance between the C_α of Pro14 and Arg17 and the back folding of the backbone justify the classification as a β turn. A clear distinction between type I and type II can be made by the $H_\alpha(i+1)$–$NH(i+2)$ distance (3.5 and 2.1 Å type II). In the representative structure this distance amounts to 3.6 Å indicating a type I β turn for the sequence PDTR.

A number of different ROE values have been reported. Schuman et al.[28] observed strong NH(i+1)–NH(i+2), NH(i+2)–NH(i+3) and H_β(i+1)–NH(i+2) ROE signals for a 9-residue peptide In the case of **13** the NH ROEs were not strong and the last ROE was missing. Moreover, additional H_β(i+1)–NH(i+3) ROE values were measured for Ala13–Asp15 and Pro14–Thr16 which were also not observed by Kirnarsky et al.[47] studying a 21-mer glycopeptide. The H_α-(i+1)–NH(i+3) cross peak observed by Schuman et al.[28] was not seen in **13**. These differences could be attributed to different test molecules and measurement conditions. Since the glycosylated peptide **13** representing the full length MUC1 repeat sequence was substituted by a complex carbohydrate typically found in cancer-associated cells and was studied under physiological conditions, we are confident to reproduce the conditions relevant for tumour immunotherapy assays. Consequently, our proposed model of a MUC1-derived glycopeptide may give a sound basis for modeling approaches in antibody design.

Experimental Section

General methods: Solvents for moisture-sensitive reactions (acetonitrile, methanol, and dichloromethane) were distilled and dried prior to use according to standard procedures.[51] DMF (amine free, for peptide synthesis) was purchased from Roth, acetic anhydride and pyridine in p.a. quality from Acros. Reagents were purchased at highest available commercial quality and used without further purification unless outlined otherwise. Fmoc-protected amino acids were purchased from Novabiochem. Rapp TentaGel was used as a resin for the solid-phase synthesis. Reactions were monitored by thin-layer chromatography with pre-coated silica gel 60 F_{254} aluminium plates (Merck KGaA, Darmstadt). Flash column chromatography was performed with silica gel (40–63 μm) purchased form Merck KGaA, Darmstadt. Optical rotations $[\alpha]_D$ were measured with a Perkin–Elmer polarimeter 241. RP-HPLC analyses were carried out on a Knauer HPLC system with Phenomenex Luna C18(2) (250×4.6 mm, 5 μ) and Phenomenex Jupiter C18 columns (250×4.6 mm, 5 μ) at a pump rate of 1 mL min^{-1}. Preparative HPLC separations were performed on a Knauer HPLC system with a Phenomenex Luna C18(2) column (250×50 mm, 10 μm) and a pump rate of 20 mL min^{-1}. Semipreparative HPLC separations were carried out on a Knauer HPLC system with Phenomenex Luna C18(2) (250×21.20 mm, 10 μ) and Phenomenex Jupiter (250×21.20 mm, 5 μ) columns at a flow rate of 10 mL min^{-1}. Water and CH_3CN were used as solvents. ^{1}H, ^{13}C, and 2D NMR spectra were recorded on Bruker AC-300, AM-400, ARX-400 or DRX-600 spectrometers. Proton chemical shifts are reported in ppm relative to residual $CHCl_3$ (δ=7.24), DMSO (δ=2.49) or water (δ=4.76). Multiplicities are given as s (singlet), d (doublet), t (triplet), q (quartet), m (multiplet). ^{13}C chemical shifts are reported relative to $CDCl_3$ (δ=77.0) or DMSO (δ=39.5). Assignment of proton and carbon signals was achieved by COSY, TOCSY, HMQC and HMBC experiments when noted. For ^{1}H and ^{13}C signals of the saccharide portions the following denominations were used: *N*-acetyl-D-galactosamine (no apostrophe); D-galactose (′); *N*-acetyl-neuraminic acid (″). MALDI-TOF mass spectra were acquired on a Micromass Tofspec E spectrometer while ESI-mass spectra were obtained on a ThemoQuest-Navigator spectrometer. HR-ESI mass spectra were recorded on a Micromass Q-TOF Ultima spectrometer (matrix: DHB: dihydrobenzoic acid).

***N*-(9*H*-Fluoren-9-yl)methoxycarbonyl-*O*-(2-acetamido-2-deoxy-3-*O*-[2,3,4-tri-*O*-acetyl-6-*O*-benzyl-β-D-galactopyranosyl]-α-D-galactopyranosyl)-L-threonine-*tert*-butylester (5)**: A solution of Fmoc-Thr(βAc_3-6-Bn-Gal(1→3)-α4,6-*O*-Bzn-GalNAc)-O*t*Bu[11] (**4**; 1.00 g, 0.94 mmol) in aqueous acetic acid (80%, 25 mL) was stirred at 80°C for 1 h. Subsequently, the reaction mixture was allowed to cool to 40°C and was diluted by the addition of toluene (25 mL). The solution was concentrated in vacuo and co-evaporated with toluene (5×25 mL). The resulting crude product was purified by flash chromatography (silica gel; cyclohexane/ethyl acetate 1:4; column: h=19 cm, ∅=3 cm) to give the title compound as a colorless, amorphous solid (755 mg, 0.77 mmol, 82%). R_f=0.10 (cyclohexane/ethyl acetate 1:4); $[\alpha]_D^{22}$ = 34.9 (c=1.00, $CHCl_3$); ^{1}H NMR (300 MHz, $CDCl_3$): δ = 7.75 (d, $J_{3,4}=J_{5,6}$=7.4 Hz, 2H, H4-, H5-Fmoc), 7.59 (d, $J_{H1,H2}=J_{H8,H7}$=7.4 Hz, 2H, H1, H8), 7.46–7.15 (m, 9H, H2-, H3-, H6-, H7-Fmoc; 5H, H_{ar}-Bn), 5.95 (d, $J_{NH,H2}$=8.5 Hz, 1H, NH-GalNAc), 5.51 (d, $J_{NH,T\alpha}$=9.2 Hz, 1H, NH-Fmoc), 5.39 (d, $J_{H3',H4'}$=2.9 Hz, 1H, H4′), 5.23–5.08 (m, 1H, H2′), 5.00–4.90 (m, 1H, H3′), 4.80 (br s, 1H, H1), 4.64–4.33 (m, 6H, H1′, H2, CH_2-Fmoc, CH_2-Bn), 4.29–3.98 (m, 5H, H9-Fmoc, T^α, T^β, H4), 3.94–3.56 (m, 5H, $H6_b$, $H6_a$, H5′, H3, H5), 3.55–3.35 (m, 2H, $H6'_a$, $H6'_b$), 2.05, 2.04, 1.98, 1.95 (4×s, 12H, CH_3-Ac), 1.43 (s, 9H, CH_3-*t*Bu), 1.24 (br s, 3H, T^γ); ^{13}C NMR (75.5 MHz, $CDCl_3$, BB): δ = 170.19, 170.10, 169.54 (C=O), 156.37 (C=O urethane), 143.65 (C1a-, C8a-Fmoc), 141.32 (C4a-, C5a-Fmoc), 137.31 (C_q-Bn), 128.51, 128.0 (C_{ar}-Bn), 127.78 (C3-, C6-Fmoc), 127.10 (C2-, C7-Fmoc), 125.18, 124.91 (C1-, C8-Fmoc), 120.07 (C4-, C5-Fmoc), 101.57 (C1′), 100.03 (C1), 83.15 (C_q-*t*Bu), 76.23 (T^β), 76.01 (C3), 73.58 (CH_2-Bn), 72.34 (C5′), 70.85 (C3′), 69.82, 69.54 (C4, C6), 68.72 (C2′), 67.84 (C6′), 67.44 (C4′), 66.83 (CH_2-Fmoc), 62.86 (C5), 59.02 (T^α), 47.59 (C2), 47.24 (C9-Fmoc), 27.95 (CH_3-*t*Bu), 23.23 (CH_3-NHAc), 20.71, 20.61, 20.55 (3×CH_3-OAc), 18.74 (T^γ); HR-ESI-TOF-MS (positive ion mode): m/z: calcd for $C_{50}H_{62}N_2O_{18}Na$: 979.4076; found: 979.4094 $[M+Na]^+$.

***N*-(9*H*-Fluoren-9-yl)methoxycarbonyl-*O*-(2-acetamido-2-deoxy-3-*O*-[2,3,4-tri-*O*-acetyl-6-*O*-benzyl-β-D-galactopyranosyl]-6-*O*-[benzyl-(5-acetamido-4,7,8,9-tetra-*O*-acetyl-3,5-dideoxy-α-D-glycero-D-galacto-2-nonulopyranosyl)onat]-α-D-galactopyranosyl)-L-threonine-*tert*-butylester (7)**: Fmoc-Thr(βAc_3-6-Bn-Gal(1→3)-αGalNAc)-O*t*Bu (**5**; 0.70 g, 0.66 mmol) and αAc_4NeuNAcCOOBnXan[17] (**6**; 1.10 g, 1.64 mmol, 2.5 equiv) were dissolved in a mixture of dry acetonitrile and dry dichloromethane (60 mL, 2:1). The solution was stirred for 1 h in a Schlenk flask (brown glass) in the presence of flame-dried molecular sieves (3 g, powdered, 3 Å) under an argon atmosphere and the exclusion of moisture. After cooling to −65°C, dry silver triflate (421 mg, 1.64 mmol) and a pre-cooled (−10°C) solution of methyl sulfenyl bromide in dry 1,2-dichloroethane[18] (1.03 mL of a 1.6 M solution, 1.64 mmol) were added slowly over 25 min. The reaction mixture was stirred at −68°C for 4 h, subsequently neutralized with Huenig's base (0.33 mL) and allowed to warm to room temperature. The suspension was diluted with dichloromethane (40 mL), filtered through Hyflo Super Cel and concentrated in vacuo. Purification of the crude product by flash chromatography (silica gel; ethyl acetate, column: h=20 cm, ∅=3 cm) gave an anomeric mixture which was separated by preparative RP-HPLC (Phenomenex LUNA, acetonitrile/water 55:45 → 80:20, 60 min; 100:0, 30 min; λ=254 nm, t_R (α anomer)=63.4 min, t_R (β-anomer)=79.0 min) to yield the desired α anomer as a colorless amorphous solid (606 mg, 0.40 mmol, 61%, conversion: 63%). In addition, the β anomer (20 mg, 0.08 mmol, 12%) as the minor component as well as fractions of unreacted **5** (26 mg, 0.027 mmol, 4%) were isolated. α Anomer: R_f=0.21 (ethyl acetate); $[\alpha]_D^{23}$ = 12.2 (c=1.00, $CHCl_3$); t_R=31.8 min (Phenomenex LUNA, acetonitrile/water 55:45 → 75:25, 40 min; 100:0, 20 min, λ=254 nm); ^{1}H NMR (600 MHz, $CDCl_3$, COSY, HMQC, HMBC): δ = 7.79–7.72 (m, 2H, H4-, H5-Fmoc), 7.60 (d, $J_{H1,H2}=J_{H8,H7}$=7.8 Hz, 2H, H1-, H8-Fmoc), 7.44–7.17 (m, 14H, H3-, H6-, H2-, H7-Fmoc; 10H, H_{ar}-Bn), 5.87 (d, $J_{NH,H2}$=8.6 Hz, 1H, NH-GalNAc), 5.50–5.39 (m, 2H, T^{NH} {5.45}, H4′ {5.42}), 5.38–5.24 (m, 2H, H8″ {5.32}, H7″ {5.28}), 5.23–5.06 (m, 4H, CH_2-COO*Bn* {5.18, 5.15}, H2′ {5.13}, NH-NeuNAc {5.09}), 4.95 (dd, $J_{H3',H2'}$=10.3, $J_{H3',H4'}$=3.0 Hz, 1H, H3′), 4.86–4.77 (m, 1H, H4″), 4.71 (d, $J_{H1,H2}$=3.0 Hz, 1H, H1), 4.66–4.44 (m, 5H, H1′ {4.59, d, $J_{H1',H2'}$=8.1 Hz}, H2 {4.49}, CH_2-Fmoc {4.51, 4.47}, CH_{2a}-Bn {4.47}), 4.43–4.31 (m, 1H, CH_{2b}-Bn), 4.30–4.19 (m, 2H, $H9_a''$ {4.27, dd, $J_{H9a'',H9b''}$=12.3, $J_{H9a'',H8''}$=2.3 Hz}, H9-Fmoc {4.24}), 4.18–4.00 (m, 5H, T^α {4.14}, T^β {4.11}, $H9_b''$ {4.05}, H5″ {4.04}, H6″ {4.03}), 3.94–3.73 (m, 4H, H4 {3.90}, $H6_a$ {3.89}, H5′ {3.84}, H5 {3.79}), 3.66–3.57 (m, 1H, H3 {3.61}), 3.55–3.46 (m, 2H, $H6_b$ {3.52}, $H6_a'$ {3.48}), 3.45–3.38 (m, 1H, $H6_b'$ {3.42}), 2.58 (dd, 1H, $J_{H3eq'',H3ax''}$=12.6, $J_{H3eq'',H4''}$=4.3 Hz, $H3_{eq}''$), 2.09, 2.08, 2.05, 2.03, 1.99, 1.98, 1.95 (7×s, 24H, 8×CH_3-Ac), 1.90 (m, 1H, $H3_{ax}''$), 1.84 (s,

3H, CH_3-Ac), 1.42 (s, 9H, CH_3-*t*Bu), 1.26 (d, $J_{T^{\gamma},T^{\beta}}=6.1$ Hz, 3H, T^{γ}); ^{13}C NMR ($CDCl_3$, chemical shifts obtained from HMQC, HMBC): δ = 170.2, 169.5, 169.4, 169.2, 166.7 (C=O), 166.4 (C1″), 155.6 (C=O urethane), 143.0 (C1a-, C8a-Fmoc), 140.5 (C4a-, C5a-Fmoc), 136.7 (C_q-Bn (C6′)), 134.1 (C_q-Bn (C1″)), 127.8, 127.4 (C_{ar}-Bn), 127.2 (C2-, C7-Fmoc), 127.1 (C_{ar}-Bn), 126.3 (C3-, C6-Fmoc), 124.1 (C1-, C8-Fmoc), 119.2 (C4-, C5-Fmoc), 100.8 (C1′), 99.5 (C1), 98.1 (C2″), 82.4 (C_q-*t*Bu), 76.7 (C3), 75.8 (T^{β}), 72.7 (CH_2-Bn (C6′)), 71.9 (C6″), 71.4 (C5′), 70.0 (C3′), 68.4 (C8″), 68.2 (C5), 68.1 (C4″), 68.0 (C2′), 67.5 (C4), 66.9 (CH_2-Bn (C1″)), 66.6 (C4′), 66.6 (C7″), 66.5 (C6′), 66.3 (CH_2-Fmoc), 63.1 (C6), 61.6 (C9″), 58.1 (T^{α}), 48.6 (C5″), 46.9 (C2), 46.6 (C9-Fmoc), 36.8 (C3″), 27.4 (CH_3-*t*Bu), 22.5, 22.3 (CH_3-NHAc), 20.2, 20.0, 19.9, 19.8 (CH_3-OAc), 17.9 (T^{γ}); HR-ES-TOF-MS (positive ion mode): *m*/*z*: calcd for $C_{76}H_{93}N_3O_{30}Na$: 1550.5742, found: 1550.5731 $[M+Na]^+$.

***N*-(9*H*-Fluoren-9-yl)methoxycarbonyl-*O*-(2-acetamido-2-deoxy-3-*O*-[2,3,4-tri-*O*-acetyl-6-*O*-benzyl-β-D-galactopyranosyl]-6-O-[benzyl-(5-acetamido-4,7,8,9-tetra-*O*-acetyl-3,5-dideoxy-α-D-glycero-D-galacto-2-nonulopyranosyl)onat]-α-D-galactopyranosyl)-L-threonine (8)**: A solution of protected trisaccharide **7** (580 mg, 0.394 mmol) in a mixture of TFA (5 mL), dichloromethane (5 mL) and anisole (0.5 mL) was stirred at ambient temperature for 2 h. The reaction mixture was then diluted with toluene (25 mL) and the solvent was removed in vacuo. The resulting residue was co-evaporated with toluene (3×25 mL) and purified by flash chromatography (silica gel; ethyl acetate/ethanol 4:1; column: $h=20$ cm, $\varnothing=3$ cm) and subsequently by preparative RP-HPLC (Phenomenex LUNA, acetonitrile/water 60:40 → 70:30, 70 min; $\lambda=254$ nm, $t_R=46.5$ min) to yield compound **8** (492 mg, 0.334 mmol, 85%) as a colorless, amorphous solid. $R_f=0.51$ (EE/EtOH 2:1); $t_R=17.1$ min (Phenomenex LUNA, acetonitrile/water + 0.1% TFA, 55:45 → 75:25, 30 min; $\lambda=254$ nm); $[\alpha]_D^{22}$ = 24.7 ($c=1.00$, $CHCl_3$); ^1H NMR (400 MHz, $CDCl_3$, COSY, HMQC): δ = 7.78–7.70 (m, 2H, H4-, H5-Fmoc), 7.63–7.52 (m, 2H, H1-, H8-Fmoc), 7.42–7.13 (m, 14H, H3-, H6-, H2-, H7-Fmoc, H_{ar}-Bn (10H)), 6.22 (d, $J_{NH,H2}=8.2$ Hz, 1H, NH-GalNAc), 5.73 (d, $J_{NH,T\alpha}=7.4$ Hz, 1H, NH-Fmoc), 5.44–5.23 (m, 3H, H4′ {5.40}, H8″ {5.33}, H7″ {5.26}), 5.23–5.05 (m, 3H, CH_2-COO*Bn* {5.17, 5.10}, H2′ {5.11}), 5.01–4.72 (m, 3H, H3′ {4.94}, H1 {4.81}, H4″ {4.80}), 4.71 (d, 1H, H1, $J_{H1,H2}=3.0$ Hz), 4.62–4.52 (m, 1H, H1′), 4.51–4.42 (m, 3H, CH_2-Fmoc {4.46}, CH_{2a}-Bn {4.47}), 4.39–4.25 (m, 5H, CH_{2b}-Bn {4.36}, H2 {4.35}, $H9_a''$ {4.30}, T^{α} {4.31}, T^{β} {4.28}), 4.24–4.17 (m, 1H, H9-Fmoc), 4.10–3.72 (m, 7H, $H9_b''$ {4.04}, H6″ {4.04}, H5″ {4.02}, H4 {3.89}, $H6_a$ {3.88}, H5′ {3.82}, H5 {3.79}), 3.71–3.60 (m, 1H, H3), 3.56–3.46 (m, 2H, $H6_b$ {3.50}, $H6_a'$ {3.48}), 3.45–3.32 (m, 1H, $H6_b'$), 2.57 (dd, $J_{H3eq'',H3ax''}=8.8$, $J_{H3eq'',H4''}=3.9$ Hz, 1H, $H3_{eq}''$), 2.15, 2.05, 2.04, 2.02, 1.98, 1.96, 1.94, 1.93 (8×s, 24H, 8×CH_3-Ac), 1.88 (m, 1H, $H3_{ax}''$), 1.85 (s, 3H, CH_3-Ac), 1.21 (d, $J_{T^{\gamma},T^{\beta}}=6.3$ Hz, 3H, T^{γ}); ^{13}C NMR (100.6 MHz, $CDCl_3$, BB, HMQC): δ = 172.70 (COOH), 170.80, 170.27, 170.15, 169.87, 169.64 (C=O), 167.30 (C1″), 155.82 (C=O urethane), 143.78 (C1a-, C8a-Fmoc), 141.25 (C4a-, C5a-Fmoc), 137.25 (C_q-Bn an C6′), 134.83 (C_q-Bn an C1″), 128.73, 128.67, 128.50, 128.43, 128.32, 127.78, 127.67 (C_{ar}-Bn), 127.12 (C2-, C7-Fmoc), 125.03 (C3-, C6-Fmoc), 124.92 (C1-, C8-Fmoc), 119.99 (C4-,C5-Fmoc), 102.11 (C1′), 101.30 (C1), 98.68 (C2″), 78.74 (T^{β}), 77.14 (C3), 73.48 (CH_2-Bn (C6′)), 73.30 (C6″), 72.81 (C5′), 70.82 (C3′), 69.25 (C8″), 68.92 (C5), 68.49 (C4″), 68.17 (C2′), 67.79 (C4), 67.73 (C7″), 67.45 (C6′), 67.02 (CH_2-Fmoc), 67.35 (C4′), 66.70 (CH_2-Bn (C1″)), 63.99 (C6), 62.42 (C9″), 58.66 (T^{α}), 49.25 (C5″), 48.40 (C2), 47.20 (C9-Fmoc), 37.46 (C3″), 23.01, 22.77 (3×CH_3-NHAc), 21.02, 20.70, 20.58, 20.53, 20.47 (7×CH_3-OAc), 18.31 (T^{γ}); HR-ESI-TOF (positive ion mode): *m*/*z*: calcd for $C_{72}H_{85}N_3O_{30}Na$: 1494.5116, found: 1494.5117 $[M+Na]^+$.

General procedure for the automated solid-phase glycopeptide synthesis: Peptide syntheses were performed according to the Fmoc protocol in an automated Perkin–Elmer ABI 433 A peptide synthesizer using Fmoc-Pro-PHB preloaded Tentagel resins.[21] In iterative cycles the peptide sequences were assembled by sequential coupling of the corresponding amino acids. In every coupling step, the *N*-terminal Fmoc group was removed by treatment of the resin (3×2.5 min) with 20% piperidine in *N*-methylpyrrolidone. Amino acid couplings were carried out using Fmoc-protected amino acids (1 mmol) activated by HBTU/HOBt[22] (1 mmol each) and DIPEA (2 mmol) in DMF (20–30 min vortex). After every coupling step, unreacted amino groups were capped by treatment with a mixture of Ac_2O (0.5 M), DIPEA (0.125 M) and HOBt (0.015 M) in NMP (10 min vortex). Attachment of the glycosylated amino acids was performed manually as described in the procedures for the corresponding glycopeptides.

Ac-Gly-Ser-Thr-Ala-Pro-Pro-Ala-His-Gly-Val-Thr-Ser-Ala-Pro-Asp-Thr-Arg-Pro-Ala-Pro-OH (10): Starting from Fmoc-Pro-*O*-Trt preloaded Tentagel S resin[21] **9** (520 mg, 0.094 mmol, loading: 0.18 mmol g^{-1}), the assembly of the eicosapeptide was performed according to the automated standard protocol. After coupling of the final amino acid, Fmoc-Gly-OH, the Fmoc group was cleaved with piperidine (20%) in NMP, and the N-terminus was acetylated with capping reagent on the resin. For the cleavage procedure under simultaneous removal of the acid-labile side-chain protecting groups, the resin was placed into a Merrifield glass reactor, washed with dichloromethane (3×15 mL) and treated with a mixture of trifluoroacetic acid (15.0 mL), distilled water (0.9 mL) and triisopropylsilane (0.9 mL) for 2 h. After filtration, the resin was washed with trifluoroacetic acid (3×3 mL), and the combined filtrates were concentrated in vacuo and co-evaporated with toluene (3×15 mL). The peptide was precipitated by addition of cold (0 °C) diethyl ether (15 mL) to furnish a colorless solid, which was washed with diethyl ether (3×10 mL), dissolved in distilled water and lyophilized. The crude product was purified by preparative RP-HPLC (Phenomenex LUNA C18, acetonitrile/water + 0.1% TFA 5:95 → 45:55; 60 min; $\lambda=212$ nm, $t_R=40.1$ min) to give the title compound (120 mg, 0.062 mmol, 66%) as a colorless solid after lyophilization. $[\alpha]_D^{22}$ = −148.8 ($c=1.00$, H_2O); t_R = 14.3 min (Phenomenex Jupiter C18, CH_3CN/H_2O + 0.1% TFA 5:95 → 45:55, 30 min; λ = 212 nm); ^1H NMR (600 MHz, H_2O/D_2O 9:1, NaH_2PO_4/Na_2HPO_4 buffer, 50 μM, pH 6.50, COSY, TOCSY, ^{15}N HSQC, ^{13}C-HSQC, HMBC, ROESY): δ = 8.55–8.47 (m, 2H, $H(8)^{Im\text{-}H2}$ {s, 8.52}, $D(15)^{NH}$ {8.50}), 8.44–8.09 (m, 12H, $H(8)^{NH}$ {8.38, d, $J_{NH,H\alpha}=7.6$ Hz}, $G(9)^{NH}$ {8.35}, $A(19)^{NH}$ {8.33}, $A(7)^{NH}$ {8.32}, $S(2)^{NH}$ {8.28}, $A(13)^{NH}$ {8.27}, $T(11)^{NH}$ {8.24}, $S(12)^{NH}$ {8.22}, $G(1)^{NH}$ {8.21}, $R(17)^{NH}$ {8.17, d, $J_{NH,r\alpha}=6.9$ Hz}, $A(4)^{NH}$ {8.15}, $T(3)^{NH}$ {8.14}), 8.06 (d, $J_{NH,V\alpha}=7.6$ Hz, 1H, $V(10)^{NH}$}), 7.97 (d, $J_{NH,T\alpha}=7.6$ Hz, 1H, $T(16)^{NH}$), 7.23 (s, 1H, $H(8)^{Im\text{-}H4}$), 7.14–7.06 (m, 1H, $R(17)^{NH\text{-}Gua}$), 4.66–4.42 (m, 8H (signal intensity reduced by H_2O suppression), $D(15)^{\alpha}$ {4.64}, $H(8)^{\alpha}$ {4.62}, $P(5)^{\alpha}$ {4.61}, $R(17)^{\alpha}$ {4.56}, $A(13)^{\alpha}$ {4.52}, $A(4)^{\alpha}$ {4.51}, $A(19)^{\alpha}$ {4.48}, $S(2)^{\alpha}$ {4.46}), 4.39–4.21 (m, 8H, $S(12)^{\alpha}$ {4.37}, $T(11)^{\alpha}$ {4.33}, $P(18)^{\alpha}$ {4.33}, $P(14)^{\alpha}$ {4.32}, $P(20)^{\alpha}$ {4.31}, $P(6)^{\alpha}$ {4.29}, $T(3)^{\alpha}$ {4.27}, $T(16)^{\alpha}$ {4.24}), 4.20–4.09 (m, 5H, $T(3)^{\beta}$ {4.16}, $A(7)^{\alpha}$ {4.15}, $V(10)^{\alpha}$ {4.14}, $T(11)^{\beta}$ {4.14}, $T(16)^{\beta}$ {4.13}), 3.98–3.65 (m, 13H, $G(9)^{\alpha a}$ {3.92}, $G(1)^{\alpha}$ {3.89}, $S(12)^{\beta a}$ {3.89}, $G(9)^{\alpha b}$ {3.87}, $S(2)^{\beta a}$ {3.82}, $S(2)^{\beta b}$ {3.78}, $S(12)^{\beta b}$ {3.75}, $P(5)^{\delta a}$ {3.74}, $P(6)^{\delta a}$ {3.73}, $P(14)^{\delta a}$ {3.72}, $P(18)^{\delta a}$ {3.73}, $P(20)^{\delta a}$ {3.69}, $P(14)^{\delta b}$ {3.53}), 3.63–3.45 (m, 4H, $P(20)^{\delta b}$ {3.58}, $P(6)^{\delta b}$ {3.58}, $P(5)^{\delta b}$ {3.53}, $P(18)^{\delta b}$ {3.53}), 3.21 (dd, 1H, $H8^{\beta a}$, $J_{H\beta a,H\beta b}=15.6$ Hz, $J_{H\beta,H\alpha}=5.9$ Hz), 3.17–3.04 (m, 3H, $R(17)^{\delta}$ {3.13}, $H(8)^{\beta b}$ {3.11}), 2.87 (dd, $J_{D\beta a,D\beta b}=16.9$, $J_{H\beta,H\alpha}=6.6$ Hz, 1H, $D(15)^{\beta a}$), 2.79 (dd, $J_{D\beta a,D\beta b}=17.1$, $J_{H\beta,H\alpha}=6.9$ Hz, 1H, $D(15)^{\beta b}$), 2.32–2.13 (m, 5H, $P(5)^{\beta a}$ {2.26}, $P(14)^{\beta a}$ {2.19}, $P(18)^{\beta a}$ {2.19}, $P(20)^{\beta a}$ {2.22}, $P(6)^{\beta a}$ {2.18}), 2.07–1.99 (m, 1H, $V(10)^{\beta}$ {2.02}), 1.99–1.70 (m, 19H, $AcNH^{terminal}$ (1.97, s), $P(5)^{\gamma}$ {1.95}, $P(20)^{\gamma}$ {1.95}, $P(14)^{\gamma}$ {1.95}, $P(6)^{\gamma}$ {1.93}, $P(18)^{\gamma}$ {1.93}, $P(20)^{\beta b}$ {1.92}, $P(14)^{\beta b}$ {1.83}, $P(5)^{\beta b}$ {1.79}, $P(18)^{\beta b}$ {1.80}, $P(6)^{\beta b}$ {1.76}, $R(17)^{\beta a}$ {1.76}), 1.70–1.51 (m, 3H, $R(17)^{\beta b}$ {1.66}, $R(17)^{\gamma}$ {1.58}), 1.33–1.19 (m, 12H, $A(19)^{\beta}$ {1.28}, $A(13)^{\beta}$ {1.28}, $A(4)^{\beta}$ {1.25}, $A(7)^{\beta}$ {1.24}), 1.15–1.04 (m, 9H, $T(11)^{\gamma}$ {1.12}, $T(3)^{\gamma}$ {1.11}, $T(16)^{\gamma}$ {1.10}), 0.85 (t, 6H, $V(10)^{\gamma}$, $J_{V\gamma,V\beta}=6.3$ Hz); ^{13}C NMR (chemical shifts taken from ^{13}C-HSQC and HMBC): δ = 176.21 ($P(20)^{C=O}$), 174.89 ($A(7)^{C=O}$), 174.05 ($P(14)^{C=O}$), 174.04 ($P(6)^{C=O}$), 173.78 ($V(10)^{C=O}$), 173.54 ($P(18)^{C=O}$), 172.61 ($D(15)^{COOH}$), 172.18 ($S(2)^{C=O}$), 172.01 ($H(8)^{C=O}$), 171.87 ($P(5)^{C=O}$), 171.64 ($T(11)^{C=O}$), 171.31 ($T(16)^{C=O}$), 171.19 ($T(3)^{C=O}$), 171.22 ($R(17)^{C=O}$), 171.20 ($G(9)^{C=O}$), 133.67 ($H(8)^{Im\text{-}C2}$), 128.39 ($H(8)^{Im\text{-}C5}$), 117.42 ($H(8)^{Im\text{-}C4}$), 67.07 ($T(11)^{\beta}$), 67.07 ($T(3)^{\beta}$), 67.07 ($T(16)^{\beta}$), 61.25 ($S(12)^{\beta}$), 61.12 ($S(2)^{\beta}$), 60.35 ($P(18)^{\alpha}$), 60.32 ($P(14)^{\alpha}$), 60.06 ($P(6)^{\alpha}$), 59.85 ($P(20)^{\alpha}$), 59.57 ($V(10)^{\alpha}$), 58.99 ($T(16)^{\alpha}$), 58.97 ($T(11)^{\alpha}$), 58.83 ($T(3)^{\alpha}$), $(P(5)^{\alpha})^{\S}$, 55.50 ($S(2)^{\alpha}$), 55.32 ($S(12)^{\alpha}$), $(H(8)^{\alpha})^{\S}$, $(D(15)^{\alpha})^{\S}$, 51.08 ($R(17)^{\alpha}$), 47.85 ($A(13)^{\alpha}$), 49.70 ($A(7)^{\alpha}$), 47.82 ($A(4)^{\alpha}$), 47.65 ($A(19)^{\alpha}$), 48.51 ($P(6)^{\delta}$), 47.73# ($P(5)^{\delta}$, $P(18)^{\delta}$), 47.65 ($P(14)^{\delta}$), 47.44 ($P(20)^{\delta}$), 42.45 ($G(1)^{\alpha}$), 40.61 ($R(17)^{\delta}$), 35.19 ($D(15)^{\beta}$), 30.18 ($V(10)^{\beta}$), 29.29 ($P(14)^{\beta}$), 29.28 ($P(6)^{\beta}$), 29.28 ($P(18)^{\beta}$), 28.88 ($P(20)^{\beta}$), 27.98 ($P(5)^{\beta}$), 27.46 ($R(17)^{\beta}$), 26.34 ($H(8)^{\beta}$), 24.55# ($P(5)^{\gamma}$, $P(6)^{\gamma}$, $P(14)^{\gamma}$, $P(18)^{\gamma}$, $P(20)^{\gamma}$), 23.98 ($R(17)^{\gamma}$), 21.61

($AcNH^{terminal}$), 18.83 ($T(16)^{\gamma}$), 18.74 ($T(3)^{\gamma}$), 18.74 ($T(11)^{\gamma}$), 18.39 ($V(10)^{\gamma a}$), 17.61 ($V(10)^{\gamma b}$), 16.40 ($A(7)^{\beta}$), 15.38 ($A(13)^{\beta}$), 15.36 ($A(4)^{\beta}$), 15.16 ($A(19)^{\beta}$); [§]: annihilated by H_2O suppression, [#]: signals overlapped; MALDI-TOF-MS (DHB, positive ion mode): *m/z*: calcd for $C_{82}H_{130}N_{25}O_{29}$: 1930.1, found: 1930.2 $[M+H]^+$, 1952.2 $[M+Na]^+$, 1968.2 $[M+K]^+$, 1974.3 $[M+2Na-H]^+$.

Fmoc-Ser(*t*Bu)-Ala-Pro-Asp(O*t*Bu)-Thr(*t*Bu)-Arg(Pmc)-Pro-Ala-Pro-Trt-Tg (11): The resin-bound peptide fragment was prepared in a 41 mL reaction vessel of peptide synthesizer according to the standard procedure starting from the Fmoc-Pro-O-Trt preloaded Tentagel S resin **9a**[21] (1.38 g, 0.28 mmol, loading: 0.20 mmol g^{-1}) and using the FastMoc (0.25 mmol) protocol for amino acid couplings. After coupling of the last amino acid, Fmoc-Ser(*t*Bu)-OH, the resin was thoroughly washed with NMP and dichloromethane and dried under a nitrogen flow. Residual solvent was removed in high vacuum to give 1.55 g dry resin, which was used in the syntheses of different glycopeptide structures.

Ac-Gly-Ser-Thr-Ala-Pro-Pro-Ala-His-Gly-Val-Thr(βAc$_3$BnGal-(1→3)-[αAc$_4$NeuNAcCOOBn-(2→6)]-αGalNAc)-Ser-Ala-Pro-Asp-Thr-Arg-Pro-Ala-Pro-OH (12): A portion of the functionalized Tentagel resin **11** (282 mg, max. 0.05 mmol) was treated in the peptide synthesizer with piperidine (20%) in NMP to remove the temporary Fmoc-protecting group. Subsequently, a solution of the (2,6)-sialyl-T threonine building block **8** (125 mg, 0.085 mmol, 1.7 equiv), HATU[24] (34 mg, 0.090 mmol, 1.8 equiv), HOAt (12 mg, 0.090 mmol, 1.8 equiv) and *N*-methylmorpholine (19.8 μL, 0.18 mmol, 3.6 equiv) in NMP (2 mL) was added to the resin. After shaking for 4 h, excess reagents were removed by filtration and the resin was washed with NMP. Remaining unreacted amino groups were acetylated with capping reagent. The eicosapeptide sequence was completed resuming the automated standard procedure according to the Fmoc protocol. After coupling of the last amino acid, the terminal Fmoc group was exchanged for an acetyl group and the resin was treated with a mixture of TFA (15 mL), distilled water (0.9 mL) and triisopropylsilane (0.9 mL) for simultaneous cleavage of the linker and the acid-labile side-chain protecting groups. Subsequently, the resin was washed with trifluoroacetic acid (3×3 mL), the combined filtrates were concentrated in vacuo and co-evaporated with toluene (3×15 mL). The peptide was precipitated by addition of cold (0°C) diethyl ether (15 mL) to give a colorless solid, which was washed with diethyl ether (3×10 mL), dissolved in distilled water and lyophilized. The crude material was purified by preparative RP-HPLC (Phenomenex Jupiter C18, grad.: acetonitrile/water + 0.1% TFA 25:75 → 50:50, 80 min, λ=212 nm, t_R=28.1 min) to furnish the partially protected glycopeptide **12** as a colorless lyophilizate (66 mg, 0.022 mmol, 44%). $[\alpha]_D^{23}=-63.8$ (c=1.00, methanol); t_R=26.6 min (Phenomenex Luna C18(2), gradient: acetonitrile/water + 0.1% TFA 15:85 → 45:55, 30 min, λ=212 nm); MALDI-TOF-MS (DHB, positive ion mode): *m/z*: calcd for $C_{135}H_{195}N_{27}O_{54}$: 3060.1, found 3059.9 $[M]^+$, 3082.0 $[M+Na]^+$, 3104.0 $[M+2Na-H]^+$.

Ac-Gly-Ser-Thr-Ala-Pro-Pro-Ala-His-Gly-Val-Thr(βAc$_3$Gal-(1→3)-[αAc$_4$NeuNAc COOH-(2→6)]-αGalNAc)-Ser-Ala-Pro-Asp-Thr-Arg-Pro-Ala-Pro-OH: For the removal of the benzyl groups, the (2,6)-sialyl-T glycopeptide **12** (73 mg, 0.024 mmol) was dissolved in anhydrous methanol (20 mL), and a catalytic amount of 5% palladium on activated charcoal was added under argon. The reaction flask was subsequently purged with H_2 and the suspension was stirred for 21 h under H_2 atmosphere. The charcoal was removed by filtration through Hyflo Super Cell which was washed with methanol (50 mL) afterwards. The combined filtrates were concentrated in vacuo, dissolved in distilled water (5 mL) and lyophilized to give the debenzylated glycopeptide (65 mg, max. 0.223 mmol) as a colorless lyophilizate, which was employed for the final deprotection without further purification. t_R=12.5 min (Phenomenex Jupiter C18, gradient: acetonitrile/water + 0.1% TFA 15:85 → 45:55, 30 min, λ=212 nm); MALDI-TOF-MS (DHB, positive ion mode): *m/z*: calcd for $C_{121}H_{184}N_{27}O_{54}$: 2880.9, found: 2880.8 $[M+H]^+$, 2902.5 $[M+Na]^+$, 2918.5 $[M+K]^+$, 2924.4 $[M+2Na-H]^+$.

Ac-Gly-Ser-Thr-Ala-Pro-Pro-Ala-His-Gly-Val-Thr(βGal-(1→3)-[αNeuNAcCOOH-(2→6)]-αGalNAc)-Ser-Ala-Pro-Asp-Thr-Arg-Pro-Ala-Pro-OH (13): The crude, debenzylated (2,6)-sialyl-T eicosapeptide (65 mg, max. 0.223 mmol) was dissolved in anhydrous methanol (20 mL) and treated with a solution of 1% sodium methoxide in methanol until a pH of 9.5 was reached. The reaction mixture was stirred for 16 h at ambient temperature and was then neutralized by the addition of acetic acid (0.05 mL). The solvent was removed in vacuo, and the resulting residue was purified by preparative RP-HPLC (Phenomenex Jupiter C18, gradient: acetonitrile/water + 0.1% TFA 5:95 → 30:70, 60 min, λ=212 nm, t_R=24.8 min), the deprotected MUC1 glycoeicosapeptide **13** (34 mg, 0.013 mmol, 55% over two steps) was isolated as colorless lyophilizate. $[\alpha]_D^{23}=-107.3$ (c=1.00, H_2O); t_R=14.2 min (Phenomenex Jupiter C18, gradient: acetonitrile/water + 0.1% TFA 5:95 → 30:70, 30 min, λ=212 nm); ^{1}H NMR (600 MHz, [D$_6$]DMSO, COSY, TOCSY, HMQC, HMBC, ROESY, NOESY): δ = 8.93 (s, 1H, $H(8)^{Im\text{-}H2}$), 8.27–8.20 (m, 2H, $D(15)^{NH}$ {8.24}, $G(9)^{NH}$ {8.22}), 8.17–8.06 (m, 10H, $S(12)^{NH}$ {8.12}, $A(19)^{NH}$ {8.11}, $T(11)^{*NH}$ {8.10}, $H(8)^{NH}$ {8.08}, $G(1)^{NH}$ {8.12}, $A(7)^{NH}$ {8.04}, NH-NeuNAc {8.02}, $S(2)^{NH}$ {7.96}, $V(10)^{NH}$ {7.94}, $A(13)^{NH}$ {7.88}), 7.82 (d, 1H, $A(4)^{NH}$, $J_{NH,A\alpha}$=6.9 Hz), 7.71 (d, 1H, $T(16)^{NH}$, $J_{NH,T\alpha}$=8.5 Hz), 7.49 (d, 1H, $R(17)^{NH}$, $J_{NH,R\alpha}$=3.8 Hz), 7.36 (s, 1H, $H(8)^{Im\text{-}H4}$), 7.32 (d, 1H, $T(3)^{NH}$, $J_{NH,T\alpha}$=7.9 Hz), 7.21 (s_b, 1H, OH), 7.13 (d, 1H, OH, J=1.5 Hz), 7.06–6.99 (m, 2H, NH-GalNAc, OH), 4.82 (d, 1H, H1, $J_{H1,H2}$=2.1 Hz), 4.60–4.41 (m, 7H, $H(8)^{\alpha}$ {4.57}, $V(10)^{\alpha}$ {4.52}, $D(15)^{\alpha}$ {4.50}, $A(4)^{\alpha}$ {4.49} $R(17)^{\alpha}$ {4.48}, $A(19)^{\alpha}$ {4.46}, $T(11)^{*\alpha}$ {4.45}), 4.40–4.25 (m, 6H, 3×P^{α} {4.34, 4.29, 4.26}, $A(13)^{\alpha}$ {4.37}, $S(2)^{\alpha}$ {4.37}, $S(12)^{\alpha}$ {4.28}), 4.23–4.07 (m, 8H, 2×P^{δ} {4.22, 4.17}, $T(3)^{\alpha}$ {4.19}, H1′ {4.18}, $T(16)^{\alpha}$ {4.17}, $T(11)^{*\beta}$ {4.16}, H2 {4.10}, $A(7)^{\alpha}$ {4.15}), 4.07–4.01 (m, 2H, $T(16)^{\beta}$ {4.04}, OH), 3.97–3.91 (m, 2H, $T(3)^{\beta}$ {3.95}, H4′ {3.93}), 3.90–3.81 (m, 5H, $G(9)^{\alpha a}$ {3.86}, H5 {3.84}, H4 {3.83}, OH), 3.80–3.27 (m, 31H, $G(9)^{\alpha b}$ {3.76}, $G(1)^{\alpha}$ {3.73}, $H6_a$ {3.73}, H3 {3.67}, 5×P^{δ} {3.64, 3.63, 3.57, 3.50, 3.44}, H7″ {3.61}, H4″ {3.55}, $S(2)^{\beta a}$ {3.61}, $H9_a''$ {3.61}, $S(12)^{\beta}$ {3.53}, $S(2)^{\beta b}$ {3.52}, $H6_a'$ {3.52}, H5″ {3.48}, $H6_b$ {3.44}, $H6_b'$ {2.47}, $H9_b''$ {3.38}, H6″ {3.33}, H2′ {3.30}, H8″ {3.30}, H5′ {3.30}), 3.25–3.20 (m, 1H, H3′), 3.15–3.02 (m, 3H, $H(8)^{\beta\alpha}$ {3.11}, $R(17)^{\delta}$ {3.08}), 3.00–2.92 (m, 1H, $H8^{\beta b}$), 2.72 (dd, 1H, $D(15)^{\beta b}$, $J_{D\beta\alpha,D\beta b}$=16.4 Hz, $J_{D\beta,D\alpha}$=5.9 Hz), 2.54–2.46 (m, 2H (partially covered by DMSO signal), $D(15)^{\beta b}$ {2.51), $H3_{eq}''$ {2.49}), 2.17–2.08 (m, 2H, 2×$P^{\beta a}$ {2.13}, {2.12}), 2.06–1.65 (m, 29H, 2×$P^{\beta a}$ {2.01, 1.98}, $V(10)^{\beta}$ {1.95}, 5×P^{γ} {1.89, 1.88, 1.87, 1.86, 1.84}, P^{β} {1.83}, 4×$P^{\beta b}$ {1.82, 1.77, 1.76, 1.75}, $AcNH''$ {s, 1.87, 3H), $AcNH^{terminal}$ (s, 1.85, 3H), $AcNH^{GalNAc}$ (s, 1.82, 3H), $R^{\beta a}$ {1.68}), 1.56–1.46 (m, 3H, $R(17)^{\beta b}$ {1.51}, $R(17)^{\gamma}$ {1.51}, $H3_{ax}''$ {1.50}), 1.22–1.10 (m, 15H, $A(7)^{\beta}$ {1.19}, $A(19)^{\beta}$ {1.18}, $A(4)^{\beta}$ {1.16}, $T(16)^{\gamma}$ {1.15}, $A(13)^{\beta}$ {1.14}), 1.01 (d, 3H, $T(11)^{*\gamma}$, $J_{T\gamma,T\beta}$=6.1 Hz), 0.99 (d, 3H, $T(3)^{\gamma}$, $J_{T\gamma,T\beta}$=6.1 Hz), 0.90 (d, 3H, $V(10)^{\gamma a}$, $J_{V\gamma,V\beta}$=6.4 Hz), 0.84 (d, 3H, $V(10)^{\gamma b}$, $J_{V\gamma,V\beta}$=6.7 Hz); ^{13}C NMR (chemical shifts obtained from ^{13}C-HSQC and HMBC): δ = 173.35, 172.64, 171.93, 171.86, 171.14, 170.50, 170.43, 170.39, 170.35, 170.00, 169.66, 169.55, 169.35 (C=O), 170.67 (C1″), 133.94 ($H(8)^{C4}$), 117.26 ($H(8)^{C4}$), 105.01 (C1′), 98.95 (C1), 98.29 C(2″), 77.98 (C3), 75.72 ($T(11)^{*\beta}$), 75.55 (C5′), 73.71 (C6″), 73.22 (C3′), 71.52 (C7″), 70.80 (C2′), 68.65 (C8″), 68.34 (C4), 68.32 (C5), 66.95 (C4′), 66.95 ($T(3)^{\beta}$), 66.48 (C4″), 66.45 ($T(16)^{\beta}$), 63.76 (C6), 63.17 (C9″), 61.95 ($S(12)^{\beta}$), 61.90 ($S(2)^{\beta}$), 60.70 (C6′), 59.54, 59.29, 59.25, 58.76, 58.04 (5×P^{α}), 58.75 ($T(11)^{*\alpha}$), 58.60 ($T(3)^{\alpha}$), 58.09 ($T(16)^{\alpha}$), 57.38 ($V(10)^{\alpha}$), 55.10 ($S(12)^{\alpha}$), 55.05 ($S(2)^{\alpha}$), 52.48 (C5″), 51.62 ($H(8)^{\alpha}$), 50.55 ($R(17)^{\alpha}$), 50.15 ($D(15)^{\alpha}$), 48.61 ($A(7)^{\alpha}$), 48.21 (C2), 46.53 ($A(7)^{\alpha}$), 46.42 ($A(4)^{\alpha}$), 46.94, 46.92, 46.80, 46.77, 46.50 (5×$P(5)^{\delta}$), 42.22 ($G(9)^{\alpha}$), 40.78 (C3″), 40.77 ($R(17)^{\delta}$), 35.76 ($D(15)^{\beta}$), 31.33 ($V(10)^{\beta}$), 29.22, 29.16, 28.85, 28.82, 28.00 (5×P^{β}), 28.48 ($R(17)^{\beta}$), 27.13 ($H(8)^{\beta}$), 24.8–24.4 (5×P^{γ})[#], 24.66 ($R(17)^{\gamma}$), 22.85 ($AcNH''$), 22.69 ($AcNH^{GalNAc}$), 22.69 ($AcNH^{terminal}$), 20.00 ($T(11)^{*\gamma}$), 19.85 ($T(3)^{\gamma}$), 19.33 ($V(10)^{\gamma a}$), 18.70 ($A(13)^{\beta}$), 18.60 ($A(4)^{\beta}$), 18.48 ($V(10)^{\gamma b}$), 18.42 ($T(16)^{\gamma}$), 17.81 ($A(7)^{\beta}$), 16.87 ($A(19)^{\beta}$); ^{1}H NMR (600 MHz, H_2O/D_2O 9:1, NaH_2PO_4/Na_2HPO_4 buffer, 50 μM, pH 6.50, COSY, TOCSY, ^{15}N-HSQC, ^{13}C-HSQC, HMBC, ROESY): δ=8.66 (d, 1H, $T^*(11)^{NH}$, $J_{NH,T\alpha}$=7.9 Hz), 8.51–7.87 (m, 16H, $S(12)^{NH}$ {8.45}, $A(13)^{NH}$ {8.43}, $D(15)^{NH}$ {8.38}, $H(8)^{H2}$ {8.38}, G(9) {8.33}, $H(8)^{NH}$ {8.33}, $A(7)^{NH}$ {8.32}, $S(2)^{NH}$ {8.28}, $A(19)^{NH}$ {8.24}, G(1) {8.22}, $R(17)^{NH}$ {8.18}, $A(4)^{NH}$ {8.15}, $T(3)^{NH}$ {8.15}, $V(10)^{NH}$ {8.02, d, $J_{NH,V\alpha}$=6.9 Hz}, $T(16)^{NH}$ {7.95}, NH-NeuNAc {7.95}), 7.54 (d, 1H, NH-GalNAc, $J_{NH,H1}$=9.9 Hz), 7.28–7.13 (m, 2H, $R(17)^{NH\text{-}Gua}$ {7.24}, $H(8)^{H4}$ {7.19}), 4.86 (m, 1H, H1 (partially covered by H_2O signal)), 4.63–4.35 (m, 10H (partially covered by H_2O signal), $P(5)^{\alpha}$ {4.61}, $H(8)^{\alpha}$ {4.59}, $T(11)^{*\alpha}$ {4.56}, $R(17)^{\alpha}$ {4.53}, $D(15)^{\alpha}$ {4.52}, $A(4)^{\alpha}$ {4.51}, $A(19)^{\alpha}$ {4.48}, $S(2)^{\alpha}$ {4.45}, $S(12)^{\alpha}$ {4.39}, $A(13)^{\alpha}$ {4.37}), 4.34–4.20 (m, 8H, H1′ {4.33}, $P(18)^{\alpha}$ {4.31},

P(14)$^{\alpha}$ {4.31}, P(6)$^{\alpha}$ {4.29}, T(3)$^{\alpha}$ {4.27}, V(10)$^{\alpha}$ {4.24}, T(16)$^{\alpha}$ {4.23}, T(11)$^{*\beta}$ {4.22}), 4.19–3.97 (m, 7H, T(3)$^{\beta}$ {4.15}, A(7)$^{\alpha}$ {4.14}, P(20)$^{\alpha}$ {4.14}, T(16)$^{\beta}$ {4.14}, H2 {4.13}, H4 {4.09}, H5 {4.01}), 3.97–3.32 (m, 34H, G(9)$^{\alpha a}$ {3.91}, H3 {3.90}, G(1)$^{\alpha}$ {3.89}, G(9)$^{\alpha b}$ {3.84}, H6$_a$ {3.83}, S(2)$^{\beta a}$ {3.82}, H4′ {3.80} H7″ {3.79}, S(2)$^{\beta b}$ {3.78}, H9$_a$″ {3.77}, S(12)$^{\beta a}$ {3.76}, H5″ {3.73}, P(5)$^{\delta a}$ {3.73}, P(14)$^{\delta a}$ {3.73}, P(18)$^{\delta a}$ {3.73}, P(6)$^{\delta a}$ {3.72}, S(12)$^{\beta b}$ {3.69}, H6$_a$′ {3.68}, P(20)$^{\delta a}$ {3.65}, H6$_b$′ {3.63}, H6″ {3.60}, P(14)$^{\delta b}$ {3.57}, H4″ {3.56}, H9$_b$″ {3.55}, P(20)$^{\delta b}$ {3.54}, P(6)$^{\delta b}$ {3.53}, P(5)$^{\delta b}$ {3.53}, H5′ {3.53}, P(18)$^{\delta b}$ {3.53}, H3′ {3.50}, H8″ {3.48}, H6$_b$ {3.48}, H2′ {3.41}), 3.25–3.02 (m, 4H, H(8)$^{\beta a}$ {3.19}, R(17)$^{\delta}$ {3.13}, H(8)$^{\beta b}$ {3.10}), 2.70–2.51 (m, 3H, D(15)$^{\beta a}$ {2.64}, H3$_{eq}$″ {2.58}, D(15)$^{\beta b}$ {2.57}), 2.31–2.08 (m, 5H, P(5)$^{\beta a}$ {2.26}, P(14)$^{\beta a}$ {2.22}, P(18)$^{\beta a}$ {2.19}, P(6)$^{\beta a}$ {2.18}, P(20)$^{\beta a}$ {2.12}), 1.96 (s, 3H, AcNH^{terminal}), 1.93 (s, 3H, AcNH″), 1.92 (s, 3H, AcNH^{GalNAc}), 2.05–1.45 (m, 23H, V(10)$^{\beta}$ {2.01}, P(14)$^{\gamma}$ {1.96}, P(5)$^{\gamma}$ {1.94}, P(6)$^{\gamma}$ {1.92}, P(18)$^{\gamma}$ {1.91}, P(20)$^{\gamma}$ {1.89}, P(14)$^{\beta b}$ {1.84}, P(5)$^{\beta b}$ {1.80}, P(18)$^{\beta b}$ {1.81}, P(20)$^{\beta b}$ {1.81}, P(6)$^{\beta b}$ {1.75}, R(17)$^{\beta a}$ {1.75}, R(17)$^{\beta b}$ {1.68}, R(17)$^{\gamma}$ {1.59}, H3$_{ax}$″ {1.54}), 1.36–1.15 (m, 15H, A(13)$^{\beta}$ {1.30}, A(19)$^{\beta}$ {1.28}, A(4)$^{\beta}$ {1.25}, A(7)$^{\beta}$ {1.24}, T(11)$^{*\gamma}$ {1.22}), 1.15–1.01 (m, 6H, T(3)$^{\gamma}$ {1.11}, T(16)$^{\gamma}$ {1.10}), 0.89 (d, 3H, V(10)$^{\gamma a}$, $J_{V\gamma,V\beta}$ = 6.9 Hz), 0.87 (d, 3H, V(10)$^{\gamma b}$, $J_{V\gamma,V\beta}$ = 6.6 Hz); ^{13}C NMR (chemical shifts obtained from ^{13}C-HMQC and HMBC): δ = 174.93, 174.90, 173.95, 173.76, 173.66, 173.61, 173.53, 173.34, 171.61, 171.25, 170.94, 170.62 (C=O), 173.24 (C1″), 134.15 (H(8)^{C2}), 117.63 (H(8)^{C4}), 104.70 (C1′), 100.07 C(2″), 99.31 (C1), 77.44 (T(11)$^{*\beta}$), 77.16 (C3), 74.91 (C5′), 72.63 (C3′), 72.49 (C6″), 71.77 (C7″), 70.65 (C2′), 69.63 (C8″), 68.99 (C4), 68.64 (C4′), 68.26 (C5), 68.26 (C4″), 66.95 (T(3)$^{\beta}$), 66.95 (T(16)$^{\beta}$), 63.85 (C9″), 62.65 (C6), 61.89 (P(20)$^{\alpha}$), 61.50 (S(12)$^{\beta}$), 61.05 (C6′), 61.04 (S(2)$^{\beta}$), 60.3 (P(18)$^{\alpha}$), 60.2 (P(14)$^{\alpha}$), 60.05 (P(6)$^{\alpha}$), 59.28 (V(10)$^{\alpha}$), 58.88 (T(16)$^{\alpha}$), 58.87 (T(3)$^{\alpha}$), 58.57 (P(5)$^{\alpha}$), 57.11 (T(11)$^{*\alpha}$), 55.49 (S(2)$^{\alpha}$), 54.96 (S(12)$^{\alpha}$), 52.49 (H(8)$^{\alpha}$), 51.85 (C5″), 51.4 (D(15)$^{\alpha}$), 51.38 (R(17)$^{\alpha}$), 48.26 (C2), 48.20 (A(7)$^{\alpha}$), 47.75 (A(13)$^{\alpha}$), 47.68 (A(4)$^{\alpha}$), 47.8 (P(5)$^{\delta}$, P(14)$^{\delta}$)$^{\#}$, 47.6 (P(6)$^{\delta}$), 47.6 (P(18)$^{\delta}$), 47.46 (A(19)$^{\alpha}$), 47.4 (P(20)$^{\delta}$), 42.52 (G(1)$^{\alpha}$), 40.56 (R(17)$^{\delta}$), 40.15 (C3″), 38.08 (D(15)$^{\beta}$), 30.13 (V(10)$^{\beta}$), 29.22 (P(18)$^{\beta}$), 29.19 (P(20)$^{\beta}$), 29.11 (P(6)$^{\beta}$), 29.11 (R(17)$^{\beta}$), 27.82 (P(5)$^{\beta}$), 26.59 (H(8)$^{\beta}$), 24.50 (P(5)$^{\gamma}$), 24.50 (P(6)$^{\gamma}$), 24.50 (P(14)$^{\gamma}$), 24.50 (P(18)$^{\gamma}$), 24.39 (P(20)$^{\gamma}$), 23.81 (R(17)$^{\gamma}$), 22.03 (AcNH^{GalNAc}), 21.90 (AcNH″), 21.67 (AcNH^{terminal}), 18.65 (T(3)$^{\gamma}$), 18.70 (T(16)$^{\gamma}$), 18.42 (V(10)$^{\gamma a}$), 18.27 (T(11)$^{*\gamma}$), 17.67 (V(10)$^{\gamma b}$), 16.28 (A(7)$^{\beta}$), 15.21 (A(4)$^{\beta}$), 15.13 (A(19)$^{\beta}$), 14.96 (A(13)$^{\beta}$); $^{\#}$: signals overlapped; MALDI-TOF-MS (DHB, positive): *m*/*z*: calcd for $C_{107}H_{169}N_{27}O_{47}$: 2584.17, found: 2585.5 $[M]^+$, 2607.1 $[M+Na]^+$, 2629.1 $[M+2Na-H]^+$.

Structural analysis—Material and methods

Structural NMR spectra

NMR spectra were recorded on Bruker 400 and 600 Avance spectrometers. All spectra were recorded in H_2O/D_2O 9:1, pH 6.5 at 298 K with peptide concentrations of 10 mM. The assignments were carried out with the help of standard DQF-COSY, TOCSY, ROESY, ^{13}C-HSQC, ^{15}N-HSQC and ^{13}C-HMBC experiments. Typically 2k data points in *F*2 and 512 experiments in *F*1 were acquired. The spectra were acquired with 16 transients and a relaxation delay of 2 s except the ROESY experiments with 80 transients. For ROESY experiments, a spinlock field of 2.8 kHz was used with a mixing time of 300 ms. The TOCSY experiments were performed with a spinlock field of 4.5 kHz using the MLEV17 sequence with mixing times of 40 ms and 80 ms. The data were zero filled and processed as 4k×1k matrix. PE COSY experiments were processed as 8k×2k matrix. To obtain the temperature coefficients of the amide proton chemical shifts, TOCSY spectra were recorded between +15 and +45 °C. The H_N–H_α coupling constants were determined by the 1D proton and DQF-COSY, PE COSY spectra.

Molecular dynamics

All molecular mechanics/dynamics simulations were performed with DISCOVER of the InsightII package (Accelrys) on a Silicon Graphics Octane workstation.[53] The simulations were done using the consistent valence force field (CVFF) that proved to account for solution NMR data to a satisfactory extent.[54] A dielectric constant (ε = 78) was used. The molecular structures were first minimized with a gradient criterion of less than 0.01 kcal mol^{-1}. The energy-minimized structures were then used for MD runs. Pseudo-atoms were used for a number of methylene proton pairs. Distance restraints derived from ROE-cross peaks, classified empirically as strong, medium, weak and very weak, were applied as biharmonic restraints with lower and upper bounds of 0.20–0.25 Å, 0.20–0.35 Å, 0.20–0.4 Å and 0.20–0.5 Å, respectively. Likewise, due to the detected *trans* configuration of all peptide bonds, the ω dihedral angle was restrained to 180°. According to a simulated annealing approach, the resulting starting molecules were heated to 600 K initially, subsequently cooled and finally, after MD at 300 K, subjected to an energy minimization using both steepest descent and conjugate gradient methods successively. Fifty structures were sampled. Eight structures within energy intervals of 15 kcal mol^{-1} and with maximum violation of upper limits less than 0.5 Å were selected. The tightness of this family of conformers was characterized by the mean pairwise RMSD for the heavy atoms or backbone atoms of the conformers and the corresponding average structure of the structural family.

Acknowledgements

This work was supported by the Deutsche Forschungsgemeinschaft (SFB-416, Project ZS and Ku 394-18) and by the Stiftung Rheinland-Pfalz für Innovation. S.D. is grateful for a doctoral fellowship provided by the Fonds der Chemischen Industrie and the Bundesministerium für Bildung und Forschung (BMBF).

[1] J. N. Blattman, P. D. Greenberg, *Science* **2004**, *305*, 200–205.
[2] P. Moingeon, *Vaccine* **2001**, *19*, 1305–1326.
[3] S. J. Danishefsky, J. A. Allen, *Angew. Chem.* **2000**, *112*, 882–911; *Angew. Chem. Int. Ed.* **2000**, *39*, 836–863.
[4] J. Taylor-Papadimitriou, J. M. Burchell, D. W. Miles, M. Dalziel, *Biochim. Biophys. Acta* **1999**, *1455*, 301–313.
[5] J. Taylor-Papadimitriou, J. M. Burchell, T. Plunkett, R. Graham, I. Correra, D. Miles, M. Smith, *J. Mammary Gland Biol. Neoplasia* **2002**, *7*, 209–221.
[6] A. M. Vlad, J. C. Kettel, N. M. Alajez, C. A. Carlos, O. J. Finn, *Adv. Immunol.* **2004**, *82*, 249–293.
[7] J. M. Burchell, A. Mungul, J. Taylor-Papadimitriou, *J. Mammary Gland Biol. Neoplasia* **2001**, *6*, 355–364.
[8] M. J. Scanlon, S. D. Morley, D. E. Jackson, M. R. Price, S. J. B. Tendler, *Biochem. J.* **1992**, *284*, 137–144.
[9] J. M. Burchell, S. J. Gendler, J. Taylor-Papadimitriou, A. Girling, A. Lewis, R. Millis, D. Lamport, *Cancer Res.* **1987**, *47*, 5476–5482.
[10] S. Dziadek, A. Hobel, E. Schmitt, H. Kunz, *Angew. Chem.* **2005**, *117*, 7803–7808; *Angew. Chem. Int. Ed.* **2005**, *44*, 7630–7635.
[11] S. Dziadek, C. Brocke, H. Kunz, *Chem. Eur. J.* **2004**, *10*, 4150–4162.
[12] B. Liebe, H. Kunz, *Angew. Chem.* **1997**, *109*, 629–631; *Angew. Chem. Int. Ed. Engl* **1997**, *36*, 618–621.
[13] B. Liebe, H. Kunz, *Helv. Chim. Acta* **1997**, *80*, 1473–1482.
[14] M. Lergenmüller, Y. Ito, T. Ogawa, *Tetrahedron* **1998**, *54*, 1381–1394.
[15] B. Helferich, F. Wedemeyer, *Liebigs Ann. Chem.* **1949**, *563*, 139–145.
[16] A. Marra, P. Sinaÿ, *Carbohydr. Res.* **1990**, *195*, 303–308.
[17] S. Keil, C. Claus, W. Dippold, H. Kunz, *Angew. Chem.* **2001**, *113*, 379–382; *Angew. Chem. Int. Ed.* **2001**, *40*, 366–369.
[18] F. Dasgupta, P. J. Garegg, *Carbohydr. Res.* **1988**, *177*, c13-c17.
[19] A. Hasegawa, H. Ohki, T. Nagahama, H. Ishida, M. Kiso, *Carbohydr. Res.* **1991**, *212*, 277–281.
[20] L. A. Carpino, G. Y. Han, *J. Am. Chem. Soc.* **1970**, *92*, 5748–5749.
[21] E. Bayer, W. Rapp, *Chem. Pept. Proteins* **1986**, *3*, 3–8; all peptide syntheses were carried out in a Perkin–Elmer ABI A 433 peptide synthesizer (Applied Biosystems).
[22] V. Dourtoglou, B. Gross, V. Lambropoulou, C. Zioudrou, *Synthesis* **1984**, 572.
[23] W. König, R. Geiger, *Chem. Ber.* **1970**, *103*, 788–798.
[24] L. A. Carpino, D. Ionescu, A. El-Faham, *J. Org. Chem.* **1996**, *61*, 2460.
[25] G. Zemplén, A. Kunz, *Chem. Ber.* **1923**, *56*, 1705–1710.

[26] P. Braun, G. M. Davies, M. R. Price, P. M. Williams, S. J. B. Tendler, H. Kunz, *Bioorg. Med. Chem.* **1998**, *6*, 1531–1545.
[27] M. Leuck, H. Kunz, *J. Prakt. Chem.* **1997**, *339*, 322–334.
[28] J. Schuman, A. P. Campbell, R. R. Koganty, B. M. Longenecker, *J. Pept. Res.* **2003**, *61*, 91–108.
[29] M. Liu, B. Acres, J.-M. Balloul, N. Bizouarne, S. Paul, P. Slos, P. Squiban, *Proc. Natl. Acad. Sci. USA* **2004**, *101*, 14567–14571.
[30] D. M. Coltart, A. K. Royyuru, L. J. Williams, P. W. Glunz, D. Sames, S. D. Kuduk, J. G. Schwarz, X.-T. Chen, S. J. Danishefsky, D. H. Live, *J. Am. Chem. Soc.* **2002**, *124*, 9833–9844.
[31] S. Mensdorff-Pouilly, L. Kirnarsky, K. Engelmann, S. E. Baldus, R. H. Verheijen, M. A. Hollingsworth, V. Pisarev, S. Sherman, F.-G. Hanisch, *Glycobiology* **2005**, *15*, 735–746.
[32] L. Kirnarsky, O. Prakash, S. M. Vogen, M. Nomoto, M. A. Hollingsworth, S. Sherman, *Biochemistry* **2000**, *39*, 12076–12082.
[33] L. Kirnarsky, M. Nomoto, Y. Ikematsu, H. Hassan, E. P. Bennett, R. L. Cerny, H. Clausen, M. A. Hollingsworth, S. Sherman, *Biochemistry* **1998**, *37*, 12811–12817.
[34] Reference [114] in S. Dziadek, C. G. Espinola, H. Kunz, *Aust. J. Chem.* **2003**, *56*, 519–543.
[35] D. S. Wishart, D. A. Case, *Methods Enzymol.* **2001**, 338, 3–34.
[36] D. E. Dorman, F. A. Bovey, *J. Org. Chem.* **1973**, *38*, 2379–2383.
[37] N. G. Delaney, V. Madison, *J. Am. Chem. Soc.* **1982**, *104*, 6635–6641.
[38] J. S. Grinstead, R. R. Koganty, M. J. Krantz, B. M. Longenecker, A. P. Campbell, *Biochemistry* **2002**, *41*, 9946–9961.
[39] D. S. Wishart, B. D. Sykes, F. M. Richards, *J. Mol. Biol.* **1991**, *222*, 311–333.
[40] N. H. Andersen, J. W. Neidigh, S. M. Harris, G. M. Lee, Z. Liu, H. Tong, *J. Am. Chem. Soc.* **1997**, *119*, 8547–8561.
[41] G. D. Rose, L. M. Gierasch, J. A. Smith, *Adv. Protein Chem.* **1985**, *37*, 1–109.
[42] H. J. Dyson, P. E. Wright, *Annu. Rev. Phys. Chem.* **1996**, *47*, 369–395.
[43] D. H. Live, L. J. Williams, S. D. Kuduk, J. B. Schwarz, D. W. Glunz, X.-T. Chen, D. Sames, R. A. Kumar, S. J. Danishefsky, *Proc. Natl. Acad. Sci. USA* **1999**, *96*, 3489–3493.
[44] G. A. Naganagowda, T. L. Gururaja, J. Satyanarayana, M. J. Levine, *J. Pept. Res.* **1999**, *54*, 290–310.
[45] D. Pal, P. Chakrabarti, *Acta Crystallogr. Sect. D* **2000**, *56*, 589–594.
[46] J. Schuman, D. Qiu, R. R. Koganty, B. M. Longenecker, A. P. Campbell, *Glycoconjugate J.* **2000**, *17*, 835–848.
[47] L. Kirnarsky, G. Suryanarayanan, O. Prakash, H. Paulsen, H. Clausen, F.-G. Hanisch, M. A. Hollingsworth, S. Sherman, *Glycobiology* **2003**, *13*, 929–939.
[48] J. S. Grinstead, J. T. Schuman, A. P. Campbell, *Biochemistry* **2003**, *42*, 14293–14305.
[49] H. Takeuchi, K. Kato, K. Denda-Nagai, F.-G. Hanisch, H. Clausen, T. Irimura, *J. Immunol. Methods* **2002**, *270*, 199–209.
[50] J. D. Fontenot, S. V. Mariappan, P. Catasti, N. Domenech, O. J. Finn, G. Gupta, *J. Biomol. Struct. Dyn.* **1995**, *13*, 245–260.
[51] D. D. Perrin, W. L. F. Armarego, *Purification of Laboratory Chemicals*, Pergamon Press, Oxford, 3 ed., **1988**.
[52] L. A. Carpino, H. Imazumi, A. El-Faham, F. J. Ferrer, C. Zhang, Y. Lee, B. M. Foxmann, P. Henklein, C. Hanay, C. Mügge, H. Wenschuh, J. Klose, M. Beyermann, M. Bienert, *Angew. Chem.* **2002**, *114*, 457–461; *Angew. Chem. Int. Ed.* **2002**, *41*, 441–445.
[53] P. Dauber-Osguthorpe, V. A. Roberts, D. J. Osguthorpe, J. Wolff, M. Genest, A. T. Hagler, *Proteins Struct. Funct. Genet.* **1988**, *4*, 31–47.
[54] M. Martín-Pastor, J. F. Espinosa, J. L. Asensio, J. Jiménez-Barbero, *Carbohydr. Res.* **1997**, *298*, 15–49.

Received: February 2, 2006
Published online: April 27, 2006

CHEMISTRY
A EUROPEAN JOURNAL

Supporting Information

Synthesis and Structural Model of a (2,6)-Sialyl-T Glycosylated MUC1 Eicosapeptide under Physiological Conditions

Sebastian Dziadek,[a] Christian Griesinger,*[b] Horst Kunz,*[a] Uwe M. Reinscheid[b]

[a] Dr. S. Dziadek, Prof. Dr. H. Kunz
Institut für Organische Chemie der Universität Mainz
Duesbergweg 10-14, 55099 Mainz (Germany)
Fax: (+49) 6131-39-24786
E-mail: hokunz@uni-mainz.de

[b] Dr. U. M. Reinscheid, Prof. Dr. C. Griesinger
Max-Planck Institute for Biophysical Chemistry
Am Fassberg 11, 37077 Göttingen (Germany)
Fax: (+49) 551-201-2202
E-mail: cigr@nmr.mpibpc.mpg.de

Table S1: ROE contacts for structure calculation of the glycopeptide **13** in H_2O/D_2O (90/10, pH = 6.5) at 298K. Spin lock: 440 ms, intensities are classified according to: S=strong, M=medium, W=weak, VW=very weak

ROE contacts from amino acids in sequential order

NH(G1)	Hα-G1	S
	Ac-NH	M
NH(S2)	Hα-S2	W
	Hα-G1	M
NH(T3)	Hα-S2	S
	Hβ-T3	M
	Hβ-S2	W
	Hγ-T3	W
NH(A4)	Hα-A4	M
	Hα-T3	S
	Hβ-T3	M
	Hβ-A4	M
Hδ(P6)	Hα-P5	S
	Hβ-P5	M
	Hγ-P5	M
NH(A7)	Hα-P6	S
	Hβb-P6	M
	Hβ-A7	M
NH(H8)	Hα-His8	W
	Hα-A7	M
NH(G9)	Hα-His8	M
	Hαa-G9	W

NH(V10)	Hα-V10	S
	Hαa,b-G9	M
	Hβ-V10	S
Hγ(V10)	Hα-S12	VW
	Hα-T11	VW
NH(T11*)	NHAc-GalNAc	M
	Hα-T11	M
	Hα-V10	S
	Hα-S12	W
	H3 GalNAc	VW
	CH_3-Ac-GalNAc	VW
	Hγ-T11	W
NH(S12)	Hα-T11	S
	Hβ-T11	M
	Hβb-S12	VW
	Hβa-S12	M
NH(A13)	Hα-A13	M
	Hα-S12	S
	CH_3-Ac-GalNAc	W
	Hβ-A13	S
Hδ(P14)	Hα-A13	M
NH(D15)	NH-T16	M
	Hα–D15	M
	Hα-P14	M
	Hδb-P14	W
	βa-P14	W
	Hβ-A13	VW
NH(T16)	NH-R17	M
	Hα-T16	S
	Hβ-T16	S

	Hγ-T16	W
NH(R17)	Hα-R17	S
	Hα-T16	S
	Hβ-T16	M
	Hβa-R17	W
	Hβb–P17	M
	Hγ–R17	M
Hδ(P18)	Hα-R17	M
NH(A19)	Hα-P18	S
	Hα-A19	M
	Hβ-P18	M
	Hβ-A19	S
Hδ-P20	Hα-A19	M

Acetylgroup of GalNAc: ROE contacts to peptide

AcNH GalNAc	Hα-S12	M
	Hα-T11	W
	Hβ-T11	W
	CH_3-Ac	S
	H1 GalNAc	S
	H1' Gal	M
	H2 GalNAc	S
	H3 GalNAc	S
CH_3-Ac-GalNAc	Hβ-T11	VW
	Hβ-A13	W
	Hγ-V10	VW

Intra-saccharide-contacts

H1 GalNAc	H2 GalNAc	W
	Hβ-T11	M
H2 GalNAc	H1' Gal	W
	H1 GalNAc	S
H3 GalNAc	H4 GalNAc	S
	H1' Gal	S
	H1 GalNAc	S
H4 GalNAc	H5 GalNAc	M
	H3 GalNAc	M
H5 GalNAc	Hγ-T11	M
	H3 GalNAc	M
	H2 GalNAc	M
	H1 GalNAc	W
H1' Gal	H6a' Gal	W
	H2' Gal	M
	H5' Gal	S
	H3' Gal	S
H2' Gal	H4' Gal	S
	H4 GalNAc	VW
	H1' Gal	S
H4' Gal	H2' Gal	M
	H5' Gal	S
	H6b' Gal	S
	H6a' Gal	M
H6a' Gal	H5' Gal	M
H3eq" NANA	H4" NANA	S
H3ax" NANA	H3eq" NANA	S
	H5" NANA	S
	H9a" NANA	VW
H9a" NANA	H8" NANA	M
	H9b" NANA	S

JOC*Article*

Helical Structure of Tercyclopropanedimethanol in Solution

Anthony G. M. Barrett,*[,†] Rachel A. James,[†] Gillian E. Morton,[†] Panayiotis A. Procopiou,[‡] Christian Boehme,[§] Armin de Meijere,[∥] Christian Griesinger,*[,⊥] and Uwe M. Reinscheid*[,⊥]

Department of Chemistry, Imperial College, South Kensington, London SW7 2AY, United Kingdom, GlaxoSmithKline Research and Development, Gunnels Wood Road, Stevenage, Herts SG1 2NY, United Kingdom, Gesellschaft für wissenschaftliche Datenverarbeitung Göttingen, Am Fassberg 11, 37077 Göttingen, Germany, Institut für Organische und Biomolekulare Chemie der Georg-August-Universität Göttingen, Tammannstrasse 2, D-37077 Göttingen, Germany, and Max-Planck-Institute for Biophysical Chemistry, Department of NMR based Structural Biology, Am Fassberg 11, 37077 Göttingen, Germany

agmb@ic.ac.uk; cigr@nmr.mpibpc.mpg.de; urei@nmr.mpibpc.mpg.de

Received December 19, 2005

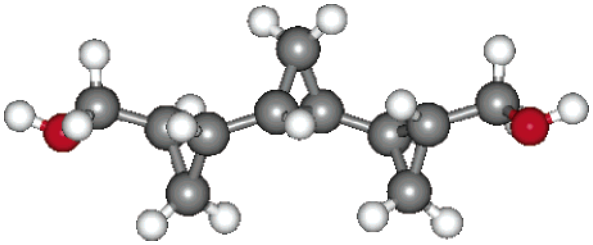

Oligocyclopropanes with repetitive stereochemistry occur in two unusual natural products with interesting bioactivity. X-ray crystal structures are available for these compounds but with partially contradicting results. Because the ^{1}H and ^{13}C NMR spectra of oligocyclopropanes are far from trivial to be assigned even at highest magnetic fields, we have prepared a specifically deuterated sample and have applied high field NMR spectroscopy and DFT calculations to determine its conformation. The helix with equal handedness shown in the stereopicture was found for tercyclopropanedimethanol. A dihedral angle of around +40° is the best representation of the experimental data and characterizes, therefore, the dominating helical conformation of tercyclopropanedimethanol with a single repetitive (+)-gauche interunit dihedral angle. This is in full agreement with the crystal structure of the all *syn,trans*-quinquecyclopropanedimethanol with an *R* configuration at the termini that also adopted an all (+)-gauche conformation. However, the crystal structure of the title compound and the solution structure are different.

Introduction

Oligocylopropane moieties have recently been shown to be important in nature as they appear in two natural products from different sources:[1] the antifungal nucleoside FR-900848[2] and the cholesteryl-transfer-protein inhibitor U-106305.[3] Some of us previously reported the total synthesis of both compounds, which relied upon a sequence of bidirectional double Simmons−Smith cyclopropanation reactions.[4] The fatty acid side chains of both compounds contain all-syn,trans disubstituted oligocyclopropanes that, as it is shown in this work, conformationally restrict these lipophilic domains to a single conformation. Compound **1** constitutes such an all-syn,trans disubstituted tercyclopropane. The nondeuterated analogue of the hydroxymethyl derivative **1** [(1*R*,3*S*,4*R*,6*R*,7*S*,9*R*)-1,9-bis(hydroxymethyl)tercyclopropane] in the solid state showed interunit dihedral angles (designated ϕ in the formula **1**) of +49.7° and

* Corresponding authors. Fax: (+44)207-594-5805 (A.G.M.B.); (+49)551-201-2202 (C.G. and U.M.R.).
† Imperial College.
‡ GlaxoSmithKline Research and Development.
§ Gesellschaft für wissenschaftliche Datenverarbeitung Göttingen.
∥ Institut für Organische und Biomolekulare Chemie der Georg-August-Universität Göttingen.
⊥ Max-Planck-Institute for Biophysical Chemistry.

(1) Pietruszka, J. *Chem. Rev.* **2003**, *103*, 1051.
(2) Yoshida, M.; Ezaki, M.; Hashimoto, M.; Yamashita, M.; Shigematsu, N.; Okuhara, M.; Kohsaka, M.; Horikoshi, K. *J. Antibiot.* **1990**, *43*, 748. Yoshida, M.; Horikoshi, K. Eur. Pat. 286 330, 1988; U.S. Patent, 4 803 074, 1989; *Chem. Abstr.* **1989**, *110*, 210961.
(3) Kuo, M. S.; Zielinski, R. J.; Cialdella, J. I.; Marschke, C. K.; Dupuis, M. J.; Li, G. P.; Kloosterman, D. A.; Spilman, C. H.; Marshall, V. P. *J. Am. Chem. Soc.* **1995**, *117*, 10629.
(4) Barrett, A. G. M.; Hamprecht, D.; White, A. J. P.; Williams, D. J. *J. Am. Chem. Soc.* **1996**, *118*, 7863. Barrett, A. G. M.; Kasdorf, K. *J. Am. Chem. Soc.* **1996**, *118*, 11030.

10.1021/jo0525985 CCC: $33.50
Published on Web 03/03/2006

SCHEME 1[a]

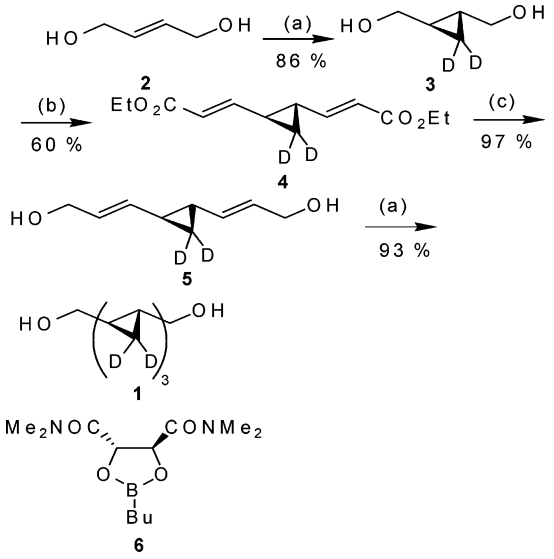

[a] Reagents: (a) (i) **6**, (ii) $Zn(CD_2I)_2$·DME, DCM, from −45 °C to rt; (b) (i) Dess−Martin periodine, DMSO/pyridine, 0 °C; (ii) PPh_3; (iii) $Ph_3P{=}CHCO_2Et$, Et_2O; (c) DIBALH, DCM, −78 °C

−58.6°, respectively, which breaks the symmetry in the conformation of a configurationally repetitive molecule.[5] In contrast, Charette and Lebel published a crystal structure of a configurationally repetitive all *syn,trans*-quinquecyclopropanedimethanol with all interunit dihedral angles as being (+)-gauche.[6] To shed some light on these partially contradicting observations, we closely examined the conformation of **1** as a model in acetone solution by NMR spectroscopy and by DFT calculations. The result of this study also clarifies whether configurationally repetitive oligocyclopropanes adopt repetitive conformations such as those of isotactic polymers.

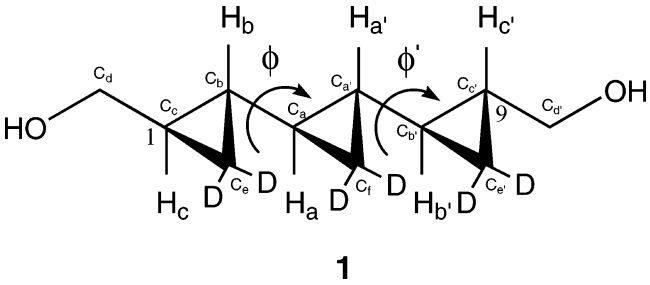

1

Results and Discussion

Synthesis. The nondeuterated cyclopropanes have been synthesized previously via iterative double cyclopropanation using the Simmons−Smith reagent derived from di-iodomethane. However, in this instance, compounds were synthesized using the Simmons−Smith reagent derived from diiodomethane-d_2 (Scheme 1). Absolute stereochemical control was effected using the chiral dioxoborolane **6**, according to the protocol of Charette and co-workers.[7] Thus, Charette cyclopropanations of diol **2** gave the cyclopropane **3** (86% yield), which was homologated using a Dess−Martin oxidation with a Wittig homologation in situ[4] to directly provide diester **4**. A DIBALH reduction gave the diene **5**, which was subjected to a second double-Charette cyclopropanation to provide the tercyclopropanedimethanol **1**.

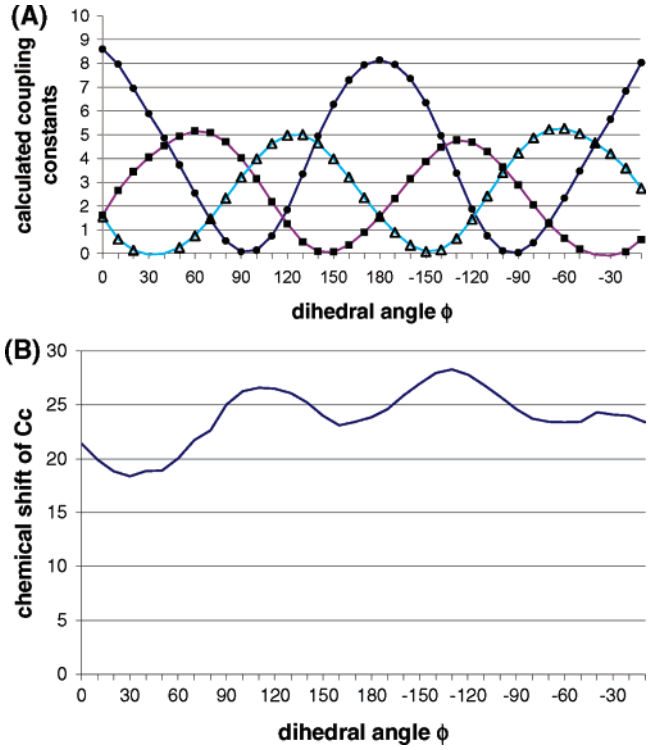

FIGURE 1. Relationship between (A) coupling constants and (B) chemical shift vs the interunit dihedral angle ϕ, as calculated by DFT.[12] (A) Filled circle: $^3J_{H_a,H_b}$ coupling constant. Filled square: $^3J_{H_a,C_c}$ coupling constant. Open triangle: $^3J_{H_a,C_e}$ coupling constant. (B) Chemical shift of C_c vs dihedral angle ϕ.

Conformational Analysis. For bicyclopropyl, the gauche conformer ($\phi \approx +50°$ or $-50°$) is stabilized in solution compared to the antiperiplanar conformer ($\phi = 180°$).[8] This was confirmed by Lüttke and co-workers, who established a Karplus relationship using the partially deuterated *cis*- and *trans*-tricyclo[5.1.0.0^{2,4}]octane as model compounds.[9] On the basis of the $^3J_{H,H}$ coupling constants, an interunit dihedral angle of 53 ± 7° was deduced for bicyclopropyl. Because analogous NMR studies of oligocyclopropanes encounter the difficulty that the cyclopropyl protons are in large part indistinguishable from one another, the partially deuterated compound **1** was synthesized to simplify spectral interpretation. Experimental NMR parameters, NOE, *J* couplings, and chemical shifts were used and compared to the predicted values for *J* couplings and chemical shifts from DFT calculations (Figure 1A,B).[10]

The one-dimensional (1D) ^{1}H and ^{13}C NMR spectra at 278 K in acetone-d_6 showed six signals each (Table 1), reflecting

(5) Barrett, A. G. M.; Hamprecht, D.; White, A. J. P.; Williams, D. J. *J. Am. Chem. Soc.* **1997**, *119*, 8608. Barrett, A. G. M.; Hamprecht, D.; James, R. A.; Ohkubo, M.; Procopiou, P. A.; Toledo, M. A.; White, A. J. P.; Williams, D. J. *J. Org. Chem.* **2001**, *66*, 2187.

(6) Charette, A. B.; Lebel, H. *J. Am. Chem. Soc.* **1996**, *118*, 10327.

(7) Charette, A. B.; Juteau, H. J. *J. Am. Chem. Soc.* **1994**, *116*, 2651. Charette, A. B.; Prescott, S.; Brochu, C. *J. Org. Chem.* **1995**, *60*, 1081.

(8) de Meijere, A.; Lüttke, W.; Heinrich, F. *Liebigs Ann. Chem.* **1974**, 306.

(9) Lüttke, W.; de Meijere, A.; Wolff, H.; Ludwig, H.; Schröter, W. *Angew. Chem.* **1966**, *78*, 141. Braun, H.; Lüttke, W. *J. Mol. Struct.* **1975**, *28*, 391.

(10) Bagno, A. *Chem.—Eur. J.* **2001**, *7*, 1652. Bagno, A.; Rastrelli, F.; Saielli, G. *J. Phys. Chem. A* **2003**, *107*, 9964. Bassarello, C.; Cimino, P.; Gomez-Paloma, L.; Riccio, R.; Bifulco, G. *Tetrahedron* **2003**, *59*, 9555. Matsumori, N.; Kaneno, D.; Murata, M.; Nakamura, H.; Tachibana, K. *J. Org. Chem.* **1999**, *64*, 866.

TABLE 1. Chemical Shifts and *J* Coupling Constants of 1 in Acetone at 278 K[a]

δ C_a	δ C_b	δ C_c	δ C_d	δ C_e	δ H_a	δ H_b	δ H_c	δ H_{d1}	δ H_{d2}	δ OH	J_{H_a,H_b}	J_{H_a,C_c}	J_{H_a,C_e}
18.2	18.2	19.8	65.2	7.13	0.57	0.67	0.73	3.27	3.37	3.6	3.45	8.4	2.4

[a] Chemical shifts, δ, in ppm (solvent signal as reference) and coupling constants, *J*, in Hz.

either static symmetry, accidental degeneracy, or dynamic symmetry of the primed and unprimed nuclei. Thus, only the dihedral angle ϕ can be determined. Three situations are possible: In the first case, ϕ and ϕ' are identical and adopt a unique value (static symmetry). One would expect that this value is close to the $\pm 50°$ previously found for the bicyclopropyl as well as the ter- and quinquecyclopropyl in the X-ray structure. In the second case, if ϕ and ϕ' each adopted one value and they were not identical (accidental degeneracy), the NMR data measured simultaneously for ϕ and ϕ' would reflect the 1:1 average of these nonidentical values. This would be the situation if the structure found in the crystal for compound **1** would also prevail in solution. In the third case (dynamic symmetry), the two angles would be identical and averaged between at least two conformations. This situation would be indistinguishable from the second case. In the following we show that all experimental data are in agreement with the first situation of static symmetry and that we do not have to assume the more complicated second and third cases. This procedure of taking the simplest structural model is justified when more NMR parameters (Table 1: chemical shifts; proton−proton and proton−carbon coupling constants; and NOE cross-peaks) are in agreement with a single value for ϕ and ϕ'.

The deuteration facilitated the extraction of the homonuclear coupling $^3J_{H_a,H_b} = 3.45$ Hz. According to the calculated Karplus relationship, this value would fit to dihedral angles of $+50 \pm 10°$, $+140 \pm 10°$, $-50 \pm 10°$, and $-140 \pm 10°$. The coupling constants predicted for the crystal structure (second case), previously reported by some of us with alternating dihedral angles ϕ and ϕ' ($-57.6°$ and $+49.7°$), would be approximately $2.9\ \text{Hz} = [J_{H_a,H_b(\phi = -57.58°)} + J_{H_a,H_b(\phi = +49.74°)}]/2$, which does not agree with this newly measured value of 3.45 ($\pm$ 0.15) Hz.[5]

Heteronuclear couplings are indispensable to further define the structure of **1**, because the deuteration removed all relevant homonuclear couplings except for the interunit $^3J_{H_a,H_b}$ coupling.[11] Applying the robust HMBC of Verdier et al.,[11] the $^3J_{H_a,C_c}$ and $^3J_{H_a,C_e}$ couplings were determined to be 8.4 and 2.4 Hz, respectively (Table 1). Two regions, $\phi = -50$ and $+140°$, are excluded by these experimental values for which $^3J_{H_a,C_c}$ is smaller than $^3J_{H_a,C_e}$. Only $\phi = +50$ or $-140°$ are compatible with the homonuclear and the heteronuclear couplings. By contrast, the values predicted for the conformation found in the crystal structure[5] would be $2.8\ \text{Hz} = [J_{H_a,C_c(\phi = -57.58°)} + J_{Ha,C_c(\phi = +49.74°)}]/2$ and $2.9\ \text{Hz} = [J_{H_a,C_e(\phi = -57.58°)} + J_{H_a,C_e(\phi = +49.74°)}]/2$, respectively, which is clearly incompatible with the experimental data. It should be stated that for the heteronuclear couplings, we relied on the difference of the $^3J_{H_a,C_c}$ and $^3J_{H_a,C_e}$ couplings and not their absolute values. It is well-established that the absolute values of the $^3J_{H,C}$ couplings calculated with DFT methods may deviate from experimental ones by approximately 2 Hz while retaining faithfully the differences.[10]

(11) Verdier, L.; Sakhaii, P.; Zweckstetter, M.; Griesinger, C. *J. Magn. Res*. **2003**, *163*, 353. Sheng, S.; van Halbeek, H. *J. Magn. Reson.* **1998**, *130*, 296. Cicero, D. O.; Barbato, G.; Bazzo, R. *J. Magn. Reson*. **2001**, *148*, 209. Marquez, B. L.; Gerwick, W. H.; Williamson, R. T. *Magn. Reson. Chem.* **2001**, *39*, 499.

Information about the dihedral angle ϕ independent of *J* couplings was obtained from NOEs. Due to the identities of the chemical shifts of primed and unprimed nuclei, the H_a-H_c NOE integral reflects the distances between the protons H_a-H_c, $H_{a'}-H_c$, $H_{a'}-H_{c'}$, and $H_a-H_{c'}$. This integral is compared to the H_a-H_b NOE integral that reflects the H_a-H_b and $H_{a'}-H_b$ distances. We found similar values for the two integrals. This is in agreement with the dihedral angle ϕ being $+50$ or $-140°$, but is inconsistent with ϕ being -50 and $+140°$ because the distances between the H_a and H_c protons would be too long.

DFT calculations of the chemical shifts of all carbon atoms of **1** and their dependence on the dihedral angle ϕ have been performed. The chemical shift of C_c shows the largest variation of 10 ppm when ϕ varies between 0 and 360° (Figure 1B).

When the calculated chemical shift of the methyl carbon of acetone is used as a reference, the δ value is 19.5 ppm on the tetramethylsilane scale for the $+50°$ conformer, and 24.2 ppm for the $-140°$ conformer. The experimental value is 19.8 ppm, which clearly fits that of the $+50°$ conformer. It should be noted that the observation of the very high-field shift of C_c further corroborates the predominant existence of a single conformation in solution, because only the ϕ values ranging between $+20$ and $+60°$ exhibit these high-field chemical shifts and exclude the presence of other conformations. The calculated chemical shifts for C_a and C_b show only small variations which, therefore, cannot deliver further information about the conformation (maximal differences for $C_a = 5.8$ ppm and $C_b = 5.1$ ppm).

All experimental information (chemical shift of C_c, homo- and heteronuclear coupling constants, ^3J, and NOE integrals of H_a-H_b ($H_{a'}-H_b$) and H_a-H_c ($H_{a'}-H_c$)) was cast into an equation of variance with the dihedral angle ϕ as the independent variable (Figure 2).

The dihedral angle with the lowest value of variance around $+40°$ is the best representation of the experimental data and characterizes, therefore, the dominating helical conformation of tercyclopropanedimethanol **1** with a single repetitive (+)-gauche interunit dihedral angle (Figure 3), in full agreement with the crystal structure of the all *syn*,*trans*-quinquecyclopropanedimethanol with *R* configuration at the termini that also adopted an all-(+)-gauche conformation. Thus, the second and third cases discussed above can be excluded and, consequently, one of the crystal structures of tercyclopropanedimethanol differs from the solution structure.

Additionally, the free energies calculated by DFT exhibited an asymmetric minimum at a dihedral angle ϕ of $+40°$, without an imaginary frequency, indicating a thermodynamically stable conformation.

The temperature dependence of the NMR parameters is quite interesting and further corroborates a unique conformation. The $^3J_{H_a,H_b}$ coupling constant increased (Figure 1A) with increasing temperature (298 K, 3.80 Hz), which normally would be interpreted as a higher population of a conformation in which the two protons are antiperiplanar or eclipsed. However, the chemical shift of C_c (Figure 1B) should also increase, which is not the case ($C_a = 18.1$ ppm, $C_b = 18.2$ ppm, $C_c = 19.8$ ppm, $H_a = 0.58$ ppm, $H_b = 0.68$ ppm, and $H_c = 0.73$ ppm). However,

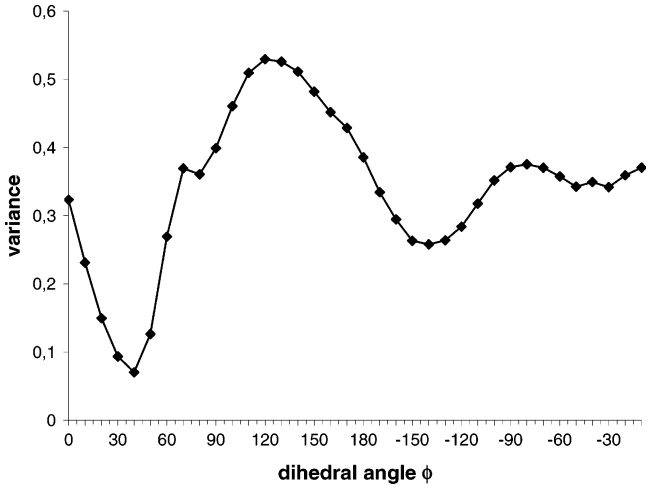

FIGURE 2. Variance with the interunit dihedral as an independent variable. The variance is defined as the following: variance = $((\delta C_{c,exp} - \delta C_{c,calc})^2/(10\ ppm)^2 + ({}^3J_{H_a,H_b,exp} - {}^3J_{H_a,H_b,calc})^2/(8.6\ Hz)^2 + (({}^3J_{H_a,C_c,exp} - {}^3J_{H_a,C_e,exp}) - ({}^3J_{H_a,C_c,calc} - {}^3J_{H_a,C_e,calc}))^2/(10.86\ Hz)^2) + (\sigma_{H_a,H_b,exp} - \sigma_{H_a,H_b,calc})^2/64^2 + (\sigma_{H_a,H_c,exp} - \sigma_{H_a,H_c,calc})^2/191.44^2)/5$. An almost identical curve was obtained when using the ratios of the heteronuclear J couplings instead of the differences.

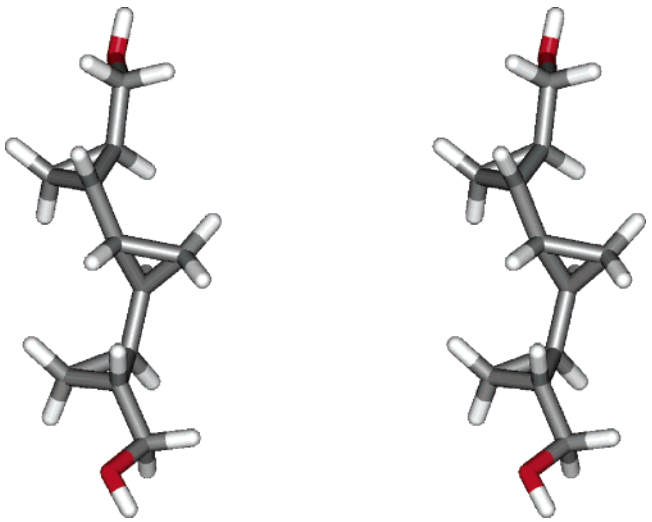

FIGURE 3. Stereoview of tercyclopropanedimethanol **1** in acetone-d_6 at 278 K.

the coupling constants and chemical shifts can be explained by a highly asymmetric potential around the $\phi = +40°$ value. Relative DFT calculated energies are 1.11, 0.98, 0, 11.12, and 14.76 kcal/mol for the angles $\phi = +20°$, $+30°$, $+40°$, $+50°$, and $+60°$. This suggests that the chemical shift of C_c stays the same while the ${}^3J_{H_a,H_b}$ increases upon temperature increase because of the strong asymmetry of the potential toward values of ϕ smaller than $+40°$.

Summary

In the present study we find for the configurationally repetitive all *syn,trans*-tercyclopropanedimethanol **1** a unique repetitive conformation with two (+)-gauche dihedral angles of $+40°$. It is induced by the *R* configuration of carbons C_c and $C_{c'}$, in complete agreement with the crystal structure of the all *syn,trans*-quinquecyclopropanedimethanol with an *R* configuration at the termini. This finding suggests conformational control of the oligocyclopropane by the configuration. The solution structure of the tercyclopropanedimethanol **1** differs from the crystal structure,[5] indicating that crystal-packing forces can supersede the intrinsic preference for the (+)-gauche, (+)-gauche conformation at least for three cyclopropane units. Our method of combining DFT with experimental restraints solves a long-standing and difficult question of conformational analysis of highly repetitive molecules and should, therefore, be applicable for other similar problems.

Experimental Section

NMR. NMR measurements were generally performed at 278 K on a 600-MHz spectrometer equipped with a cryoprobe and a 400-MHz spectrometer. The sample consisted of 3 mg of **1** in acetone-d_6. A total of 8 scans per t_1 increment were acquired for COSY and 28 scans per t_1 increment were acquired for NOESY spectra. A mixing time of 800 ms was used. The ^{13}C-HSQC and ^{13}C-HMBC experiments were performed according to Verdier and co-workers.[11] A delay of 50 ms was chosen. From these spectra, the heteronuclear ${}^3J$ coupling constants and ^{13}C chemical shifts were extracted. ${}^3J_{H,H}$ values were extracted from 1D-proton spectra and confirmed by selective versions. Measured chemical shifts are referenced with respect to the solvent signal relative to tetramethylsilane.

DFT. Structures were optimized using the hybrid B3LYP functional and the 6-31G(d,p) basis set.[12] The vibrational analysis provided $\Delta G_{calc}°$ values for the different conformations. With the obtained geometries, the calculations of the chemical shifts and the ${}^3J$ coupling constants were run using the same functional and basis set. Spin−spin coupling constants were calculated taking into account the contributions of the following interactions: Fermi contact, paramagnetic spin−orbit, diamagnetic spin−orbit, and spin−dipole. The calculated chemical shift values were referenced to the calculated acetone values computed at the same level of theory. The experimental and the calculated shifts were obtained with deuterated compound and computer models. Nondeuterated models exhibited similar chemical shifts, supporting the conformational analysis. However, it is not possible to obtain the same amount of experimental data of the nondeuterated compound, rendering a comparison impossible.

Acknowledgment. This work was supported by the EPSRC, GlaxoSmithKline, Max-Planck Society, the DFG (SFB 416), and the Fonds der Chemischen Industrie.

Supporting Information Available: Syntheses of **1**, **3**, **4**, and **5**. This material is available free of charge via the Internet at http://pubs.acs.org.

JO0525985

(12) Frisch, M. J.; Trucks, G. W.; Schlegel, H. B.; Scuseria, G. E.; Robb, M. A.; Cheeseman, J. R.; Montgomery, J. A., Jr.; Vreven, T.; Kudin, K. N.; Burant, J. C.; Millam, J. M.; Iyengar, S. S.; Tomasi, J.; Barone, V.; Mennucci, B.; Cossi, M.; Scalmani, G.; Rega, N.; Petersson, G. A.; Nakatsuji, H.; Hada, M.; Ehara, M.; Toyota, K.; Fukuda, R.; Hasegawa, J.; Ishida, M.; Nakajima, T.; Honda, Y.; Kitao, O.; Nakai, H.; Klene, M.; Li, X.; Knox, J. E.; Hratchian, H. P.; Cross, J. B.; Bakken, V.; Adamo, C.; Jaramillo, J.; Gomperts, R.; Stratmann, R. E.; Yazyev, O.; Austin, A. J.; Cammi, R.; Pomelli, C.; Ochterski, J. W.; Ayala, P. Y.; Morokuma, K.; Voth, G. A.; Salvador, P.; Dannenberg, J. J.; Zakrzewski, V. G.; Dapprich, S.; Daniels, A. D.; Strain, M. C.; Farkas, O.; Malick, D. K.; Rabuck, A. D.; Raghavachari, K.; Foresman, J. B.; Ortiz, J. V.; Cui, Q.; Baboul, A. G.; Clifford, S.; Cioslowski, J.; Stefanov, B. B.; Liu, G.; Liashenko, A.; Piskorz, P.; Komaromi, I.; Martin, R. L.; Fox, D. J.; Keith, T.; Al-Laham, M. A.; Peng, C. Y.; Nanayakkara, A.; Challacombe, M.; Gill, P. M. W.; Johnson, B.; Chen, W.; Wong, M. W.; Gonzalez, C.; Pople, J. A. *Gaussian 03*, revision C.02; Gaussian, Inc.: Pittsburgh, PA, 2003.

Supporting information

The exact experimental procedures are the same as reported for the non-deuterated compounds with the exception that d_2-diiodomethane was used in all Charette cyclopropanation reactions rather than diiodomethane. The scale of reaction and yields are given in parenthesis following the compound numbers.

(*R*,*R*)-2,2-Dideuterio-1,3-cyclopropanedimethanol 3 (409 mg, 86 %)[4]

R_f=0.27 (EtOAc); IR ($CHCl_3$) 3349br, 2875, 1435, 1109, 1066, 1019cm^{-1}; ^{1}H NMR ($CDCl_3$, 400MHz) δ 4.25 (s, 2H), 3.83 (dd, *J* = 11.3, 4.4Hz, 2H), 2.98 (dd, *J* = 11.3, 8.8Hz, 2H), 0.96-0.99 (m, 2H); ^{13}C NMR ($CDCl_3$, 100MHz) δ 66.0 (2C), 19.8 (2C), 6.0-7.0 (m, CD_2); *m/z* (Cl^+; NH_3); 122 $[M+NH_4]^+$, 104 $[M]^+$; HRMS calcd for $C_5H_{12}D_2NO_2$ $[M+NH_4]^+$: 122.1150, found: 122.1148.

***(R,R)*-2,2-Dideuterio-1,3-bis[(*E*)-2-ethoxycarbonylethenyl]cyclopropane 4** (470 mg, 60 %)[4]

R_f=0.37 (hexanes : EtOAc, 4 : 1); IR (neat) 2982, 2938, 1711, 1644, 1368, 1263, 1187, 1142, 1043, 977, 859cm^{-1}; ^{1}H NMR ($CDCl_3$, 400MHz) δ 6.40-6.48 (m, 2H), 5.89 (d, *J* = 15.4Hz, 2H), 4.16 (q, *J* = 7.1Hz, 4H), 1.81 (d, *J* = 9.1 Hz, 2H), 1.27 (t, *J* = 7.1Hz, 6H); ^{13}C NMR ($CDCl_3$, 100MHz) δ 166.3, 149.5, 119.9, 60.3, 25.0, 16.1-17.4 (m, CD_2), 14.3; *m/z* (Cl^+; NH_3); 241 $[M+H]^+$, 258 $[M+NH_4]^+$; HRMS calcd for $C_{13}D_2H_{17}O_4$ $[M+H]^+$: 241.1409, found: 241.1408.

(*R,R)*-2,2-Dideuterio-1,3-bis[(*E*)-3-hydroxy-1-propen-1-yl]cyclopropane 5 (232 mg, 97 %)[4]

R_f= 0.47 (EtOAc); IR (neat) 3315br, 3014, 2924, 2866, 1667, 1000, 963cm^{-1}; ^{1}H NMR ($CDCl_3$, 400MHz) δ 5.68 (dt, *J* = 15.3, 6.1Hz, 2H), 5.23-5.30 (m, 2H), 4.06 (dd, *J* = 6.1, 1.2Hz, 4H), 1.58 (s, br, 2H), 1.42 (d, *J* = 7.7Hz, 2H); ^{13}C NMR ($CDCl_3$, 100MHz) δ 134.8, 127.3, 63.5, 23.2, 14.0-15.2 (m, CD_2); *m/z* (Cl^+; NH_3); 174 $[M+NH_4]^+$, 156 $[M+H]^+$; HRMS calcd for $C_9H_{16}D_2NO_2$ $[M+NH_4]^+$: 174.1463, found: 174.1465.

(1*R*, 3*S*,4*R*,6*R*,7*S*,9*R*)-2,2,5,5,8,8-hexadeuterio-1,9-biscyclopropanedimethanol 1 (209 mg, 93 %)[4]

R_f=0.42 (hexanes : EtOAc: ^{i}PrOH, 5 : 5 : 1); $[\alpha]^{25}_D$= -122.9 (*c* 0.28, EtOH); IR (neat) 3342br, 3002, 2871, 1425, 1309, 1061, 1031, 734cm^{-1}; ^{1}H NMR ($CDCl_3$, 400MHz) δ 3.36-3.42 (m, 4H), 1.48 (s, br, 2H), 0.77-0.84 (m, 2H), 0.68-0.70 (m, 2H), 0.56-0.59 (m, 2H); ^{13}C NMR ($CDCl_3$, 100MHz) δ 66.9, 19.5, 18.0, 17.9, 7.0-8.2 (m, CD_2); *m/z* (Cl^+; NH_3); 206 $[M+NH_4]^+$, 188 $[M]^+$; HRMS calcd for $C_{11}H_{16}D_6NO_2$ $[M+NH_4]^+$: 206.2027, found: 206.2029.

ELSEVIER

Journal of Molecular Structure: THEOCHEM 820 (2007) 85–89

THEO CHEM

www.elsevier.com/locate/theochem

Energetic, geometric and magnetic analysis of all-*syn*,*trans* cyclic cyclopropanes

Stefan G. Wehner [a], Christian Boehme [b], Uwe M. Reinscheid [a,*]

[a] *Max-Planck-Institute for Biophysical Chemistry, Department of NMR based Structural Biology, Am Fassberg 11, 37077 Göttingen, Germany*
[b] *Gesellschaft für wissenschaftliche Datenverarbeitung Göttingen, Am Fassberg 11, 37077 Göttingen, Germany*

Received 17 October 2006; received in revised form 12 June 2007; accepted 12 June 2007
Available online 15 June 2007

Abstract

Structural, energetic and magnetic properties of a series of cyclic cyclopropanes have been investigated on the DFT (B3LYP/6-31G(d)) level. The cyclization of these oligomeric all-*syn*,*trans* cyclopropanes, designated [*N*]rondelanes, should be possible on energetic grounds, since no substantial destabilization energies were calculated for the larger homologues. However, the high strain for the smaller rondelanes might prevent their successful synthesis. Thermochemical reactions, structural data, and NICS values were investigated in order to test for homoaromatic stabilization. The careful choice of a homoisodesmic reaction revealed weak aromatic stabilization energies for [3] and [7]rondelane, 2.3 kcal/mol and 2.2 kcal/mol, respectively. However, we could not observe a pattern according to the Hückel rule and the stabilization energies are small compared to the stabilization of cyclopropane due to σ-aromaticity. Calculated structural data indicate homoconjugation for the smaller homologues. [3]Rondelane showed a NICS value of −2.54 indicating a weak neutral homoaromaticity.

Keywords: Computational chemistry; Cyclopropane; Trannulene; DFT; Homoaromaticity; Rondelane; Strain

1. Introduction

The concept of aromaticity has been the subject of recent reviews [1,2]. One important reason for the scientific interest is the thermodynamic stability of aromatic compounds which is relevant for chemical synthesis. Starting from the classical aromatic benzene and its higher homologues, the annulenes, two modifications were successfully introduced into the basic skeleton: *cis* annelation of three cyclopropane rings leading to tris-homobenzene [3–5], and exclusively *trans*-configurated C=C bonds in annulenes forming the so-called trannulenes [6,7]. During our work on oligomeric cyclopropanes we became interested in the combination of the two principles mentioned above, i.e. the homoconjugation and all-*trans* configuration resulting in cyclic all-*syn*,*trans* cyclopropanes which were designated [*N*]rondelanes (with *N* indicating the number of cyclopropane units). A computational study about the stability and aromatic character of these compounds is presented.

2. Theoretical approach

All calculations were done using Gaussian™ [8]. The models were geometry optimized using Becke's three parameter hybrid functional in conjunction with the correlation functional of Lee, Yang, and Parr [9,10] and the 6-31G(d) basis set. This level of theory, B3LYP/6-31G(d) for short, was also used for all other calculations. For [3]rondelane larger basis sets were additionally used (6-311G(d), 6-311G(d,p), 6-311G(2d,p) and 6-311G++(2d,p)). Frequency calculations were carried out to characterize the optimized structures as energy minima and to obtain the zero-point vibrational energy (ZPVE) corrections. The latter were used unscaled to correct the B3LYP/6-31G(d) energies. The NBO

* Corresponding author. Fax: +49 551 201 2202.
E-mail address: urei@nmr.mpibpc.mpg.de (U.M. Reinscheid).

0166-1280/$ - see front matter © 2007 Elsevier B.V. All rights reserved.
doi:10.1016/j.theochem.2007.06.008

program (version 3.1) was used for the calculation of bond orders and bond bendings [11]. NICS values [12] have been calculated 1.28 Å above the inner ring center formed by the cyclopropanes (e.g. the cyclohexane-type ring for [3]rondelane). Generally, the more negative the NICS values, the more aromatic the rings are [13].

3. Results and discussion

A comparison of the solution structure of all-*syn*,*trans* tercyclopropanedimethanol with the X-ray crystal structure [14] showed an unexpected flexibility which allowed the synthesis of coronanes bridged by a stretch of five and seven cyclopropane units [15]. Cyclization of oligomeric all-*syn*,-*trans* cyclopropanes should lead to a macrocyclic ring exclusively composed of twisted bent bonds [16]. However, molecular mechanics and DFT calculations indicate an energetic minimum for a dihedral of 180° (defined by H_a—C_a—C_b—H_b in Fig. 1, see Supplementary information) and attempts to cyclisize an 8-membered all-*syn*,*trans* oligomeric cyclopropane have proved inconclusive so far [17]. Therefore, we started a computational investigation about the energetic, geometric and magnetic properties of the [*N*]rondelanes shown in Fig. 1. Due to the helical geometry constrained to the plane of the macrocyclic ring, one series of enantiomers was chosen which is classified as *M* according to standard stereochemical rules [18].

The stabilization energies (STE) of the six rondelanes shown in Fig. 1 were calculated on the DFT (B3LYP/6-31G(d)) level (Table 1) [9,10]. Stabilization energies (STE) were defined by the homodesmotic reaction type I depicted in Scheme 1 ($E_{products} - E_{educts}$). The STE combines strain energy due to opening of the inner ring, potential homoaromatic stabilization energy (HASE), and arrangement-strain of the cyclopropane units with a strain-free arrangement at an interunit dihedral of 180°.

Table 1
Stabilization energies (STE, in kcal/mol, according to reaction type I of Scheme 1), bond orders (BO) and valence non-Lewis electron representation (in %) of rondelanes and open rondelanes

	STE	BO of C_a—C_b	BO of C_b—C_c	BO of C_b—C_d	Valence non-Lewis electron representation in %
[3]Rondelane	−106.0	1.034	0.976	0.979	1.2
[4]Rondelane	−59.2	1.009	1.007	0.997	1.0
[5]Rondelane	−33.0	1.010	1.012	1.005	0.9
[6]Rondelane	−18.8	1.010	1.013	1.009	0.9
[7]Rondelane	−11.1	1.010	1.015	1.010	0.9
[8]Rondelane	−6.8	1.009	1.016	1.010	0.9
Cyclopropane	−26.1[a]	1.037	1.037	1.037	0.6
Open [3]rondelane	–	1.009[b]	1.013[b]	1.013[b]	0.8
Open [7]rondelane	–	1.011[b]	1.012[b]	1.013[b]	0.8

[a] According to the ring opening reaction: E(cyclopropane) + E(ethane) = E(pentane) [14].
[b] For the central cyclopropane unit.

The STE of −6.8 kcal/mol is probably not preventing the synthesis of [8]rondelane whereas the STE of −106.0 kcal/mol for [3]rondelane (Table 1) is at the limit of compounds stable at room temperature similarly to the trannulenes which are unstable unless embedded into fullerene cages [19,20]. Within a NBO analysis, bond orders of the rondelanes were calculated in order to quantify the bonding [11]. A strengthening of the cyclopropane C_b—C_c and C_b—C_d bonds with increasing ring size was accompanied by a decreasing bond order for the interunit C_a—C_b bonds. Interestingly, the value of the interunit bond (C_a—C_b) for [3]rondelane is as high as for cyclopropane. Additionally, the percentage of valence non-Lewis electron

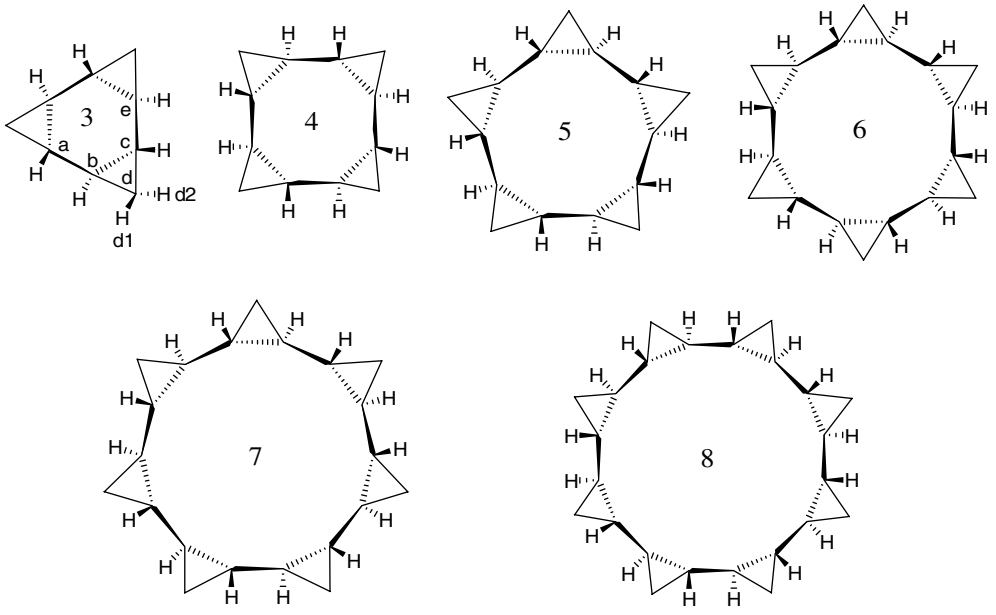

Fig. 1. Chemical formulas of the series from [3]rondelane to [8]rondelane.

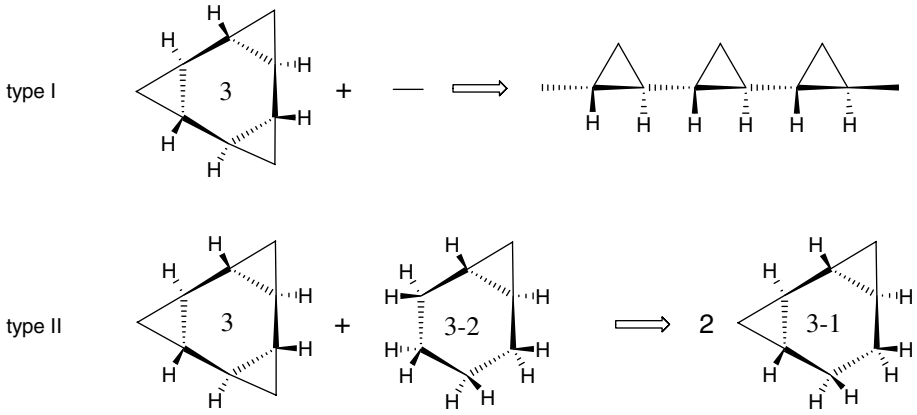

Scheme 1. Reaction types for thermochemical calculations exemplified for [3]rondelane.

representation was calculated. High values (benzene: 2.8%) indicate substantial electron delocalization. Going from smaller to larger rondelanes the non-Lewis representation decreases from 1.2% for [3]rondelane to 0.9% for [8]rondelane (Table 1). In comparison to the value for a linear rondelane (0.8%) with an interunit dihedral of 180° (designated open [3]rondelane) this might indicate a higher degree of delocalization and therefore a weak homoaromatic character.

The composition C_nH_{2n} of the rondelanes is identical with the homoconjugated annulenes and thus [3]rondelane is related to tris-homobenzene (*cis* annelation of three cyclopropane rings) with the six π-electrons fulfilling the Hückel rule $[4n + 2]$ for aromatic systems [3,4], and to the trannulenes [6,7]. Recently, neutral tris-homoaromaticity [1] was suggested for tris(bismethano)benzene after a long period of controversy [21] whereas the parent tris-homobenzene was not found to be homoaromatic [22]. Strain partially counteracts the stabilizing effects from electron delocalization via homoconjugation and was found to be dominant for some derivatives of tris(bismethano)benzene, thus obscuring the homoaromaticity [21]. In order to evaluate the presence of electron delocalization in the rondelanes, we calculated stabilization effects, specifically asking the question: are the rondelanes – at least to some extent – aromatic? If so, [3]rondelane would be classified as neutral, tris-homoaromatic.

Keeping the above strain analysis in mind, a methodological problem occurs, since at least for the lower order members of the series, the major effects of strain must be distinguished from the possibly smaller effects of homoaromaticity.

Additionally, this energetic criterion is highly dependent on the reference compound chosen. The calculated aromatic stabilization energy of benzene exhibits differences up to 50 kcal/mol due to referencing and choice of reaction type [2]. Therefore, we used the homodesmotic reaction type II of Scheme 1 to calculate the homoaromatic stabilization energy (HASE).

For the linear reaction products on the right side of Scheme 1 we assumed negligible strain except the cyclopropane ring strain itself which is cancelled in the reactions since the same number cyclopropanes occurs on both sides.

According to reaction type II, [3]rondelane and [7]rondelane might be considered as homoaromatic, with homoaromatic stabilization energies (HASE) of 2.3 kcal/mol and 2.2 kcal/mol, respectively (Table 2). Larger basis sets were tested for [3]rondelane. In the case of compounds with bond angle distortions such as cyclopropanes, it is important to add polarization functions to allow the system to build deformed bonds [1,23]. Additionally, electron correlation has to be taken into account which is properly done with the B3LYP functional [24]. The larger basis sets resulted in homoaromatic stabilization energies (HASE) in the range 2.4–2.6 kcal/mol (see Supplementary information). These values should be seen as lower limits for stabilization since the negative values for [4] and [5]rondelane show that the destabilizing strain is partly overcome in [3]rondelane. However, the alternating stabilization/destabilization pattern expected from the Hückel rule could not be found for the investigated series of rondelanes. Moreover, the calculated stabilization energies are much smaller than the σ-aromatic stabilization of cyclopropane (11.3 kcal/mol) [25].

In the next step, the magnetic criterion of aromaticity was applied using Nucleus-Independent-Chemical-Shift (NICS) values [12,13]. To avoid contact to protons of type H_b (or H_c) and to decrease the influence of σ-electrons, the probe was positioned 1.28 Å above the ring center. In the series of rondelanes going from [3] to [8], the NICS values increased from −2.54, −0.38, +0.41, +0.68, +0.83 to

Table 2
Thermochemical reactions of [*N*]rondelane (in kcal/mol)

	STE (type I)	HASE (type II)
[3]Rondelane	−106.0	+2.3
[4]Rondelane	−59.2	−15.1
[5]Rondelane	−33.0	−15.3
[6]Rondelane	−18.8	−3.7
[7]Rondelane	−11.1	+2.2
[8]Rondelane	−6.8	+1.0

Table 3
Calculated structural data (bond length r in Å, bond angle a and bond bending in °) of [N]rondelanes and open [N]rondelanes

	[3]Rondelane	[4]Rondelane	[5]Rondelane	[6]Rondelane	[7]Rondelane	[8]Rondelane	Open [3]rondelane	Open [7]rondelane
$r(C_a—C_b)$	1.502	1.508	1.503	1.501	1.501	1.503	1.499	1.499
$r(C_b—C_c)$	1.584	1.528	1.521	1.518	1.516	1.514	1.514	1.514
$r(C_b—C_d)$	1.521	1.520	1.517	1.515	1.514	1.514	1.513	1.514
$r(C_b—H_b)$	1.090	1.091	1.091	1.091	1.091	1.091	1.091	1.091
$r(C_c—H_c)$	1.090	1.091	1.091	1.091	1.091	1.091	1.091	1.091
$r(C_d—H_{d1})$	1.089	1.088	1.088	1.088	1.088	1.087	1.088	1.088
Size of cyclopropane ring	4.626	4.568	4.554	4.548	4.545	4.540	4.540	4.541
$a(C_a—C_b—C_c)$	104.3	112.8	116.7	118.8	119.9	121.8	121.0	120.9
$a(C_a—C_b—C_d)$	142.9	138.2	132.8	128.7	125.6	125.0	120.8	121.0
$a(C_b—C_d—H_{d1})$	122.7	121.5	120.3	119.4	118.8	118.2	118.0	118.0
$a(C_c—C_d—H_{d1})$	133.7	115.3	116.2	116.9	117.4	117.4	118.3	118.3
$a(H_{d1}—C_d—H_{d2})$	113.0	113.5	113.7	113.9	114.1	114.1	113.9	114.0
$a(C_d—C_b—H_b)$	106.6	109.2	111.2	112.5	113.5	114.1	115.6	115.4
$a(C_c—C_b—H_b)$	110.3	111.6	112.7	113.4	114.1	113.1	115.3	115.3
$a(C_a—C_b—H_b)$	110.4	111.2	112.2	112.9	113.5	112.9	113.9	114.0
Bond bending $C_a—C_b$	19.3	12.6	7.9	4.9	2.8	1.5	1.3	1.2
Bond bending $C_b—C_c$	18.2	19.7	21.4	22.4	23.0	23.5	23.8	23.8
Bond bending $C_b—C_d$	24.0	24.4	24.1	23.9	23.8	23.8	23.9	23.8

+0.96. Since non-aromatic compounds also exhibit NICS values different from zero, there is no magnetic indication of aromaticity for the larger rondelanes. However, [3]rondelane shows a NICS value at 1.28 Å of −2.54 which should be compared to −10.2 and −7.6 for benzene at 1.0 Å and 1.5 Å, respectively [13].

As a last criterion structural data were investigated since these are directly linked to experimental data. Cyclopropane has been an ideal candidate for this type of research since its discovery in 1884 [26]. Being the centrepiece in the development of concepts such as σ-delocalization (surface delocalization), σ-aromaticity, homoaromaticity and strain [25,27–30] the rondelanes should also be useful test compounds. As structural basis, the bond lengths and bond angles of the rondelanes and the open chain analogues (designated open [N]rondelane) are listed in Table 3.

The general trend going from smaller to larger macrocyclic ring systems is the shortening of the cyclopropane bonds $C_b—C_c/C_b—C_d$ bonds, until they reach the typical values for the open rondelanes (1.513 Å). This is further illustrated by the decreasing ring size (sum of C—C distances of the cyclopropane ring). The stretching of a C—C bond affords less energy than comparable shortening [31] and consequently, the lower order rondelanes achieve their stabilization with increased bond lengths of the cyclopropane units. The annelation of cyclopropane ring systems distorts the central cyclohexane ring of [3]rondelane (Fig. 2). The cyclopropane rings bend the typical dihedral angle of −60° in cyclohexane to −71.8° (dihedral of $C_a—C_b—C_c—C_e$) in [3]rondelane. The orientation of the skewed cyclopropane rings is controlled by the configuration – and hence related to the helicity – for the present series M (Fig. 2). Strengthening of the $C_a—C_b$ bond, with concurrent weakening of the $C_b—C_c$ bond, is reflected by

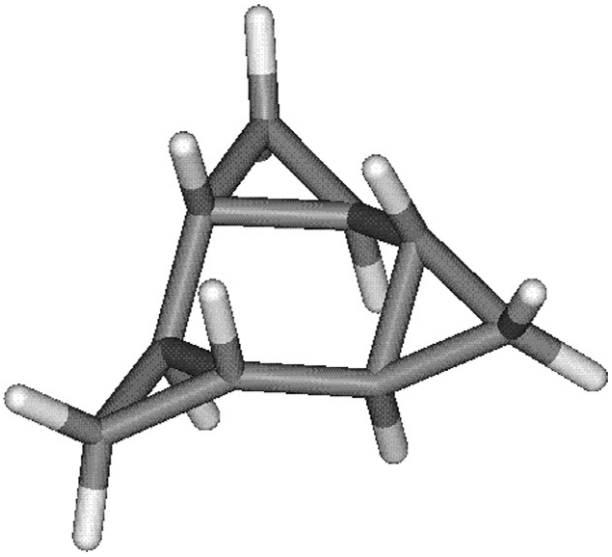

Fig. 2. Geometry optimized (B3LYP/6-31G(d)) structure of [3]rondelane.

the increased bond order (BO $C_a—C_b = 1.0343$, Table 1). This type of interaction resembles the electron conjugation in *s-trans* butadiene. The observed bond alternation is reversed compared to the open rondelanes. This in itself does not exclude homoaromaticity, since a number of compounds are known such as annulene [18] to show bond alternation while being aromatic with a delocalized electron distribution [32]. The bond bending, which shows the deviation from the nuclei-connecting line, was calculated within the NBO analysis. As shown in Table 3, the deviation from the nuclei-connecting line is substantially in [3]rondelane, which correlates with a bond angle of 104.25° ($C_a—C_b—C_c$) for the macrocyclic inner ring carbons. A substantial bond bending ($C_a—C_b$ of 19.3° for

[3]rondelane) is needed for the small rondelanes to retain bonding under geometrically unfavourable conditions.

4. Conclusions

The preparation of [3]rondelane will require the embedding into a stabilizing framework such as fullerenes for [18]trannulene. Higher homologues could be synthesized since the strain decreases substantially with larger ring size.

We have found indications for homoconjugation (bond lengths indicative of C=C bonds, increased percentages of non-Lewis valence electrons, energetic stabilization for [3]rondelane and [7]), but since other features are missing (e.g. no Hückel pattern of energetic stabilization, no planar ring system, which was found to be a prerequisite in the case of cyclooctatetraene[32]), only [3]rondelane seems to be a candidate for neutral homoaromaticity.

Acknowledgements

This work was supported by the Max-Planck Society and the DFG (SFB 416). We gratefully acknowledge the support of Prof. Griesinger and the inspiring ideas of F. Wetter.

Appendix A. Supplementary data

Supplementary data associated with this article can be found, in the online version, at doi:10.1016/j.theochem.2007.06.008.

References

[1] R.V. Williams, Chem. Rev. 101 (2001) 1185.
[2] M.K. Cyrański, Chem. Rev. 105 (2005) 3773.
[3] J. Spanget-Larsen, R. Gleiter, Angew. Chem. Int. Ed. 17 (1978) 441.
[4] W. Spielmann, D. Kaufmann, A. de Meijere, 17 (1978) 440.
[5] (a) G. Person, M. Keller, H. Prinzbach, Liebigs Ann. (1996) 967; (b) C. Rücker, H. Müller-Bötticher, W.-D. Braschwitz, H. Prinzbach, U. Reifenstahl, H. Irngartinger, Liebigs Ann./Recl. (1997) 967.
[6] A.A. Fokin, H. Jiao, P.v.R. Schleyer, J. Am. Chem. Soc. 120 (1998) 9364.
[7] G.A. Burley, Angew. Chem. Int. Ed. 44 (2005) 3176.
[8] M.J. Frisch et al., Gaussian 03, Gaussian, Inc., Pittsburgh, PA, 2003.
[9] A.D. Becke, J. Chem. Phys. 98 (1993) 5648.
[10] C. Lee, W. Yang, R.G. Parr, Phys. Rev. B. 37 (1988) 785.
[11] E.D. Glendening, A.E. Reed, J.E. Carpenter, F. Weinhold, F. NBO Version 3.1.
[12] P.v.R. Schleyer, C. Maerker, A. Dransfeld, H. Jiao, N.J.R. van Eikema Hommes, J. Am. Chem. Soc. 118 (1996) 6317.
[13] Z. Chen, C.S. Wannere, C. Corminboeuf, R. Puchta, P.v.R. Schleyer, Chem. Rev. 105 (2005) 3842.
[14] A.G.M. Barrett, R.A. James, G.E. Morton, P.A. Procopiou, C. Boehme, A. de Meijere, C. Griesinger, U.M. Reinscheid, J. Org. Chem. 71 (2006) 2756.
[15] A.G.M. Barrett, D. Hamprecht, R.A. James, M. Ohkubo, P.A. Procopiou, M.A. Toledo, A.J.P. White, D.J. Williams, J. Org. Chem. 66 (2001) 2187.
[16] P.G. Gassman, J. Chem. Soc. Chem. Commun. (1967) 793.
[17] A.G.M. Barrett, Personal Communication.
[18] E.L. Eliel, S.H. Wilen, Basic Organic Stereochemistry, Wiley, New York, 2001.
[19] X.-W. Wei, A.D. Darwish, O.V. Boltalina, P.B. Hitchcock, J.M. Street, R. Taylor, Angew. Chem. Int. Ed. 40 (2001) 2989.
[20] G.A. Burley, P.W. Fowler, A. Soncini, J.P.B. Sandall, R. Taylor, Chem. Commun. (2003) 3024.
[21] F. Stahl, P.v.R. Schleyer, H. Jiao, H.F. Schaefer III, K.-H. Chen, N.L. Allinger, J. Org. Chem. 67 (2002) 6599.
[22] R.V. Williams, H.A. Kurtz, Adv. Phys. Org. Chem. 29 (1994) 273.
[23] I.N. Levine, Quantum Chemistry, Prentice Hall, NJ, 2000.
[24] M. Nendel, K.N. Houk, L.M. Tolbert, E. Vogel, H. Jiao, P.v.R. Schleyer, Angew. Chem. Int. Ed. 36 (1997) 748.
[25] K. Exner, P.v.R. Schleyer, J. Phys. Chem. A 105 (2001) 3407.
[26] A. de Meijere, S.I. Kozhushkov, A.A. Fokin, I. Emme, S. Redlich, P.R. Schreiner, Pure Appl. Chem. 75 (2003) 549.
[27] D. Cremer, J. Gauss, J. Am. Chem. Soc. 108 (1986) 7467.
[28] J. Gauss, D. Cremer, J.F. Stanton, J. Phys. Chem. A 104 (2000) 1319.
[29] B. Rozsondai, in: Z. Rappoport (Ed.), The Chemistry of the Cyclopropyl Group, vol. 2, Wiley & Sons, Chichester, UK, 1995 (Chapter 3).
[30] D. Cremer, E. Kraka, K.J. Szabo, in: Z. Rappoport (Ed.), The Chemistry of the Cyclopropyl Group, vol. 2, Wiley & Sons, Chichester, UK, 1995 (Chapter 2).
[31] C.S. Wannere, K.W. Sattelmeyer, H.F. Schaefer III, P.v.R. Schleyer, Angew. Chem. Int. Ed. 43 (2004) 4200.
[32] P.W. Fowler, R.W.A. Havenith, L.W. Jenneskens, A. Soncini, E. Steiner, Angew. Chem. 114 (2002) 1628.

Supplementary information

Calculated energies for [N]rondelanes, [N-1]rondelanes, [N-2]rondelanes, cyclopropane and benzene. No imaginary frequencies were found unless indicated.

Table S1:

Calculated energies (zero point energy (ZPE), sum of electronic and zero point energy, SZPE) of bicyclopropyl in hartree (B3LYP/6-31G(d)) at different conformations (H_a-C_a-C_b-H_b)

dihedral/ energies	0° (1 imag. freq.)	30 (0 imag. freq.)	60° (0 imag. freq.)	90° (0 imag. freq.)	120° (1 imag. freq.)	150° (0 imag. freq.)	180° (0 imag. freq.)
ZPE	0.14468	0.144746	0.144853	0.144787	0.144531	0.144462	0.144604
SZPE	-234.442089	-234.446150	-234.448377	-234.447292	-234.44600	-234.447302	-234.448636

Table S2:

Calculated energies (zero point energy (ZPE), sum of electronic and zero point energy, SZPE) of [N]rondelanes in hartree (B3LYP/6-31G(d))

rondelane/ energies	[3]rondelane	[4]rondelane	[5]rondelane	[6]rondelane	[7]rondelane	[8]rondelane
ZPE	0.186248	0.250433	0.313209	0.375495	0.437515	0.500231
SZPE	-349.737440	-466.447405	-583.12460	-699.783011	-816.430685	-933.073195

Table S3:

Calculated energies (zero point energy (ZPE), sum of electronic and zero point energy, SZPE) of [N-1]rondelanes in hartree (B3LYP/6-31G(d))

rondelane/ energies	[3-1]rondelane	[4-1]rondelane	[5-1]rondelane	[6-1]rondelane	[7-1]rondelane	[8-1]rondelane
ZPE	0.181498	0.245197	0.307560	0.369776	0.432497	0.495094
SZPE	-311.730352	-428.417226	-545.077584	-661.723925	-778.365789	-895.008259

Table S4:

Calculated energies (zero point energy (ZPE), sum of electronic and zero point energy, SZPE) of [N-2]rondelanes in hartree (B3LYP/6-31G(d))

rondelane/ energies	[3-2]rondelane	[4-2]rondelane	[5-2]rondelane	[6-2]rondelane	[7-2]rondelane	[8-2]rondelane
ZPE	0.176390	0.239674	0.302059	0.364987	0.427107	0.489943
SZPE	-273.726970	-390.363153	-507.006145	-623.658989	-740.304461	-856.944901

Table S5:

Calculated energies (zero point energy (ZPE), sum of electronic and zero point energy, SZPE) of cyclopropane and benzene in hartree (B3LYP/6-31G(d))

compound/ energies	cyclopropane	benzene
ZPE	0.081779	0.100768
SZPE	-117.813425	-232.14788

Table S6:

Calculated energies (zero point energy (ZPE), sum of electronic and zero point energy, SZPE) of [3]rondelane in hartree with different basis sets

rondelane/ energies	6-311G(d)	6-311G(d,p)	6-311G(2d,p)	6-311G++(2d,p)
ZPE	0.184764	0.184229	0.184232	0.183933
SZPE	-349.807637	-349.826354	-349.833149	-349.835864

Table S7:

Calculated energies (zero point energy (ZPE), sum of electronic and zero point energy, SZPE) of [3-1]rondelane in hartree with different basis sets

rondelane/ energies	6-311G(d)	6-311G(d,p)	6-311G(2d,p)	6-311G++(2d,p)
ZPE	0.180321	0.179746	0.179786	0.179612
SZPE	-311.793528	-311.811333	-311.817361	-311.819387

Table S8:

Calculated energies (zero point energy (ZPE), sum of electronic and zero point energy, SZPE) of [3-2]rondelane in hartree with different basis sets

rondelane/ energies	6-311G(d)	6-311G(d,p)	6-311G(2d,p)	6-311G++(2d,p)
ZPE	0.175300	0.174708	0.174766	0.174621
SZPE	-273.783377	-273.800083	-273.805559	-273.807048

DOI: 10.1002/ejoc.200500878

^{13}C Chemical Shifts and $^{1}J_{CH}$ Coupling Constants of Cytidine at Different χ Dihedrals Based on DFT Calculations

Jörg T. Fischer[a] and Uwe M. Reinscheid*[a]

Keywords: ^{13}C chemical shift / ^{1}J coupling constant / Quantum chemistry / Density functional calculations / Conformation analysis / Cytidine

A molecular dynamic simulation of cytidine reproduced the dominating ^{3}E-*endo*, the so-called North conformation of the sugar and the *anti* base orientation with $\chi = -120°$. Taken as starting structures for a geometry optimisation, ^{13}C chemical shifts and ^{1}J coupling constants were calculated by DFT [functional: B3LYP, basis set: 6-31G(d,p)]. As for the first time no minimal structural model was used, the results can be interpreted without further approximations except solvent dependence which was not included. The influence of the glycosidic torsion angle was studied. The ^{13}C chemical shifts correlated with a North conformation of the sugar independent of the base orientation when using an empirically derived coordinate analysis. However, the $^{1}J_{CH}$ coupling constants and ^{13}C chemical shifts clearly showed a dependence on the glycosidic torsion which enables the identification of χ. The $^{1}J_{CH}$ analysis showed that the sugar pucker is not the major determinant for $^{1}J_{C1'H1'}$. Instead, the base orientation caused major changes, with a maximal difference of 14 Hz. Additionally, $^{1}J_{C2'H2'}$, $^{1}J_{C3'H3'}$ and $^{1}J_{C4'H4'}$ are differently influenced by the glycosidic torsion which can be exploited for assigning χ. Analysis of electrostatic and steric effects showed that an isolated view is not able to explain all NMR spectroscopic data but gives some useful ideas. A higher charge on C3′ and the $^{1}J_{C6H6}$ coupling constants were explained by through-space effects. Depending on the glycosidic torsion, the base non-planarity changes substantially. The results clearly show that also for ribonucleotides ^{13}C chemical shifts and $^{1}J_{CH}$ coupling constants are dependent on the base orientation which was questioned in the past.

Introduction

A number of biological functions of RNA and nucleotide analogues are related to inherent structural flexibility, e.g. the puckering of the ribose and the orientation of the base through the glycosidic linkage, which have been studied in the past by NMR spectroscopy.[1] Four conformational parameters are required to define the shape of a nucleoside:[2] i. the glycosidic torsion angle χ which determines the *syn* (+60°) or *anti* (–120°) orientation of the base relative to the sugar; ii. the torsion angle γ; iii. the pseudorotation phase angle, *P*, which is 140°–180° around the C-2′-*endo* conformation, the so-called South conformation, and 0°–40° around the C-3′-*endo* conformation, the so-called North conformation; iv. the puckering amplitude ν_{max} = falling mainly in the range of 30°–45°. For the majority of nucleosides, the value of *P* normally falls in a tight range in the vicinity of either one of the North or South extremes. In solution, the two conformations are in a rapid dynamic equilibrium dictated by the balance of stereoelectronic effects, which are in turn influenced by the electronegativity, ionisation state, steric bulk, and relative stereochemistry.

The key for a better operational understanding lies in a thorough description of the factors governing this mobility. To this end quantum mechanical calculations of derivatives of the smallest units, the four bases, were performed due to experimental and computational limitations.[3,4] Consequently, results derived from these studies have to be interpreted cautiously when dealing with experimental results of native RNA bases. To overcome these difficulties we focus in this report on the genuine nucleoside cytidine and its structural features with special emphasis on the torsional angle χ between C1′ of the ribose and N1 of the base. We present calculated data of ^{13}C chemical shifts and $^{1}J_{CH}$ coupling constants of cytidine in relation to rotation of the pyrimidine base.

Results and Discussion

In a molecular dynamics approach, models of cytidine with three values of ν_{max} were built (30°, 38° and 45°). The chemical formula of cytidine is shown in Figure 1. After minimisation no differences in the location of the energy minima were observed. The DFT calculations were then performed with a structural model of the North conformation (energy minimum) derived from ν_{max} = 38° with only one geometrical constraint for the sugar (C4′–O–C1′–C2′

[a] Max-Planck Institute of Biophysical Chemistry, Department of NMR-based Structural Biology,
Am Fassberg 11, 37077 Göttingen, Germany
Fax: +49-551-201-2202
E-mail: urei@nmr.mpibpc.mpg.de

was set to 0°). A structure of cytidine in the North conformation with a χ dihedral of –120° is shown in Figure 2.

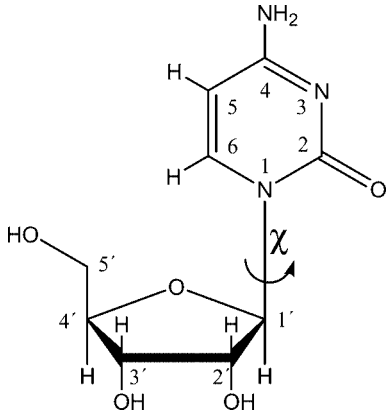

Figure 1. Chemical formula of cytidine. Base torsional angle χ is defined according to Wijmenga et al.[2] as O4′–C1′–N1–C2.

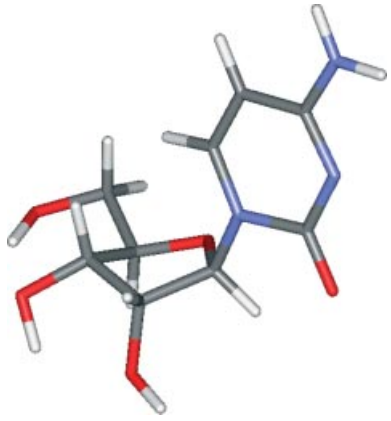

Figure 2. Structure of cytidine in the North conformation and *anti* (χ = –120°) glycosidic orientation of the base.

The importance of a careful treatment of the geometrical data was illustrated by Cloran.[6] During geometry optimisation in their computational study on 2-deoxy-β-D-ribofuranosylamine and analogues spontaneous bond rotations occurred to yield final structures different from starting structures. Consequently, an additional structural constraint was added to fix the desired envelope form. This in turn might influence the geometrical data and subsequently the calculated NMR spectroscopic data (vide infra). The same study showed that conformational preferences and energy barriers to pseudorotation were affected by changes in the C1′ substitution. This clearly advocated the analysis of natural RNA bases instead of model compounds.

The crystal structure of cytidine[7] showed a North conformation, a ν_{max} = of 38.7°, χ of 18.4° and for the hydroxymethyl group a *gg* orientation which is in agreement with the modelling. Similarly, the global energy minimum of methyl β-D-ribofuranoside was assigned to the North conformation.[4] The South conformer was found as a local minimum, 2.4 kcal/mol higher in energy. The east barrier (P = 90°) was estimated 3.7 kcal/mol and the west barrier (P = –90°) 4.4 kcal/mol.[8] In agreement, we found that the North conformer of cytidine is energetically more stable than the South conformer with the same base torsional angle of –120° (Table 1). The local minimum with χ of +60° is only reached by higher energy conformations at +110° and –145°.

In Table 1 the calculated ^{13}C chemical shifts of the North and South conformation of cytidine in relation to different glycosidic torsion angles are shown. First we analysed the reproduction of the North conformation.

^{13}C Chemical Shift and Sugar Pucker

The effects of sugar puckering on the C1′, C4′, and C5′ resonances of the North and South and C3′ ribose conformations were established by Harbison[9] based on empirical, structural, and NMR spectroscopic data. For the first canonical coordinate *can*1 > –6.25 ppm the sugar is in the North conformation, for *can*1 < –6.25 ppm, the sugar adopts a South conformation (*can*1 = 0.179·δC1′ – 0.225·δC4′ – 0.0585·δC5). In a subsequent study they conducted DFT calculations of the four conformations N-*anti*-*gg*, N-*anti*-*gt*, S-*anti*-*gg*, and S-*syn*-*gg* of a model pyrimidine-type base.[10] Computations yielded ^{13}C chemical shifts that were systematically different from experimentally derived values in the range from 4.23 to 6.17 ppm depending on the geometrical approach used. These authors again emphasised the need for geometry optimisation because differences in distances and angles influence the calculated chemical shifts. They concluded that unconstrained minimisation

Table 1. Calculated ^{13}C chemical shifts (in ppm) and relative energies of the North (N) and South (S) conformation of cytidine with restrained glycosidic torsion angles; experimental ^{13}C chemical shifts in ppm in DMSO as solvent.

χ/Atom	N60°	N110°	N180°	N–145°	N–120°	N–60°	S–120°	Experimental
C2	144.8	144.5	147.3	146.4	146.5	144.8	146.3	156.2
C4	152.0	151.4	153.1	151.9	151.7	151.8	150.8	166.4
C5	84.2	86.1	83.9	83.2	84.1	84.7	84.9	94.5
C6	137.5	140.2	134.1	134.8	136.6	133.0	135.5	142.3
C1′	101.2	97.0	93.6	90.8	88.1	91.0	88.6	90.0
C2′	82.5	75.2	75.6	76.8	78.6	75.3	73.9	74.7
C3′	76.1	79.3	76.5	77.4	79.5	79.0	78.2	70.1
C4′	80.8	77.7	80.0	78.0	79.9	79.3	84.6	84.7
C5′	60.8	63.1	64.0	63.3	65.1	64.3	65.6	61.3
Rel. energy[a]	4.5	5.5	7.3	11.4	0	25.1	4.9	–

[a] Relative energies (in kcal/mol) corresponds to the difference to the minimum energy for χ = –120° (absolute value in hartree = –886.061148).

of average crystal-structure coordinates with the B3LYP/6-31+G(d) method gives a reliable starting structure.

Applying an averaged systematic correction (subtraction of 5.2 ppm), our ^{13}C chemical shifts can be assigned to the North and South conformers and confirm the canonical coordinate analysis for the determination of the sugar pucker. For χ = –120° a borderline result is obtained that might be explained by a different approach (empirical vs. calculated, vide infra).

Preliminary ^{13}C data in relation to sugar pucker were presented by Case.[4] They found that the chemical shieldings of the C3′ and C5′ were the most sensitive to the sugar ring pucker. In contrast, our data for cytidine show that the C2′ resonance is sensitive to the sugar pucker and is deshielded by 4.7 ppm in the North conformation whereas C4′ is shielded by 4.7 ppm (Table 1). Furthermore, the C1′, C3′ and C5′ resonances are not much affected by pseudorotation. Additional correlations between sugar pucker and ^{13}C chemical shifts have been found by Tinoco.[11] A 5–6 ppm downfield shift of the C3′ resonance was attributed to a North to South conversion which is not observed in our calculations. The effect was explained by steric interaction between H3′ and O5′: repulsion of the σ-bonding electrons toward the carbon would increase the diamagnetic shielding.[12] It is known that steric strain produces significant shielding in the tensor component perpendicular to the plane of the strain but there is no simple model to quantify this effect.[13]

^{13}C Chemical Shifts and Glycosidic Torsion

In contrast to the large amount of correlation data between the sugar pucker and ^{13}C chemical shifts, at least for model compounds, the glycosidic torsion could not be determined from sugar ^{13}C chemical shift data only.[9] Prestegard[3] calculated a difference of 6 ppm between the two conformational minima (*syn* and *anti*) for a base carbon of a model compound. However, in our analysis of cytidine the calculated carbon chemical shifts and $^1J_{CH}$ coupling constants of the sugar clearly separate the two major conformations *syn* and *anti* around the glycosidic torsion angle (Table 1). The use of this information as a tool in the NMR structure elucidation of RNA and the structural evaluation of existent structural models requires the assignment of the sugar pucker as North conformer, which can be easily done with the above-mentioned analysis of Harbison.[9] A reason why a canonical coordinate for the base conformation was not established might be the different methods applied. Harbison[9] used experimental data of real molecules for which they tried to derive a correlation, whereas in our study the calculated NMR spectroscopic data were used.

Another possibility to derive conformational information is to study the temperature dependence of ^{13}C chemical shifts. In RNA oligomers C3′, C4′, and C5′ showed downfield shifts with increasing temperature.[14,15] This was explained by an increased population of the South conformer with increasing temperatures. C1′ chemical shifts were observed to move upfield with increasing temperature, while C2′ resonances were not affected much.[14,15] By analysing the ^{13}C chemical shifts of cytidine in D_2O, H_2O/D_2O mixture (90:10), H_2O-based phosphate buffer (50 mM, pH 6.7) and cryo mixtures of H_2O/DMSO (70:30) we could not verify this observation. The maximal temperature shift was +0.4 ppm going from 263 K to 298 K. Therefore, we expect no substantial influence on the sugar pucker populations in this temperature region and assign the major conformation to the North conformer.

$^1J_{CH}$ Coupling Constants and Sugar Pucker

In the analysis of cytidine and a model compound it was proposed that the sugar conformation is the major determinant of the $^1J_{C1'H1'}$ in nucleosides.[16] The measured $^1J_{C2'H2'}$ coupling constant (exp. value: 153.4 Hz) should increase with a quasi-equatorial orientation of the proton, which would correspond to the North conformation rather than the South conformation. Similarly, a larger $^1J_{C1'H1'}$ coupling constant (exp. value: 170.3 Hz) would indicate a preference for the North conformer. The calculated data for cytidine show these trends but indicate the influence of the χ dihedral on the $^1J_{CH}$ coupling constants (Table 2). In general, deviations of 10% between experimental and calculated ^1J coupling constants were observed for methyl α-D-xylopyranoside.[17] The difference of $^1J_{C1'H1'}$ coupling constants between purine and pyrimidine bases were attributed in ribonucleotides to a different preference of the North and South conformers.[16] In contrast, for the deoxyribonucleotides studied by Sklenár[18] it was found that only the bases itself are responsible for this difference and it was speculated that this also holds for ribonucleosides. The calculated $^1J_{C1'H1'}$ coupling constants of cytidine in the present study show that the sugar pucker is not the major factor favouring the hypothesis of Sklenár.[18]

Additionally, as several effects are operating in the flexible cytidine, only the sum of all can reproduce experimental data. As an example, a correlation for the $^1J_{CH}$ coupling constants was proposed:[19] $^1J_{CH} = -3432 + 182.2 q_C q_H + 3889/r_{CH}$.

where q_C and q_H are the total atomic charges on carbon and hydrogen from Mulliken population analysis, and r_{CH} is the C–H bond length. Using this formula and the calculated values (Table 3 and Table 4) one obtains for χ = +60°, –120° and –60° $^1J_{C1'H1'}$ coupling constants constants of 125.3 Hz, 139.6 Hz, and 144.2 Hz, respectively. All deviate substantially from the calculated and experimental values indicating that charge and bond length of the directly involved atoms is not sufficient to obtain good ^1J correlations and/or the parametrisation has to be changed for the specific molecule. The latter seems to be appropriate for cytidine. The inclusion of solvent might influence atomic charges due to specific interactions and/or global electrostatic interactions. In a study on Schiff base models using the simple COSMO model of solvent simulation, different

Table 2. Calculated sugar carbon $^{1}J_{CH}$ coupling constants of cytidine with restrained glycosidic torsion angles, experimental $^{1}J_{CH}$ coupling constants in DMSO as solvent.

χ/Atom pair	N60°	N110°	N180°	N–145°	N–120°	N–60°	S–120°	Experimental
C5–H5	143.3	143.4	143.4	143.4	143.2	143.5	146.5	172.4
C6–H6	150.0	153.3	155.3	153.4	150.2	146.7	153.9	180.1
C1′-H1′	164.2	170.3	178.3	175.1	169.5	175.7	169.2	169.0
C2′-H2′	157.3	170.1	159.2	155.2	152.1	154.8	158.1	147.5
C3′-H3′	167.1	163.6	155.5	154.4	152.3	154.3	162.8	146.5
C4′-H4′	150.5	151.7	159.8	159.7	159.1	153.6	155.3	142.4

Table 3. Calculated Mulliken charges of selected atoms with restrained glycosidic torsion angles.

χ/Atom	N60°	N110°	N180°	N–145°	N–120°	N–60°	S–120°
C4′	–0.025	–0.032	–0.017	–0.019	–0.014	–0.023	–0.041
H4′	0.178	0.178	0.228	0.228	0.223	0.186	0.203
O4′	–0.475	–0.484	–0.489	–0.482	–0.476	–0.457	–0.480
C3′	–0.186	0.001	0.002	0.003	0.001	0.002	–0.040
H3′	0.276	0.255	0.229	0.226	0.226	0.225	0.251
O3′	–0.556	–0.551	–0.552	–0.552	–0.553	–0.549	–0.541
C2′	–0.052	–0.073	–0.054	–0.036	–0.042	–0.077	0.014
H2′	0.239	0.274	0.245	0.224	0.216	0.231	0.211
O2′	–0.540	–0.545	–0.563	–0.562	–0.559	–0.544	–0.554
OH2′	0.353	0.351	0.372	0.373	0.371	0.367	0.341
C1′	0.243	0.233	0.262	0.241	0.226	0.242	0.230
H1′	0.210	0.224	0.244	0.253	0.258	0.254	0.237
N1	–0.728	–0.731	–0.742	–0.738	–0.734	–0.738	–0.741
C2	0.833	0.827	0.823	0.816	0.813	0.826	0.825
O2	–0.503	–0.512	–0.540	–0.524	–0.508	–0.497	–0.505
N3	–0.659	–0.658	–0.662	–0.663	–0.663	–0.665	–0.664
C5	–0.287	–0.291	–0.291	–0.291	–0.289	–0.281	–0.293
C6	0.179	0.193	0.171	0.177	0.181	0.170	0.232
H5	0.188	0.189	0.185	0.185	0.187	0.187	0.182
H6	0.233	0.245	0.258	0.247	0.242	0.232	0.232

Table 4. Calculated bond lengths [Å] of cytidine with restrained glycosidic torsion angles.

χ/ Bonds	N60°	N110°	N180°	N–145°	N–120°	N–60°	S–120°
C5′–C4′	1.5218	1.5233	1.5212	1.5216	1.5223	1.5229	1.5342
C4′–O4′	1.4764	1.4727	1.4803	1.4799	1.4742	1.4699	1.4807
C4′–C3′	1.5461	1.5423	1.5374	1.5417	1.5429	1.5406	1.5286
O4′–C1′	1.4526	1.4808	1.4618	1.4633	1.4697	1.4837	1.4793
C3′–H3′	1.0848	1.0892	1.0921	1.0923	1.0921	1.0925	1.0879
C3′–O3′	1.4496	1.4513	1.4518	1.4508	1.4504	1.4486	1.4744
C3′–C2′	1.534	1.5323	1.5313	1.5346	1.5361	1.5385	1.5464
C2′–C1′	1.5522	1.5457	1.5495	1.5437	1.5443	1.5384	1.5511
C1′–H1′	1.0961	1.095	1.0914	1.0907	1.0921	1.0907	1.0932
C1′–N1′	1.4794	1.4742	1.4825	1.4727	1.4655	1.4674	1.4495
N1–C2	1.4642	1.4591	1.451	1.4605	1.4719	1.4803	1.4685
N1–C6	1.3715	1.3738	1.3612	1.3627	1.3667	1.3688	1.3643
C2–N3	1.3712	1.3694	1.3659	1.3677	1.3687	1.3711	1.3712
C5–C6	1.3554	1.3553	1.3599	1.3585	1.3564	1.3565	1.3565

ε values did not influence the calculated charges justifying our gas-phase approach.[20] Although inappropriate taken alone, atomic charges are helpful in explaining conformational preferences as can be shown for the increased negative charge on C3′ of –0.186 at χ = +60° (Table 3).

Chattopadhyaya[21] investigated the electronic transmission from a purine base to the backbone torsions in nucleotides. On protonation of the base, the North conformation is favoured. A decreased *gauche* effect between $\sigma_{C3'H3'}$ and $\sigma^*_{C4'O4'}$ leaves more electron density at the C3′ atom (Figure 3A). In the present study on cytidine the high negative charge of C3′ for the χ = +60° conformer cannot be simply related to the north conformation because this was held constant. Furthermore, the $\sigma_{C3'H3'}$ and $\sigma^*_{C4'O4'}$ interaction is geometrically not changed during rotation around the glycosidic angle. The high positive charge of H3′ (+0.2764) might therefore indicate the influence of O2 on the C3′–H3′ bond (vide infra). The decreased bond length corresponds to a high $^{1}J_{C3'H3'}$ coupling constant (N60°: 167.1 Hz, Table 2).

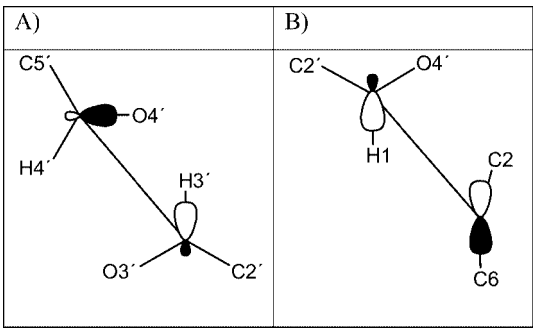

Figure 3. Newman projections of the (A) $\sigma_{C3'H3'}$ and $\sigma^*_{C4'O4'}$ interaction of the North conformer with χ = +60°, and (B) $\sigma_{C1'H1'} \rightarrow \pi^*_{N1C6}$ interaction of the North conformer with χ = –60°.

$^1J_{CH}$ Coupling Constants and χ Torsion

Serianni[16] suggested that the $^1J_{C1'H1'}$ coupling constants are unaffected by N-glycosidic torsion. It was speculated that bond length and orientation influences the $^1J_{C1'H1'}$ coupling. This was tested with a model compound with constrained sugar pucker. Rotation of the χ torsion resulted in a small change of 0.8 Hz in $^1J_{C1'H1'}$. The molecular size of the model compound limited the calculations to the HF level of theory. In contrast, Davies[22] had found a strong dependence on the χ torsion for a cyclic pyrimidine nucleoside.

Supporting this view the $^1J_{C1'H1'}$ coupling constant as a function of χ could be reproduced by a generalized Karplus equation in the analysis of deoxyribonucleotides.[18] For this analysis, the SD (spin-dipolar) term was neglected for *J*-coupling calculations. In the present study, the ribonucleoside cytidine also shows a strong dependence of the $^1J_{C1'H1'}$ coupling on the glycosidic torsion (Table 2) which is in contrast to Serianni.[16]

The most important effect defining the angular dependence of one-bond carbon–proton coupling constants is their sensititivy to the lone-pair orientation belonging to an atom placed α to the C–H bond. The glycosidic nitrogen bears a lone pair perpendicular to the base plan (partially delocalised within the base) whose orientation with respect to the sugar is given by χ. For χ around +30° and –150° the overlap between n_{N1} and C1′–C2′ is maximized. Such hyperconjugative charge transfer into $\sigma^*_{C1'-C2'}$ weakens the C1′–C2′ bond and reduces the absolute value of other-bond contribution to $^1J_{C1'H1'}$. In our calculations the bond length C1′–C2′ for χ = +60° (1.5522 Å) is increased but not for χ = –145° (1.5437 Å) indicating that additional factors are relevant. Furthermore, the $\sigma_{C1'H1'} \rightarrow \pi^*_{N1C6}$ interaction with an overlap at a χ torsion around +60° would weaken the C1′–H1′ bond and its contribution to $^1J_{C1'H1'}$ (Figure 3, B). In agreement, the C1′–H1′ bond length in cytidine was found to be increased at a glycosidic torsion of +60° when compared with the other torsional angles (N60°: 1.0961 Å, N-145°: 1.0907 Å).

Recently, Cuevas[23] hypothesized that delocalisation is not the origin of the decreased $^1J_{CH}$ coupling constants found in cases of the Perlin effect. In their calculation of oxane and acyclic ethers the minimum $^1J_{CH}$ value occurred at an angle near 0°, when the C–H bond is not antiperiplanar to any lone pair of electrons contradicting the convential reasoning of hyperconjugative $n_O \rightarrow \sigma^*_{CH}$ delocalisation discussed above. They suggested a dipolar interaction with the electric field of the oxygen dipole polarizing the electron distribution in the C–H bond. This is supported by a charge distribution at the H atom that can better be correlated with a dipolar interaction than by a delocalisation. These dipolar effects might also operate for H6 of the cytidine base. A C–H·····O contact influencing the charge of the proton could explain the calculated $^1J_{C6H6}$ coupling constants (Table 2 and Table 3). The maximum (155.3 Hz) is found for χ = 180°, concomitantly with the highest positive charge on H6 (+0.258) and with H6 positioned near to O4′.

In addition to electrostatic data describing structural preferences, bond lengths also monitor steric factors. In the deoxyribonucleotides studied by Sklenár[18] a maximum of $r_{C1'H1'}$ vs. χ was found for the *syn* (+60° to +150°) and a minimum for the *anti* orientation (–135° to –105°). The difference between these two was 0.01 Å. As a comparison, the maximal bond-length difference between axial and equatorial C–H bonds in cyclohexane amounts to 0.002 Å, but becomes large for methylene groups adjacent to oxygen and nitrogen (in oxane: 0.011 Å, in azane: 0.013 Å).

For cytidine a maximum of 1.0961 Å was found for χ = +60°, in a region of repulsion between O4′ of the sugar and O2 of the base (Table 4). In contrast to the data of Sklenár[18] this trend reflected the $^1J_{C1'H1'}$ coupling constant dependence on $r_{C1'H1'}$.

Base Planarity and χ Torsion

In deoxyribonucleotides a base nonplanarity was observed in such a way that the N1–C6 bond was moved away

Table 5. Calculated dihedrals related to base planarity and hybridisation of C1′–N1 with restrained glycosidic torsion angles.

χ/Dihedral	N60°	N110°	N180°	N–145°	N–120°	N–60°	S–120°
C6–N1–C2–N3	1.3°	–6.9°	1.4°	5.9°	8.8°	1.8°	6.5°
C2–N1–C6–C5	1.3°	4.5°	–1.0°	–6.7°	–8.7°	–3.5°	–5.8°
N1–C2–N3–C4	–2.5°	4.8°	–0.9°	–1.7°	–3.7°	0.2°	–3.0°
C2–N3–C4–C5	1.1°	–0.3°	0.1°	–1.8°	–1.5°	–0.5°	–1.1°
N3–C4–C5–C6	1.6°	–2.4°	0.3°	1.2°	1.9°	–1.1°	2.1°
C4–C5–C6–N1	–2.7°	0.1°	0.2°	3.0°	3.3°	3.1°	1.5°
Sum of pos. ring dihedrals	5.3°	9.4°	2.0°	10.1°	14.0°	5.1°	10.1°
C1′–N1–C6–C5	172.6°	–179.6°	–179.1°	–174.0°	–171.8°	–166.9°	–177.6°
C1′–N1–C2–N3	–169.8°	177.6°	179.6°	174.1°	172.7°	166.8°	178.6°

from the C2′ atom.[18] The deviation from planar geometry increased for χ between –120° and –60° with decreasing H6–H2′ distance. A base nonplanarity of 8–9° with a χ torsion of –120° corresponded to $r_{H6H2'}$ = 2.4 Å. It was suggested that the driving force is the repulsion between H6 and H2′. In the present study of cytidine we found a different base planarity at different χ values (Table 5). The highest non-planarity was found for +60° and –60°, but in the opposite direction. The bending at χ = –60° can be explained by steric repulsion between H6 and H2′ and electrostatic repulsion between O2 and O4′ (Figure 4). However, for the +60° torsion we hypothesize electrostatic repulsion between O2 and the ring oxygen and steric repulsion between O2 and H3′. As a consequence the aromatic ring remains almost planar but the connecting bond C1′–N1 is bend in the direction of O4′. This is indicated by the low sum of positive ring dihedrals and the deviation from 180° for the hybridisation dihedrals φ_{hyb} (C1′–N1–C6–C5) and ξ_{hyb} (C1′–N1–C2–N3) (Table 5).

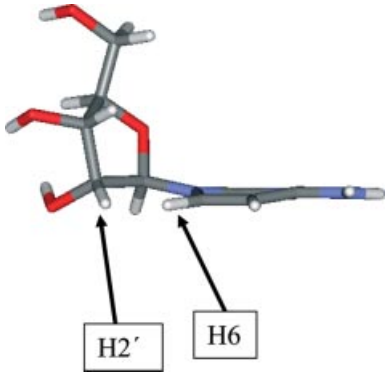

Figure 4. Base bending and repulsion of H6 and H2′ of cytidine in the North conformation with χ = –60°.

Conclusion

The calculated ^{13}C chemical shifts of cytidine correlated with a North conformation of the sugar. Moreover, the $^{1}J_{CH}$ coupling constants and ^{13}C chemical shifts clearly showed a dependence on the glycosidic torsion that enables the identification of χ. The $^{1}J_{CH}$ analysis revealed that the sugar pucker is not the major determinant for $^{1}J_{C1'H1'}$. Instead, the base orientation caused major changes, with a maximal difference of 14 Hz. The calculated base non-planarity gives an important view on the geometrical flexibility of the aromatic bases in RNA and protein-RNA complexes.

Experimental Section

Computational Methods: Molecular modelling of cytidine was done with "Discover" in the Insight program package (Accelrys™).[24] The puckering amplitude of the ribose was set at 30°, 38°, and 45°. Chemical shifts of ^{13}C (isotropic shielding) and $^{1}J_{CH}$ coupling constants (including all four contributions PSO: paramagnetic spin orbit, DSO: diamagnetic spin orbit, FC: Fermi contact and SD: spin dipole) were calculated by DFT methods for geometry optimised cytidine (Gaussian™).[5] The shifts are reported relative to the computed shielding for TMS (tetramethylsilane). The coupling constants are presented as total values of all four contributions. The B3LYP functional and a 6-31G(d,p) basis set[25] were used for geometry optimisation and calculation of NMR parameters. The sum of electronic and thermal free energy was calculated. Different sets of constraints were applied on the ribose dihedrals and the glycosidic torsion angle. One of the five ribose ring dihedrals was set at 0° in order to fix an envelope conformation.

NMR: Solutions of 5 mM and 50 mM cytidine were prepared with the following solvents: D_2O, H_2O/D_2O (90:10), H_2O/D_2O phosphate buffer (50 mM, pH = 6.7), H_2O/DMSO (70:30). ^{13}C NMR spectra were recorded at different temperatures with a Avance Bruker 400 spectrometer with standard techniques and a data size of 16 K. Standard ^{1}H-^{13}C-HSQC spectra without decoupling were performed to obtain $^{1}J_{CH}$ coupling constants.

Acknowledgments

We like to thank Prof. Griesinger for supporting this work. We gratefully acknowledge the help in preparing the manuscript by F. Wetter.

[1] C. W. Hilbers, S. S. Wijmenga, *Nucleic Acids: Spectra, Structures, & Dynamics*, in: Encyclopedia of nuclear magnetic resonance (Eds.: D. M. Grant, R. K. Harris), Wiley, Chichester, England, **1996**, 3346–3359.
[2] S. S. Wijmenga, B. N. M. van Buuren, *Prog. NMR Spectrosc.* **1998**, *32*, 287–387.
[3] R. Ghose, J. P. Marino, K. B. Wiberg, J. H. Prestegaard, *J. Am. Chem. Soc.* **1994**, *116*, 8827–8828.
[4] A. P. Dejaegere, D. A. Case, *J. Phys. Chem. A* **1998**, *102*, 5280–5289.
[5] M. J. Frisch, G. W. Trucks, H. B. Schlegel, G. E. Scuseria, M. A. Robb, J. R. Cheeseman, J. A. Montgomery Jr, T. Vreven, K. N. Kudin, J. C. Burant, J. M. Millam, S. S. Iyengar, J. Tomasi, V. Barone, B. Mennucci, M. Cossi, G. Scalmani, N. Rega, G. A. Petersson, H. Nakatsuji, M. Hada, M. Ehara, K. Toyota, R. Fukuda, J. Hasegawa, M. Ishida, T. Nakajima, Y. Honda, O. Kitao, H. Nakai, M. Klene, X. Li, J. E. Knox, H. P. Hratchian, J. B. Cross, C. Adamo, J. Jaramillo, R. Gomperts, R. E. Stratmann, O. Yazyev, A. J. Austin, R. Cammi, C. Pomelli, J. W. Ochterski, P. Y. Ayala, K. Morokuma, G. A. Voth, P. Salvador, J. J. Dannenberg, V. G. Zakrzewski, S. Dapprich, A. D. Daniels, M. C. Strain, O. Farkas, D. K. Malick, A. D. Rabuck, K. Raghavachari, J. B. Foresman, J. V. Ortiz, Q. Cui, A. G. Baboul, S. Clifford, J. Cioslowski, B. B. Stefanov, G. Liu, A. Liashenko, P. Piskorz, I. Komaromi, R. L. Martin, D. J. Fox, T. Keith, M. A. Al-Laham, C. Y. Peng, A. Nanayakkara, M. Challacombe, P. M. W. Gill, B. Johnson, W. Chen, M. W. Wong, C. Gonzalez, J. A. Pople, *Gaussian 03, Revision 6.0*, Gaussian, Inc., Pittsburgh PA, **2003**.
[6] F. Cloran, Y. Zhu, J. Osborn, I. Carmichael, A. S. Serianni, *J. Am. Chem. Soc.* **2000**, *122*, 6435–6448.
[7] S. Furberg, C. S. Peterson, C. Romming, *Acta Crystallogr., Sect. B* **1965**, *18*, 313.
[8] C. A. Podlasek, W. A. Stripe, I. Carmichael, M. Shang, B. Basu, A. S. Serianni, *J. Am. Chem. Soc.* **1996**, *118*, 1413–1425.
[9] M. Ebrahimi, P. Rossi, C. Rogers, G. S. Harbison, *J. Magn. Reson.* **2001**, *150*, 1–9.
[10] P. Rossi, G. S. Harbison, *J. Magn. Reson.* **2001**, *151*, 1–8.
[11] G. Varani, I. Tinoco, *J. Am. Chem. Soc.* **1991**, *113*, 9349–9354.
[12] R. A. Santos, P. Tang, G. S. Harbison, *Biochemistry* **1989**, *28*, 9372–9378.
[13] J. C. Facelli, *Concepts Magn. Reson.* **2004**, *20A*, 42–69.
[14] P. P. Lankhorst, C. Erkelens, C. A. G. Haasnoot, C. Altona, *Nucleic Acid Res.* **1983**, *11*, 7215–7230.

[15] M. P. Stone, S. A. Winkle, P. N. Borer, *J. Biomol. Struct. Dyn.* **1986**, *3*, 767–781.
[16] T. Bandyopadhyay, J. Wu, W. A. Stripe, I. Carmichael, A. S. Serianni, *J. Am. Chem. Soc.* **1997**, *119*, 1737–1744.
[17] O. L. Malkina, M. Hricovíni, F. Bízik, V. G. Malkin, *J. Phys. Chem. A* **2001**, *105*, 9188–9195.
[18] M. L. Munzarová, V. Sklenár, *J. Am. Chem. Soc.* **2003**, *125*, 3649–3658.
[19] S. Wolfe, B. M. Pinto, V. Varma, R. Y. N. Leung, *Can. J. Chem.* **1990**, *68*, 1051–1062.
[20] E. Tajkhorshid, S. Suhai, *Chem. Phys. Lett.* **1999**, *299*, 457–464.
[21] P. Acharya, A. Trifonova, C. Thibaudeau, A. Földesi, J. Chattopadhyaya, *Angew. Chem. Int. Ed.* **1999**, *38*, 3645–3650.
[22] D. B. Davies, M. MacCoss, S. S. Danyluk, *J. Chem. Soc., Chem. Commun.* **1984**, *6*, 536–538.
[23] G. Cuevas, K. Martínez-Mayorga, M. C. Fernández-Alonso, J. Jiménez-Barbero, C. L. Perrin, E. Juaristi, N. López-Mora, *Angew. Chem. Int. Ed.* **2005**, *44*, 2360–2364.
[24] Discover in the Insight program package (Accelrys™), version 2.98: P. Dauber-Osguthorpe, V. A. Roberts, D. J. Osguthorpe, J. Wolff, M. Genest, A. T. Hagler, *Proteins: Struct., Funct., Genet.* **1988**, *4*, 31–47.
[25] B3LYP functional and a 6-31G(d,p) basis set: A. Bagno, *Chem. Eur. J.* **2001**, *7*, 1652–1661.

Received: November 7, 2005
Published Online: February 24, 2006

ELSEVIER

Journal of Molecular Structure: THEOCHEM 767 (2006) 81–85

THEO CHEM

www.elsevier.com/locate/theochem

Interpretation of cytidine proton chemical shifts and J coupling constants calculated by DFT

J.T. Fischer [1], S.G. Wehner [1], U.M. Reinscheid *

Department of NMR-based Structural Biology, Max-Planck Institute of Biophysical Chemistry, Am Fassberg 11, 37077 Göttingen, Germany

Received 29 March 2006; received in revised form 28 April 2006; accepted 1 May 2006
Available online 12 May 2006

Abstract

With a DFT approach [B3LYP/6-31G(d,p)] the geometry of the ribonucleoside cytidine was optimized and NMR parameters (proton chemical shifts and *J* couplings) were calculated. Calculations of proton chemical shifts with varied base orientations of a North sugar conformer revealed a through-space effect between the OH2′ proton and the carbonyl oxygen of the base. The $^{3}J_{H1'C6}$ couplings were found to be similar for *trans* and *gauche* orientation of proton and carbon. This was rationalized by a NBO analysis of interaction energies between donor and acceptor natural bond orbitals. The different $^{3}J_{H1'C6}$ coupling constants upon rotation of the base could be correlated to the charge delocalization along the coupling pathway which was independent of the ribose conformation. The $^{1}J_{H6C6}$ and $^{1}J_{H1'C1'}$ coupling constants seem to be less dominated by the hybridization of the corresponding carbon atoms.

Keywords: ^{1}H chemical shift; J coupling constant; DFT; Conformation; Cytidine

1. Introduction

The nucleosides have been studied in the past by NMR methods which deliver means to evaluate the inherent structural flexibility [1]. At least the following four parameters are needed to describe the conformation: (1) the glycosidic torsion angle χ (O4′–C1′–N1–C2) which determines the *syn* (+60°) or *anti* (−120°) orientation of the base relative to the sugar; (2) the torsion angle γ; (3) the pseudorotation phase angle *P* which around the C-2′-endo conformation, the so called South conformation, amounts to 140–180°, and around the C-3′-endo conformation, the so-called North conformation, amounts to 0–40°; (4) the puckering amplitude ν_{max} falling mainly in the range of 30–45°. For the majority of nucleosides, the value of *P* normally falls in a tight range in the vicinity of either one of the North or South extremes. In solution, the two conformations are in a rapid dynamic equilibrium dictated by the balance of stereoelectronic effects, which are in turn influenced by the electronegativity, ionization state, steric bulk, and relative stereochemistry.

Apart from experimental approaches, a number of computations with mostly minimal models of ribonucleosides [2,3], or on deoxyribonucleosides lacking the OH2′ group have been performed [4,5]. Recently, calculated ^{13}C chemical shifts and $^{1}J_{CH}$ coupling constants for the full cytidine model were reported [6]. In extension to this report we now present calculated values of the conformational relevant *J* couplings and proton chemical shifts. With our NBO analysis [7], a number of hypotheses of the past can be substantiated with the genuine ribonucleoside cytidine.

2. Theoretical approach

Molecular dynamic simulations were done with Discover in the Insight program package using a CVFF forcefield (Accelrys™) and constant-temperature, constant-volume ensemble (NVT). The ribose puckering amplitude was set at 38°. One of the five ribose ring dihedrals (C4′–O4′–C1′–C2′) was set at 0° in order to fix an North or South sugar pucker (Fig. 1). Water as solvent was simulated with a dielectric constant ε of 78. The molecular structure was first minimized with a gradient criterion of less than 0.5 kcal/mol. A high temperature (600 K) molecular dynamic simulation yielded 100 conformers with high RMSD values. These served as starting structures for a simulated annealing protocol. The resulting starting molecules were heated to 600 K initially, subsequently cooled and finally, after a MD run for 10 ps at

* Corresponding author. Tel.: +49 551 201 2215; fax: +49 551 201 2202.
E-mail address: urei@nmr.mpibpc.mpg.de (U.M. Reinscheid).
[1] Contributed equally.

0166-1280/$ - see front matter © 2006 Elsevier B.V. All rights reserved.
doi:10.1016/j.theochem.2006.05.002

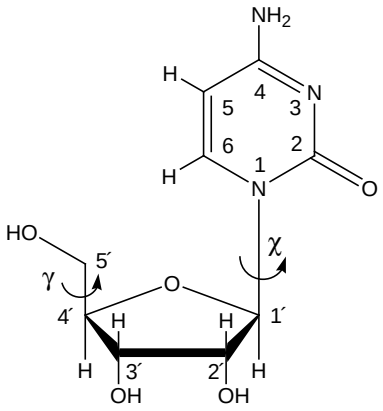

Fig. 1. Chemical formula of cytidine. Dihedral angles are indicated according to [1].

300 K, subjected to an energy minimization using both steepest descent and conjugate gradient methods successively. Hundred structures were sampled and the lowest in energy were taken representing different base orientations.

Chemical shifts of ^{1}H (isotropic shielding) and $^{3}J_{CH}$ coupling constants (including all four contributions PSO, DSO, FC and SD) were calculated by DFT methods for geometry optimized cytidine (Gaussian) [8]. The shifts are reported relative to the computed shielding for TMS at the same level of theory. The coupling constants are presented as total values of all four contributions. The B3LYP functional [9,10] and a 6-31G(d,p) basis set were used for geometry optimization and calculation of NMR parameters. Natural bond orbital (NBO) analysis [7] was performed to evaluate delocalization effects and charges for different glycosidic torsional angles (version 3.2 implemented in Gaussian, [8]).

3. Results and discussion

In the starting geometry for the MD simulations a ribose puckering amplitude of 38° ($\nu_{max}=38°$) was used. Atom numbering and two dihedrals of cytidine (γ and χ) are indicated in Fig. 1. The simulations were done with one geometrical constraint for the sugar (C4′–O4′–C1′–C2′ or C3′–C4′–O4′–C1′ were set to 0°) to obtain North and South conformers, respectively. The resulting North and South conformers of lowest energy were used for subsequent DFT calculations.

3.1. Proton chemical shifts and glycosidic torsion

When the glycosidic torsion is changed and no restraints for the OH dihedrals are applied, the OH2′ dihedral changes between two orientations: $-160°\pm8°$ and $-47°\pm9°$ which is reflected by the proton chemical shift of OH2′ (Table 1). Low ppm values correspond to the almost antiperiplanar orientation of the protons with the sugar in the North conformation (e.g. N60; δOH2′ = 1.44 ppm; OH2′ dihedral = −165.2°). A through-space contact between OH2′ proton and the carbonyl oxygen of the base is optimal with a base torsion of 180° and leads to a deshielding (δOH2′ = 3.03 ppm). The OH2′ proton plays an important role being the only difference between RNA and DNA backbone. Molecular dynamic simulations showed that only few orientations of the OH2′ dihedral are possible in RNA including the above mentioned [11]. The calculated proton chemical shifts can now be correlated with the different OH2′ orientations. For the North conformer the rotation of the base does not influence the OH3′ dihedral, which remains at $-153°\pm4°$, and the OH3′ proton chemical shift does not change significantly. With the same glycosidic torsion angle of −120° it is clearly seen that the South conformation influences the proton chemical shifts which relates to changed dihedrals of OH2′ and OH3′, +147° and +160°, respectively (Table 1). The chemical shifts of H1′, H2′and H3′ are most sensitive upon rotation around χ. Since in some cases (compare N60°, N110°, N-60°) the exocyclic OH2′ and OH3′ dihedrals are not influenced by the glycosidic torsion, the differences in proton chemical shifts are not solely due to a locally changed environment. A particular case is found for H1′.

For the North conformer with an *anti* orientation of the base the H1′ proton is deshielded (N-120°; δH1′ = 7.31 ppm) compared to the South conformer (δH1′ = 6.52 ppm) because the carbonyl oxygen of the base is in closest proximity to H1′. Atomic charge calculations within the NBO approach [7] indicate a charge dependence with the highest positive value

Table 1
Calculated proton chemical shifts, dihedrals and charges (NBO) of cytidine in the North (N) or South (S) conformation with restrained glycosidic torsion angles

χ/proton	N60°	N110°	N180°	N-145°	N-120°	N-60°	S-120°
H5	5.35	5.67	5.61	5.31	5.31	5.41	4.65
H6	7.22	7.53	8.08	7.54	7.46	7.24	7.02
H1′	5.14	5.17	5.7	6.54	7.31	6.55	6.52
H2′	4.39	6.31	5.72	4.27	4.21	4.45	3.92
OH2′	1.44	1.23	3.03	2.87	2.71	2.04	3.92
H3′	6.58	5.04	3.93	3.96	4.31	4.14	4.39
OH3′	3.73	4.37	4.83	4.83	4.84	4.55	1.29
H4′	3.99	3.89	4.51	4.87	4.6	4.01	3.48
Dihedral OH2′–H2′	−165.2°	−166.2°	−39.2°	−50.4°	−54.1°	−153.6°	147.8°
Dihedral OH3′–H3′	−152.0°	−150.1°	−157.3°	−157.6°	−157.9°	−156.2°	160.3°
Charge H1′	+0.260	+0.250	+0.269	+0.283	+0.292	+0.280	+0.276
Charge H6	+0.253	+0.260	+0.274	+0.251	+0.245	+0.242	+0.248

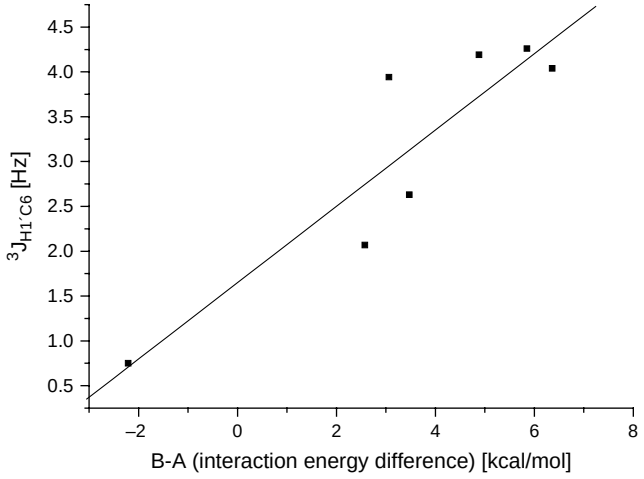

Fig. 2. Differences ($B-A$) of the sums of second-order perturbation stabilization energies (ΔE_2) of bonds within the pathway for $^3J_{H1'C6}$ couplings at different torsional angles.

of +0.292 at the N-120° conformation with the highest ppm value of H1′. A good correlation was found between $\delta_{H1'}$ and charge q at H1′ ($\delta_{H1'} = -8.76$ ppm $+ 54.59q$, $R = 0.961$).

In contrast to DNA, the sugar pucker of ribonucleotides is preferentially C3′ endo (North conformer) which directs the H2′ proton away from its base. Consequently, downfield shifts are expected for H2′ resonances in North puckered sugars only when the χ angle is between 90 and 150° (N110; δH2′ = 6.31 ppm/N-120; δH2′ = 4.21 ppm). Calculations of Dejaegere et al. (1998) [2] showed that H2′ and H3′ proton shifts differed by 0.5 ppm between the North and South conformations in opposite directions: H2′ moved upfield and H3′ downfield when going from North to South. A similar trend is observed in our calculations. Additionally, both H2′ and H3′ resonances depend on the glycosidic torsion with the maximum ppm values at $\chi = +110°$ and +60°, respectively. The usually North-puckered sugars in RNA will place the H3′ proton close to the base ring which explains the dependence on the glycosidic torsion angle. With a glycosidic torsion of -120° (Fig. 1) the distance between H3′ and H6 amounts to 2.18 Å which increases to 3.83 Å at a χ of 180°. Upfield shifts in the H6 resonance have been associated with increasing χ [12]. The highest ppm value is reached at a glycosidic torsion of 180° (δH6 = 8.08 ppm). Since this corresponds to the shortest distance between H6 and O4′ (2.26 Å at $\chi = 180°$ and 2.61 Å at $\chi = -120°$) this unshielding of H6 could be explained by a C–H···O contact interaction which is supported by the increased charge on H6 (+0.274) for the N180° conformation.

3.2. J couplings and glycosidic torsion

The calculated ^3J couplings for fixed OH2′ dihedrals of cytidine in the North conformation and *syn* or *anti* base orientation are shown in Table 2. The homonuclear and heteronuclear ^3J couplings follow Karplus relationships. The only differences between *anti* and *syn* orientations of the base ($^3J_{H3'OH3'}$ and $^3J_{C2'OH3'}$) are found for the OH2′ dihedral of +60° and arise from a changed OH3′ dihedral (*anti*: +71.7°, *syn*: +167.3°).

The calculated ^3J couplings for different base orientations are shown in Table 3. ^3J couplings in the base are independent of the sugar conformation since the values for N-120° and S-120° are almost the same. In most cases, in the synperiplanar (*cis*) orientation the ^3J coupling constant is smaller than in the antiperiplanar (*trans*) orientation, a relation which was found for the base. If the opposite relation holds, this might indicate a through-space component which is transmitted while the two atoms are close to each other in the synperiplanar orientation [13]. The $^3J_{H1'C2}$ couplings follow the typical dihedral dependence *trans* > *cis* whereas for $^3J_{H1'C6}$ almost the same values were found for two North conformations (N-120°:N60°; *trans*:*cis*; 4.25 Hz:4.18 Hz). The *trans* dihedral (+162.2°) was observed for the *anti* (N-120°) and the *cis* dihedral (−6.0°) for the *syn* (N60°) orientation of the base. Consequently, an additional effect operates at the *syn* orientation of the base for $^3J_{H1'C6}$ which is absent for $^3J_{H1'C2}$ in the *anti* orientation (N-120: $^3J_{H1'C2} = 2.79$ Hz). This effect could be attributed to a delocalization. In general, charge transfer from bonds within a saturated coupling pathway into antibonds (here shown for σ bonds only: $\sigma_{pathway} \rightarrow \sigma^*$ designated B) leads to increased ^3J coupling constants whereas the opposite relation leads to decreased coupling constants ($\sigma \rightarrow \sigma^*_{pathway}$ designated *A*) [14]. The second-order perturbation stabilization energies (ΔE_2) associated with this charge transfer [7] between donor and acceptor natural bond orbitals were summed up for all bond/antibond combinations for each base conformation and the difference between sum *B* and sum *A* was taken as overall delocalization effect. A good correlation was found with different torsional angles ($R = 0.9036$, $^3J_{H1'C6} = 1.649$ Hz + $0.426 \cdot (B-A)$, Fig. 2). This indicates the influence of delocalization effects on the $^3J_{H1'C6}$ coupling constant for different base orientations while the ribose conformation can be neglected since values for the N-120° and S-120° conformations are similar ($^3J_{H1'C6}$: 4.25 Hz; 4.03 Hz/$B-A$: 5.87; 6.38). The $^3J_{H1'C6}$ coupling constant was not dominated by charge dependent effects which is supported by a theoretical analysis with ethane although the latter is highly unpolar compared to cytidine [15]. The sum of charges of the four atoms H1′, C1′, N1 and C6 did not correlate with the calculated $^3J_{H1'C6}$ coupling (e.g. the highest and lowest coupling constants for N60° and N180° correspond to nearly the same sum of charges, +0.102 and +0.096, respectively). A multiple regression yielded $R^2 = 0.8164$ with the ($B-A$) difference as independent variable, and $R^2 = 0.8241$ with charge as additional independent variable, only slightly improving the fit. We conclude that the $^3J_{H1'C6}$ coupling constant is dominated by a charge transfer effect and possibly minor steric effects.

The different OH2′ dihedrals due to different base orientations (dihedral OH2′ is *trans* for N60°, N110°, N-60°, S-120° and *gauche* for N180°, N-145° and N-120°) result in a *trans–gauche* difference for $^3J_{OH2'C3'}$ of about 6 Hz (Tables 1 and 3). The main difference when comparing the different base orientations is found for OH2′ due to a different dihedral.

Table 2
Selected calculated ^3J coupling constants (in Hz) of cytidine in the North conformation at $\chi = -120°$ or $+60°$ with restrained OH2′ dihedrals

OH2′ dihedral $\chi = -120°$/atom pair	0°	+60°	+120°	180°	−120°	−60°
H2′–OH2′	7.26	0.67	1.56	12.58	2.51	0.58
H3′–OH3′	10.98	−0.32	−0.01	8.33	10.04	10.12
C1′–OH2′	2.20	11.93	3.11	0.28	3.42	−0.18
C3′–OH2′	2.2	0.29	4.73	0.79	1.40	5.82
C2′–OH3′	2.36	6.20	5.97	3.40	3.07	3.22
C4′–OH3′	−0.62	1.17	0.94	−0.79	−0.84	−0.89
Dihedral OH3′	−163.4°	+71.7°	+69.1°	−144.3°	−156.1°	−160.4°
OH2′ dihedral $\chi = +60°$/atom pair	0°	+60°	+120°	180°	−120°	−60°
H2′–OH2′	6.92	1.04	1.53	11.89	2.80	0.44
H3′–OH3′	11.2	12.5	0.28	9.77	10.80	10.92
C1′–OH2′	2.07	11.23	3.11	0.42	3.40	−0.31
C3′–OH2′	1.75	0.24	4.24	1.09	1.19	5.75
C2′–OH3′	2.71	−0.14	5.52	3.64	3.27	3.07
C4′–OH3′	−0.48	1.10	1.64	−0.86	−0.65	−0.66
Dihedral OH3′	−163.1°	+167.3°	+68.9°	−149.2°	−159.8°	−160.8°

Table 3
Calculated ^3J coupling constants, dihedrals of the North and South conformation and sum of charges of cytidine with restrained glycosidic torsion angles

χ/$^3J_{pair}$	N60°	N110°	N180°	N-145°	N-120°	N-60°	S-120°
H6–C4	7.64	7.82	7.79	7.69	7.60	7.37	7.67
H6–C2	4.78	4.76	4.86	4.82	4.87	4.83	4.68
H1′–C2	4.02	3.43	0.36	1.82	2.79	0.73	2.52
H1′–C6	4.18	2.62	0.74	2.06	4.25	3.93	4.03
H1′–C3′	2.29	2.30	1.99	2.53	2.74	2.41	0.24
H1′–C4′	1.50	1.61	2.16	1.99	1.87	1.65	0.09
H2′–C4′	4.42	3.69	4.05	4.29	4.24	4.13	0.29
OH2′–C1′	1.84	1.86	−0.91	−0.72	−0.66	2.36	−1.18
OH2′–C3′	0.15	0.05	5.75	6.17	6.31	−0.38	4.10
OH2′–H2′	11.00	12.06	3.54	1.71	1.22	9.04	8.54
H3′–C1′	0.18	0.25	0.16	0.14	0.15	0.15	5.36
H3′–C5′	3.70	3.88	3.86	3.84	3.94	3.70	2.01
OH3′–C2′	3.61	3.35	3.07	3.01	3.13	3.14	−0.18
OH3′–C4′	−0.82	−0.07	−0.67	−0.72	−0.60	−0.61	1.98
H4′–C2′	0.86	0.94	0.89	0.93	0.94	1.16	1.65
H4′–C1′	0.28	0.06	0.26	0.22	0.28	0.11	1.75
Dihedral H1′–C2	+165.3°	−133.4°	−59.2°	−24.7°	−1.5°	+55.6°	−0.1°
Dihedral H1′–C6	−6.0°	+50.9°	+119.0°	+143.3°	+162.2°	−140.1°	+172.1°
sum of charges (H1′–C1′–N1–C6)	+0.102	+0.063	+0.096	+0.095	+0.092	+0.061	+0.089

This results for $\chi = -120°$ in a *gauche* orientation with respect to H2′ (−54.1°) and a *trans* orientation to C3′ and correspondingly a weak homonuclear ($^3J_{OH2'H2'} = 1.22$ Hz) and strong heteronuclear ($^3J_{OH2'C3'} = 6.31$ Hz) coupling, respectively (Tables 1 and 3).

It was found that $^1J_{CH}$ coupling constants depend on the base orientation for cytidine [6] which was questioned in the past [5]. Additionally, charge and bond lengths were not sufficient for obtaining good ^1J correlations in the case of cytidine [6]. Glycosidic torsion influences the two $^1J_{CH}$ couplings between H6–C6 and H1′–C1′. The s-orbital percentage for the corresponding carbon atoms are shown in Table 4. The difference between $^1J_{H6C6}$ of N-60° and S-120° amounts to 7.2 Hz and corresponds to a change in s-orbital contribution of 1.21% which is supported by the well known empirical correlation between hybridization and $^1J_{CH}$ coupling constants ($s_{CH}\% = 0.2\ ^1J_{CH}$)

Table 4
Calculated ^1J coupling constants [6] and s-orbital percentages of the corresponding carbon atoms at different glycosidic torsion angles of cytidine

χ/$^1J_{pair}$/s-orbital (%)	N60°	N110°	N180°	N-145°	N-120°	N-60°	S-120°
H6–C6	150.0	153.3	155.3	153.4	150.2	146.7	153.9
H1′–C1′	164.2	170.3	178.3	175.1	169.5	175.7	169.2
(H6–)C6	31.88	32.08	32.97	32.53	32.08	31.76	32.06
(H1′–)C1′	26.71	26.21	28.06	27.93	27.77	27.26	27.94

[16]. According to this relation the change of 7.2 Hz of the $^1J_{H6C6}$ coupling constants would correspond to a change in s-orbital percentage of 1.44% which matches the calculated difference of 1.21%. However, the correlation coefficient of $R=0.7719$ indicates that additional factors such as charge and bond lengths also influence the $^1J_{H6C6}$ coupling constant to a minor extent. A similar relation holds for the $^1J_{H1'C1'}$ coupling constants (Table 4) but the correlation coefficient is even worse ($R=$ 0.4958). Consequently, for the N60° (syn) base orientation additional effects such as bond lengths have to be taken into account to explain the further reduced coupling constant ($r_{H1'C1'}=1.0961$ Å at N60° and 1.0950 Å at N110° [6]). Again, the ribose conformation seems to play only a minor role for the $^1J_{H6C6}$ and $^1J_{H1'C1'}$ couplings.

4. Conclusions

The dependence of J couplings on the torsional angle of cytidine was documented by DFT calculations. Especially the $^3J_{H1'C6}$ and $^1J_{H6C6}$ coupling constants can be correlated to NBO derived quantities such as donor–acceptor interaction energies and sp-hybridization effects, respectively. Additionally, the close contact of H6 to the ribose O4′ is related to increased deshielding, i.e. increased ppm values for the base torsion of 180°. The conformation of the ribose plays only a minor role in the above mentioned NMR parameters enabling the evaluation of base orientations within RNA structures.

Acknowledgements

We like to thank Prof. Griesinger for supporting this work. We gratefully acknowledge the help in preparing the manuscript by F. Wetter.

References

[1] S.S. Wijmenga, B.N.M. van Buuren, Prog. NMR Spectrosc. 32 (1998) 287.
[2] A.P. Dejaegere, D.A. Case, J. Phys. Chem. 102 (1998) 5280.
[3] F. Cloran, Y. Zhu, J. Osborn, I. Carmichael, A.S. Serianni, J. Am. Chem. Soc. 122 (2000) 6435.
[4] M.L. Munzarová, V. Sklenar, J. Am. Chem. Soc. 125 (2003) 3649.
[5] T. Bandyopadhyay, J. Wu, W.A. Stripe, I. Carmichael, A.S. Serianni, J. Am. Chem. Soc. 119 (1997) 1737.
[6] J.T. Fischer, U.M. Reinscheid, Eur. J. Org. Chem. 9 (2006) 2074.
[7] A.E. Reed, L.A. Curtiss, F. Weinhold, Chem. Rev. 88 (1988) 899.
[8] M.J. Frisch et al., Gaussian 03, Gaussian Inc., Pittsburgh, PA, 2003.
[9] A.D. Becke, J. Chem. Phys. 98 (1993) 5648.
[10] C. Lee, W. Yang, R.G. Parr, Phys. Rev. B 37 (1988) 785.
[11] P. Auffinger, E.J. Westhof, Mol. Biol. 274 (1997) 54.
[12] J.A. Cromsigt, C.W. Hilbers, S.S. Wijmenga, J. Biomol. NMR 21 (2001) 11.
[13] M.L. Munzarová, V. Sklenar, J. Am. Chem. Soc. 124 (2002) 10666.
[14] R.H. Contreras, J.E. Peralta, C.G. Giribet, M.C. Ruiz de Azúa, J.C. Facelli, Ann. Rep. NMR Spectrosc. 41 (2000) 55.
[15] R.H. Contreras, J.E. Peralta, Prog. NMR Spectrosc. 37 (2000) 321.
[16] G. Binsch, J.B. Lambert, B.W. Roberts, J. Am. Chem. Soc. 86 (1964) 5564.

Available online at www.sciencedirect.com
ScienceDirect
Journal of Molecular Structure 872 (2008) 145–149
Journal of MOLECULAR STRUCTURE
www.elsevier.com/locate/molstruc

Conformational analysis of menthol diastereomers by NMR and DFT computation

Julia Härtner, Uwe M. Reinscheid *

Max Planck Institute for Biophysical Chemistry, NMR II, Am Fassberg 11, 37077 Göttingen, Germany

Received 19 October 2006; received in revised form 21 February 2007; accepted 21 February 2007
Available online 28 February 2007

Abstract

Correlations between experimental and calculated ^{13}C chemical shifts were performed with the series of all menthol diastereomers. In this way it could be shown that identification problems with newly isolated natural products can be solved. Starting from simulated, low energy conformers of menthol, neomenthol, isomenthol, and neoisomenthol the ^{13}C chemical shifts were obtained using DFT calculations [functional: B3LYP, basis set: 6-31G(d,p)]. Due to differences in chemical shifts, the prochiral methyl groups of the isopropyl substituent of menthol could be differentiated using the correlations between experimental and calculated values. A conformational scan of the dihedral angle of the isopropyl group allowed the determination of the dominating rotamers of menthol (+68.4°) and neomenthol (+172.5°) using ^{13}C chemical shifts. The results were supported by energy calculations, $^{1}J_{CH}$ and $^{3}J_{HH}$ measurements. The correlations and $^{3}J_{HH}$ measurements for isomenthol indicate conformational averaging impeding the determination of the isopropyl group rotamer. For neoisomenthol, MD simulations showed two chair conformations. However, in contrast to calculated energies and correlations between theoretical and experimental ^{13}C chemical shifts, the measured $^{3}J_{H3H2}$ coupling of 6.3 Hz indicates an equally populated equilibrium of both conformers.

Keywords: ^{13}C chemical shift; Menthol; Neomenthol; Isomenthol; Neoisomenthol; DFT; Conformation

1. Introduction

Menthol (Fig. 1a) is the major constituent of the essential oil of the *Labiaceae* (peppermint: *Mentha x piperita* and spearmint: *Mentha spicata*) and is used industrially. The determination of menthol in the natural mixture with its four diastereomers isomenthol, neomenthol, and neoisomenthol (Fig. 1b, c, and d) can be done chromatographically or using NMR spectroscopy. In the presence of isomeric forms the high resolution of ^{13}C NMR is advantageous compared to proton NMR. For a reliable assignment the possibility of a mixture of conformers has to be taken into account which has been partially done in the past for some natural products [1–5]. A simulation using the Sybyl force field [6] generated conformers of the menthol isomers and tried to correlate structural with organoleptic parameters [7]. Additionally, the equilibrium between menthone and isomenthone was calculated using the DFT approach [8]. Conflicting results concerning the ^{13}C resonances of the menthol isomers [9,10] prompted us to evaluate the conformations of the series of menthol diastereomers using a combined NMR–DFT approach.

2. Experimental

2.1. Computational

The four isomeric compounds menthol, neomenthol, isomenthol, and neoisomenthol were built using DISCOVER in the InsightII program package (Accelrys™, [11]). A CVFF force field was chosen. The series of enantiomers starting from (+) menthol (1*S*,3*S*,4*R*) shown in Fig. 1a–d was chosen. A high temperature (600 °C) molecular

* Corresponding author. Tel.: +49 551 201 2215; fax: +49 551 201 2202.
E-mail address: urei@nmr.mpibpc.mpg.de (U.M. Reinscheid).

0022-2860/$ - see front matter © 2007 Elsevier B.V. All rights reserved.
doi:10.1016/j.molstruc.2007.02.029

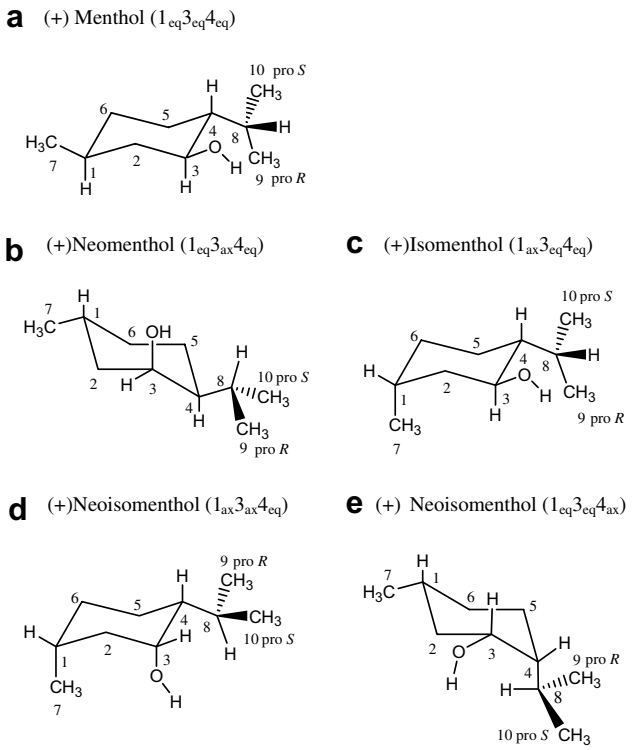

Fig. 1. (a–e) Menthol and the diastereomers neomenthol, isomenthol, and neoisomenthol.

dynamic/minimization simulation was performed and the resulting energy minimized structures were used as starting structures for Gaussian™ calculations [12]. Geometry optimization, energy calculations and ^{13}C chemical shift calculations were done using B3LYP and a 6-31G(d,p) basis set. The chemical shifts were calibrated with calculated values for TMS ($\delta_C = 188.85$). Correlation coefficients and standard deviations (SD) of the fits between calculated and experimental data were obtained using Origin™.

2.2. NMR spectroscopy

A solution of (+) menthol (50 mM) in DMSO-d_6, and solutions of all menthol diastereomers in $CDCl_3$ (50 mM) were measured at 298 K. 1D proton, ^1H,^1H-COSY (4 K × 1 K, 8 scans) and ^1H,^{13}C-HSQC spectra (4 K × 1 K, 16 scans) were recorded with a 400 MHz Bruker Avance spectrometer.

3. Results and discussion

In cyclohexane derivatives such as the menthol diastereomers a chair conformation is the dominating conformation (Fig. 1a–e). The position of the three substituents is designated by a shorthand notation. In order to avoid misassignments, we introduce the clear pro*R*/pro*S* nomenclature for the methyl groups of the isopropyl substituent.

In the first step of our conformational analysis a direct comparison of the measured ^{13}C chemical shifts of menthol

Table 1
^{13}C chemical shifts of menthol

Numbering	Senda and Imaizumi [10] ($CDCl_3$)	This study (DMSO-d_6)	Sassa et al. [9] ($CDCl_3$)
C-1	32.20	32.08	31.60
C-2	45.90	45.94	45.10
C-3	71.20	70.24	71.60
C-4	50.70	50.40	30.20
C-5	23.80	23.64	23.10
C-6	35.30	35.20	34.50
C-7	22.60	23.05	22.20
C-8	26.10	25.80	25.90
C-9	16.30	16.80	16.10
C-10	21.30	21.80	21.00

(Table 1) revealed that the natural product isolated by Sassa et al. [9] should not be regarded as menthol. The isolated compound tentatively assigned as menthol by Sassa et al. [9] neither fits to the experimental and calculated chemical shifts of all four menthol isomers nor to the calculated chemical shifts of three positional isomers (same numbering shown in Fig. 1a; isomer I: 1-OH, 4-isopropyl, 6-methyl; isomer II: 1-methyl, 2-OH, 4-isopropyl; isomer III: 4-isopropyl, 5-methyl, 6-OH, data not shown). This inconsistency could be traced back to a typing error [13].

Only minor variations were found between the ^{13}C chemical shifts of menthol in DMSO-d_6 and the results of Senda and Imaizumi [10] obtained in $CDCl_3$ (Table 1, Fig. 2).

The correct assignment of C-9 and C-10 was accomplished by the DFT calculations of ^{13}C chemical shifts and can be rationalized by the γ-gauche effect [14] of C-9 in the dominating rotamer. The correlation coefficient of 0.999 and the standard deviation of 0.27 illustrate variation due to experimental conditions (Fig. 2). A nearly perfect linear fit indicates that solvent effects ($CDCl_3$ or DMSO-d_6) are not important, and can be disregarded in this case.

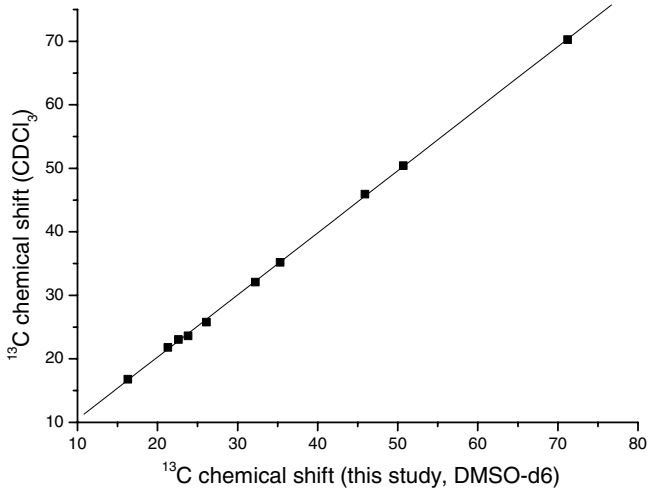

Fig. 2. Fit between ^{13}C experimental values of menthol in two solvents (Senda and Imaizumi [10]: $CDCl_3$; this study: DMSO-d_6).

The dominating chair of neoisomenthol was predicted to bear the isopropyl group in the axial position (Fig. 1e) [10]. The high-field shift of C-1 compared to menthol would then be explained by a γ-effect [14] due to the axial positions of the OH-group and the methyl group in the minor $1_{ax}3_{ax}4_{eq}$ conformer (Fig. 1d). To evaluate the correct chair conformer of neoisomenthol the structure of Fig. 1e, ($1_{eq}3_{eq}4_{ax}$) was obtained by a MD simulation and the ^{13}C chemical shifts were calculated. The best fit was obtained for the +79.9° rotamer of the isopropyl group with a correlation coefficient of 0.9811 and a standard deviation of 3.17. This conformer was 1.76 kcal/mol higher in energy compared to the conformer of Fig. 1d. However, the experimental value of 6.3 Hz for the $^3J_{H2H3}$ coupling indicates conformational averaging between the two chair conformers (calculated values: $^3J_{H2axH3ax} = 10.1$ Hz of Fig. 1e and $^3J_{H2axH3eq} = 2.67$ Hz of Fig. 1d). The conflicting theoretical results might be explained by the exclusion of solvent effects in the calculations. In 3-substituted cyclohexanols hydrogen bonds were found to stabilize conformers depending on the temperature and this stabilization is not adequately modeled in our calculations [15].

MD simulations in DISCOVER (Accelrys™) revealed different conformations for the four menthol isomers. For isomenthol and neoisomenthol two different chairs were found. The conformers of the other isomers differed only in the dihedral angle of the isopropyl group. This is in agreement with the $^3J_{HH}$ couplings measured in this work ($^3J_{H4,H8}$: menthol (2.5 Hz), neomenthol (9.2 Hz), isomenthol (5.5 Hz). The last value indicates conformational averaging and could be explained by the existence of a conformer with an axial isopropyl group [16]. The $^3J_{H4,H8}$ coupling for neoisomenthol could not be determined due to overlapping resonances.

We next studied the dependence of the ^{13}C chemical shifts on the dihedral angle of the isopropyl group. The resulting fits between calculated and experimental ^{13}C chemical shifts of menthol are shown in Fig. 3a–c. The experimental and corrected values were taken from Senda and Imaizumi [10]. The statistical values are shown in

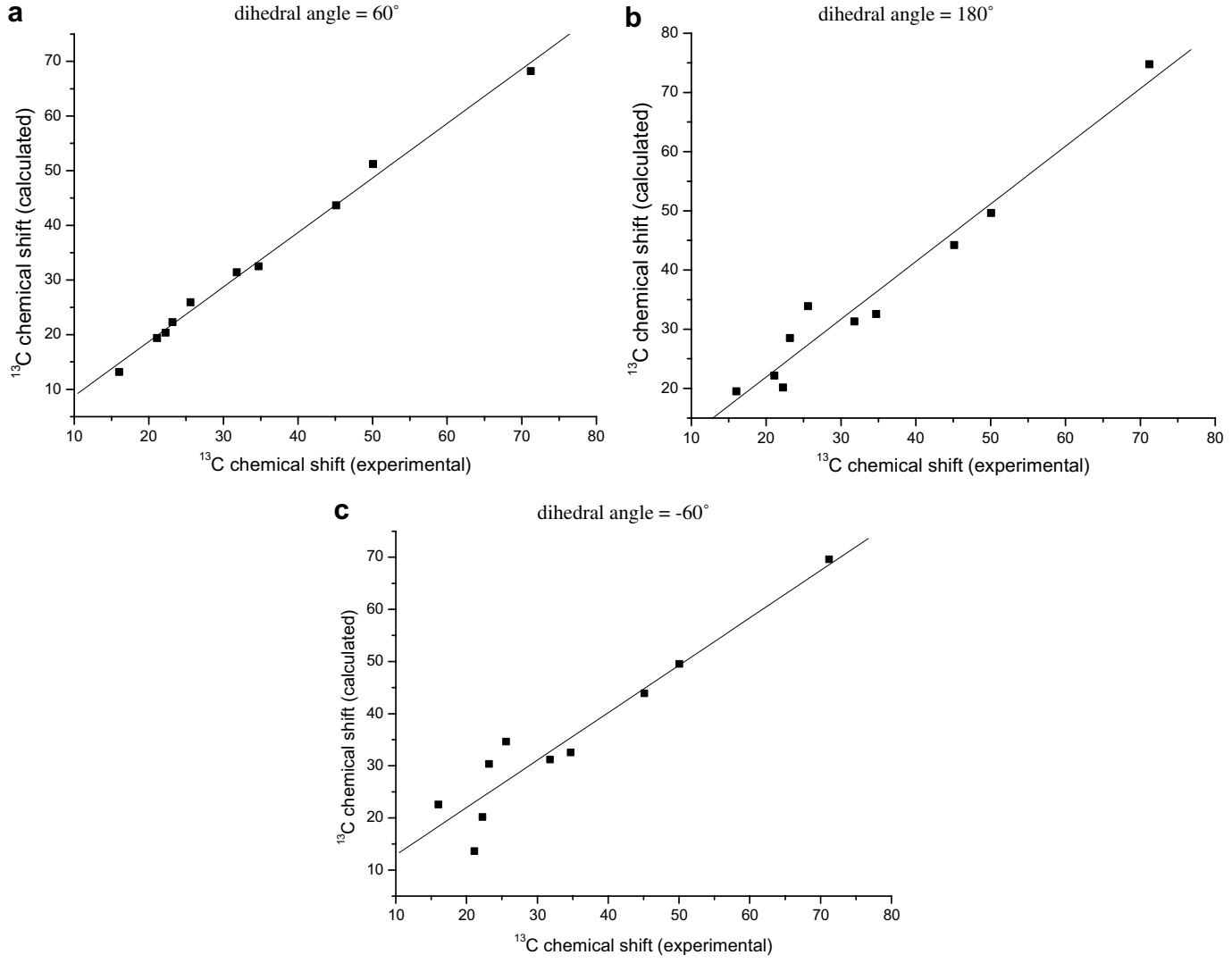

Fig. 3. (a–c) Fits between experimental and calculated ^{13}C chemical shifts for menthol conformers with different dihedral angles of the isopropyl group (H8–C8–C4–H4).

Table 2
Correlation coefficients and standard deviation (in brackets) of the linear fits between experimental and calculated ^{13}C chemical shifts of the four diastereomeric menthols at different H8–C8–C4–H4 dihedral angles (dominating conformers are in bold)

Isomer/dihedral angle	60°[a]	180°[b]	−60°[c]
Menthol (Fig. 1a)	**0.9969 (1.42)**	0.9788 (3.67)	0.9524 (5.24)
Neomenthol (Fig. 1b)	0.9817 (3.33)	**0.9943 (1.85)**	0.9814 (3.81)
Isomenthol (Fig. 1c)	0.9752 (4.32)	0.9824 (3.68)	0.9777 (3.66)
Neoisomenthol (Fig. 1d)	0.9825 (3.47)	0.9935 (1.86)	0.9833 (3.01)

[a] Optimized values for menthol, neomenthol, isomenthol, and neoisomenthol: +68.4°/+55.0°/+68.2°/+74.4°.
[b] −174.0°/+172.5°/+163.4°/−174.7°.
[c] −77.9°/−75.4°/−78.4°/−54.8°.

Table 2. The best fit was obtained with a dihedral angle of +68.4° in agreement with a recently obtained crystal structure for (−)menthol [17].

Additionally, we were able to differentiate between the two methyl groups of the isopropyl substituent (pro*R* and pro*S*, Fig. 1a). The exchange of pro*R* and pro*S* carbon assignments in the dominating +68.4° conformation led to a worse fit between experimental and calculated values and enabled the assignment of the methyl groups of menthol (correct assignment: correlation coefficient: 0.9969/SD = 1.42, exchanged assignment: correlation coefficient: 0.9846/SD = 3.15). No measurements of residual dipolar couplings in orienting media [18] were needed for this determination.

The performance of this approach was tested by fitting the experimental values of neomenthol, isomenthol, and neoisomenthol with calculated values of the low energy conformers obtained by simulations with DISCOVER (Fig. 4a–c, Table 2). In contrast to the energetic data (Table 3), the best fit for isomenthol was obtained with

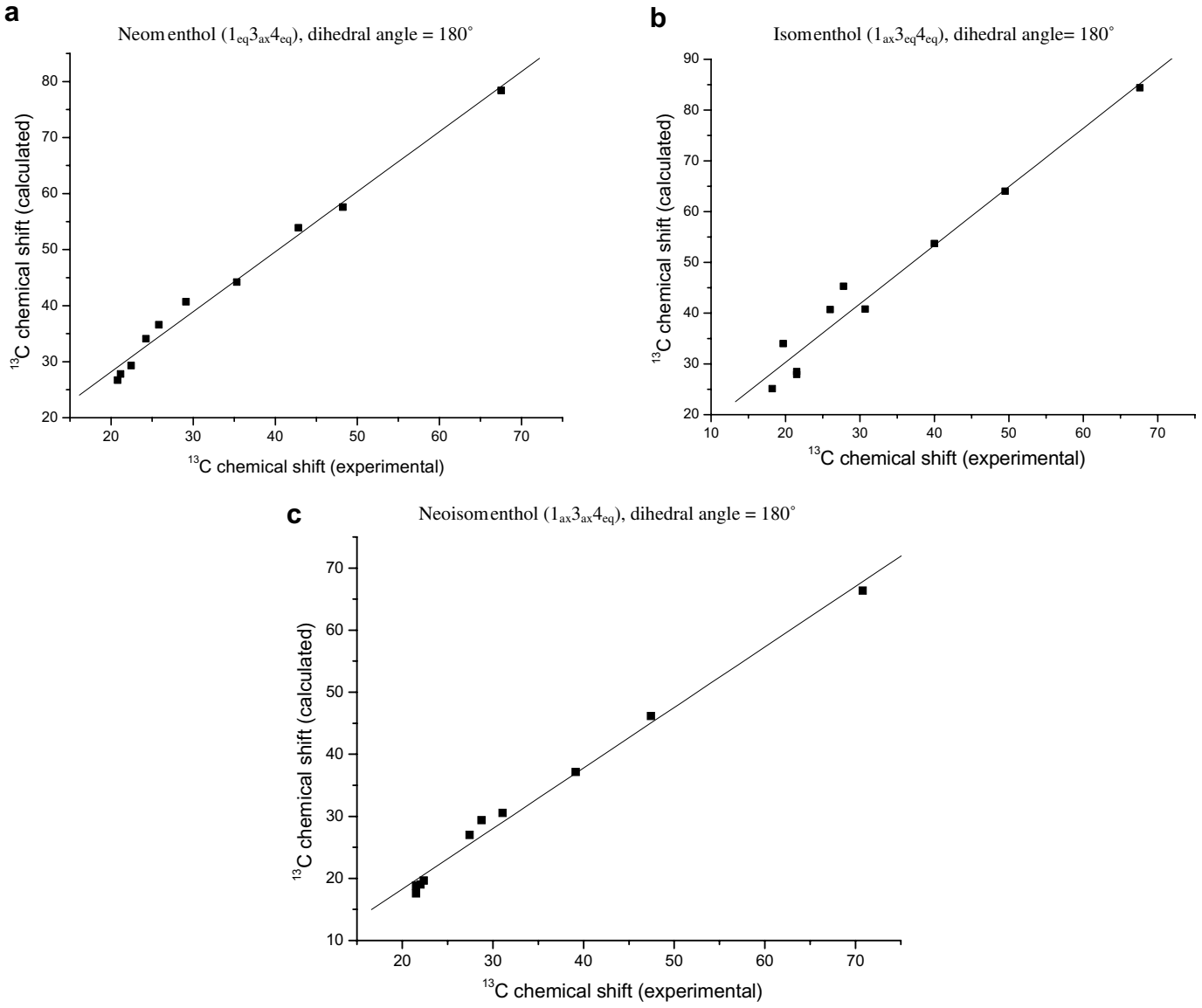

Fig. 4. (a–c) Fits to experimental data of the conformers of neomenthol, isomenthol, and neoisomenthol (isopropyl dihedral angle: H8–C8–C4–H4).

Table 3
Energy differences in kcal/mol of the four diastereomeric menthols at different H8–C8–C4–H4 dihedral angles

Isomer/dihedral angle	60°	180°	−60°
Menthol (Fig. 1a)	0[a]	1.82	0.56
Neomenthol (Fig. 1b)	1.03	0[b]	0.83
Isomenthol (Fig. 1c)	0[c]	1.78	0.67
Neoisomenthol (Fig. 1d)	0.98	0[d]	1.11

[a] Basis value set to 0: −468.088633 Hartree.
[b] −468.087743 Hartree.
[c] −468.084991 Hartree.
[d] −468.081991 Hartree.

a dihedral angle of +163.4° (Table 2). Since the correlation coefficient is substantially smaller compared with the other isomers, we calculated the Boltzmann average with 76% of the +68.2° rotamer and 24% of the −78.4° rotamer. However, even for this mixture a poor correlation coefficient of 0.9786 and a SD of 3.93 were obtained. Since the contributions of other conformers can be assumed to be small on energetic grounds (the lowest energy conformer with the isopropyl group in axial position is 1.47 kcal/mol higher in energy than the basis conformer (Table 3)), the approach is not sufficient to determine the dihedral angle of the isopropyl group of isomenthol.

However, dihedral angles of 180° determined for the rotamers of neomenthol and neoisomenthol are supported by energetic data (Table 3) and measurements of $^1J_{CH}$ couplings (neomenthol: $^1J_{C8,H8} = 123.6$ Hz; neoisomenthol $^1J_{C8,H8} = 123.7$ Hz). Axial CH groups have smaller ^1J couplings in cyclohexanes [19] due to the $\sigma_{C-H} \rightarrow \sigma^*_{C-H}$ delocalization which is pronounced for the *anti* arrangement [20].

4. Conclusions

In this study, the dominating conformers of menthol and neomenthol were identified based on the comparison between experimental and calculated ^{13}C chemical shifts. The determinations of the rotamers of the isopropyl group based on ^{13}C chemical shift correlations were additionally supported by thermochemical data. Calculated and experimental data for isomenthol and neoisomenthol indicate conformational averaging which excludes a simple approach using solely calculated ^{13}C chemical shifts for the conformational analysis. However, the approach helped to identify assignment problems in a recently isolated natural product.

Acknowledgements

We are grateful for the support of Prof. C. Griesinger, Prof. M. Keusgen (Marburg), and Dr. Panten (Symrise GmbH, Holzminden).

References

[1] E. Kolehmainen, K. Laihia, R. Laatikainen, J. Vepsäläinen, M. Niemitz, R. Suontamo, Magn. Reson. Chem. 35 (1997) 463.
[2] K.-Y. Kim, S.-G. Lee, Magn. Reson. Chem. 35 (1997) 451.
[3] J.M. Torres-Valencia, M. Meléndez-Rodríguez, R. Álvarez-García, C.M. Cerda-García-Rojas, P. Joseph-Nathan, Magn. Reson. Chem. 42 (2004) 898.
[4] G. Barone, D. Duca, A. Silvestri, L. Gomez-Paloma, R. Riccio, G. Bifulco, Chem. Eur. J. 8 (2002) 3240.
[5] G. Barone, L. Gomez-Paloma, D. Duca, A. Silvestri, R. Riccio, G. Bifulco, Chem. Eur. J. 8 (2002) 3233.
[6] M. Clark, R.D. Cramer III, N. Van Opdenbosch, J. Comp. Chem. 10 (1989) 982.
[7] M. Chastrette, E. Rallet, Flavour Frag. J. 13 (1998) 5.
[8] W.B. Smith, C. Amezcua, Magn. Reson. Chem. 36 (1998) S3.
[9] T. Sassa, H. Kenmoku, M. Sato, T. Murayama, N. Kato, Biosci. Biotechnol. Biochem. 67 (2003) 475.
[10] Y. Senda, S. Imaizumi, Tetrahedron 31 (1975) 2905.
[11] P. Dauber-Osguthorpe, V.A. Roberts, D.J. Osguthorpe, J. Wolff, M. Genest, A.T. Hagler, Proteins Struct. Funct. Genet. 4 (1988) 31.
[12] M.J. Frisch et al., Gaussian 03, Inc., Pittsburgh, PA, 2003.
[13] T. Sassa, personal communication.
[14] H. Günther, NMR Spectroscopy: Basic Principles, Concepts, and Applications in Chemistry, Wiley, Chichester, 1998.
[15] P.R. de Oliveira, L. Tasic, S.A. Rocco, R. Rittner, Magn. Reson. Chem. 44 (2006) 790.
[16] T. Egawa, M. Sakamoto, H. Takeuchi, S. Konaka, J. Phys. Chem. A 107 (2003) 2757.
[17] P. Bombicz, J. Buschmann, P. Luger, N.X. Dung, C.B. Nam, Z. Kristallogr. 214 (1999) 420.
[18] L. Verdier, P. Sakhaii, M. Zweckstetter, C. Griesinger, J. Magn. Reson. 163 (2003) 353.
[19] G. Cuevas, E. Juaristi, J. Am. Chem. Soc. 124 (2002) 13088.
[20] L. Goodman, V. Pophristic, Nature 411 (2001) 565.